Heat transfer by steam condensing onto rotating cones

Malcolm Howe

HEAT TRANSFER BY STEAM CONDENSING ONTO ROTATING CONES

by

Malcolm Howe, A.M.Inst.F. C.Eng.

Thesis submitted for the degree of
Doctor of Philosophy
in the
University of Durham

Department of Engineering Science,
University of Durham.

July 1972.

Abstract.

A theoretical analysis is made for the condensation of steam in a laminar film on the outer surface of an axisymmetrical body. The body rotates about a vertical axis and the film is assumed to drain under the combined influence of gravitational and centrifugal accelerations. A differential equation which governs the film thickness is derived and is numerically integrated for two types of axisymmetrical body to calculate the theoretical film to surface heat transfer coefficient.

The first type of body is the cone. A decrease in the apex angle on stationary cones leads to an increase in the component of gravitational acceleration along the surface and to an increase in the theoretical heat transfer coefficient. However, an increase in the apex angle of a cone rotating at high speed increases the component of the centrifugal acceleration along the surface and increases the heat transfer coefficient. A comparison is made between the heat transfer coefficient for discs and for cones.

The second type of body has a concave surface described by the rotation of a circular arc and represents part of a turbine rotor at the transition from shaft to blade disc. Theoretical film thicknesses and heat transfer coefficients are presented and discussed for bodies with an arc radius of 0.2 m and shaft diameters between 0.002 m and 0.6 m.

An apparatus for making measurements of heat transfer coefficient from steam to rotating axisymmetrical bodies with

diameters up to 0.6 m, is described.

The heat transfer results for steam condensing on cooled rotating cones with apex angles 10^{o}, 20^{o} and 60^{o} are presented and discussed. The condensate film supports various patterns of waves as it drains along the surface of the 10^{o}, 20^{o} and 60^{o} cones. At high speeds, drainage on the 10^{o} and 20^{o} cones is assisted by the formation and detachment of drops. The pattern of waves and the mode of drainage are shown to be dependent on the apex angle, the speed of rotation, the cone diameter and the distance from the starting point of condensation. With either mode of drainage the experimental heat transfer coefficients are generally larger than the theoretical laminar values.

Acknowledgements.

Many people have given useful advice and practical assistance particularly during the design and construction of the apparatus and I am greatly indebted to them.

My sincere thanks are extended to Professor Russell Hoyle, who was Head of Department and leader of the project until his retirement in October 1971. Without the benefit of his skilful supervision throughout the work many of my efforts would have been misguided.

I am also extremely grateful for the keen interest taken in all aspects of my work by Professor Harry Marsh who has recently become the leader of the project. I have learnt much from discussions with him about the theoretical side of my work.

I would like to extend my thanks to Senior Technicians Harker and Johnson for looking after the steam supply and doing many jobs on the apparatus over a period of five years.

My thanks are due to the Science Research Council for sponsoring this work.

Finally I would like to thank my wife for patiently transforming pages of poor hand writing into typed script.

Contents

List of figures.

Notation.

Upper case

A Surface area.

B A constant whose value defines $\frac{dt}{dX}$ as being small compared with $\frac{dt}{dy}$.

C Constants of integration.

D Diameter of cone.

E $\frac{3H}{\nu^2} = \frac{3\ c\theta}{Pr(1+\frac{3}{8}\ c\theta)}$ H as defined on page 62

F Body force.

$\dot{G}$ Condensation rate per unit area.

N Speed of rotation of body.

P Function of y.

Q Energy flow/unit time.

R $(1 + \beta t)$.

S Shear force.

U Average velocity of condensate flow in X direction.

V Volume.

X Directions parallel to the generator of a body.

Y Directions perpendicular to the generator.

Z Function of y.

Lower case

a Acceleration parallel to X direction.

a_y Acceleration parallel to Y direction.

b Coefficient relating the normal n to the cone wall thickness w.

c Specific heat of condensate.

d Diameter of body at the starting point of condensation.

f Function.

g Gravitational acceleration.

h Heat transfer coefficient.

k Coefficient of thermal conductivity.

k_o Coefficient of thermal conductivity of cone material at 0^o C.

l Specific enthalpy of condensation.

$\mathring{m}$ Mass flow rate.

n Distance from the axis of rotation to the inner surface of cone in direction Y.

p Point on the generator.

r Radius of curvature of the generator curve.

t Temperature.

u Velocity of condensate flow in X direction at distance y from outer surface of cone.

v Variable relating δ^4 to x.

w Wall thickness of hollow cone.

x Distance in X direction from starting point of condensation.

x' Distance in X direction from apex of inner surface of cone.

y Distance in Y direction.

Greek symbols

Upper case

Γ Mass flow rate per unit perimeter $\frac{\dot{m}}{\pi D}$

Δ Small increment.

Lower case.

2α Apex angle of cone.

β Temperature coefficient of thermal conductivity.

δ Thickness of laminar film of condensate.

ζ Fraction whose value lies between zero and unity ($0 < \zeta < 1.0$).

η Co-ordinate parallel to axis of rotation.

θ Steam to surface temperature difference ($t_s - t_o$), or film temperature difference.

θ_w Temperature difference across the cone wall.

μ Dynamic viscosity.

ν Kinematic viscosity.

ξ Co-ordinate in direction perpendicular to axis of rotation.

π Constant 3.14159.

ρ Density.

σ Surface tension.

τ Shear stress.

ϕ Heat flux (energy transfer/unit time.unit area).

ψ Angle of rotation of generator about vertical axis.

ω Angular velocity.

Subscripts

o Outer surface of cone.

i Inner surface of cone.

w Wall.

z Speed of rotation = zero.

N Speed of rotation N.

S+G Refers to work of Sparrow and Gregg.

S+H Refers to work of Sparrow and Hartnett.

exp Quantity measured by experiment.

lam quantity calculated from laminar theory.

Dimensionless groups.

L dimensionless distance along the cone $\frac{x\omega^2 \mathrm{Sin}^2\alpha}{g\mathrm{Cos}\alpha}$

λ dimensionless laminar film thickness $\frac{\delta}{\left[\frac{\nu}{\mathrm{Sin}\alpha}\right]^{\frac{1}{2}} E^{\frac{1}{4}}}$

Nu	Nusselt number	$\frac{hx}{k}$
Pr	Prandtl number	$\frac{c\mu}{k}$
Re	Reynolds number	$\frac{4\Gamma}{\mu}$
We	Weber number	$\frac{D^3 \rho \omega^2}{4g\sigma}$

Other symbols defined in the text.

1.0 Introduction.

The work reported in this thesis is concerned with the filmwise condensation of steam on rotating axisymmetrical bodies and has applications in several fields.

Large acceleration fields created by rotating the condensing surface lead to improvements in the rate of condensation. In the field of condenser design such improvements could reduce the area of the condensing surface for a given thermal load and thus reduce the size of the condenser. This advantage might be used in space-flight applications where the condition of zero gravitational acceleration demands the creation of an acceleration field at the condensing surface to induce film drainage. Creating the field by rotating the surface, as opposed to vibrating it, has the operational advantage of being both silent and dynamically balanced.

The present work forms part of a wider investigation into the transient thermal stresses which occur in all steam turbine rotors during cold starting and during the maneouvring of marine steam turbines. If the rate of change of rotor temperature is not limited during these operations, the rotors can become over stressed and eventually suffer thermally induced fatigue which in turn leads to the risk of rotor disintegration. In the past the duration of the warm through period has been determined empirically by what has been considered to be safe practice in the operation of steam turbines. With the advent of the large rotors used in land based turbines and the use of steam turbines in nuclear submarines, there has been the need for

turbine designers to minimise the duration of the warm through period while maintaining safe levels of stress in the rotor. To calculate the thermal stresses during the warm through period requires a knowledge of the temperature on any part of the rotor at a given time.

With steam turbines the problem of finding the rotor temperature at a given time is complicated by the deposition of condensate on the rotor whenever the temperature of the outer surface of the rotor is below the saturation temperature of the steam. Since the rotors are usually cleaned by the steam during full load operation, the condensate forms a continuous film which becomes an additional barrier to heat transfer and influences the rate of change of rotor temperature. The importance of the film as a heat transfer barrier depends on the thickness of the film which increases until the rates of condensation and of drainage are equal. Rates of drainage are governed by the shape of the rotor and by the magnitude and direction of the rotor's acceleration field.

Thus an experimental study of the heat transfer by steam condensing onto turbine rotors is required to determine the change in rotor temperature with time. Because of the variety in shape and in the size of turbine rotors any experimental heat transfer study based on tests with one rotor has a limited scope. The study must be more broadly based so the results can be applied to any rotor.

If an axisymmetrical body such as a rotor is cut into a number of thin slices by planes normal to the axis of symmetry, each slice approximates to the frustum of a cone. Thus

a more fundamental approach to the problem has been made by studying the heat transfer by steam condensing onto rotating cones with a variety of apex angles.

As described in section 2.4 an experimental and theoretical study has already been made of the condensation of steam on rotating horizontal cylinders which are 0^{o} cones and represent the shaft part of the turbine rotor. The film of condensate was found to drain from the cylinder by the formation and detachment of drops. The condensation of steam on a rotating disc, which is the 180^{o} cone and represents the outer part of a blade disc, has also been studied by others. The condensate was found to support wave regimes and to drain along the surface of the disc as a continuous film.

The main purpose of the present work is to make an experimental study of the condensation of steam on rotating cones with apex angles of 10^{o}, 20^{o} and 60^{o}. Film drainage on this range of cones was primarily along the surface. However at high speeds of rotation on the 10^{o} and 20^{o} cones drainage was assisted by the formation and detachment of drops.

The experimental results for the cylinders and for discs were compared with a laminar model of the condensation process on cylinders and discs respectively. In order to make a similar comparison for the experimental results from cones, a theory was developed for the condensation of steam in a laminar film on the surface of a cone rotating about a vertical axis. The film was assumed to drain along the generator of the cone under the influence of both gravitational and centrifugal accelerations.

The theory is shown to link the previous theories which consider drainage by either gravitational or centrifugal accelerations alone.

The laminar theory was extended to cover the drainage of condensate along the surface of axisymmetrical bodies with generators formed by smooth curves. Such an extension enables the experimental heat transfer data for cones to be applied to turbine rotors.

2.0 PREVIOUS WORK

2.0 Introduction.

The condensation of vapours has long been of interest to engineers, not only because of its importance in the overall performance of heat engines, but also because of its importance in the chemical manufacturing processes.

Over the years of this century the general techniques of theoretical analysis and of modelling have improved with the aid of modern computing facilities. These techniques have been applied to develop theoretical models of the condensation process for a variety of fluid flow conditions and for a variety of fluids. The latest methods of modelling the process are the result of several separate advances in technique. This section will review and discuss the basic advances which have been made.

Because the condensation process has been of such practical interest, a considerable amount of experimental work has been done to verify the mathematical models and to fill in gaps where the models are inaccurate. Only the general findings of this experimental work can be reported here, because of a lack of space.

2.1 Types of condensation.

Condensation may be defined for engineering purposes as the removal of energy from a vapour in such a way that a change of phase occurs in which the vapour is converted to liquid. In the steady state, condensation usually occurs when the vapour is reduced to a temperature below that of saturation at the given

pressure of the vapour. There are exceptions to this where under certain conditions the vapour can become sub-cooled and remain in a quasi-stable state without changing phase. If the vapour is cooled uniformly, as it might be by expansion in the last stages of a steam turbine, droplet nucleation will occur throughout the vapour system. If the vapour is cooled locally, as in a condenser, the phase change is confined to the locality of the energy sink, i.e. to the condenser tubes. The scope of this review is limited to the latter kinds of condensation.

The liquid deposited on the surface of the energy sink has been observed to take on one, or possibly a combination of two, basically different forms. These two different forms or types of condensation are:-

(i) filmwise condensation, and

(ii) dropwise condensation.

These two forms are analogous to film and nucleate boiling respectively. But whereas film boiling is desirable and not easily maintained, film condensation is more usually encountered in practice and is the least effective form of condensation.

The type of condensation that occurs on a given surface depends to a large extent on the cleanliness of the surface. Most experimentalists have found that clean vapours, whether or not they contain non-condensable gases, will form a complete film on chemically clean metal surfaces, whether the surfaces are rough or polished. This rule has been found to be true for steam condensing on the common metals used in commercial condensers. The term 'clean vapours' means free from contaminants such as oil vapour. Erb and Thelen (1)* gave a

---

* References given in section 9.

quantitative description of the surface characteristics necessary for particular types of condensation in terms of the number of free bonds at the surface. If a relatively large number of free bonds are available, sufficient molecules of liquid are adsorbed to form the base for a complete film. This type of surface could be called wettable and would favour filmwise condensation. If relatively few free bonds exist the surface density of adsorbed molecules is insufficient to form a film and the liquid is weakly bonded to the surface at what are termed nucleation sites. This type of surface could be termed non-wettable. Surface tension forces acting on the liquid at the nucleation sites forms the liquid into drops. The angle of contact made between the drop and the metal surface has been used as a measure of the wettability of the surface; a contact angle of 0^{o} signifies perfectly non-wettable surfaces and a contact angle of 180^{o} signifies perfectly wettable surfaces.

No justice could be done to the previous studies of dropwise condensation by a shortened account, so the detailed review of previous work will concentrate only on filmwise condensation which is the direct concern of the present work. However, one can direct the reader, who is making a literature survey in the field of dropwise condensation, to several important papers. Extensive lists of work published prior to 1965 are given in two papers by Tanner, Potter, Pope and West (2, 3) who report their own experimental findings on the effects of heat flux, of vapour velocity, of non-condensable gas concentration and of surface chemistry on dropwise condensation. Later works of importance are those of Umur and Griffith (4) who investigated the

existance of thin liquid layers between drops:
of McCormick and Westwater (5) who investigated the density of nucleation sites;
of Le Fevre and Rose (6) and Rose (7) on the theory of dropwise condensation;
and to the work of Mikic (8) who considered the effects of the thermal properties of the condensing surface of dropwise condensation.

2.2 Filmwise condensation on stationary surfaces.

Filmwise condensation occurs only on wettable surfaces. Condensate deposited on the surface during the initial transfer of energy from the vapour to the surface forms a complete liquid film. Further energy transfer from the vapour to the surface has to be transported across the film, which acts as a barrier. Once the film is established, the energy transfer, which is a function of the condensation rate, becomes directly related to and limited by the drainage rate.

In 1916 Nusselt (9) produced a very simple model for film condensation. Nusselt considered the problem in two parts. First he considered the drainage of a film of liquid under the action of an acceleration field, and derived an expression for the velocity distribution across the film by making a balance between the body forces and the viscous forces in the direction of flow. The thickness of the film was assumed to be maintained constant and the direction of drainage of the film was assumed to be parallel to the solid surface. In the second part, the rate of energy transfer across the film from the vapour to the

solid surface was related to the condensation rate through the specific enthalpy of the condensation. The two parts were combined to obtain equations for film thickness and for heat transfer coefficient, by equating the rate of drainage to the rate of condensation. To simplify the mathematics of the analysis, Nusselt made the following assumptions about the film of condensate:-

(i) The film was in laminar flow along a smooth isothermal surface under the action of an acceleration field, and that the thickness of the film was small compared with the radius of curvature of the surface.

(ii) Energy liberated by condensation at the liquid-vapour interface was transported across the film only by conduction.

(iii) Fluid accelerations and inertia effects were neglected.

(iv) The temperature dependent physical properties of the film were evaluated at the mean film temperature.

(v) The temperature at the liquid vapour interface was at the saturation temperature of the vapour.

(vi) Under-cooling of the film was neglected.

(vii) The vapour was relatively stationary with respect to the surface and did not exert drag at the liquid-vapour interface.

(viii) The vapour was free from non-condensable gases.

More recent theoretical models of the condensation process have relaxed these restrictions.

In a review of Nusselt's published work by Monrad and Badger (10) we are told that Nusselt subsequently considered the condensation process under five different sets of conditions.

(i) Vapour condensing on a smooth inclined surface with negligible vapour velocity.

(ii) Vapour condensing on the outside of a horizontal tube with negligible vapour velocity.

(iii) Vapour condensing on an inclined plane with appreciable vapour velocity.

(iv) Superheated vapour condensing on any surface.

(v) Impure vapour condensing on any surface.

Nusselt derived the following equations for condensation on a vertical plate with negligible vapour velocity.

The film thickness was expressed as

$$\delta = 1.414 \left[\frac{k \mu \theta x}{l \rho^2 g} \right]^{\frac{1}{4}} \quad ; \quad \delta \propto x^{\frac{1}{4}}$$

and the heat transfer coefficient was expressed as $h = \frac{k}{\delta}$

giving $$h = 0.707 \left[\frac{k^3 l \rho^2 g}{\mu \theta x} \right]^{\frac{1}{4}} \quad ; \quad h \propto x^{-\frac{1}{4}}$$

Similar equations were developed for inclined planes, and horizontal tubes; the main differences being in the numerical constant, in the length parameter x or in the component of the acceleration field.

Monrad and Badger compared the Nusselt heat transfer coefficient for condensation on the outer surface of a horizontal tube with data for condensing steam, benzene and carbon

tetrachloride, and found reasonable agreement when the vapour to surface temperature difference was small. More recently, Hampson and Ozisik (11) have compared the mean experimental heat transfer coefficient for steam condensing on inclined plates with the Nusselt value. The experimental heat transfer coefficients were shown to be between 1.18 and 1.28 times the Nusselt values for all angles of inclination away from the horizontal. However, experimental heat transfer coefficients for condensation on the underside of a horizontal plate were shown to be 1.5 times the Nusselt values. This increase in the experimental heat transfer coefficients at angles close to the horizontal was attributed to the formation and detachment of pendant drops from the surface of the film.

The Nusselt theory was extended by Bromley (12) who considered the effects of undercooling the film of condensate and by Rohsenow (13) who considered the effects of cross flow in the film to determine the true temperature distribution. After some discussion, Bromley and Rohsenow agreed that the effects of undercooling, and of cross flow or energy convection, could be accounted for by replacing the specific enthalpy l used in Nusselt's equations, by the term $(l + 0.68\ c\ \theta)$.

Sparrow and Gregg applied the mathematical techniques of boundary layer theory to the condensation of vapours in laminar films on vertical plates (14) and on the outer surfaces of horizontal tubes (15). This study took into account the full effects of energy convection and of inertia. Similarity transforms were used to reduce the partial differential equations for the

conservation of mass, momentum, and energy to ordinary differential equations which were then solved numerically. Solutions were obtained for values of the parameter $\frac{c\theta}{l}$ between 0 and 2 and for Prandtl numbers between 0.003 and 100. The effects of inertia were shown to be negligible for fluids with Prandtl numbers greater than ten. The factor $(1 + 0.68\ c\ \theta)$ given by Rohsenow was verified and found to predict heat transfer coefficients of $1.05\ h_{S+G}$ at $\frac{c\theta}{l} = 2$ with Prandtl numbers of unity. Inertia effects were shown to be much more significant for liquid metals where the Prandtl numbers are less than unity. With a Prandtl number of 0.003 and a value of $\frac{c\theta}{l} = 0.1$, the Nusselt model, which neglects both inertia and convection, predicts heat transfer coefficients of $1.75\ h_{S+G}$

Chen (16) and Koh, Sparrow and Hartnett (17) published studies of the influence of shear stresses at the liquid-vapour interface due to induced vapour velocity. Both studies were for laminar films on vertical surfaces and both utilised two-phase boundary layer theory. Chen used the equations of momentum and of energy in a modified integral form and provided a solution using a perturbation method for the condition of $\mu\rho_{vapour} \ll \mu\rho_{liquid}$. Koh et al used the partial differential form of the boundary layer equations and provided a solution through the use of similarity transforms.

Both studies showed that the effect of induced vapour velocity increased film thickness and reduced the heat transfer coefficient by causing a negative velocity gradient at the liquid-vapour interface. The reduction in heat transfer coefficient at $\frac{c\theta}{l} = 2.0$ was negligible at Prandtl numbers

greater than 10, but the reduction reached 0.91 of the value without shear at a Prandtl number of unity. In the liquid metal range the adverse effect of interfacial shear is maintained even in thin films; at Prandtl number 0.003 and $\frac{c\theta}{l} = 0.06$, the heat transfer coefficient is reduced to 0.75 of the value without shear. The values without shear are based on heat transfer coefficients given in (14) which account only for the effects of inertia and convection. Chen proferred the following expression to relate his published results with those of Nusselt's simple expression for mean heat transfer coefficient

$$\frac{h_m}{h_{m\ \text{Nusselt}}} = \left[\frac{1 + 0.68\ \frac{c\theta}{l} + 0.02\ \frac{c\theta}{l}\ \gamma}{1 + 0.85\ \gamma - 0.15\ \frac{c\theta}{l}\ \gamma}\right]^{\frac{1}{4}}$$

where γ is a parameter for the effect of inertia and is equal to $\frac{k\theta}{l}$. The expression is accurate to 1% over the range

$\frac{c\theta}{l} \leqslant 2$; $\gamma \leqslant 20$

$Pr > 1$ and $Pr < 0.05$.

Koh et al showed that the heat transfer coefficient remained unchanged by increasing the ratio $\left[\frac{\mu\rho \text{liquid}}{\mu\rho \text{vapour}}\right]^{\frac{1}{2}}$ from 100 to 600.

Chen (18) extended his study of the effects of interfacial shear on heat transfer coefficient, to laminar condensation on single and on multiple horizontal tubes. Interfacial shear was found to effect the heat transfer coefficient for single tubes in the same way as was the case for vertical plates. The model for multiple horizontal tubes arranged in vertical banks appeared to provide a lower limit for the experimental results for condensing freon 11, freon 12, water, n-butane and acetone on banks of 2, 3, 4 and 5 tubes. Chen explained the difference between his results and the experimental results as being due

to the irregular dripping of condensate from higher tubes.

The experimental heat transfer data available for condensates with Prandtl numbers greater than unity are for values of $\frac{c\theta}{l}$ less than 1.0. This data shows fair agreement with the laminar theories of Rohsenow, of Sparrow et al and of Chen, which are almost indistinguishable from one another at $\frac{c\theta}{l}$ less than unity where they all become asymptotic to the Nusselt theory. The modified laminar theories show a significant decrease in heat transfer coefficient from the Nusselt value when the Prandtl number is less than unity. Experimental data for liquid metals appear to be as much as two orders of magnitude below the modified laminar theories. Sukhatme and Rohsenow (19) showed that part of this discrepancy could be explained by the presence of a significant temperature difference between the vapour and the liquid-vapour interface. This temperature difference caused a decrease in the film temperature difference used in the laminar theory, and was attributed to a decrease in vapour pressure in the neighbourhood of the liquid vapour interface. The concentration gradient necessary for the migration of vapour molecules towards the liquid-vapour interface caused the pressure drop. The accommodation coefficient, which is the fraction of the molecules striking the surface and condensing, also effects the rate of heat transfer. Previous attempts to explain the discrepancy between the experimental heat transfer coefficients for liquid metals and the values predicted by the modified laminar theory, suggested that the accommodation coefficient decreased from near unity at low pressures to approximately 0.06 at one

atmosphere. Wilcox and Rohsenow (20) have made precise measurements of the accommodation coefficient for potassium and have found the value to be unity up to pressures of one atmosphere, thus contradicting the dependence on pressure.

Poots and Miles (21) made a theoretical study of the effects of temperature dependent physical properties on the condensation of steam on a plane vertical surface. They compared their results, with those obtained from the constant property models of Nusselt (9) Rohsenow (13) and Chen (16). The comparison yielded a reference temperature at which the fluid properties could be evaluated for inclusion in the constant property models. Using the reference temperature corrects the constant property models for the effects of variable properties. The reference temperature recommended for correcting the Nusselt model was the Drew reference temperature $t_{ref} = t_o + 0.25\,(t_s - t_o)$ where t_o = wall temperature and t_s = steam temperature.

The presence of waves on films of condensate have been recognised as a possible source of the discrepancy between the experimental heat transfer coefficients and those predicted by laminar theory which presupposes a smooth liquid-vapour interface.

Kirkbride (22) made micrometer measurements of the maximum film thickness for oil and water film flowing down vertical tubes. The films at Reynolds numbers $\frac{4\Gamma}{\mu}$ up to 8 were observed to be smooth and the measured maximum film thickness agreed with the theoretical laminar value. At Reynolds numbers between 8 and 1800, the film was observed to support waves. The measured maximum film thicknesses were

found to be larger than the theoretical laminar values by a factor of approximately two at a Reynolds number of 1000.

Friedman and Miller (23) and Dukler and Bergelin (24) published mean film thicknesses for kerosene, toluene and water films flowing down vertical tubes. The mean film thicknesses were found to agree, with the theoretical laminar film thicknesses within the limits of experimental error. The wave profiles were observed to be regular up to Reynolds numbers of 1080 and thereafter to become irregular.

Grimley (25) measured the Reynolds numbers at the onset of waves in several fluids and obtained the correlation

$$\frac{\sigma^3 \rho}{\mu^4 g} = 0.3\ \mathrm{Re}^8$$

Binnie (26) measured the Reynolds number, the wave length and the wave velocity at the onset of waves in water flowing down a plane inclined surface, and found that waves appeared at Reynolds numbers down to 4.

Kapitza (27) made a theoretical study of long sinusoidal waves in thin films of liquid flowing down plane vertical surfaces, and showed that once the plane laminar surface of a film was disturbed, the effects of surface tension became as large as the effects of viscosity. After the onset of waves in the flow, the amplitude of the waves was shown to increase until the energy dissipated by viscosity was balanced by the imparted kinetic and capillary energies. Thus Kapitza argued that the wave regime was more stable than plane laminar flow. Kapitza predicted the onset of waves to occur at

$$\mathrm{Re} = 2.43 \left[\frac{\sigma^3 \rho}{\mu^4 g}\right]^{\frac{1}{11}},$$

and compared the film thicknesses beneath the wave crests and the mean film thicknesses for wave flow with the film thicknesses for plane laminar flow. For a given flow rate the film thickness beneath wave crests was shown to be 1.36 times the value for plane laminar flow and the mean film thickness was shown to be 0.93 times the value for plane laminar flow. Both of these results provided a quantitative explanation for the previous experimental results of Grimley and of Friedmann and Miller.

Brooke Benjamin (28) and Yih (29) examined the stability characteristics of the full Navier-Stokes equations and directed their work towards predicting the stability of liquid films flowing down inclined surfaces. Their work suggested that the films were unstable at all finite Reynolds numbers. By different methods, they both arrived at the same stability criterion which was expressed in terms of the amplification factor A for the most unstable wave as

$$A = \exp\left[0.1737 \frac{\rho^2 x^3 g}{\mu^2} \cdot \frac{\mu^4 g}{\sigma^3 \rho} \cdot \mathrm{Re}^7\right]$$

The above equation shows that the amplification factor is always greater than unity.

Brooke Benjamin argued that waves would remain invisible while the amplification factor remained close to unity and that the wave with the largest rate of growth would be the first to become visible at the onset of waves. The above equation was evaluated at the test conditions used by Binnie, and showed that the amplification factor only became significantly greater than unity at Reynolds numbers greater than four.

Binnie found that waves became visible at Reynolds numbers greater than four.

It is interesting to note that Grimley correlated his experimental results in terms of $\frac{\sigma^2 \rho}{\mu^4 g}$ and Re^8 and that Kapitza predicted the onset of waves in terms of $\frac{\sigma^3 \rho}{\mu^4 g}$ and Re^{11}.

The variables used in the Nusselt equation for mean heat transfer coefficient on plane vertical surfaces may be rearranged as:-

$$\frac{h_m}{k}\left[\frac{\nu^2}{g}\right] = 1.47\left[\frac{4\Gamma}{\mu}\right]^{-\frac{1}{3}}$$

where $\frac{4\Gamma}{\mu}$ is the film Reynolds number.

Kirkbride (22) found that experimental mean heat transfer coefficients for condensing organic vapours with large temperature differences across the film, were greater than those predicted by the above equation when the Reynolds number exceeded 2000. This increase was attributed to turbulence in the film of condensate.

Colburn (30) made use of an empirical correlation between the turbulent friction factor and the heat transfer factor j for turbulent gas flow along large rectangular ducts, to derive the following equation for the mean heat transfer coefficient in the turbulent region of the film of condensate.

$$\frac{h_m}{k}\left[\frac{\nu^2}{g}\right]^{\frac{1}{3}} = \frac{Re}{\frac{22}{Pr^{\frac{1}{3}}}\left[Re^{0.8} - 364\right] + 12,800}$$

This equation predicts that the mean heat transfer coefficient in the turbulent region increases with both Reynolds number and Prandtl number. Colburn assumed that the transition to turbulent flow occurred at a Reynolds number of 1600.

The equation showed reasonable agreement with experimental mean heat transfer coefficients for condensing diphenyle.

Carpenter and Colburn (31) measured the effect of positive vapour velocity on the condensation of steam, methanol, ethanol, toluene and trichlorethylene on the inside of a vertical tube. They recommend the equation:-

$$h_m = 0.065\left[\frac{c\rho kf}{2\mu\rho}\right]^{\frac{1}{2}}_{vapour} \cdot G_m$$

where G_m was the mass flow of vapour/unit time.unit surface area

and f was the fanning friction factor for the vapour. As the vapour velocity increased the heat transfer coefficient became larger at lower Reynolds numbers; a finding which led these workers to conclude that an appreciable vapour velocity causes a transition to turbulent flow at Reynolds number of less than 2000. At a vapour velocity of 80 $\frac{m}{s}$, the transition to turbulence occurred at a Reynolds number of approximately 240.

The Prandtl-Von Karman velocity distribution for a turbulent boundary layer was adopted by Seban (32) to develop a theory for predicting the heat transfer coefficient for pure vapours condensing in turbulent films on vertical surfaces. Seban made the assumption that the eddy thermal diffusivity was equal to the eddy kinematic viscosity and the assumption that the transition to turbulence occurred at a Reynolds number of 1600. The predicted heat transfer coefficients agreed with Colburn over the range of Prandtl number 2 to 5. However

at Prandtl numbers less than approximately 0.05 and at Reynolds numbers below 10^5, the mean heat transfer coefficient in the turbulent region was found to be less than that given by the Nusselt theory extended into the turbulent region. Seban attributed this finding for the low Prandtl numbers to the turbulent transport of energy being negligible in the region immediately after transition. The turbulent transport of energy was shown to make an important contribution to energy transfer at Reynolds numbers greater than 10^5.

Seban's theory was extended by Rohsenow, Weber and Ling (33) to include the effects of positive interfacial shear stress at the liquid-vapour interface. The transition Reynolds number was assumed to decrease from 1600 at a dimensionless interfacial shear stress $\tau^+ = 0$ to a Reynolds number of 57 at $\tau^+ = 9$ and thereafter to remain constant with τ^+ : where $\tau^+ = \frac{\tau_{vapour}}{g(\rho - \rho_{vapour})} \left[\frac{g}{\nu^2}\right]^{1/3}$

Over the range of Prandtl number 0.01 to 10, the heat transfer coefficient was shown to increase with τ^+ at any Reynolds number.

Dukler (34) predicted the mean heat transfer coefficient for turbulent condensation on vertical surfaces with positive interfacial shear by working from the definition of eddy viscosity and utilising the Deissler equation for its variation near a solid boundary. Dukler assumed that the ratio of the eddy thermal diffusivity to the eddy viscosity was unity and obtained expressions for the velocity distribution in terms of the film thickness and the interfacial shear stress.

The results with zero interfacial shear stress agreed well with Nusselt at low Reynolds numbers and with both Colburn's empirical equation and Seban's theoretical equation in the turbulent region at Prandtl numbers greater than unity. An objection to one of the assumptions made by Dukler was raised by Lee (35), who pointed out that Dukler had neglected the molecular conductivity in comparison with the eddy conductivity when deriving the temperature distribution in the film at dimensionless thicknesses of $y^+ = \frac{y}{\nu}\sqrt{\frac{\tau}{\rho}}$ greater than 20. This assumption was acceptable at Prandtl numbers greater than unity but not at Prandtl numbers of less than unity, for here the assumption led to a decrease in the heat transfer coefficient. Thus Dukler's analysis at first sight appeared to account for the low experimental heat transfer coefficients for liquid metals. Lee repeated Dukler's analysis for no interfacial shear while retaining both the molecular and eddy conductivities. The modified results agreed with Dukler's original results at high Prandtl numbers and with Seban's result at low Prandtl numbers. Kunz (36) extended Lee's work to account for interfacial shear stress and the predicted heat transfer coefficients show good agreement with the experimental values measured by Carpenter and Colburn.

The effects of non -uniform gravity fields on film condensation were considered by Dhir and Leinhard (37) in connection with their work on boiling heat transfer. The gravitational constant g which appears in the Nusselt equation for heat transfer coefficient was replaced by an effective gravitational constant g_{eff}. given by:-

$$g_{eff.} = \frac{x\,(g\,R)^{\frac{4}{3}}}{\int_0^x g^{\frac{1}{3}}\,R^{\frac{4}{3}}\,dx}$$

where R is the local radius of the body.

By a different method the author has arrived independently at a similar expression. The author's expression accounts for the effects of gravitational and centrifugal acceleration on the condensation of steam in laminar films on rotating cones and on rotating axisymmetrical bodies. A complete derivation of this expression is given in section 3.

Gerstmann and Griffith (38) observed freon 113 condensing on the underside of horizontal and inclined plane surfaces. A random array of drops formed at the free surface of the film on the underside of the horizontal surface. These drops moved over the free surface of the film as neighbouring drops detached themselves from the film. At a small angle of inclination the drops ran down the surface and became elongated. At angles greater than 5^{o}, the drops became elongated in the direction of flow and formed uniform ridges which were pitched 0.01 m apart. For angles up to 19^{o} drops continued to form and be detached from the ridges. At angles greater than 19^{o}, drop formation ceased and the flow pattern changed to one of jagged roll waves. A theory was developed to predict heat transfer coefficients during drainage by drops and by ridges and this was used to correlate the experimental results. For horizontal surfaces

$$Nu = 0.81\,(Ra)^{0.193} \quad ; 10^{10} > Ra > 10^{8}$$

$$Nu = 0.81\,(Ra)^{0.2} \quad ; 10^{8} > Ra > 10^{6}$$

and for inclined surfaces

$$Nu = 0.9 \frac{Ra^{\frac{1}{6}}}{(1 + 1.1\, Ra^{-\frac{1}{6}})}$$

where $$Nu = \frac{h_m}{k}\left[\frac{\sigma}{g(\rho - \rho_{VAPOUR})\,\mathrm{Sin}\,\alpha}\right]^{\frac{1}{2}}$$

the Rayleigh number $$Ra = \frac{g\,\mathrm{Sin}\alpha\,\rho(\rho - \rho_{VAPOUR})}{k\,\theta\,\mu}\,l\left[\frac{\sigma}{g(\rho - \rho_{VAPOUR})\,\mathrm{Sin}\,\alpha}\right]^{\frac{3}{2}}$$

Small quantities of non-condensable gases such as O_2, N_2 or CO_2 are often present in condensing vapours. The gases may be introduced into the boiler by either the make-up feed water or by the feed water treatment and into a condenser working under vacuum by imperfect sealing. Non-condensable gases in the vapour accumulate at the liquid-vapour interface and have an adverse effect on heat transfer coefficient by creating a gas barrier through which vapour must diffuse before condensing. Non-condensable gases effect dropwise condensation more than they affect filmwise condensation. The presence of an 0.5% concentration of non-condensables in the vapour has been shown to reduce the heat transfer coefficient for filmwise condensation to 0.5 of the value for pure vapour condensing. Increasing the vapour velocity clears the gas barrier from the liquid-vapour interface and leads to an improvement in heat transfer coefficient.

Provan (39) made a survey of the theoretical and the experimental work done prior to 1962 on the effects of non-condensable gases on filmwise condensation. This topic has continued to receive considerable attention at the National Engineering Laboratory where the effects of non-condensable gases on the performance of tube condensers has been investigated (40).

2.3 Methods of improving the condensation process.

Many methods have been proposed for improving the performance of condensers operating under filmwise conditions. Apart from inducing dropwise condensation by introducing contaminants into the vapour, the methods for improving filmwise condensation consist of either creating turbulence in the film or of reducing the thickness of the film.

Frankel and Bankoff (41) made a theoretical study of the filmwise condensation of vapours on a horizontal porous cylinder. The films were assumed to drain from the outer surface of the cylinder by the action of gravitational acceleration and by suction through the porous wall. Increases in heat transfer coefficient of 1.5 times the value without suction were predicted for fluids with Prandtl numbers of 10. In the presence of zero gravitational acceleration, the heat transfer coefficient was predicted to be proportional to the suction velocity.

In 1965, Velkoff and Miller (42) presented experimental heat transfer coefficients for freon 113 condensing in the presence of uniform electrostatic fields created between the condensing surface and an anode grid held in the vapour. The field strength was varied by applying voltages up to 50 kV and currents up to 14 μA. Applying the electrostatic field induced waves in the film and caused jets of condensate to be emitted from the film. Experimental heat transfer coefficients 2.5 times the value without the field were measured for these low electrical power inputs. Recently Holmes and Chapman (43) published experimental heat transfer coefficients for

freon 114 condensing in the presence of alternating electric fields. The fields were created between the condensing surface and a plate held in the vapour by the application of voltages up to 60 kV at 60 Hz. Experimental heat transfer coefficients with the field applied were found to be as much as 10 times the value without the field.

Considerable effort has been directed towards improving the heat transfer coefficients for filmwise condensation by increasing the acceleration field to improve film drainage. The centrifugal acceleration field created on a rotating condensing surface can lead to sustained improvements in film drainage. For mechanical reasons, the types of surfaces suitable for rotation are usually axisymmetrical and may take the form of either discs, cylinders or cones. However, any surface can be used if provision is made to balance the rotating parts.

2.4 Filmwise condensation on rotating surfaces.

2.4.1. Introduction.

Broadly speaking, the experimental and theoretical studies of the heat transfer between rotating surfaces and either single or two-phase fluids have been undertaken for two reasons. The first reason is to gain knowledge of the beneficial effects of rotation on heat transfer with a view to improving the performance of evaporators and condensers. The second reason for the study is to enable calculations to be made for the heat transfer between the working fluid

and the rotating parts of power producing machines.

The present work is undertaken for the second reason and is part of a wider investigation, which has been undertaken by Hoyle and his colleagues, of the transient thermal stresses on rotating axisymmetrical bodies. In particular, the investigation has been directed towards predicting the transient thermal stresses in steam turbine rotors during cold starting and during manoeuvring. The problems involved during these operations have been given by Terrel (44), by Hall and Britten (45) and more recently by Moore (46). Methods for calculating the rotor temperatures during the cold starting of steam turbines have been given by Chow and Hoyle (47) and Hoyle and Mahabir (48).

As shown in the sketch below, any axisymmetrical body can be simulated by a combination of truncated cones with various apex angles α.

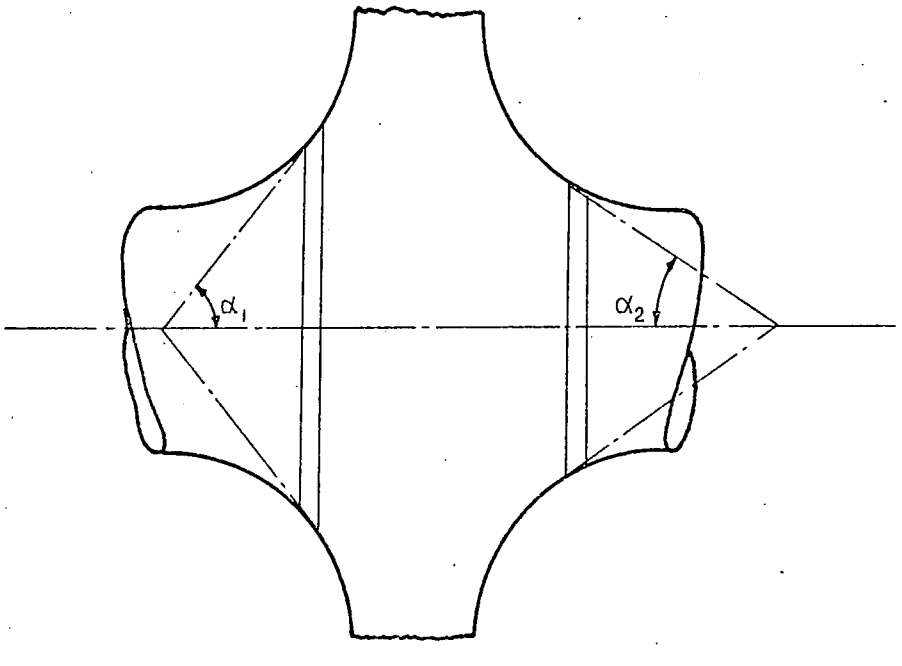

An investigation of the transient thermal stresses in a rotating axisymmetrical body such as the turbine rotor, requires the study of the heat and mass transfer to the outer surface of cones with many apex angles. Such a study was undertaken by Hoyle and his colleagues and their experimental and theoretical work on discs, cylinders and cones is reviewed, together with the work of others, in the following sections.

2.4.2

Filmwise condensation on rotating discs.

An important advance in the theoretical understanding of the filmwise condensation process on rotating surfaces was made in 1959 by Sparrow and Gregg (49). They used the mathematical techniques of boundary layer theory to study the condensation of pure vapour in a laminar film on the surface of a rotating disc. The disc was assumed to rotate with its axis of symmetry vertical and the film of condensate was assumed to be drained by centrifugal acceleration acting radially over the surface of the disc. Gravitational acceleration was neglected because it acted perpendicular to the surface and did not affect film drainage.

The problem of condensation on a rotating disc lent itself to a solution of the Navier Stokes and energy equations using boundary layer approximations and thus enabled the full effects of energy convection and of inertia to be taken into

account. Similarity transforms were used to reduce the partial differential equations which express the conservation of mass, momentum and energy to ordinary differential equations. An overall energy balance was made for the film and the boundary conditions at the surface of the disc and at the liquid-vapour interface were introduced to enable a simultaneous solution of the conservation equations to be made. This solution for the conservation equations was obtained numerically for the range of Prandtl numbers 0.003 to 100 and for the range of values of $\frac{c\theta}{1}$ 0.0001 to 1.0.

The results showed that for a given angular velocity ω and a given film temperature difference, the heat flux and heat transfer coefficient were uniform over the surface of the disc. This finding confirmed one of Sparrow and Gregg's initial assumptions; that the temperature distribution across the film depended only on the perpendicular distance from the surface of the disc and not on the radius of the disc. This assumption implied that the thickness of the film of condensate was uniform over the entire surface of the disc. The heat flux and the heat transfer coefficient where shown to increase with $\omega^{\frac{1}{2}}$.

Sparrow and Gregg's heat transfer results are shown below.

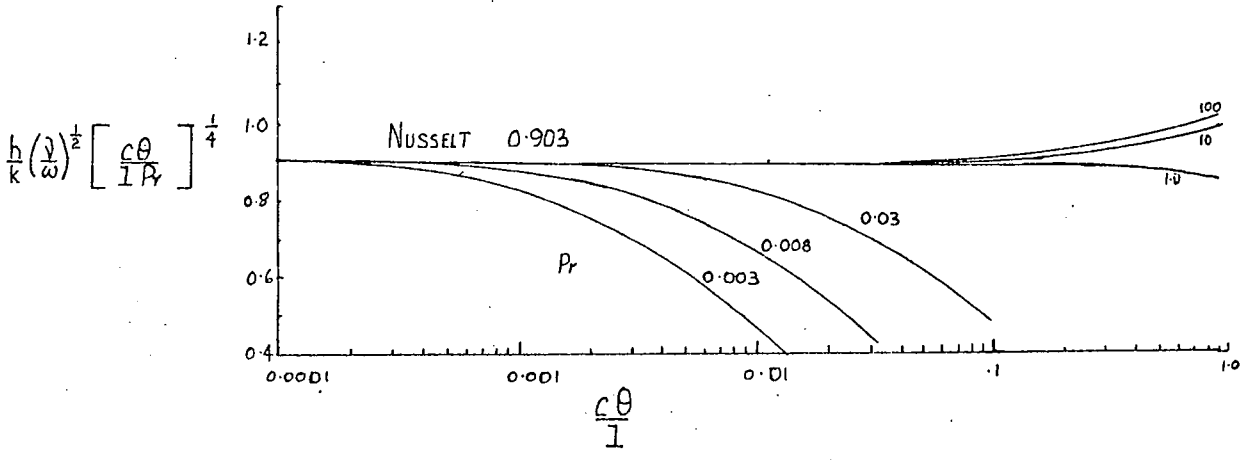

At small values of $\frac{c\theta}{l}$, which imply small film thicknesses, and over the range of Prandtl number 1 to 100, the heat transfer coefficient was expressed by

$$\frac{h}{k}\left[\frac{\nu}{\omega}\right]^{\frac{1}{2}} = 0.904\left[\frac{Pr}{c\theta/l}\right]^{\frac{1}{4}}$$

This equation was shown to correspond exactly to the solution of the conservation equations when the effects of energy convection and of inertia were neglected. Thus the film could be assumed to drain radially over the surface of the disc and be described by a simple analysis of the Nusselt type.

At $\frac{c\theta}{l}$ greater than 0.1, the effects of energy convection, which improve the heat transfer coefficient, tend to dominate when the Prandtl number is greater than unity. At a Prandtl number of unity, the effects of inertia, which reduce the heat transfer coefficient, tend to dominate the condensation process on the rotating disc. The effects of inertia continue to dominate the heat transfer coefficient for the rotating disc as the Prandtl number becomes less than unity. Also the effects of inertia also become important at values of $\frac{c\theta}{l}$ less than 0.1. It is interesting to note that at Prandtl numbers of unity the effects of convection dominates the condensation process on stationary vertical surfaces and on stationary horizontal cylinders.

Over the full range of both Prandtl number and $\frac{c\theta}{l}$, the temperature distributions across the film on the rotating disc were shown to have little departure from linearity. This finding supported Nusselt's assumption of a linear temperature

distribution across thin laminar films.

Later in 1959, Nandapurka and Beatty (50) published experimental heat transfer coefficients for methanol, ethanol and freon 113 condensing at atmospheric pressure on a rotating disc. The disc had a diameter of 0.127 m and rotated at speeds between 400 and 2400 rev/min. with the axis of symmetry vertical.

Experimental heat transfer coefficients were obtained at values of $\frac{c\theta}{l}$ less than 0.1 and were compared with the theoretical prediction given by Sparrow and Gregg, namely

$$\frac{h}{k}\left[\frac{\nu}{\omega}\right]^{\frac{1}{2}} = 0.904\left[\frac{Pr}{c\theta/l}\right]^{\frac{1}{4}}$$

The experimental heat transfer coefficients were consistantly about 0.75 of the value given by the above equation. Also the experimental heat transfer coefficients were found to increase in proportion to $\omega^{0.45}$.

Dye was introduced to the film through a No. 20 hyperdermic needle to detect the direction of drainage. The streamline of dye followed a radial path near the centre of the disc. Near the outer edge of the disc, the dye followed a path which was slightly curved backwards from the direction of rotation. The dye also revealed the presence of ripples moving over the surface of the film in the direction of drainage. Nandapurka and Beatty attributed the low experimental heat transfer coefficients to the effects of vapour drag acting on the waves and causing a reduction in drainage. In the discussion on this paper, the low experimental results were attributed to errors in temperature measurement caused by

conduction along the thermocouple leads which were taken through the thickness of the disc directly from the hot junction.

Sparrow and Gregg (51) extended their previous theoretical study of the condensation process on rotating discs to include the effects of induced shear stresses at the liquid-vapour interface of a laminar film of condensate. Interfacial shear was found to cause reductions in the heat transfer coefficient on rotating surfaces in much the same way as it did on stationary surfaces (16, 17, 18). The effects of induced shear stress on a smooth film at the experimental temperatures reported by Nandapurka and Beatty was shown to reduce the heat transfer coefficient to 0.9936 of the value without interfacial shear. Since this theoretical study did not take into account the effect of shear stress when waves were present on the film of condensate, the discrepancy between experiment and theory was not resolved.

Measurements of the maximum thickness of water films flowing outwards over the horizontal surface of a rotating disc were reported by Espig and Hoyle (52). The measurements were made with a micrometer for Reynolds numbers between 10 and 600, and the results were correlated by

$$\delta \left[\frac{D\omega^2}{2\nu^2} \right]^{\frac{1}{2}} = 1.3 \left[\frac{4\Gamma}{\mu} \right]^{\frac{1}{3}} \quad ; \quad \Gamma = \frac{\text{mass flow rate of water}}{\pi D}$$

The correlation for the maximum film thicknesses on the rotating disc agreed with the correlation given by Kirkbride (22) for water films on stationary vertical surfaces, and with the prediction of maximum film thickness given by Kapitza (27) for long waves on vertical surfaces.

Bromley, Humphreys and Murray (53) studied both the evaporation of liquid films and the condensation of vapours on rotating discs. Discs with various combinations of smooth and radially grooved surfaces were used. A series of experiments were undertaken to measure the overall heat transfer coefficient between steam condensing on one side of the rotating disc and vapour evaporating from a film of liquid on the second side of the rotating disc. The experimental overall heat transfer coefficient for the disc grooved on both sides was found to be 1.13 times the experimental value for the disc with smooth surfaces on both sides.

In 1968 Espig and Hoyle (54) published experimental heat transfer coefficients for steam condensing on a smooth rotating disc. In connection with their work on transient thermal stresses in rotating axisymmetrical bodies, the disc could be considered as the cone with an apex angle of 180°. The disc, which was made of copper, had a diameter of 0.25 m, and could be rotated at speeds up to 2500 rev/min with the axis of symmetry horizontal. Thermocouples were arranged in isothermal regions on the steam and cooling water sides of the disc. The thermocouple leads were taken from the rotating part of the apparatus to the potentiometer through mercury slip rings. A resistance network analogue was used to represent part of the cross-section of the disc between radii 0.03 m and 0.125 m. Temperature readings taken at the inner and the outer surfaces of the disc were used in the resistance network to calculate the temperature gradient in the disc at the condensing surface. This temperature gradient was used to calculate the

heat flux from the condensate to the outer surface of the disc.

Espig and Hoyle also made a thecretical study of the condensation process but used the integral form of the equations for the conservation of mass, momentum and energy. For thin laminar films of condensate their analysis also gave the equation

$$h = 0.903 \left[\frac{k^3 \rho^2 \omega^2}{\theta \mu}\right]^{\frac{1}{4}}$$

The experimental heat transfer coefficients were found to be about 1.5 to 2.0 times the value predicted by the above equation, and to be related to the above equation by the expression

$$\frac{h_{exp}}{h} = 113\, N^{-0.415}\, \theta^{-0.6}$$

where N was the rotational speed in rev/min
and θ was the steam to surface temperature difference in ^{o}F.
Espig and Hoyle argued that the kind of waves observed on a film of water draining from the surface of a rotating disc (52) would also be present on a film of condensate draining from a rotating disc. The wave motion on the film of condensate was proposed as the reason for the experimental heat transfer coefficients being greater than those predicted by the laminar theory.

2.4.3 Filmwise condensation on rotating cylinders.

In 1953 Yeh (55) made an experimental study of the effects of steam pressure and of rotation on the heat transfer

coefficient for filmwise condensation on a rotating cylinder. Yeh worked with Hoyle on the transient thermal stress problem. In connection with this problem, the cylinder was considered to be a cone with an apex angle of 0^{o}. The cylinder had a diameter of 0.0254 m and rotated with the axis of symmetry horizontal at speeds up to 2000 rev/min. Heat transfer coefficients were calculated from temperature readings taken at the inner and outer surfaces of the cylinder. Temperatures were measured with thermocouples whose leads were taken from the rotor through slip rings. The experimental results are shown plotted in terms of the Nusselt number $\frac{h_m D}{2K}$ and the Weber number $\frac{D\rho\omega^2}{4g\sigma}$ on the graph below. Yeh found that the heat transfer coefficient decreased slightly with increases in speed up to 30 rev/min, but an increase in heat transfer coefficient was observed with further increases in speed up to 1500 rev/min. This increase was attributed to the formation and detachment of drops from the surface of the film of condensate. At speeds of over 1500 rev/min, the heat transfer coefficient was observed to decrease to almost the stationary value. This decrease was attributed to the effects of vapour drag acting on the drops and reducing the rate of drainage. Some doubt has been cast on Yeh's results because a faulty mechanical seal was suspected of leaking air and oil into the steam space.

In order to clarify Yeh's findings, Singer and Preckshot (56) also studied the condensation of steam on an 0.0254 m diameter horizontal cylinder rotating at speeds up to 6,500 rev/min. They calculated the mean experimental steam-side heat transfer

coefficient h_{mo} indirectly from the equation

$$\frac{1}{U} = \frac{1}{h_{mo}} + \frac{x}{k} + \frac{1}{h_{mi}}$$

The overall heat transfer coefficient U was based on the measured mass flow rate of condensate per unit surface area of the cylinder and on the difference between the steam temperature and the mean cooling water temperature. These temperatures were measured by stationary thermocouples placed in the steam space and in the cooling water. The water-side heat transfer coefficient was obtained from data presented by Kuo et al (57).

The experimental heat transfer coefficient was correlated in terms of a Nusselt number $Nu = \frac{h_m D}{2k}$ and a Weber number

$$We = \frac{D^3 \rho \omega^2}{4g\sigma}$$

Three distinct regimes of condensate drainage were reported and these are illustrated below by the sketches (a, b, c, d and e)

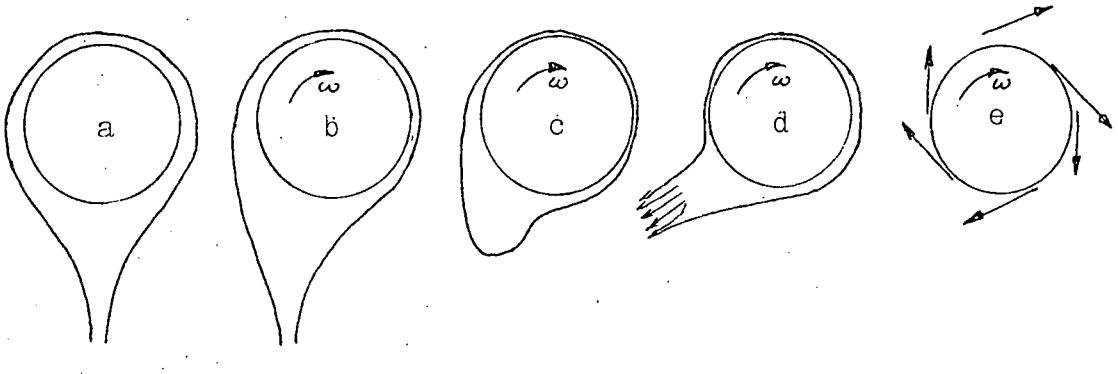

At zero speed, the condensate drained from the underside of the cylinder as shown in (a). The position at which the film drained from the cylinder moved in the direction of rotation with increasing speed while $\frac{D\omega^2}{2g} < 1$ (b). The film

thickness increased and caused a reduction in mean heat transfer coefficient to 0.8 of the stationary value. At moderate speeds between $500 < We < 1800$ the film remained continuous and supported circumferential waves (c). Drainage occurred at the wave crests (c, d) due to the actions of centrifugal acceleration and gravitational acceleration. The heat transfer coefficient increased to three times the stationary value over this range of Weber number. At a Weber number of approximately 1800, the circumferential wave regime degenerated to one where drops were drawn from the film. The drops were detached from all points around the circumference of the film by the action of the centrifugal acceleration (e). Over the range $1800 < We < 34{,}000$ the heat transfer coefficient was found to decrease, almost to the stationary value. This decline in heat transfer coefficient was also observed by Yeh and was attributed to a significant interfacial drag between the drops and the steam. Singer and Preckshot argued that steam drag acted on the drops in the direction opposite to the direction of drop detachment and reduced the drainage rate by delaying detachment.

Further experimental work on the heat transfer from steam condensing on rotating cylinders was undertaken by Hoyle and Matthews (58) who studied the effect of changes in cylinder diameter and of rotation on the heat transfer coefficient. They used cylinders of 0.10 m, 0.2 m and 0.254 m diameter rotating at speeds up to 1500 rev/min with the axis of symmetry horizontal. The mean heat transfer coefficient was calculated from temperature readings taken from rotating

thermocouples at the inner and outer surfaces of the cylinders. The heat transfer results for these three cylinders were compared with the data produced by Yeh and by Singer and Preckshot.

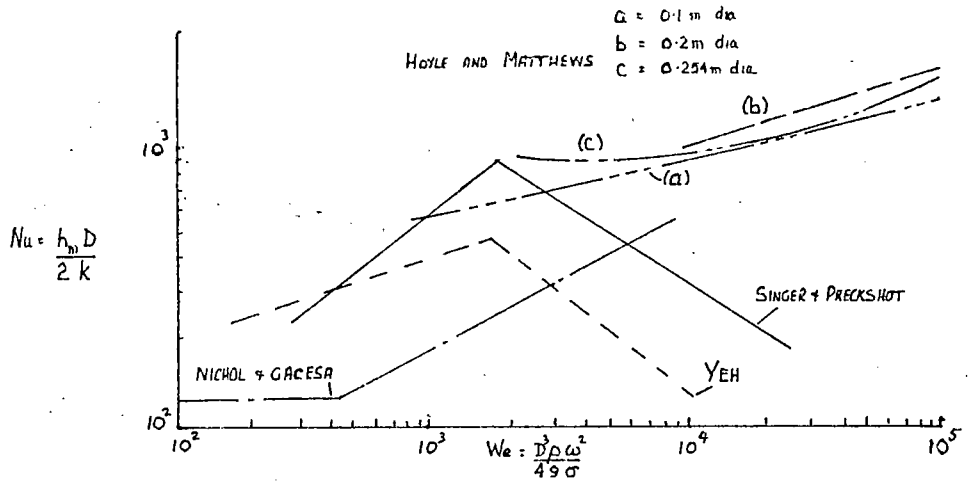

Hoyle and Matthews did not observe any decrease in heat transfer coefficient when the Weber number increased beyond 1800; this being contrary to the work of Yeh, and of Singer and Preckshot. No reason was offered for this variance. Hoyle and Matthews correlated mean transfer coefficients for their three rotating cylinders by using a simple modification of the Nusselt equation for stationary horizontal cylinders:-

$$h_m = 0.72 \left[\frac{k^3 \rho^2 g}{\mu \theta D} \right]^{\frac{1}{4}}$$

The constant 0.72 was replaced by a variable B which accounted for the effects of rotation. An expression for

$$B = \left[1.9 - \frac{0.9}{1.095^{\frac{D\omega^2}{2g}}} \right] \frac{1.5}{\left(D\sqrt{\frac{\rho}{\sigma}}\right)^{0.19}}$$

was derived from the experimental results.

The continued increase in heat transfer coefficient for Weber numbers greater than 1800 found by Hoyle and Matthews

was supported by the findings of Nichol and Gacesa (59) who investigated the heat transfer coefficients for steam condensing on a vertical cylinder 0.0254 m diameter, which rotated at speeds up to 2700 rev/min. The Nusselt number was found to remain constant at 110 for Weber number up to 430 and thereafter to increase according to $Nu = 6.13\ We^{0.496}$.

In a continuation of their study of the condensation process on rotating cylinders, Hoyle and Matthews (60) used photographs of the condensing surface taken during tests, together with the experimental heat transfer results, to demonstrate that the film on the 0.1 m diameter cylinder remained laminar during the formation of protrusions. By 'protrusions' the authors meant drops in their early stages of formation on the film. On the assumption that the area of condensing surface taken by the photograph was representative of the remaining surface, the number of protrusions, or drops, per unit area were counted and the drop diameter was measured. The heat flux per drop and hence the mass flow rate of condensate into each drop was calculated, together with the circumference of the drop. Reynolds numbers for the flow from the film into the drop were calculated from

$$Re = \frac{4\Gamma}{\mu}$$

where Γ = mass flow rate per drop/circumference of drop. These calculations were made for a range of rotational speeds and showed that the Reynolds number decreased from 17 at $\frac{D\omega^2}{2g} = 12$

to approximately 5 at $\frac{D\omega^2}{2g} = 160$. Thus the Reynolds number remained well below the value of 2000 at the transition to turbulence. Increases in $\frac{D\omega^2}{2g}$ were shown to cause a reduction in the size of the drops leaving the film and to increase the number of drops per unit area. These results taken together showed that the percentage area of the film covered by drops reached a maximum of 18% at $\frac{D\omega^2}{2g} = 20$.

2.4.4. Filmwise condensation on rotating cones.

Practical use has been made of rotating conical heat transfer elements for the evaporation of liquid films during food processing and for both evaporation and condensation during the desalination of sea water.

Hickman (61) in 1957 described and gave performance data for a centrifugal boiler and compression still in which the evaporating liquid flowed in a thin film along the inner surface of a rotating inverted cone. Vapour from the inner surface of the cone was collected and compressed before being released to condense on the outer surface of the cone. The pressure rise was only 0.025 bar. Energy liberated at the outer surface of the cone during condensation was transferred by conduction to the inner surface to maintain the evaporation process.

The evaporation and condensation process described by Hickman was given theoretical consideration by Bromley (62). Assuming that the movement of the evaporating film and of the condensate film was due only to centrifugal acceleration, Bromley replaced the gravitational term in the Nusselt equation

for the velocity profile through a thin laminar film with the term $\frac{D\omega^2}{2}$, to obtain an equation for the film thickness in terms of the mass flow rate. This equation for film thickness enabled Bromley to derive an equation for the overall heat transfer coefficient between the vapour condensing on the outer surface of the cone and the vapour evaporating from the film on the inner surface of the cone. Agreement between the theory and the scatter of the experimental overall heat transfer coefficients was reasonable. The theoretical predictions were between 0.6 and 1.43 times the data; with the greatest deviation between theory and experiment occurring at small values of temperature difference and at low flow rates.

More recently, Bruin (63) has given radial, tangential and meridional velocity profiles for laminar films of liquid moving along the inner surface of an inverted rotating cone.

Some of the theoretical work on the heat transfer from rotating discs and cones to single phase fluids made a significant contribution towards the development of a theory for condensation on rotating cones. Wu (64) made a theoretical study of the laminar motion of an incompressible viscous fluid induced by a rotating cone. The Karman-Cochran solution of the Navier-Stokes equations for the boundary layer induced by a rotating infinite disc was adapted for the boundary layer induced by a rotating cone.

Heat transfer from the rotating infinite disc to the boundary layer was studied by Millsaps and Pohlhausen (65) and by Sparrow and Gregg (66), but their results were valid

only where the fluid properties remained constant, and where the temperature differences and speeds of rotation remained small. The technique used by Millsaps et al was adapted by Tien (67) to study the heat transfer from the rotating cone to the induced boundary layer. The results were valid for cones with apex angles large enough to sustain the character of the boundary layer.

Sparrow and Hartnett (68) used the findings of Wu and of Tien to modify the theory for condensation on rotating discs (49) to include condensation on rotating cones. The film was considered to drain along the surface of the cone under the influence of the component of centrifugal acceleration resolved parallel to the surface. In effect, the change from disc to cone merely required that the angular velocity ω in the dimensionless variables for the disc should be multiplied by $\sin\alpha$. Thus the solution of the conservation and energy equations for condensation on the rotating cone was obtained by the method used for rotating discs. The component of the gravitational acceleration resolved parallel to the surface could not be included in the dimensionless variables, therefore the modified theory was valid only where the centrifugal acceleration dominated drainage.

Comparing the heat transfer coefficients for rotating discs and for rotating cones gave

$$\frac{h_{cone}}{h_{disc}} = (\mathrm{Sin}\,\alpha)^{\frac{1}{2}}$$

This equation which applies to laminar flow, predicts that the heat transfer coefficient for the cone is always less than that

for a disc. The presence of waves may alter the above relationship.

Heat transfer coefficients for steam condensing on a rotating 60^{o} cone were given by Howe and Hoyle (69). The experimental results were obtained on the apparatus which is described in detail in section 4 of this thesis; where it will be found that the 60^{o} cone has a base diameter D = 0.61 m and is mounted with the axis of symmetry vertical. Experimental results were taken with the cone rotating at speeds between zero and 700 rev/min under steam pressures between 1 and 8 bar. The experimental heat transfer coefficients were correlated in terms of the Nusselt number $Nu = \frac{hD}{k}$, the ratio of accelerations $\frac{D\omega^2}{2g}$ and the non-dimensional group $\frac{D\sigma\rho}{\mu^2}$.

The non-dimensional group $\frac{D\sigma\rho}{\mu^2}$ included the fluid properties relevant both to the motion of the film and to the character of the surface of the film. The fluid properties were evaluated at the Drew reference temperature $t_f = t_o + .25(t_s - t_o)$. Between the largest and the smallest values of t_f, the viscosity increased by a factor of 1.4, the surface tension increased by a factor of 1.2 and the density increased by a factor of 1.05. Thus it was argued that by increasing t_f the body force remained substantially unchanged, while the freedom of movement of the film increased. Therefore at a constant $\frac{D\omega^2}{2g}$ an increase in t_f improves the drainage rate and so reduces the equilibrium film thickness. Ideally the diameter D in the group $\frac{D\sigma\rho}{\mu^2}$ should be replaced by the local film thickness δ, but as measurements of this were not available, D was used to relate the local film

thickness to the distance from the starting point of condensation near the apex of the cone.

The Nusselt number was shown to increase with $\frac{D\sigma\rho}{\mu^2}$ over the range of $\frac{D\omega^2}{2g}$ zero to 77.

At $\frac{D\omega^2}{2g}$ = zero, the Nusselt number was a function of $\left[\frac{D\sigma\rho}{\mu^2}\right]^{\frac{3}{4}}$

At $\frac{D\omega^2}{2g} > 8$, the Nusselt number was a function of $\left[\frac{D\sigma\rho}{\mu^2}\right]^{1.0}$

This change in the dependence of Nusselt number on $\frac{D\sigma\rho}{\mu^2}$ was explained in terms of the wave regimes, which changed pattern with increases in $\frac{D\omega^2}{2g}$.

The behaviour of the film of condensate on the surface of the rotating 60° cone was studied by Robson (70) who used still photography to observe the formation and drainage of the film. Film drainage was found to occur only in a direction parallel to the surface of the cone over the speed range 100 to 1400 rev/min. The patterns of the waves on the film were found to be dependent on $\frac{D\omega^2}{2g}$. Irregular patterns of roll-waves were observed on the film at speeds between 100 and 400 rev/min. Over this range of speeds, the wave length decreased and the number of waves per unit surface area increased with speed. At about 400 rev/min, the roll-waves degenerated to rivulets or streaks of fluid which continued to exist up to 1400 rev/min. As the speed increased over this range, the amplitude of the rivulets appeared to decrease and the number of rivulets per unit surface area increased.

At speeds below 100 rev/min, the direction of drainage was along the generator of the cone; that is along the meridian of the cone. As the speed increased to about 300 rev/min, the angle made between the drainage path and the generator of the cone increased to about 30° where it remained constant with

further increases in speed.

A reliable method for measuring the local film thickness of the condensate on the rotating 60° cone was not available. To overcome this difficulty, Robson attempted to simulate the drainage of this film of condensate by studying the drainage of cold water films on a second rotating 60° cone. The validity of the simulation was based on the assumption that the mean thicknesses of the films of condensate and of water were equal when the same mass flow rates occurred on each cone at a common cone diameter and speed of rotation.

Robson measured the mean film thickness of cold water films flowing down the outer surface of a rotating 60° cone, which was mounted on Holgate's apparatus (71). Cold water was introduced to the outer surface of the cone by a distributor at the apex of the cone. Measurements of the mean film thickness were made at several stations along the generator of the cone using a capacitance probe. The water flow rate was varied between 0.009 and 0.127 m^3/h and the speed of rotation was varied between zero and 660 rev/min. Thus mean thicknesses of the water film were obtained for given cone diameters, speeds of rotation and mass flow-rates. Robson then used Howe's heat transfer results (69) to obtain the mass flow rate of condensate at any cone diameter for a particular speed of rotation. At a given speed and at a given cone diameter, the calculated mass flow rate of condensate was matched with the mass flow rate of cold water to obtain a value of the mean thickness for the water film. Under these matched conditions the mean thickness of the water film was assumed to be the mean thickness of the condensate film.

The mean thicknesses for the condensate films were correlated by

$$\delta \left[\frac{D\omega^2 \, \mathrm{Sin}(30^\circ)}{2\,\nu^2} \right]^{\frac{1}{2}} = 1.1 \, \mathrm{Re}^{\frac{1}{3}}$$

This equation predicts mean thicknesses of 1.22 times the Nusselt value.

Holgate (71) made measurements of wave length, mean film thickness and wave velocity for cold water films flowing down the stationary 60° cone. The wavelengths were found to be between 0.01 m and 0.03 m. These wave lengths were in broad agreement with the values for condensate films measured by Robson from photographs of the condensate film taken at very low speeds of rotation. The mean film thickness of water films on the stationary cone was found to be 0.93 of the Nusselt value, which was exactly the reduction predicted by Kapitza (27) and the velocity of the waves was found to be 2.5 to 2.6 times the local mean film velocity, which was only marginally greater than the 2.4 times predicted by Kapitza. Waves on the cold water films may not be exactly the same as the waves on the condensate films, due to the basically different methods of sustaining the two films, i.e. the former has variable mass flow rate while the latter has constant mass flow rate. Thus the mean film thicknesses may not be comparable under the matched conditions of mass flow rate, cone diameter and speed. However, if one accepts that the two thicknesses are comparable, the larger mean thicknesses reported by Robson could be caused by substantial components

of centrifugal acceleration resolved perpendicular to and acting outwards from the cone surface.

Present work.

As stated in section 2.4.1 the present work is part of a wider investigation into the transient thermal stresses in the rotors of steam turbines during cold starting and manoeuvring. In this investigation the heat transfer to such a body has been simulated by studying the heat transfer from steam to the surfaces of cones with many apex angles.

Heat transfer data for steam condensing on a rotating disc (54) and on rotating cylinders (55, 56, 58 and 59) have been published by other workers. One of the aims of the present work is to extend this heat transfer study to include cones with intermediate apex angles. To achieve this aim, apparatus was designed and constructed for the measurement of heat transfer coefficients from steam to rotating cones and to rotating axisymmetrical bodies. Experimentally determined heat transfer coefficients for rotating cones with apex angles of 10^{o}, 20^{o} and 60^{o} are presented. Some of the author's results for the latter cone have been discussed in 2.4.4 (69).

The published heat transfer data for discs and for cylinders was correlated against a laminar theory for the condensation process. In the present work a theory is developed for laminar filmwise condensation on rotating cones with apex angles between 0^{o} and 180^{o}. The cones are assumed to rotate with the axis of symmetry vertical and the films of condensate are assumed to

drain under the influence of both gravitational and centrifugal acceleration. Since the eventual aim of the research is to make an experimental study of the heat transfer to a rotating axisymmetrical body such as a turbine rotor, the laminar theory for condensation on rotating cones is extended to cover the condensation on an axisymmetrical body whose profile is described by a smooth curve. This laminar theory for filmwise condensation on rotating cones and on rotating axisymmetrical bodies is given in the next section.

3.0 THEORY

3.0 Introduction.

This section covers the theory used in presenting the experimental results and is divided into two main parts.

The first part is concerned with a theoretical study of the condensation of steam in laminar films on the external surfaces of rotating axisymmetrical bodies. These films are assumed to be drained in a direction parallel to the condensing surface by the action of both gravitational and centrifugal accelerations. Two kinds of axisymmetrical bodies are considered during the study. The first is the circular cone which is a special case where the profile is formed by a straight line. The second is of a more general nature where the profile is formed by a smooth curve.

A differential equation, which relates the condensate film thickness to the distance from the starting point of condensation, is developed from the study. Several analytical solutions for this equation are given for cones with certain limiting conditions of apex angle and of speed of rotation. A method of numerical integration is given to enable the equation to be applied to a wider range of conditions. The numerical solution to the equation is used to calculate film thicknesses and heat transfer coefficients for a large range of speeds of rotation and of steam to surface temperature differences. These calculations are made and presented for cones with various apex angles and for one other kind of axisymmetrical body, where the profile is formed by a circular arc. This body is designed to represent the shape of a turbine rotor at a position where

the shaft meets a blade disc.

The second part of this section deals with the temperature distribution across the wall of the hollow cone. Two temperature distributions are considered. The first is for wall materials which have a constant thermal conductivity. The second temperature distribution is for materials where the thermal conductivity is assumed to have a linear dependence on temperature.

3.1 The condensation of steam in laminar film on the surface of a rotating cone.

The important and extensive theoretical work reported by Sparrow and his associates has already been referred to as being of particular interest because the complete Navier-Stokes and energy equations were solved using a boundary layer approach. One general conclusion, which has relevance to the present research, can be drawn from the results of their previous work. This conclusion is that, for fluids with Prandtl Numbers in the region of unity and with film conditions where the value of $\frac{c\theta}{1}$ is less than 0.1, the effects of both energy convection and of inertia can be neglected. Such a conclusion yields a quantitative criterion which defines the high limit of the region where thin film approximations may be made.

When applied to the present research work on film condensation, which covers both stationary and rotating cones, the boundary layer approach is seen to have several disadvantages which are:-

(i) When either the speed of rotation becomes zero, or the apex angle becomes small, the boundary layer character ceases to exist. Tien (67).

(ii) The effects of gravitational acceleration are not considered.

(iii) The given equations for film thickness and heat transfer coefficient apply only to condensate films starting at the apex of the cone.

The following theoretical analysis for laminar films of condensate on conical surfaces uses a different line of approach and attempts to overcome these disadvantages of the boundary layer approach. The theory is designed to be applied to the present research conditions, where the condensate (water) has a Prandtl Number near unity and the films are such that the value of $\frac{c\theta}{l}$ is less than 0.1. Because these conditions meet the criteria for "thin films", the effects of both energy convection and of inertia are neglected. Thus the condensate film is assumed to be thin and in laminar flow in a direction parallel to the surface and along a meridian of the cone. Film drainage is provided by the combined effects of both gravitational and centrifugal acceleration resolved parallel to the meridian. As such the present laminar theory for thin films may be applied to:-

(i) condensate films which start at any distance from the apex of the cone,

(ii) to cones of any apex angle between 0^{o} and 180^{o},

(iii) to cones which are either stationary or rotating.

3.1.1 The co-ordinate system.

Consider the truncated cone shown in fig. 1. The conical surface is described by the rotation of a straight line generator, about the vertical axis. The angle of rotation is denoted by ψ , but since the usual assumption of angular symmetry is made, this dimension becomes redundant. The root of the generator lies at a radius of $\frac{1}{2}d$ from the axis of rotation and the generator makes an angle α with axis of rotation. Angle α becomes the semi-apex angle of the cone. Throughout the text, cones are referred to by their apex angle, which is 2α.

Directions parallel to the generator are denoted by X and distances from the root to some point on the generator in this direction are denoted by x. Both X and x are considered to be positive in the direction of increasing cone diameter. Directions perpendicular to the generator are denoted by Y, which is considered to be positive in a direction away from the axis of rotation. The distance from the generator to some point in the condensate film is denoted by y.

3.1.2 Acceleration field.

The acceleration field for the cone rotating about its vertical axis may be resolved in two principal directions:-

(i) In the X direction, or parallel to the generator,

$$a = \tfrac{1}{2}D\,\omega^2\,\mathrm{Sin}\alpha + g\,\mathrm{Cos}\,\alpha \qquad \ldots\ldots\ldots (3.1.1)$$

where $$D = (d + 2x\,\mathrm{Sin}\alpha) \qquad \ldots\ldots\ldots (3.1.2)$$

FIG 1

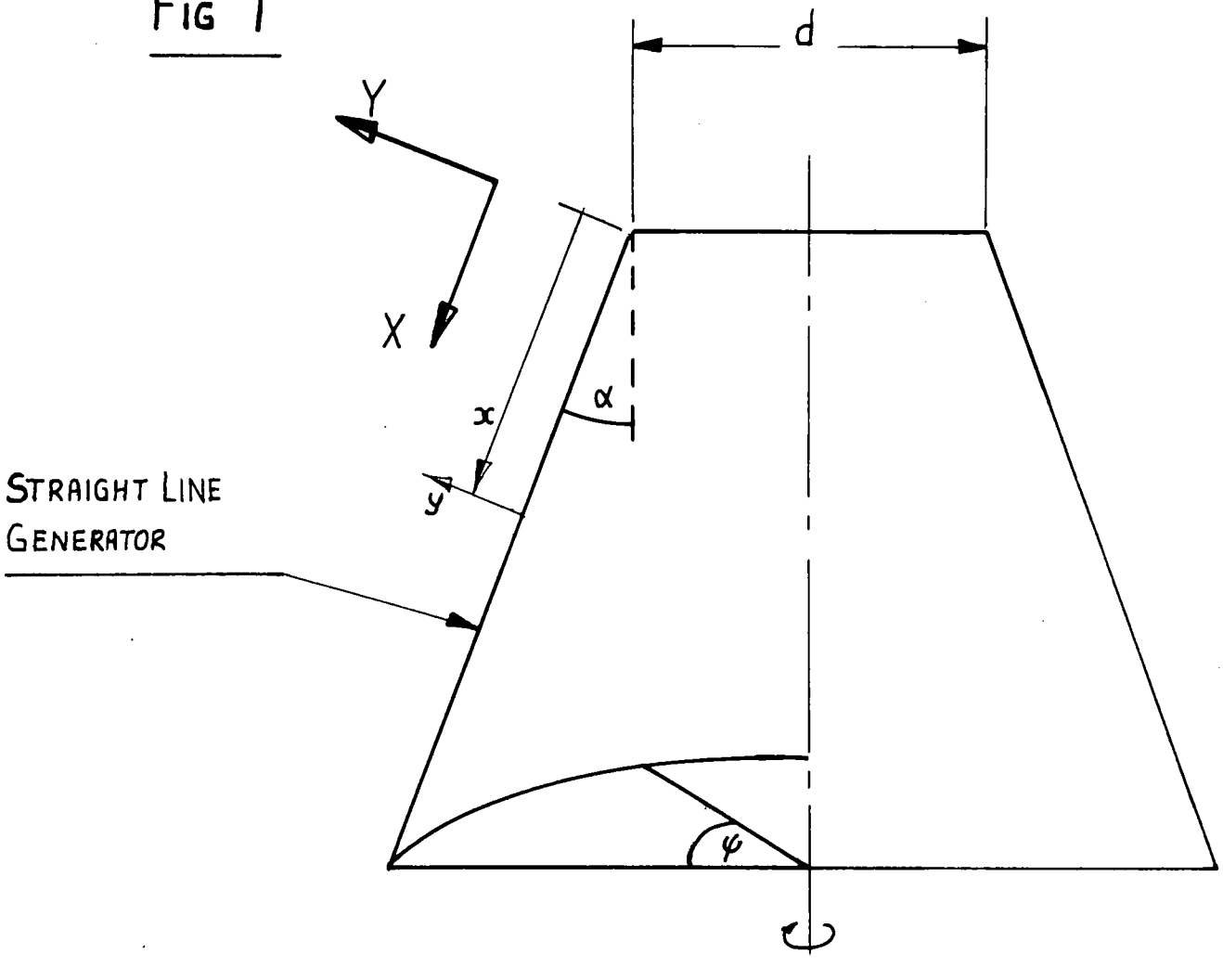

APEX ANGLE OF CONE. 2α.
DISTANCE FROM THE STARTING POINT OF THE FILM
IN X DIRECTION x.
DISTANCE FROM THE OUTER SURFACE OF THE CONE
IN Y DIRECTION. y.
DIAMETER OF THE CONE AT THE STARTING POINT OF
THE FILM. d.

and (ii) in the Y direction, or perpendicular to the generator,

$$a_y = \tfrac{1}{2} D \omega^2 \cos\alpha - g \sin\alpha \qquad \ldots\ldots\ldots (3.1.3)$$

In this study, the thin laminar film of condensate is assumed to drain from the cone surface only in the positive X direction under the influence of acceleration a. Consequently the acceleration in the Y direction is neglected even though its magnitude may greatly exceed that of a.

3.1.3 Velocity distribution across a laminar film of condensate.

The laminar film of condensate is assumed to start on the cone surface at some distance away from the apex. In fig. 2, the diameter of the cone at the starting point of the film is denoted by d and at that point, both x and the film thickness δ are zero.

A small elemental ring of fluid whose cross-section has a length Δx and a thickness Δy is positioned inside the condensate film. The upper surface of the element lies at a distance x from the starting point of the film and the inner surface of the element lies at a distance y from the cone surface.

If the change in the volume of the elemental ring with change in distance y is neglected, then the volume of the elemental ring of fluid is given by

$$V = \pi D \ \Delta x \ \Delta y$$

The body force on the element in the X direction is

$$F = \rho \pi D \ \Delta x \ \Delta y \ a \qquad \ldots\ldots\ldots (3.1.4)$$

FIG 2

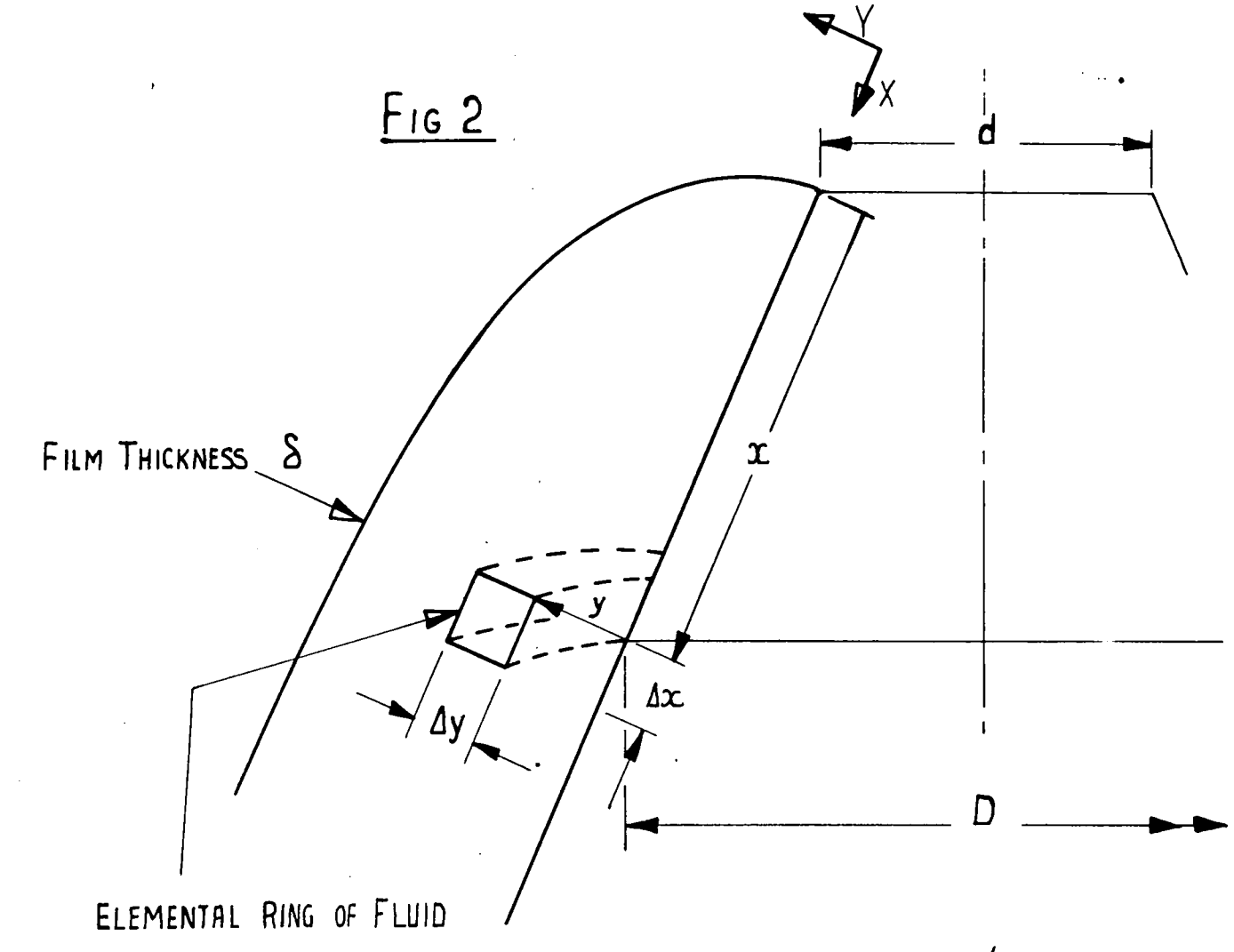
Y
X
d
x
FILM THICKNESS δ
y
Δy
Δx
D
ELEMENTAL RING OF FLUID

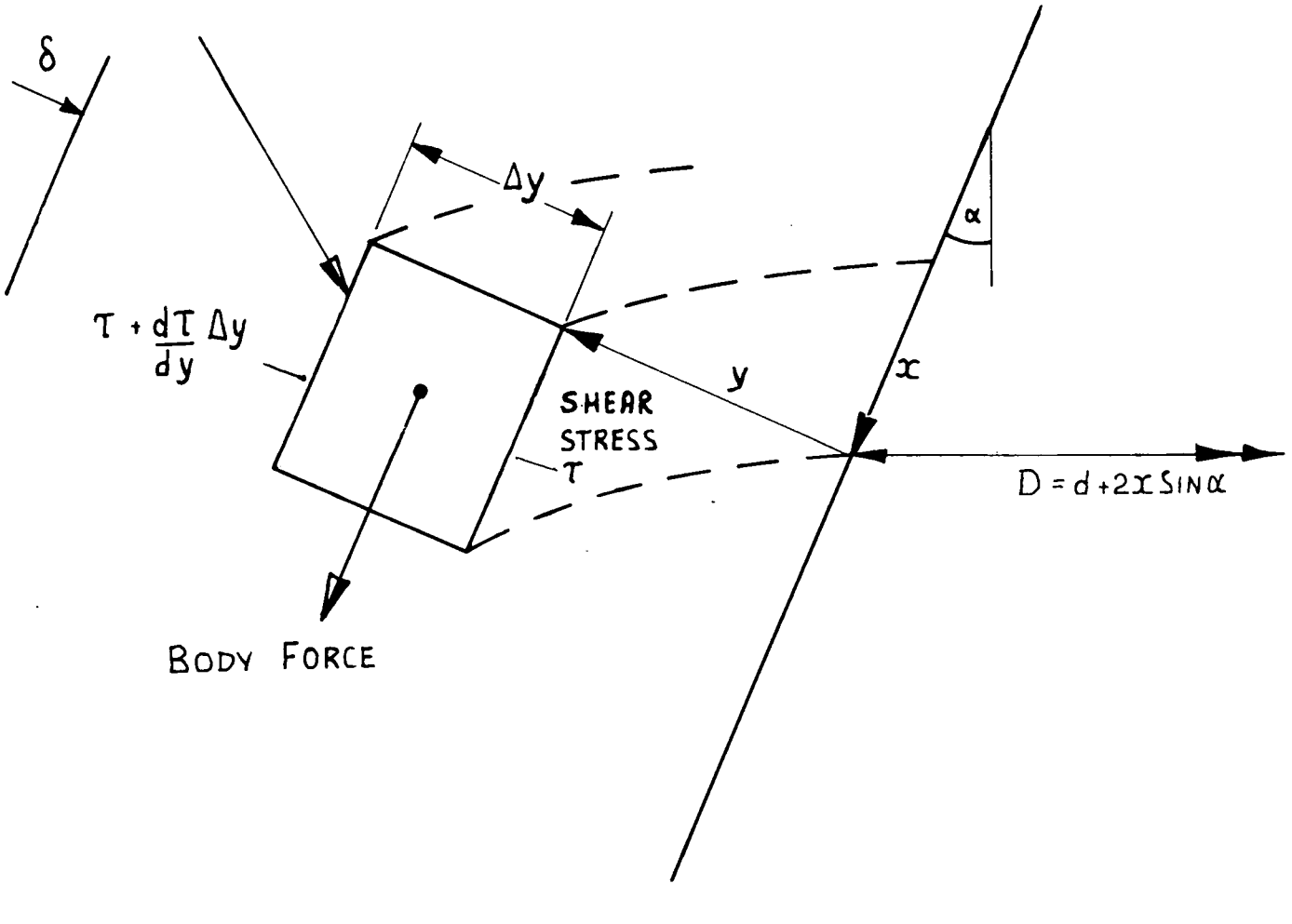
δ
Δy
α
τ + dτ/dy Δy
y
x
SHEAR STRESS τ
D = d + 2x SIN α
BODY FORCE

The shear stress at the point y = τ

and at the point (y + Δy) = $\tau + \frac{d\tau}{dy}\Delta y$.

In terms of the velocity gradient $\frac{du}{dy}$ and dynamic viscosity μ the shear stress $\tau = \mu \frac{du}{dy}$

and $$\frac{d\tau}{dy} = \mu \frac{d^2u}{dy^2}$$

The area of the inner surface of the element is given approximately by $\pi D \Delta x$. Therefore the shear force on the inner surface of the element at the point y becomes

$$S = \pi D \Delta x \tau \qquad \ldots\ldots\ldots (3.1.5)$$

Assuming that there is no change between the areas of the inner and outer surfaces of the element, the shear force on the outer surface of the element, at the point (y + Δy), becomes:-

$$(S + \Delta S) = \pi D \Delta x \left(\tau + \frac{d\tau}{dy} \Delta y\right) \qquad \ldots\ldots\ldots (3.1.6)$$

To maintain a balance of forces acting on the element in the direction X: shear force + body force = 0. $\ldots\ldots\ldots$ (3.1.7)

Substituting from equations (3.1.4), (3.1.5) and (3.1.6) into equation (3.1.7) we have

$$\pi D \mu \frac{d^2u}{dy^2} \Delta x \Delta y + \rho \pi D a \Delta x \Delta y = 0$$

and simplifying we have

$$\frac{d^2u}{dy^2} = -\frac{\rho}{\mu} a \qquad \ldots\ldots\ldots (3.1.8)$$

Integrating equation (3.1.8) gives an expression for the velocity distribution across the film at the point x

$$u = -\frac{\rho}{\mu} a \frac{y^2}{2} + C_1 y + C_2 \qquad \ldots\ldots\ldots (3.1.9)$$

Introducing the boundary conditions for the film we have, at $y = 0$, velocity $u = 0$ and therefore $C_2 = 0$.

On the assumption that the shear stress at the free surface of the film is negligible, then at $y = \delta$; $\frac{du}{dy} = 0$

and therefore $C_1 = \frac{\rho}{\mu} a \delta$

Hence equation (3.1.9) becomes:-

$$u = \frac{\rho}{\mu} a \left[\delta y - \frac{y^2}{2} \right] \qquad \ldots\ldots\ldots (3.1.10)$$

This equation predicts a semi-parabolic velocity distribution across the film and has a form similar to that given by Nusselt for thin laminar films on plane surfaces.

In equation (3.1.5) the area of the inner surface of the elemental ring of fluid may be correctly written as

$$(D + 2y \operatorname{Cos}\alpha) \Delta x$$

and in equation (3.1.6) the area of the outer surface of the element becomes

$$(D + (2y + 2\Delta y) \operatorname{Cos}\alpha) \Delta x$$

Carrying these additional terms through to the differential equation for the velocity distribution introduces a new term

$$\frac{2 \operatorname{Cos}\alpha}{(D + 2y \operatorname{Cos}\alpha)} \frac{du}{dy}$$

to the left-hand side of equation (3.1.8). The presence of this additional term modifies the solution for the velocity distribution and gives, after introducing the boundary conditions,

$$u = -\frac{\rho a}{\mu} \left\{ \frac{Dy}{4 \operatorname{Cos}\alpha} + \frac{y^2}{4} - \left[\frac{D^2}{8 \operatorname{Cos}\alpha} + \frac{D\delta}{2 \operatorname{Cos}\alpha} + \frac{\delta^2}{2} \right] \left[\ln \left| 1 + \frac{2y \operatorname{Cos}\alpha}{D} \right| \right] \right\}$$

The above equation may be simplified by using a series

expansion for the ln term:-

$$\ln\left[1 + \frac{2y\,\mathrm{Cos}\alpha}{D}\right] = \frac{2y\,\mathrm{Cos}\alpha}{D} - \frac{2y^2\,\mathrm{Cos}^2\alpha}{D^2} + \frac{8}{3}\frac{y^3\,\mathrm{Cos}^3\alpha}{D^3} - \frac{4y^4\,\mathrm{Cos}^4\alpha}{D^4} + \text{other terms}$$

For thin film conditions where y is very much less than D, all terms of $\frac{y^3}{D}$ and of higher orders may be neglected to give a velocity distribution of

$$u = \frac{\rho a}{\mu}\left[\delta y - \frac{y^2}{2}\right]$$

This equation for u agrees with that obtained by the integration of equation (3.1.8).

By integrating equation (3.1.10) between the limits y = 0 and y = δ the mean velocity of flow U at the point x can be determined

$$U = \frac{\rho}{\mu} a\,\frac{\delta^2}{3} \qquad \ldots\ldots\ldots (3.1.11)$$

3.1.4 Conservation of energy.

Consider a second element abcd shown in fig. 3. When rotated about the vertical axis, the element forms a control volume in the condensate film.

The equation for conservation of energy in the control volume may be written in a differential form as:-

$$\pi(d+2x\mathrm{Sin}\alpha)k\left[\frac{dt}{dy}\right]_{y=o}\Delta x = \frac{\rho d}{dx}\left[1\int_o^\delta \pi(d+2x\mathrm{Sin}\alpha)u\,dy\right]\Delta x + \frac{\rho d}{dx}\left[\int_o^\delta \pi(d+2x\mathrm{Sin}\alpha)uc(t_s-t)\,dy\right]x \qquad \ldots\ldots\ldots (3.1.12)$$

FIG 3

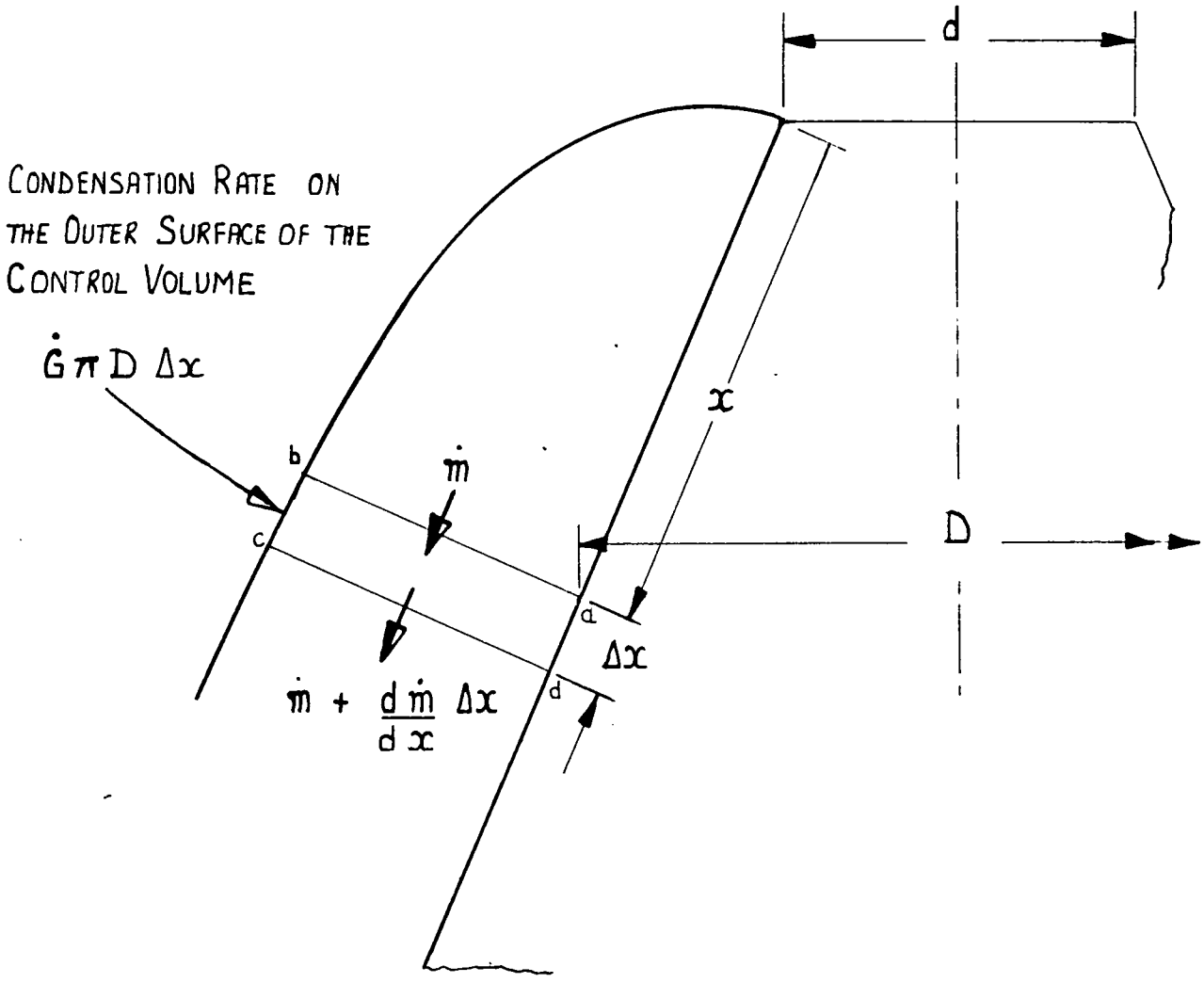

ELEMENT abcd

THE CONTROL VOLUME IS DESCRIBED BY ROTATING THE ELEMENT ABOUT THE VERTICAL AXIS.

The term on the left hand side of the equation represents the energy transfer to the inner surface of the control volume denoted by line ad. The first term on the right hand side of the equation represents the energy liberated by the vapour condensing on the outer surface of the control volume denoted by line bc. The second term on the right hand side represents the energy liberated by under-cooling the condensate.

For thin films it has been shown by Sparrow et al that the temperature distribution is linear.

Therefore the temperature at any point y may be expressed as:-

$$t = t_o + \frac{y}{\delta}\theta$$

and the temperature gradient at the surface becomes:-

$$\left[\frac{dt}{dy}\right]_{y=o} = \frac{\theta}{\delta}$$

Thus the conservation equation becomes:-

$$\pi(d+2x\mathrm{Sin}\alpha)k\left[\frac{\theta}{\delta}\right]\Delta x = \rho\frac{d}{dx}\left[\, 1\int_o^{\delta}\pi(d+2x\mathrm{Sin}\alpha)u\ dy\,\right]\Delta x + \rho\frac{d}{dx}\left[\int_o^{\delta}\pi(d+2x\mathrm{Sin}\alpha)uc\theta\left(1-\frac{y}{\delta}\right)dy\right]\Delta x \quad \ldots\ldots (3.1.13)$$

The terms in brackets [ ] on the right hand side, may be integrated at constant x between the limits of δ and zero giving:-

$$\pi(d+2x\mathrm{Sin}\alpha)k\,\frac{\theta}{\delta}\,\Delta x = \rho\frac{d}{dx}\left[\pi\frac{\rho}{\mu}1(d+2x\mathrm{Sin}\alpha)a\,\frac{\delta^3}{3}\right]\Delta x + \rho\frac{d}{dx}\left[\pi\frac{\rho}{\mu}c\theta(d+2x\mathrm{Sin}\alpha)a\,\frac{\delta^3}{8}\right]\Delta x \quad \ldots\ldots (3.1.14)$$

Equation (3.1.14) can be simplified to:-

$$(d + 2x\ \mathrm{Sin}\alpha)\ k\,\frac{\theta}{\delta} = \frac{\rho^2}{3\mu}\left[1 + \frac{3}{8}c\theta\right]\frac{d}{dx}\left[D\ a\ \delta^3\right]$$

where $D = (d + 2x \sin\alpha)$

Completing the differentiation of the right hand side of the equation we have:-

$$Dk\frac{\theta}{\delta} = \frac{\rho^2}{3\mu}\left(1+\frac{3}{8}c\theta\right)\left[3Da\delta^2\frac{d\delta}{dx} + D\delta^3\frac{da}{dx} + a\delta^3\frac{dD}{dx}\right]$$

and simplifying we have:-

$$a\,\delta^3\frac{d\delta}{dx} + \frac{\delta^4}{3}\left[\frac{da}{dx} + \frac{a}{D}\frac{dD}{dx}\right] = \frac{\mu\, k\,\theta}{\rho^2\left[1 + \frac{3}{8}\,c\,\theta\right]}$$

The group of fluid properties $\frac{\mu\, k\,\theta}{\rho^2}$ may be written as $\frac{c\,\theta\,\nu^2}{Pr}$ which is the form used by Sparrow & Gregg.

$$a\,\delta^3\frac{d\delta}{dx} + \frac{\delta^4}{3}\left[\frac{da}{dx} + \frac{a}{D}\frac{dD}{dx}\right] = \frac{c\,\theta\,\nu^2}{Pr\left[1 + \frac{3}{8}\,c\,\theta\right]} \qquad (3.1.15)$$

The fraction $\frac{3}{8}$ which appears in the above equation is only valid if the velocity distribution is semi-parabolic and the temperature distribution is linear. For thick films, $0.1 < \frac{c\theta}{1} < 2.0$ Rohsenow (13) has shown that the fraction should be 0.68.

3.1.5 Mass flow rate at point x.

It can be shown that equation (3.1.15) can be found from a simple mass balance on a control volume in the film. Again consider the control volume shown in fig. 3.

The mass flow rate across plane ab

$$\dot{m} = \pi\, D\, \delta\, U \qquad \ldots\ldots\ldots (3.1.16)$$

At plane cd, which intersects the cone surface at point $(x + \Delta x)$, the mass flow rate is

$$\dot{m} + \frac{d\dot{m}}{dx}\Delta x$$

Differentiating equation (3.1.16) we get

$$\frac{d\dot{m}}{dx} = \pi\left[D\,\delta\frac{dU}{dx} + DU\frac{d\delta}{dx} + \delta U\frac{dD}{dx}\right] \qquad \ldots\ldots\ldots (3.1.17)$$

3.1.6 Condensation rate

Condensation takes place at the liquid vapour interface which coincides with the outer surface of the control volume. This outer surface is denoted by line bc in fig. 3.

When the film thickness δ is very small in comparison with diameter D, the area of the outer surface of the element is approximately = $\pi D \Delta x$.

Assuming that the heat transfer from the steam through the film to the surface of the cone is by conduction only, we can express the energy flow rate per unit area of surface by Fourier's Equation

$$\frac{\text{energy flow rate}}{\text{unit area}} \quad \phi = - \frac{k\,(t_o - t_s)}{\delta} \qquad \ldots\ldots\ldots (3.1.18)$$

thus the $\frac{\text{condensation rate}}{\text{unit area}}$ $\dot{G} = \frac{\phi}{l}$ $\ldots\ldots\ldots (3.1.19)$

Hence the condensation rate over the outer surface of the element is

$$\dot{G}\, \pi\, D\, \Delta x \qquad \ldots\ldots\ldots (3.1.20)$$

3.1.7 Conservation of mass.

A mass balance may be made on the three sides of the control volume through which fluid may pass, namely sides ab, bc and cd.

The equation for the conservation of mass on the control becomes:-

$$\dot{m} + \frac{d\dot{m}}{dx} \Delta x = \dot{m} + \dot{G}\, \pi\, D\, \Delta x$$

or

$$\frac{d\dot{m}}{dx} = \dot{G}\, \pi\, D \qquad \ldots\ldots\ldots (3.1.21)$$

Expanding equation (3.1.21) using equation (3.1.17) and (3.1.20) we have:-

$$D\,\delta\frac{dU}{dx} + DU\frac{d\delta}{dx} + \delta U\frac{dD}{dx} = \frac{\dot{G}D}{\rho} \qquad \ldots\ldots\ldots (3.1.22)$$

The substitution for $\frac{dU}{dx}$ is obtained by differentiating equation (3.1.11)

$$\frac{dU}{dx} = \frac{\rho}{u}\left[\frac{2}{3}\,a\,\delta\,\frac{d\delta}{dx} + \frac{\delta^2}{3}\frac{da}{dx}\right]$$

On collecting terms the equation (3.1.22) becomes:-

$$a\,\delta^3\frac{d\delta}{dx} + \frac{\delta^4}{3}\left[\frac{da}{dx} + \frac{a}{D}\frac{dD}{dx}\right] = \frac{c\,\theta\,\nu^2}{Pr\left[1 + \frac{3}{8}\,c\,\theta\right]} \qquad \ldots\ldots\ldots (3.1.23)$$

We can show from equation (3.1.15) that the specific enthalpy of condensation in equation (3.1.22) can be replaced by $(1 + \frac{3}{8}\,c\,\theta)$ to account for the energy transferred to the cone by the under-cooling of the condensate.

3.1.8 Behaviour of Equation (3.1.15).

Equation (3.1.15) is the governing equation for condensate films on the outer surfaces of rotating cones. Before investigating the behaviour of the governing equation it should be rearranged into a more suitable form:-

$$\frac{d\delta^4}{dx} = 4\,H - \frac{4\delta^4}{3}\left[\frac{da}{dx} + \frac{a}{D}\frac{dD}{dx}\right] \qquad \ldots\ldots\ldots (3.1.24)$$

where $$H = \frac{c\,\theta\,\nu^2}{Pr\,(1 + \frac{3}{8}\,c\,\theta)}$$

For the cones considered in this study, a is given by equation (3.1.1) from which

$$\frac{da}{dx} = \omega^2\,\mathrm{Sin}^2\alpha \qquad \ldots\ldots\ldots (3.1.25)$$

and D is given by equation (3.1.2) from which

$$\frac{dD}{dx} = 2\,\mathrm{Sin}\,\alpha \qquad \ldots\ldots\ldots (3.1.26)$$

Therefore the governing equation becomes:-

$$\frac{d\delta^4}{dx} = \frac{4\left\{H - \frac{\delta^4}{3}\left[2\omega^2 \sin^2\alpha + \frac{2\,g \sin\alpha \cos\alpha}{D}\right]\right\}}{\left[\frac{1}{2} D\omega^2 \sin\alpha + g \cos\alpha\right]} \quad \ldots\ldots\ldots (3.1.27)$$

At zero speed, the above equation reduces to:-

$$\frac{d\delta^4}{dx} = \frac{4\,H - \frac{8}{3}\frac{\delta^4}{D}\left[g \sin\alpha \cos\alpha\right]}{g \cos\alpha} \quad \ldots\ldots\ldots (3.1.28)$$

When α is zero the slope $\frac{d\delta^4}{dx}$ remains finite and positive. Since the second term in the numerator also remains positive for all finite values of α, the slope $\frac{d\delta^4}{dx}$ will decrease as the film grows. The slope will only become zero when

$$H = \frac{2}{3}\frac{\delta^4}{D} g \sin\alpha \cos\alpha$$

or $$\delta^4 = \frac{3}{2}\frac{D\,H}{g \sin\alpha \cos\alpha}$$

The rate of change of slope is

$$\frac{d}{dx}\left[\frac{d\delta^4}{dx}\right] = \frac{8}{3}\sin\alpha\left[\frac{\delta^4}{D^2}\frac{dD}{dx} - \frac{1}{D}\frac{d\delta^4}{dx}\right]$$

By inspection, it can be seen that both the rate of change of slope $\frac{d}{dx}\left[\frac{d\delta^4}{dx}\right]$ and the slope $\frac{d\delta^4}{dx}$ are zero when D becomes infinite. Therefore the film thickness grows monotonically from zero to infinity. If the film starts at some position away from the apex, the presence of the cone diameter $D\ (= d + 2\,x \sin\alpha)$ in equation (3.1.28) will have the effect of reducing the magnitude of the second term. If this occurs, the film thickness should be greater than that which would occur if the film started at the apex.

When $g = 0$, equation (3.1.27) reduces to:-

$$\frac{d\delta^4}{dx} = \frac{4\left[H - \frac{2\delta^4}{3}\omega^2 \operatorname{Sin}^2\alpha\right]}{\frac{1}{2} D\omega^2 \operatorname{Sin}\alpha} \qquad \ldots\ldots\ldots (3.1.29)$$

If the film starts at the apex ($D = 0$), the slope $\frac{d\delta^4}{dx}$ becomes infinite. If the film starts at some point away from the apex, the slope becomes finite for all finite values of ω and $\operatorname{Sin}\alpha$. The slope $\frac{d\delta^4}{dx}$ should tend towards zero very rapidly because in equation (3.1.29) both the second term in the numerator and the presence of the cone diameter D in the denominator, are contributing to the rate of decrease of slope.

$\frac{d\delta^4}{dx}$ can only be zero when D is infinite or when

$$H = \frac{\delta^4}{3} 2\omega^2 \operatorname{Sin}^2\alpha$$

or $$\delta^4 = \frac{3}{2} \frac{H}{\omega^2 \operatorname{Sin}^2\alpha}$$

It can be shown that $\frac{d}{dx}\left[\frac{d\delta^4}{dx}\right]$ is also zero when $\frac{d\delta^4}{dx}$ is zero. At this point the film thickness becomes independent of D or x, and will remain uniform.

3.2 The condensation of steam in a laminar film on the surface of a rotating axisymmetrical body whose profile is formed by a smooth curve.

Having completed the study of the condensation of steam in a laminar film on the surface of a rotating cone, the general method of analysis may be taken one stage further and thereby made more widely applicable. The next stage is to consider the condensation of steam in a thin laminar film on the surface of a rotating axisymmetrical body whose generator is formed by a smooth curve. The essential difference between the body with the curved generator and the cone lies in the angle α. For the cone the angle α is the semi-apex angle and is uniform with x. The angle for the curved generator becomes a variable dependent on x and as such needs to be re-defined. Therefore new expressions must be derived to relate both the angle α and the diameter of the body, to the distance along the curve. In this study, the reasoning applied to the fluid flow in the film and to the energy transfer across the film is almost the same as that already given for cones. In most instances the same assumptions are made. As such, the presentation of these two aspects of the study will be kept brief to avoid too much repetition. However the presentation will verify that the general method of analysis can be extended to cover bodies with curved generators.

The first step is to introduce a new pair of co-ordinates. These are the cartesian co-ordinates η and ξ, which specify directions parallel to the axis of rotation, and directions perpendicular to the axis of rotation, respectively.

Their introduction eases the task of specifying the shape of the curve which forms the generator. The co-ordinates X and Y remain as before in the analysis for cones; but their existence on the curved generator needs to be clarified. At any point on the curved generator, the X direction is always tangential to the curve and the Y direction is always perpendicular to X and in the direction of the radius of curvature. The distance along the curve from the starting point of the condensate film is still represented by x and the distance from the surface of the body to some point in the film is still denoted by y. The new co-ordinate system is shown in fig. 4. The curve of the generator is specified in terms of the cartesian co-ordinates η and ξ and may be defined as

$$\xi = f(\eta) \qquad \ldots\ldots\ldots (3.2.1)$$

The length of a very small part of the curve, denoted by Δx, is related to the co-ordinates η and ξ by the equation

$$\Delta x^2 = \Delta \eta^2 + \Delta \xi^2 \qquad \ldots\ldots\ldots (3.2.2)$$

As Δ approaches zero, then

$$\frac{dx}{d\eta} = \left[1 + \left[\frac{d\xi}{d\eta} \right]^2 \right]^{\frac{1}{2}} \qquad \ldots\ldots\ldots (3.2.3)$$

The length of the curve x from the origin at $\eta = 0$ to some point P may be expressed as

$$x = \int_{\eta=0}^{\eta=P} \left\{ 1 + \left[\frac{d\xi}{d\eta} \right]^2 \right\}^{\frac{1}{2}} d\eta \qquad \ldots\ldots\ldots (3.2.4)$$

In most instances the equation for the curve will not permit equation (3.2.4) to be integrated without using a numerical method of integration.

FIG 4

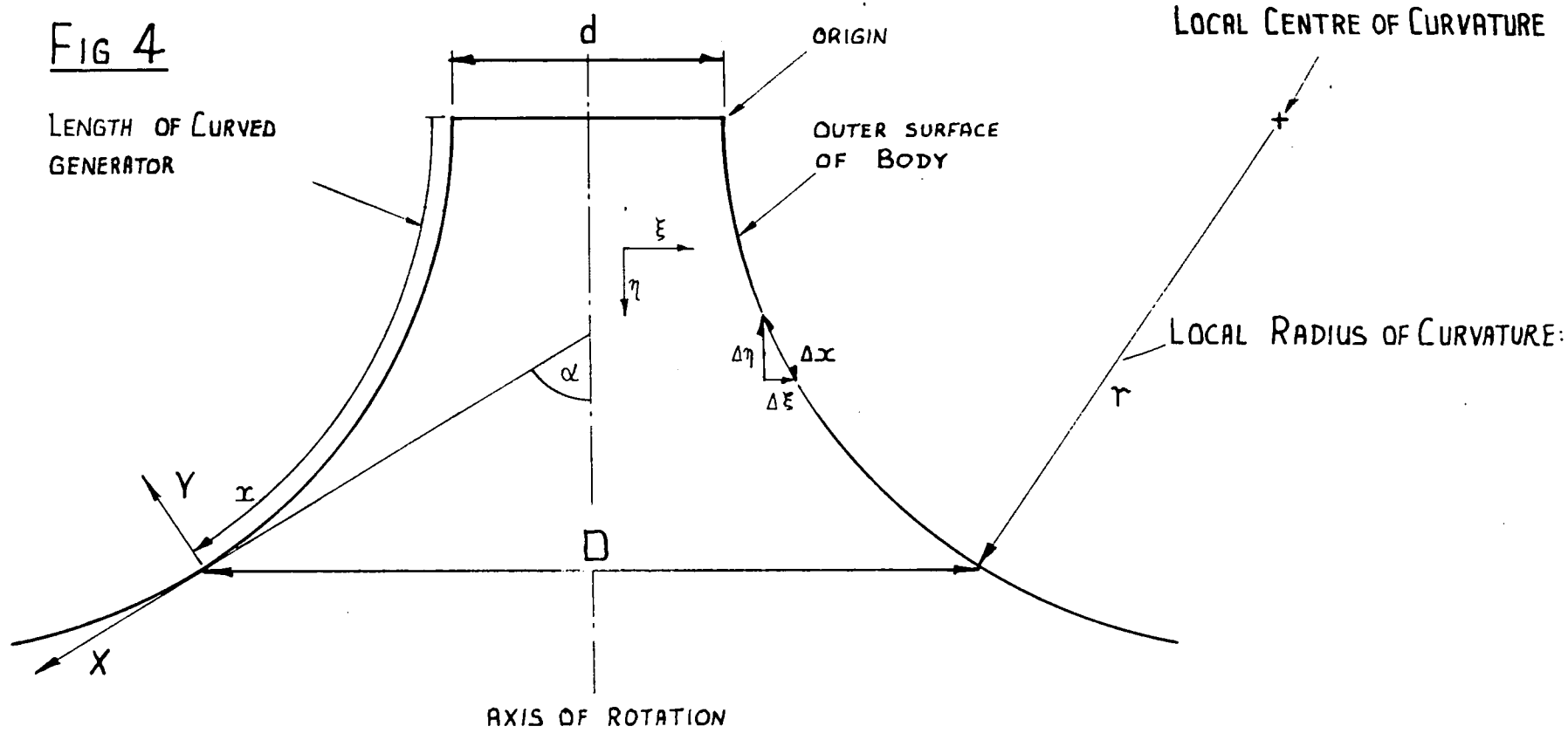

THE OUTER SURFACE OF THE BODY IS DESCRIBED BY THE ROTATION OF THE CURVED GENERATOR ABOUT THE VERTICAL AXIS

Fig. 4 shows the origin of the generator curve positioned at a point $\frac{1}{2}d$ from the axis of rotation; that is the vertical axis. Rotating the generator curve about the vertical axis describes the outer surface of the axisymmetrical body.

The diameter of the body at any point on the surface then becomes:-

$$D = d + 2\,f(\eta) \qquad \ldots\ldots\ldots (3.2.5)$$

or $$D = d + 2\,\xi \qquad \ldots\ldots\ldots (3.2.6)$$

Therefore $$\frac{dD}{d\eta} = 2\,\frac{d\xi}{d\eta} \qquad \ldots\ldots\ldots (3.2.7)$$

From (3.2.7) and (3.2.3)

$$\frac{dD}{dx} = \frac{2\,\frac{d\xi}{d\eta}}{\left\{1 + \left[\frac{d\xi}{d\eta}\right]^2\right\}^{\frac{1}{2}}} \qquad \ldots\ldots\ldots (3.2.8)$$

The angle α is shown in fig. 4 and is re-defined to be the angle made between the tangent to the generator curve and the vertical axis. Since the curve is defined in terms of η and ξ, equation (3.2.1) gives

$$\frac{d\xi}{d\eta} = \tan\alpha \qquad \ldots\ldots\ldots (3.2.9)$$

from which

$$\frac{d^2\xi}{d\eta^2} = \frac{1}{\mathrm{Cos}^2\alpha}\,\frac{d\alpha}{d\eta} \qquad \ldots\ldots\ldots (3.2.10)$$

where $$\frac{1}{\mathrm{Cos}^2\alpha} = 1 + \tan^2\alpha$$

equation (3.2.10) becomes

$$\frac{d\alpha}{d\eta} = \frac{\frac{d^2\xi}{d\eta^2}}{\left\{1 + \left[\frac{d\xi}{d\eta}\right]^2\right\}} \qquad \ldots\ldots\ldots (3.2.11)$$

Substituting for $\frac{dx}{d\eta}$ from equation (3.2.3) gives

$$\frac{d\alpha}{dx} = \frac{\frac{d^2\xi}{d\eta^2}}{\left\{1 + \left[\frac{d\xi}{d\eta}\right]^2\right\}^{3/2}} \qquad \ldots\ldots\ldots (3.2.12)$$

The acceleration field for the body with the curved generator may be resolved, as before, into two components

(i) In the X direction

$$a = \tfrac{1}{2} D\omega^2 \operatorname{Sin}\alpha + g \operatorname{Cos}\alpha \qquad \ldots\ldots\ldots (3.2.13)$$

and (ii) In the Y direction

$$a_y = \tfrac{1}{2} D\omega^2 \operatorname{Cos}\alpha - g \operatorname{Sin}\alpha \qquad \ldots\ldots\ldots (3.2.14)$$

Consider the small elemental ring of fluid, whose cross-section has a length Δx and a thickness Δy, shown in fig. 5 . The element is positioned inside the film and has co-ordinates for its uppermost and innermost surfaces of x and y respectively. Making the thin film approximation gives the volume of the elemental ring of fluid as

$$V = \pi D \, \Delta x \, \Delta y \qquad \ldots\ldots\ldots (3.2.15)$$

The body force on the element in the X direction is

$$F = \rho \pi D \, \Delta x \, \Delta y \, a \qquad \ldots\ldots\ldots (3.2.16)$$

The shear stress at the inner surface of the element at the point y is τ and at the outer surface of the element, at the point $(y + \Delta y)$, is $\left(\tau + \frac{d\tau}{dy} \Delta y\right)$

since $\tau = \mu \frac{du}{dy}$

and $\frac{d\tau}{dy} = \mu \frac{d^2u}{dy^2}$

The shear force at the inner surface of the element becomes

FIG 5

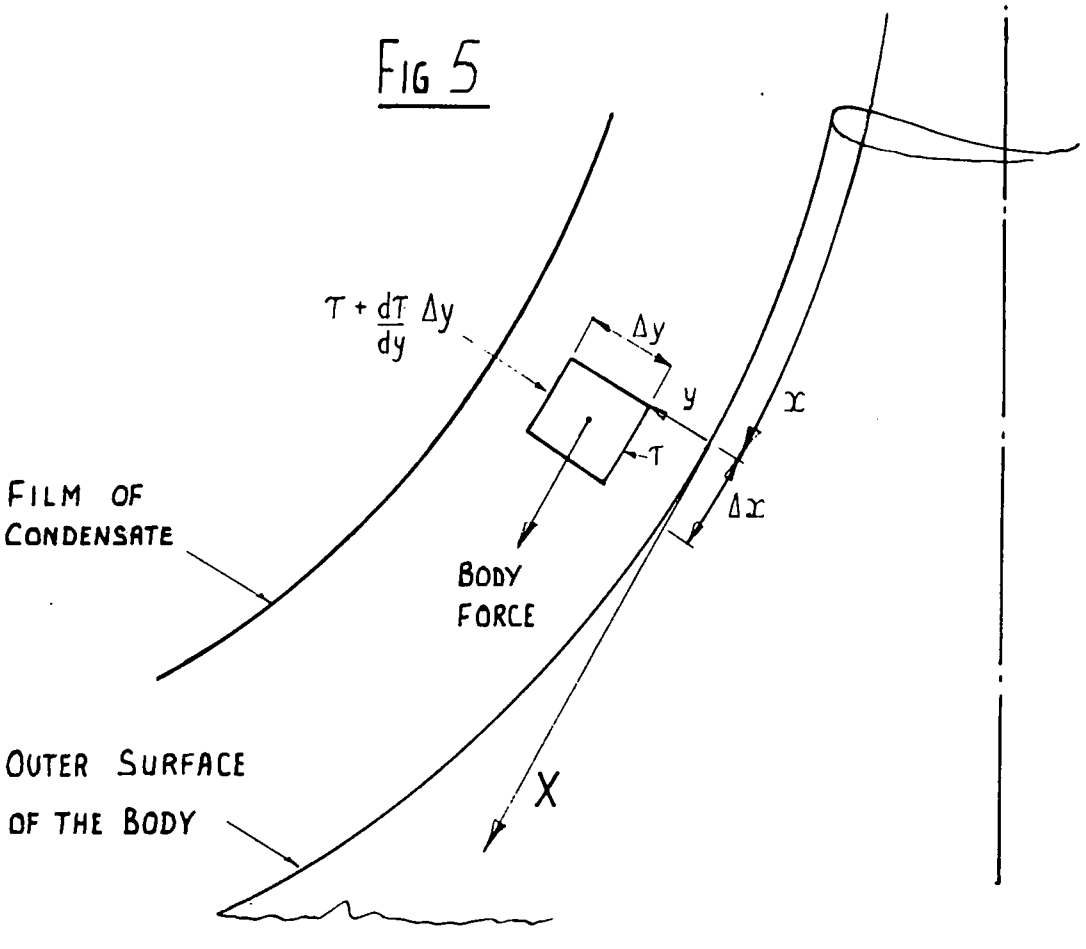

FIG 6

CONDENSATION RATE ON THE OUTER SURFACE OF THE CONTROL VOLUME $\dot{G}\pi D \Delta x$

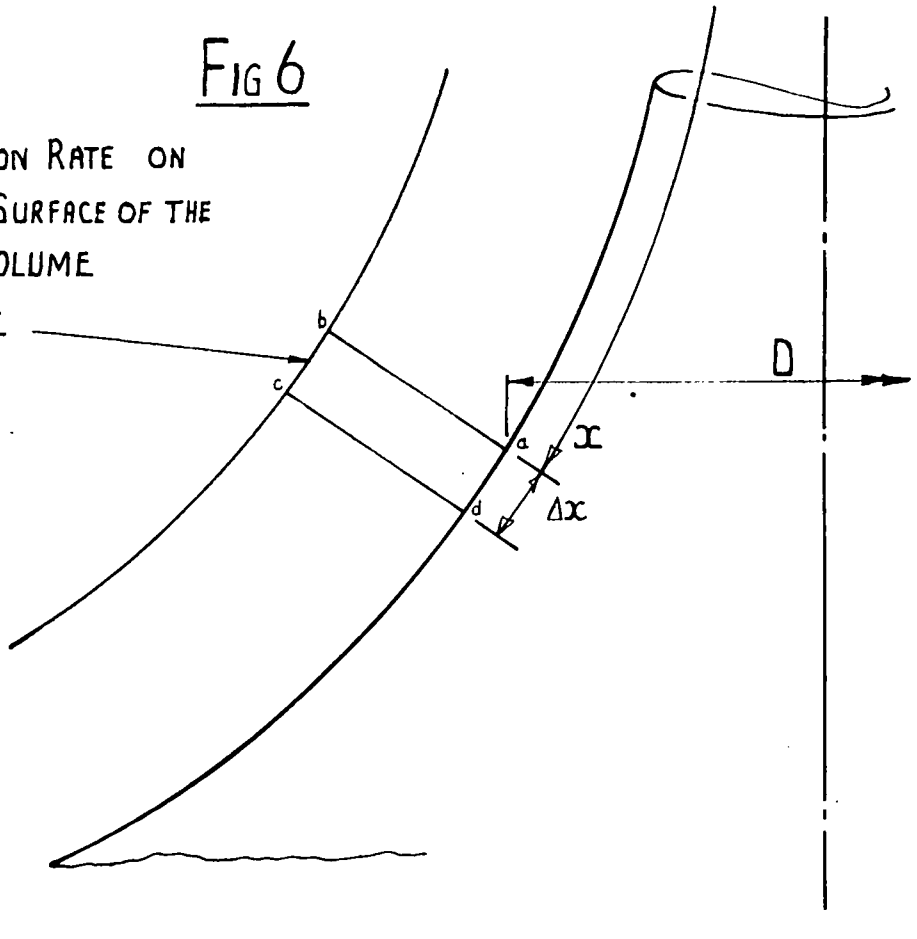

$$S = \pi D \, \Delta x \, \tau \qquad \ldots\ldots\ldots (3.2.17)$$

and the shear force at the outer surface of the element becomes:-

$$(S + \Delta S) = \pi D \, \Delta x \left[\tau + \frac{d\tau}{dy} \Delta y \right] \qquad \ldots\ldots\ldots (3.2.18)$$

A balance of the forces acting on the element in the X direction is maintained by the equation:-

net shear force + body force = 0

Thus

$$\pi D \, \mu \frac{d^2u}{dy^2} \Delta x \, \Delta y + \rho \pi D \, a \, \Delta x \, \Delta y = 0 \qquad \ldots\ldots (3.2.19)$$

hence

$$\frac{d^2u}{dy^2} = - \frac{\rho}{\mu} a \qquad \ldots\ldots\ldots (3.2.20)$$

The boundary conditions for the film on the curved generator are the same as those used for the cone:-

at $y = \delta$, $\frac{du}{dy} = 0$

and at $y = 0$, $u = 0$

Integrating equation (3.2.20) twice, and imposing the above boundary conditions, yields an expression for the velocity distribution across the film.

$$u = \frac{\rho}{\mu} \left[\delta y - \frac{y^2}{2} \right] \qquad \ldots\ldots\ldots (3.2.21)$$

which gives a mean velocity of flow in the X direction

$$U = \frac{\rho a \, \delta^2}{3\mu} \qquad \ldots\ldots\ldots (3.2.22)$$

These two equations have the same form as their counterparts for the cone.

Consider a second element abcd shown in fig. 6. When the element rotates about the vertical axis a control volume is formed in the film. The equation for conservation of energy in the control volume may be written in a differential form as:-

$$\pi Dk\left[\frac{dt}{dy}\right]_{y=o}\Delta x = \rho\frac{d}{dx}\left[1\int_o^\delta \pi Du\ dy\right]\Delta x + \rho\frac{d}{dx}\left[\int_o^\delta \pi Duc(t_s-t)\ dy\right]\Delta x \quad \ldots\ldots (3.2.23)$$

If the assumption of a linear temperature gradient across the film is made

$$t = t_o + \frac{y}{\delta}\theta$$

and the temperature gradient at the condensing surface becomes:-

$$\left[\frac{dt}{dy}\right]_{y=o} = \frac{\theta}{\delta}$$

Thus the energy equation becomes:-

$$\pi Dk\frac{\theta}{\delta}\Delta x = \rho\frac{d}{dx}\left[1\int_o^\delta \pi Du\ dy\right]\Delta x + \rho\frac{d}{dx}\left[\int_o^\delta \pi Duc\theta(1-\frac{y}{\delta})\ dy\right]\Delta x \quad \ldots\ldots (3.2.24)$$

The right hand side of equation (3.2.24) may be integrated for constant x and simplified to give:-

$$D\frac{\theta}{\delta} = \frac{\rho^2}{3\mu}(1 + \tfrac{3}{8}c\theta)\frac{d}{dx}(D a \delta^3) \quad \ldots\ldots (3.2.25)$$

Completing the differentiation of the right hand side gives:-

$$Dk\frac{\theta}{\delta} = \frac{\rho^2}{3\mu}(1 + \tfrac{3}{8}c\theta)\left[3Da\delta^2\frac{d\delta}{dx} + D\delta^3\frac{da}{dx} + a\delta^3\frac{dD}{dx}\right]$$

which simplifies to give

$$a\delta^3\frac{d\delta}{dx} + \frac{\delta^4}{3}\left[\frac{da}{dx} + \frac{a}{D}\frac{dD}{dx}\right] = \frac{c\theta\nu^2}{Pr(1 + \frac{3}{8}c\theta)} \quad \ldots\ldots (3.2.26)$$

Where the group of fluid properties

$\frac{\mu k \theta}{\rho^2}$ has been written as $\frac{c \theta \nu^2}{Pr (1 + \frac{3}{8} c \theta)}$

The preceding analysis has shown that the governing equation for the film thickness on the curved body is the same as that derived for the cone.

Equation (3.2.13)is used to obtain

$$\frac{da}{dx} = \tfrac{1}{2}\omega^2 Sin\alpha \frac{dD}{dx} + (\tfrac{1}{2}D\omega^2 Cos\alpha - gSin\alpha) \frac{d\alpha}{dx} \qquad \ldots\ldots\ldots (3.2.27)$$

where $\frac{dD}{dx}$ and $\frac{d\alpha}{dx}$ are given by equations (3.2.8) and (3.2.12) respectively.

Although the acceleration in the Y direction a_y, has been neglected for the reason already stated, this acceleration has appeared on the right hand side of equation (3.2.27) after differentiating acceleration a with respect to the changing angle α. Acceleration ay is accompanied by the multiplier $\frac{d\alpha}{dx}$ which is by definition the local radius of curvature of the generator curve. The average curvature of a small arc on any curve is defined as the rate of turning of the tangent to the arc with respect to the length of arc, or as

$$\text{curvature} = \frac{\Delta\alpha}{\Delta x}$$

In the limit as Δ approaches zero, the curvature at a point on the curve becomes

$$\text{curvature} = \frac{d\alpha}{dx}$$

which is expressed for any curve in terms of the co-ordinates η and ξ by equation (3.2.12). The local radius of curvature at a point on the curve is by definition equal to the reciprocal of the curvature, therefore

$$\frac{d\alpha}{dx} \equiv \frac{1}{r}$$

3.3 Analytical solutions for equation (3.1.15)

Equation (3.1.15) for cones where the apex angle is uniform with x has the form

$$a \quad \delta^3 \frac{d\delta}{dx} + \frac{\delta^4}{3}\left[\frac{da}{dx} + \frac{a}{D}\frac{dD}{dx}\right] = \frac{c\,\theta\,\nu^2}{Pr\left[1 + \frac{3}{8}c\,\theta\right]}$$

Equation (3.1.15) does not appear to have a complete analytical solution for the general case because of the non-linear coefficients. However a partial analytical solution to the equation may be obtained by introducing a new variable v such that

$$\delta^4 = v\,x \qquad \ldots\ldots\ldots (3.3.1)$$

gives $$4\delta\frac{d\delta}{dx} = v + x\frac{dv}{dx} \qquad \ldots\ldots\ldots (3.3.2)$$

Substituting the new relationships for δ and for $\frac{d\delta}{dx}$ into equation (3.1.15) gives:-

$$\frac{dv}{dx} + v\left[\frac{1}{x} + \frac{4}{3}\left(\frac{\omega^2\,Sin^2\alpha}{a} + \frac{2\,Sin\alpha}{D}\right)\right] = \frac{4}{a}H \qquad \ldots\ldots\ldots (3.3.3)$$

where $$H = \frac{c\,\theta\,\nu^2}{Pr\,(1 + \frac{3}{8}c\,\theta)}$$

The integrating factor for (3.3.3) becomes:-

$$I.F. = x\,a^{4/3}\,D^{4/3} \qquad \ldots\ldots\ldots (3.3.4)$$

and equation (3.3.3) reduces to

$$\frac{d}{dx}\left(x\,a^{4/3}\,D^{4/3}\,v\right) = 4\,H\,a^{1/3}\,D^{4/3}$$

or $$\delta^4\,a^{4/3}\,D^{4/3} = 4\,H\int a^{1/3}\,D^{4/3}\,dx \qquad \ldots (3.3.5)$$

where $$x\,v = \delta^4$$

A numerical method must be used to evalute the integral on the right hand side of equation (3.3.5) except where certain

simplifying assumptions can be made.

Consider one of the extreme conditions of rotation where the film drainage is dominated by centrifugal acceleration, such that $\frac{1}{2}(d + 2 \times \mathrm{Sin}\alpha)\omega^2 \mathrm{Sin}\alpha$ is much greater than $g \mathrm{Cos}\alpha$. Then equation (3.3.5) reduces to:-

$$\delta^4 \, 2^{\frac{4}{3}} \, (d+2x\mathrm{Sin}\,)^{\frac{8}{3}} (\omega^2 \mathrm{Sin}\alpha)^{\frac{4}{3}} = 4H \int 2^{\frac{1}{3}} (d+2x\mathrm{Sin}\alpha)^{\frac{5}{3}} (\omega^2 \mathrm{Sin}\alpha)^{\frac{1}{3}} dx \quad \ldots\ldots\ldots (3.3.6)$$

The right hand side can be integrated. If the film starts at cone diameter d, then $x = 0$ at d and $\delta = 0$ at $x = 0$. Using these limits to evaluate the constant of integration gives an equation in terms of the film thickness

$$\delta^4 = \frac{3}{2} \frac{H}{\omega^2 \mathrm{Sin}^2\alpha} \left[\frac{(d + 2 \times \mathrm{Sin}\alpha)^{8/3} - d^{8/3}}{(d + 2 \times \mathrm{Sin}\alpha)^{8/3}} \right] \quad \ldots\ldots\ldots (3.3.7)$$

This equation applies to the condition of zero gravitational acceleration which was considered by Sparrow et al. When the condensate film starts at the apex, $d = 0$ and equation (3.3.7) reduces to

$$\delta = 1.1068 \left[\frac{k \theta \mu}{l \rho^2 \omega^2 \mathrm{Sin}^2\alpha} \right]^{\frac{1}{4}} \quad \ldots\ldots\ldots (3.3.8)$$

where under-cooling has been neglected.

$$h = 0.904 \left[\frac{k^3 l \rho^2 \omega^2}{\theta \mu} \right]^{\frac{1}{4}} (\mathrm{Sin}\alpha)^{\frac{1}{2}} \quad \ldots\ldots (3.3.9)$$

These equations for δ and for h agree with those given by Sparrow and Hartnett (68) for thin films on rotating cones in the absence on gravity. Making the apex angle $2\alpha = 180^\circ$ reduces the two equations to those given by Sparrow and Gregg (49) for thin films on rotating discs. Under such conditions

the condensate film remains uniform with x, but when the film starts at some distance away from the apex, the film thickness and the heat transfer coefficient become dependent on both d and x.

Consider the other extreme condition of rotation where the cone is stationary. Equation (3.3.5) reduces to

$$\delta^4 (g\mathrm{Cos}\alpha)^{1/3} (d+2x\mathrm{Sin}\alpha)^{4/3} = 4H \int (g\mathrm{Cos}\alpha)^{1/3} (d+2x\mathrm{Sin}\alpha)^{4/3} dx \quad \ldots\ldots\ldots (3.3.10)$$

and the right hand side can be integrated. Introducing the boundary conditions, $x = 0$ at cone diameter d, and $\delta = 0$ at $x = 0$, enables the constant of integration to be evaluated and equation (3.3.10) reduces to

$$\delta^4 = \frac{6}{7} \frac{H}{g\ \mathrm{Cos}\alpha\ \mathrm{Sin}\alpha} \left[\frac{(d + 2\ x\ \mathrm{Sin}\alpha)^{7/3} - d^{7/3}}{(d + 2\ x\ \mathrm{Sin}\alpha)^{4/3}} \right] \quad \ldots\ldots\ldots (3.3.11)$$

If under-cooling is neglected and the film starts at the apex where $d = 0$

$$\delta = 1.1442 \left[\frac{k\ \theta\ \mu\ x}{l\ \rho^2\ g\ \mathrm{Cos}\alpha} \right]^{1/4} \quad \ldots\ldots\ldots (3.3.12)$$

and

$$h = 0.8739 \left[\frac{k^3\ l\ \rho^2\ g\ \mathrm{Cos}\alpha}{\theta\ \mu\ x} \right]^{1/4} \quad \ldots\ldots\ldots (3.3.13)$$

These two equations agree with those given by Dhir and Leinhard (37) for stationary cones. As the apex angle approaches zero, the cone is almost reduced to a line, for which the thin film approximation is violated and equations (3.3.12) and (3.3.13) become invalid.

Returning to equation (3.3.11) it can be shown that when the apex angle of the truncated cone approaches 0^o; that is for condensate films on a vertical cylinder wall

$$\delta^4 = 4\ H\ \frac{x}{g}$$

or $$\delta = 1.414 \left[\frac{k \theta \mu x}{l \rho^2 g} \right]^{\frac{1}{4}} \quad \ldots\ldots\ldots (3.3.14)$$

and $$h = 0.707 \left[\frac{k^3 l \rho^2 g}{\theta \mu x} \right]^{\frac{1}{4}} \quad \ldots\ldots\ldots (3.3.15)$$

These two equations agree with those given by Nusselt for thin films of condensate on plane vertical surfaces.

Although equation (3.1.15) cannot be solved completely, the partial solution is interesting because it shows that the integral is only a function of two terms, (i) the combined gravitational and centrifugal accelerations resolved in the X direction and (ii) the cone diameter. Thus it can be seen that the complete equation for the film thickness will have a similar form to that given by Nusselt and others, but with an additional multiplier which is a function of the resolved accelerations and the cone diameter

$$\delta = \left[\frac{4k\theta\mu}{l\rho^2} \right]^{\frac{1}{4}} \left[\frac{\int (a^{1/3} D^{4/3}) \, dx}{a^{4/3} D^{4/3}} \right]$$

The integral needs separate numerical solutions for intermediate conditions of rotation between zero and high speed, but this numerical solution is not difficult to achieve. However, very recently Professor H. Marsh has shown that by reducing equation (3.1.15) to a dimensionless form, only one numerical integration is required to cover all intermediate conditions of rotation. This solution is given in appendix A. Equation (3.1.15) may also be used within the limits of the thin film approximation for variable steam to surface temperature differences. The experimental temperature distribution along the outer surface will be used in equation (3.1.15) to calculate the theoretical laminar film thickness

and the theoretical heat transfer coefficient for the test conditions. A comparison may then be made between the theoretical and the experimental heat transfer coefficients. Therefore a numerical solution to equation (3.1.15) would also assist the introduction of the variable temperature difference.

A solution of equation (3.2.26) for bodies with curved generators will almost certainly have to be obtained numerically, since most curves do not furnish simple equations for the angle α in terms of the distance along the curve x.

In the next section a method of numerical integration, which enables equations (3.1.15) and (3.2.26) to be solved in their complete and unsimplified forms, is developed.

3.4 A numerical solution of the governing equations for film thickness.

The equations governing the film thickness on both rotating cones and on bodies with curved generators have the same general form. Because of this, the numerical method given in this section is applicable to both equations. The governing equation, which is a first order differential equation, should first be rearranged to give:-

$$\frac{d\delta}{dx} = \frac{H - \frac{\delta^4}{3}\left[\frac{a}{D}\frac{dD}{dx} + \frac{da}{dx}\right]}{\delta^3 a} \qquad \ldots\ldots\ldots (3.4.1)$$

This is the form required for the numerical solution, which integrates along the slope $\frac{d\delta}{dx}$ from the starting point of the film, to produce a curve of film thickness against the distance from the starting point x.

The numerical solution for equation (3.4.1) in the general case, (see section 3.1.8), presents one major problem. At the starting point of condensation the equation exhibits a singularity, which means that at that point, the film thickness is zero and the slope $\frac{d\delta}{dx}$ is infinite. Clearly numerical integration cannot proceed under this handicap, therefore the film thickness at the starting point of condensation must be given a very small but finite value. An initial value of 10^{-12} m was used by the author. This, together with the author's logarithmic system for specifying the integration interval (shown in fig. 7) permitted the governing equation to be solved using the Milne fifth-order variable step predictor-corrector method of numerical integration, in conjunction with the IBM Continuous System Modelling Program (C.S.M.P.) The computer program was run

FIG 7

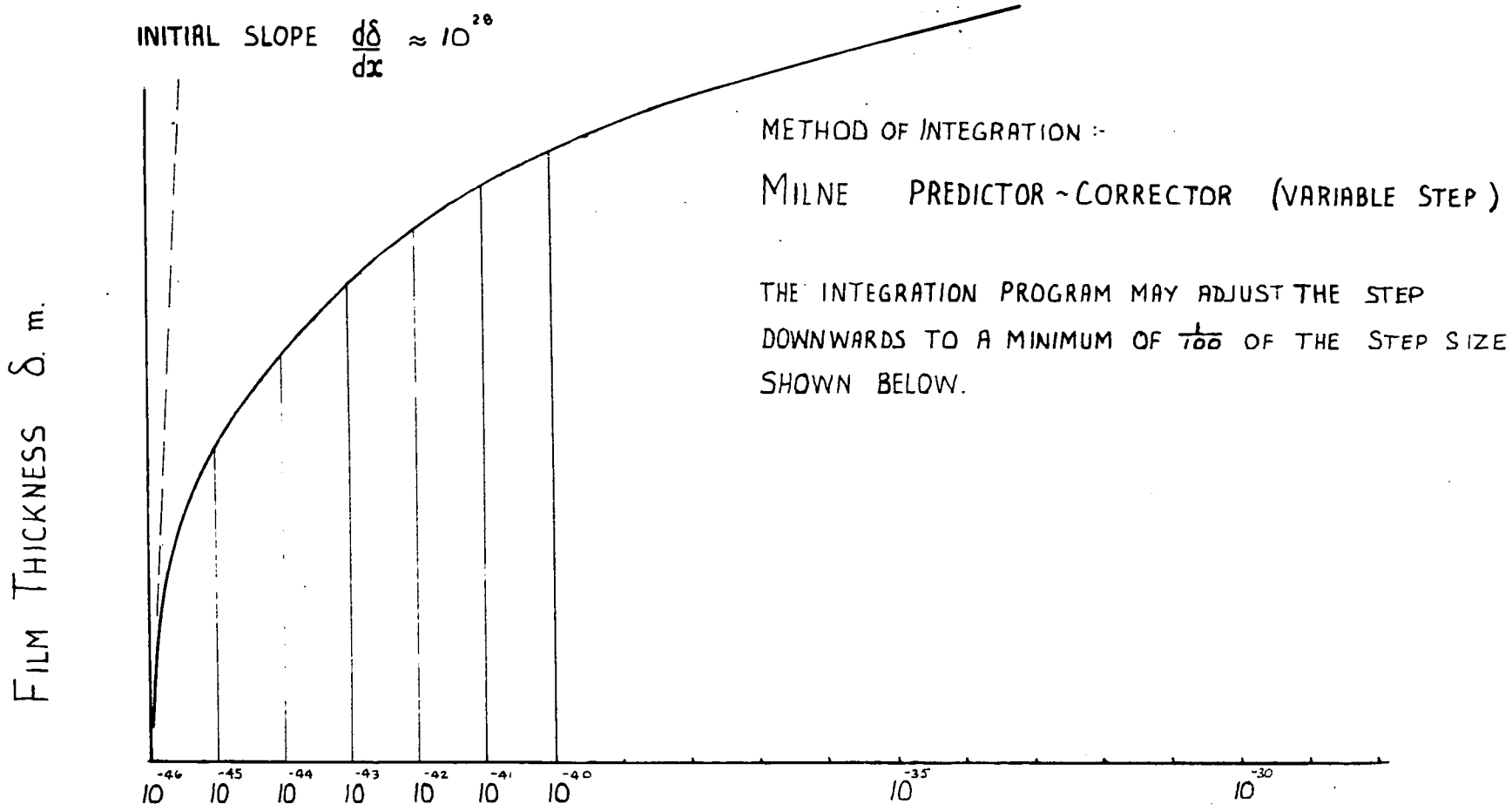

METHOD OF INTEGRATION :-

MILNE PREDICTOR - CORRECTOR (VARIABLE STEP)

THE INTEGRATION PROGRAM MAY ADJUST THE STEP DOWNWARDS TO A MINIMUM OF $\frac{1}{100}$ OF THE STEP SIZE SHOWN BELOW.

on an IBM 360/67 digital computer.

The use of the logarithmic system for specifying the integration interval is essential because of the very large slope of $\frac{d\delta}{dx}$ which can be in the order of 10^{28} at the starting point of condensation. With the logarithmic system, integration commences at intervals of 10^{-46} m for the first ten integration steps; the next ten steps have an interval of 10^{-45} m: the next ten steps have an interval of 10^{-44} m and so on. By using this system the integration interval increases as the slope $\frac{d\delta}{dx}$ decreases. Thus it is possible to achieve extremely accurate integration with less than 500 steps, because the majority of the steps are confined to that part of the curve where the slope $\frac{d\delta}{dx}$ undergoes its most rapid rate of change with x.

Because the numerical integration starts at such a large slope $\frac{d\delta}{dx}$, it is necessary to provide a check for the values of film thickness at distances away from the singularity. For certain conditions of rotation and apex angle, exact values of film thickness may be obtained from the analytical solutions given in section (3.3). It is convenient to use these exact values of film thickness to provide an accurate standard against which the values obtained from the numerical solution can be compared.

Fig. 8 shows the film thickness given by the numerical solution of the governing equation for a disc rotating at 100 rev./min. The condensate film is assumed to start at the centre of the disc, the Prandtl number for the condensate is 1.37 and the steam to disc surface temperature difference is 10° C. Also shown on fig. 8 is the film thickness, given

FIG 8

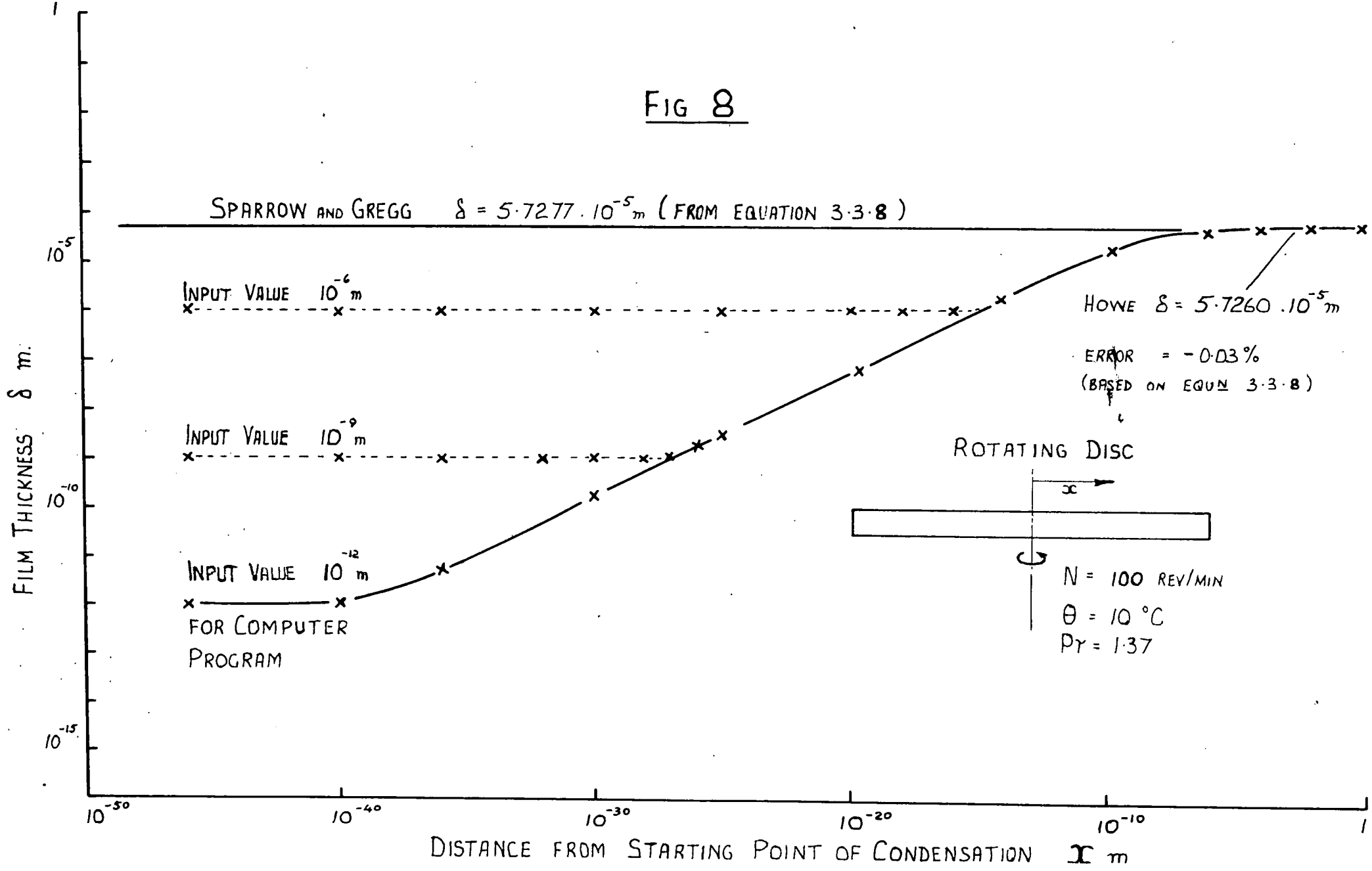
SPARROW AND GREGG $\delta = 5{\cdot}7277 \cdot 10^{-5}$ m (FROM EQUATION 3·3·8)
INPUT VALUE 10^{-6} m
INPUT VALUE 10^{-9} m
INPUT VALUE 10^{-12} m
FOR COMPUTER PROGRAM
HOWE $\delta = 5{\cdot}7260 \cdot 10^{-5}$ m
ERROR = −0·03%
(BASED ON EQUN 3·3·8)
ROTATING DISC
x
N = 100 REV/MIN
θ = 10 °C
Pr = 1·37
FILM THICKNESS δ m.
1
10^{-5}
10^{-10}
10^{-15}
10^{-50}
10^{-40}
10^{-30}
10^{-20}
10^{-10}
1
DISTANCE FROM STARTING POINT OF CONDENSATION x m

by the analytical solution for a rotating disc with the same film conditions. At a point approximately 10^{-6} m from the starting point of condensation, the computed values of the film thickness converge and thereafter remain almost the same as the analytical values to within an error of less than - 0.03% based on the latter values.

Other initial values for the film thickness of 10^{-6} m or 10^{-9} m could also be used for starting the numerical integration (see fig. 8). If the initial logarithmic step intervals are set to 10^{-30} m and 10^{-20} m respectively, the same value of film thickness is obtained. The much lower initial film thickness of 10^{-12} m used by the author, ensured that the film thicknesses calculated for a wide range of conditions were not adversely affected by the initial value.

The experimental temperature distribution along the outer surface of the cone is to be used in the numerical solution of the governing equation to give theoretical values of the film thickness and of the heat transfer coefficients for the test conditions. Therefore it is essential that the numerical integration procedure remains stable when the temperature difference changes the first term in the numerator on the right hand side of equation (3.4.1). Increasing the temperature difference will cause an immediate increase in slope $\frac{d\delta}{dx}$ and a decrease in the temperature difference will have the reverse effect.

A second test for stability in the numerical solution was made by introducing a step change in the temperature difference. A 60° cone rotating at 100 rev/min was chosen for the solution. Fig. 9 shows the effect on film thickness,

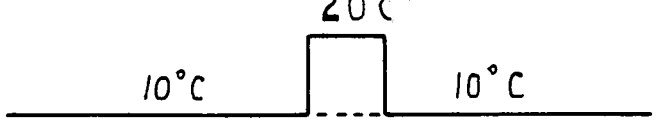

FILM TEMPERATURE DIFFERENCE θ °C

FIG 9

$2\alpha = 60°$

N = 100 REV/MIN

UNIFORM θ - - - - -

STEP CHANGE θ ——

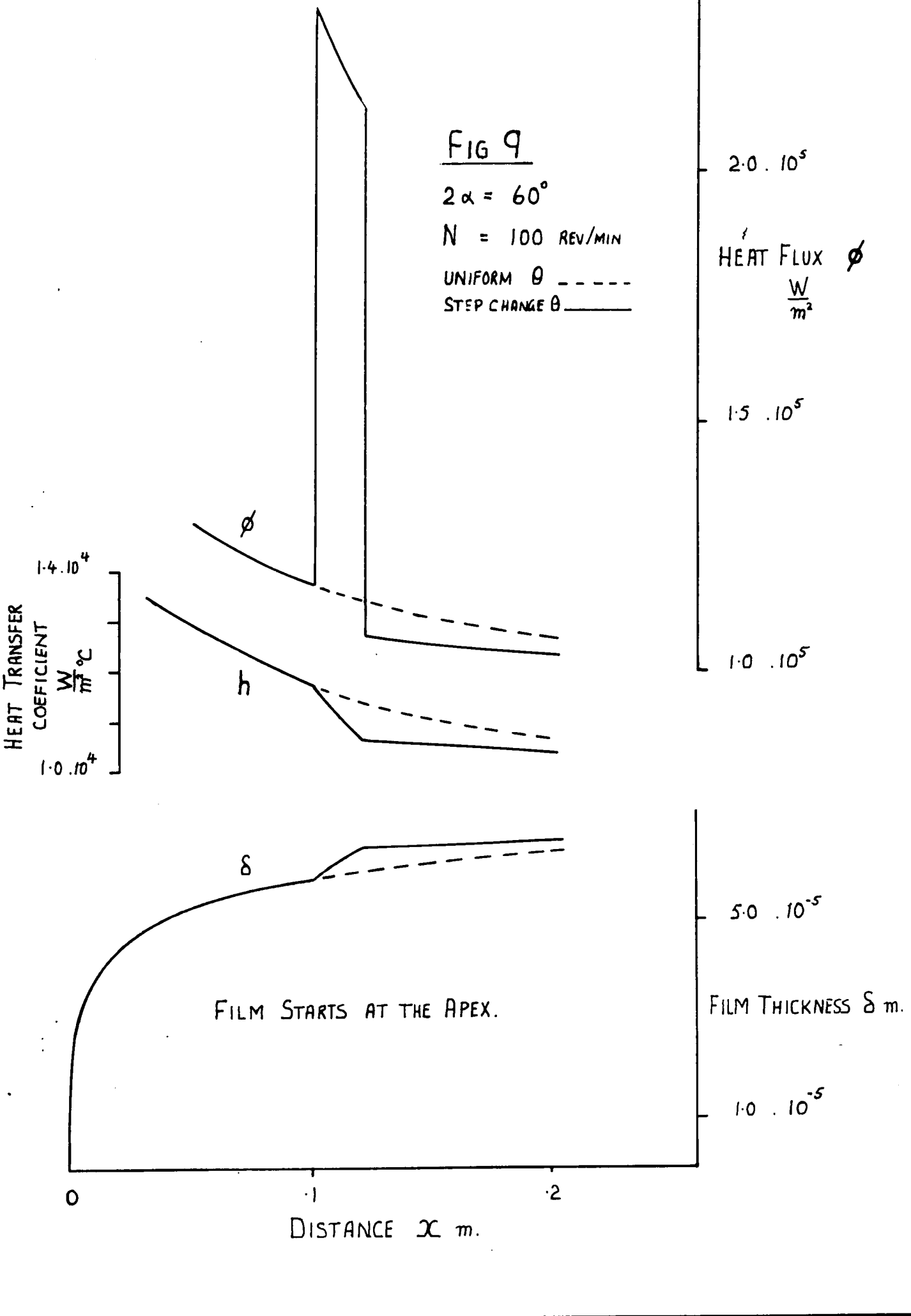

heat flux and heat transfer coefficient, of a step increase in temperature difference from 10^{o} C to 20^{o} C between x = 0.1 m and x = .12 m. The dotted lines indicate values for a completely uniform temperature distribution of 10^{o} C. The sudden increase in slope $\frac{d\delta}{dx}$ caused by the step change in temperature difference, produces sharp changes in the film thickness. These changes in film thickness are clean and free from spurious fluctuations which could occur with an unstable numerical method of integration. At a later stage when the experimental temperature differences, which will not be absolutely uniform, are used to calculate theoretical heat transfer coefficients etc., it will be difficult to visualise what is happening to the condensate film. To this end the curves in fig. 9 merit some further consideration, because they illustrate what happens to the film and to the energy transfer when a simple change in temperature difference occurs.

The immediate effect of the stepped increase in temperature difference is to double the heat flux. The extra energy transfer causes an increase in the condensation rate and the film starts to grow more rapidly. At the position where the temperature difference is restored to 10^{o}, the film thickness has increased by only 6.5%. This extra condensate quickly spreads out as the film moves down the surface of the cone, and becomes a small addition to the steady state film which is indicated by the dotted line. Restoring the temperature difference to 10^{o} C immediately reduces the heat flux by half, but the new value lies below the steady state value (dotted line). This occurs because the condensate

deposited during the stepped increase in temperature difference now becomes an extra barrier to further energy transfer.

The curve for the heat transfer coefficient reflects in a reverse sense, the movement in the curve for the film thickness. An important point to notice about the three curves is that both the film thickness and the heat transfer coefficient remain relatively unaffected by doubling the temperature difference when compared to the heat flux, which is shown to be very sensitive to changes in temperature difference. This result has some bearing at a later stage when the theoretical values of heat flux and of heat transfer coefficient are compared with the experimental values. These two tests for the stability of the numerical method for solving the governing equations have demonstrated that the method is stable and capable of accurately negotiating regions in the film where the slope $\frac{d\delta}{dx}$ is subjected to rapid rates of change.

3.5 The effect of rotation on heat transfer coefficient.

In the preceding pages it has been shown that none of the available analytical equations take into account the combined effects of both gravitational and centrifugal accelerations during the calculation of the heat transfer coefficient for steam condensing on rotating cones.

However, after establishing confidence in both the validity of the governing equation (3.1.15) and in the accuracy of the method of numerical integration, it was possible to apply the complete form of the equation to the problem of film condensation on rotating cones with the certainty that meaningful results would be obtained. Thus a theoretical study of the combined effects of gravitational and centrifugal accelerations on the film thickness and on the heat transfer coefficient was made.

The governing equation was integrated numerically to give values of film thickness and of heat transfer coefficient for condensate films starting at the apex on cones with apex angles of 0^{o}, 10^{o}, 60^{o}, 120^{o}, 170^{o} and 180^{o}. Each cone was given speeds of rotation which increased by orders of magnitude from 0 to 10, 100, 1000, and 10,000 rev/min. The calculations were made for uniform steam to surface temperature differences of 1, 10 and 100^{o} C. For the sake of clarity only the heat transfer coefficients resulting from the calculations will be presented and discussed. Bearing in mind the remarks made in the latter part of section (3.4), concerning the relationship between the curves for the heat transfer coefficient and film thickness, the behaviour of the film thickness can also be detected from the curves which follow.

By changing only the temperature difference θ, it was found that the heat transfer coefficient was a function of $\left(\frac{1}{\theta}\right)^{\frac{1}{4}}$, which corresponded to the dependence on θ given by the analytical solutions for the governing equation (section 3.3).

Figs. 10, 11 and 12 show the theoretical heat transfer coefficients for cones with apex angles of 10^{o}, 60^{o} and 170^{o} respectively. The heat transfer coefficients are plotted against the distance from the starting point of condensation x for several values of speed N rev/min and for a common value of temperature difference $\theta = 10^{o}$ C. The curves on figs. 10, 11 and 12 show that for the stationary cones the heat transfer coefficient is a function of $\left(\frac{1}{x}\right)^{\frac{1}{4}}$ and has the largest values on the cone with the smallest apex angle. Stationary cones with small apex angles have the benefit of a proportionately large component of gravitational acceleration resolved parallel to their surface, that is in the X direction, to assist drainage and hence to improve heat transfer. But the small apex angle also means that the component of the centrifugal acceleration resolved in the X direction remain relatively small until high speeds are attained.

Generally speaking, the curves show that the heat transfer coefficient h becomes less dependent on x as the speed increases. The position at which h becomes independent of x depends upon a combination of speed and apex angle. Cones with large apex angles have correspondingly large components of the centrifugal acceleration resolved in the X direction. Since the magnitude of this acceleration increases with the square of the speed, the benefit to film drainage is such that h can become independent of x at very short distances from the starting

FIG 10

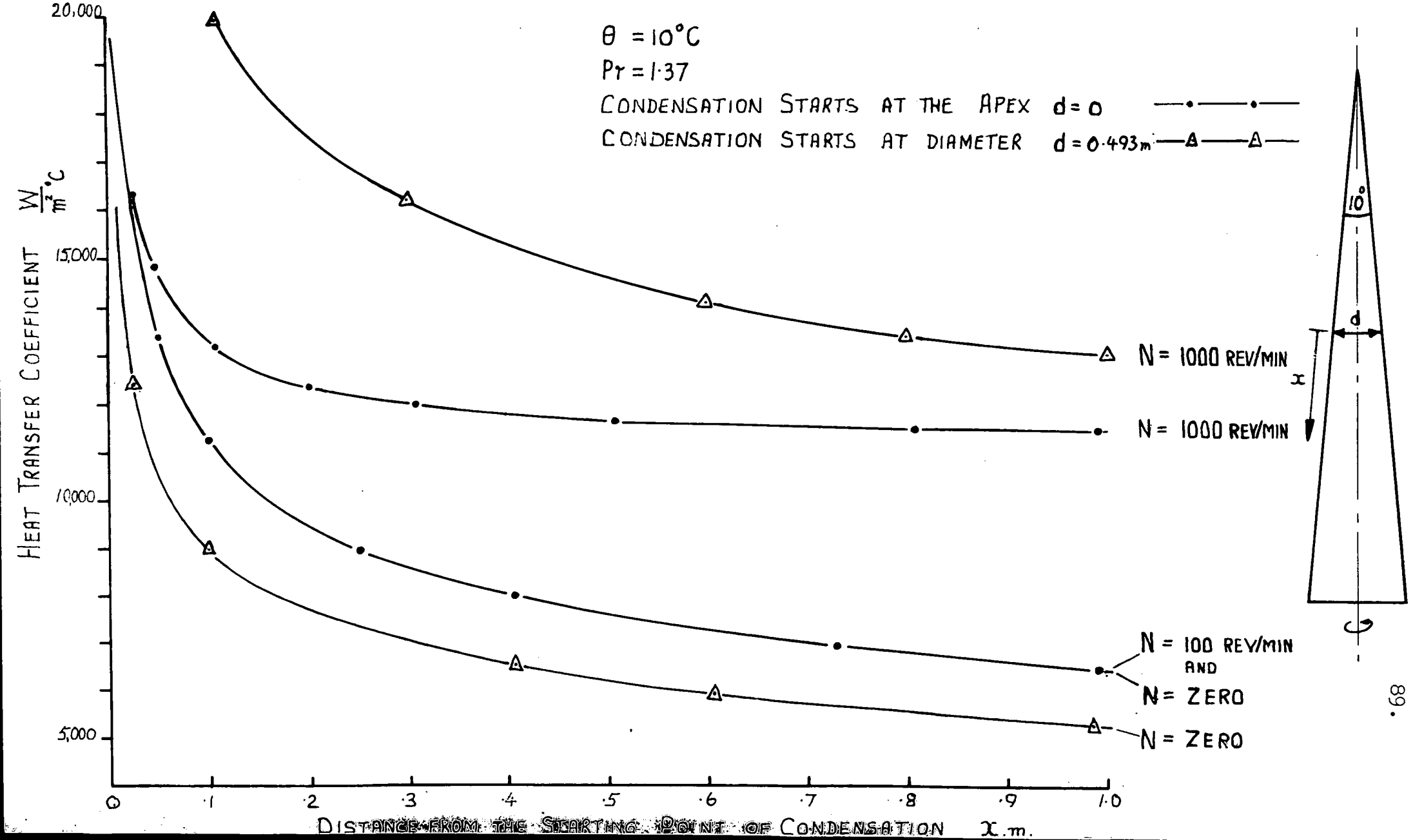
θ = 10°C
Pr = 1·37
CONDENSATION STARTS AT THE APEX d = 0
CONDENSATION STARTS AT DIAMETER d = 0·493m
N = 1000 REV/MIN
N = 1000 REV/MIN
N = 100 REV/MIN AND N = ZERO
N = ZERO
HEAT TRANSFER COEFFICIENT W/m²°C
20,000
15,000
10,000
5,000
0
·1
·2
·3
·4
·5
·6
·7
·8
·9
1·0
DISTANCE FROM THE STARTING POINT OF CONDENSATION x.m.
10°
d
x

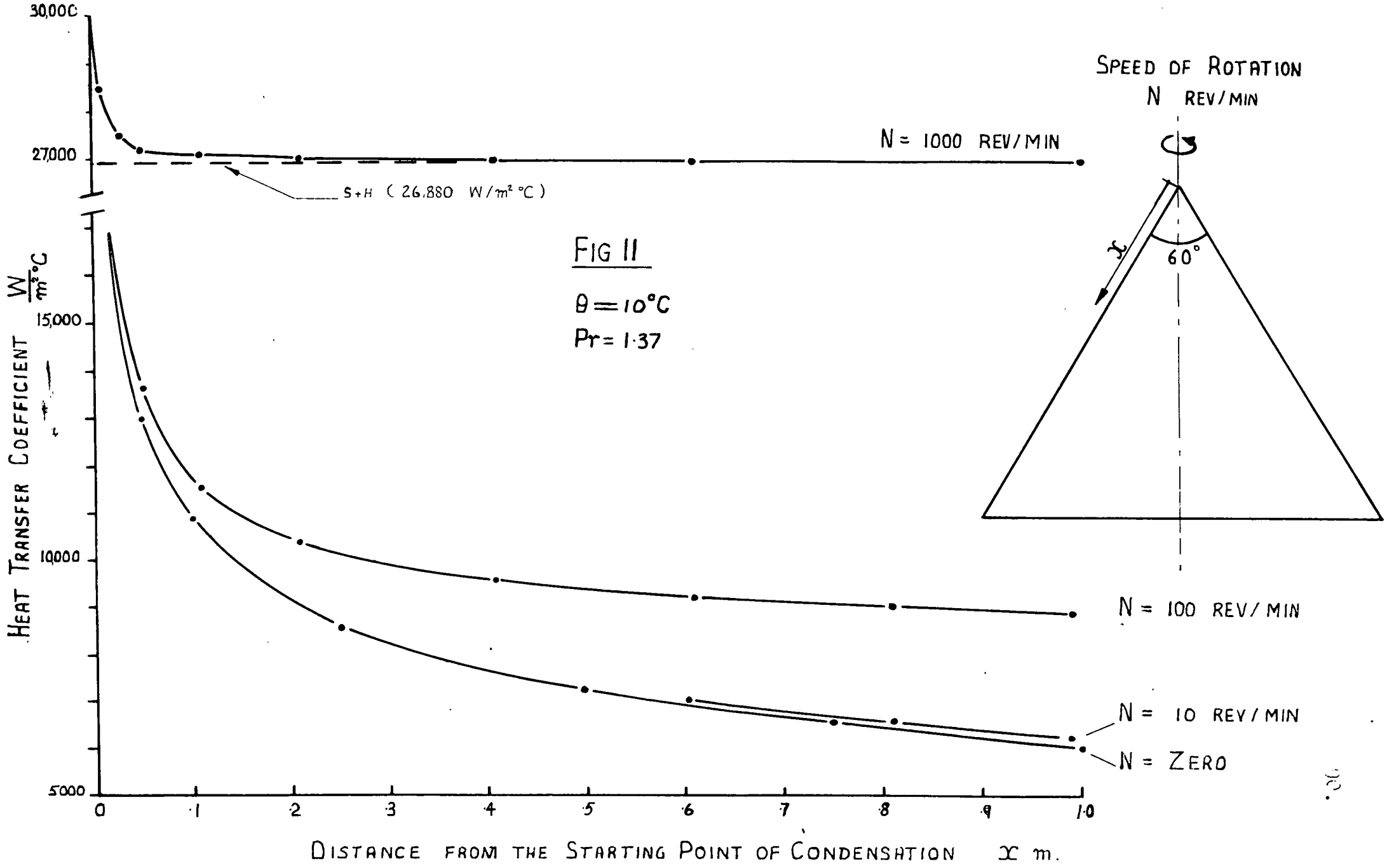
30,000
27,000
N = 1000 REV/MIN
S+H (26,880 W/m² °C)
SPEED OF ROTATION
N REV/MIN
x
60°
θ = 10°C
Pr = 1·37
HEAT TRANSFER COEFFICIENT W/m²°C
15,000
10,000
5000
N = 100 REV/MIN
N = 10 REV/MIN
N = ZERO
0
·1
·2
·3
·4
·5
·6
·7
·8
·9
1·0
DISTANCE FROM THE STARTING POINT OF CONDENSATION x m.

FIG 11

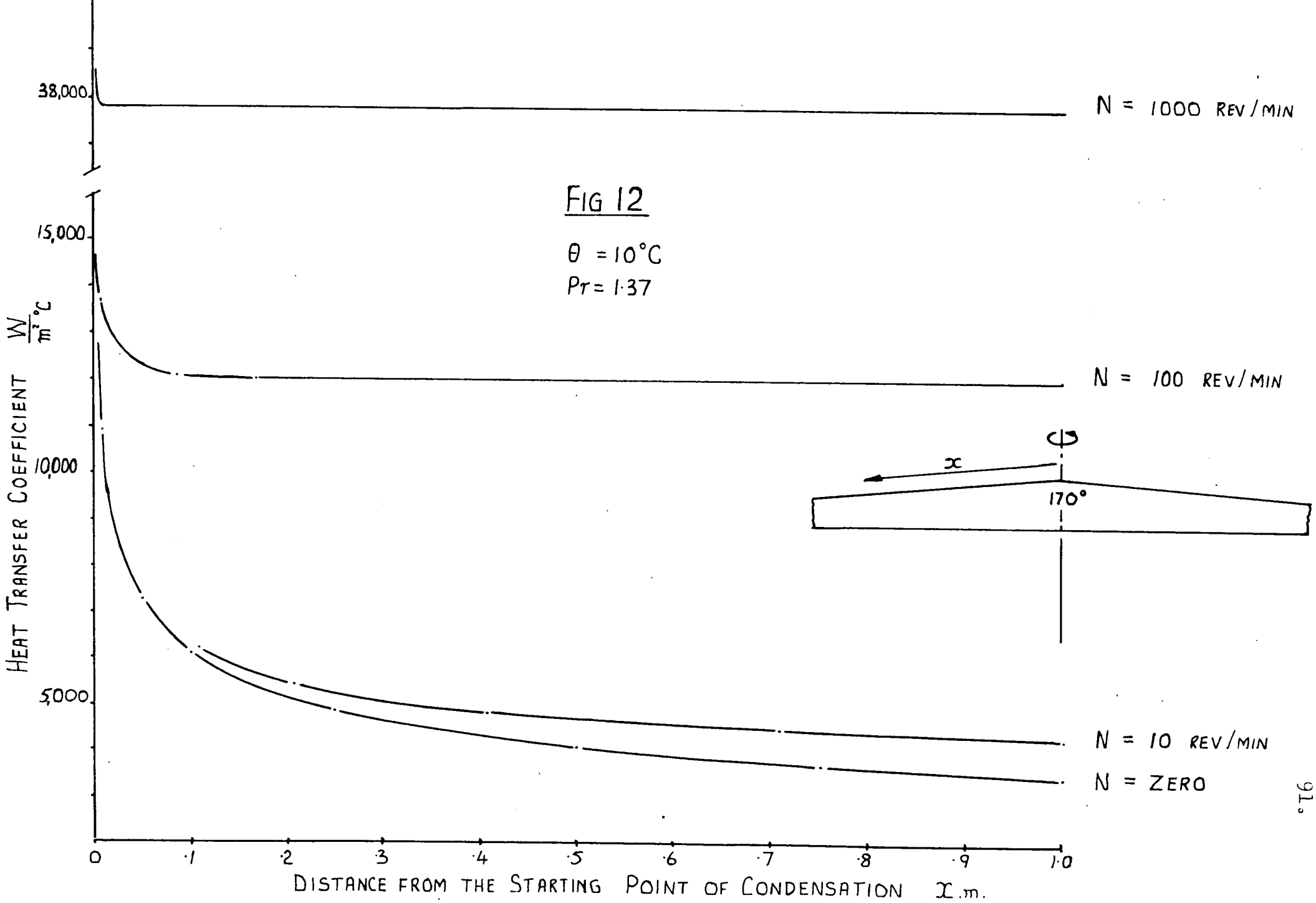

FIG 12

$\theta = 10°C$

$Pr = 1{\cdot}37$

point of the film. It is in this region of uniform heat transfer coefficient, i.e. where the centrifugal acceleration dominates the film drainage, that the work by Sparrow et al is seen to apply.

The above points are illustrated by the curves for the 10^{o} and 170^{o} cones. Fig. 10 shows that for a 10^{o} cone at 1.0 m from the starting point of condensation, h increases from 6350 $\frac{W}{m^{2}{}^{o}C}$ at zero to 11500 $\frac{W}{m^{2}{}^{o}C}$ at 1000 rev/min. At this point the heat transfer coefficient is just starting to become independent of x. In contrast to this, fig. 12 shows that on the 170^{o} cone, at 1.0 m from the starting point of condensation, h has a lower value of 3400 $\frac{W}{m^{2}{}^{o}C}$ at zero but attains a value of 12,000 $\frac{W}{m^{2}{}^{o}C}$ at only 100 rev/min. Even at this comparatively low speed of rotation, h is uniform after the point x = 0.15 m.

For cones with apex angles of 20^{o} and less it is more appropriate to the present work to consider condensation heat transfer on truncated cones. The curves for the heat transfer coefficient on a truncated cone with a 10^{o} apex angle are also shown in fig. 10. The condensate film on the truncated cone starts at a diameter d = 0.493 m, which is also the starting point of the film on the experimental 10^{o} truncated cone. At zero speed the heat transfer coefficient is seen to be less than that obtained for a film starting at the apex. This condition was predicted in section (3.1.8). For any given finite speed of rotation, the film starting at some

point away from the apex has the advantage of forming in a region where larger centrigual accelerations exist to improve drainage. At 1000 rev/min, the curve for the truncated 10^{o} cone shows that there is an improvement in the heat transfer coefficient in comparison with the values given for the film starting at the apex.

To illustrate the effect of rotation on heat transfer in a more general way, the subscripts Z and N can be added to the heat transfer coefficients h to represent h at zero speed and h at some speed of rotation N respectively, for any given set of fluid properties and steam to surface temperature difference. Forming the ratio $\frac{h_N}{h_z}$ gives a new parameter which shows the improvement in heat transfer coefficient gained by rotation. Within the limits of the thin film approximation, this parameter has the added advantage of being independent of the fluid properties and of the steam to surface temperature difference. The parameter $\frac{h_N}{h_z}$ is used as the ordinate for the curves shown in figs.13, 14 and 15. Each of these three figs. present curves on log-log scales. The parameter $\frac{h_N}{h_z}$ may also be interpreted either as the ratio of the film thicknesses $\frac{\delta_z}{\delta_N}$ or as the ratio of the heat flux at speed N and at zero, $\frac{\phi_N}{\phi_z}$.

Fig.13 gives curves for the ratio $\frac{h_N}{h_z}$ against speed N rev/min. The ratio is taken at a distance of 0.5 m from the starting point of condensation for cones with apex angles of 10^{o}, 60^{o}, 120^{o} and 170^{o} and with films starting at the apex. These

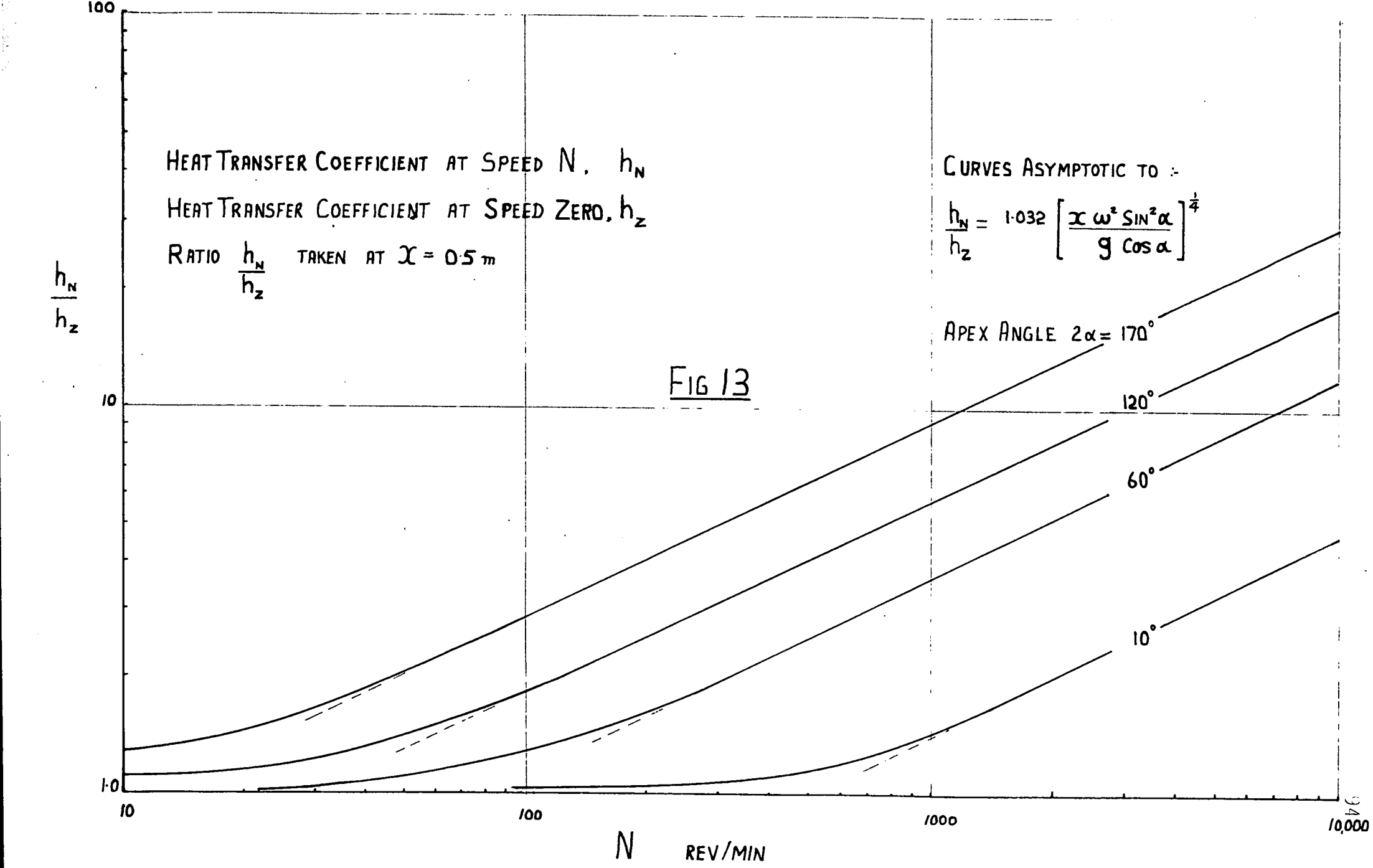
HEAT TRANSFER COEFFICIENT AT SPEED N, h_N
HEAT TRANSFER COEFFICIENT AT SPEED ZERO, h_z
RATIO $\frac{h_N}{h_z}$ TAKEN AT $x = 0.5\,m$
CURVES ASYMPTOTIC TO :-
$\frac{h_N}{h_z} = 1.032 \left[\frac{x\,\omega^2 \sin^2\alpha}{g \cos\alpha}\right]^{\frac{1}{4}}$
APEX ANGLE $2\alpha = 170°$
120°
60°
10°
$\frac{h_N}{h_z}$
100
10
1·0
10
100
1000
10,000
N REV/MIN

FIG 13

curves show the magnitude of the improvement in heat transfer coefficient for any given combination of apex angle and speed rotation. It should be noted that the position of these curves depends upon the value of x at which the ratio $\frac{h_N}{h_z}$ is taken. As x increases, the curves tend to be displaced diagonally from right to left. All of the curves in fig.13 have an origin at N = 0, and $\frac{h_N}{h_z} = 1.0$, and form smooth transition curves to become straight lines with a slope approaching 0.5 at higher speeds. In this region $\frac{h_N}{h_z}$ is a function of $N^{\frac{1}{2}}$ or $\omega^{\frac{1}{2}}$, which shows that the heat transfer is dominated by the centrifugal acceleration. When this occurs, the curves become asymptotic to the equations given by Sparrow and Hartnett (68). The equation for the asymptote becomes:-

$$\frac{h_N}{h_z} = 1.034 \left[\frac{x\omega^2 \, \mathrm{Sin}^2\alpha}{g \, \mathrm{Cos}\alpha} \right]^{\frac{1}{4}}$$

Although the term $\frac{x\omega^2 \, \mathrm{Sin}^2\alpha}{g \, \mathrm{Cos}\alpha}$ in the above equation is derived from $\omega^2 \, \mathrm{Sin}^2\alpha \div \frac{g \, \mathrm{Cos}\alpha}{x}$, the term may also be interpreted as the quotient of the centrifugal acceleration resolved in the X direction and the gravitational acceleration resolved in the X direction.

The curves given in fig.13 show that the cones with the larger apex angles gain the most rapid improvement in heat transfer with increases in speed. The curve for the 170° cone is very close to its asymptote at N = 80 rev/min, while the curve for the 10° cone needs speeds of over 1000 rev/min to become asymptotic. One of the experimental cones has an

apex angle of 60^{o} and a working slant length of approximately 0.5 m. Looking at the 60^{o} curve on fig.13 shows that if the film on the experimental cone remains laminar, the heat transfer coefficient should show a 4.5 fold increase over the range of test speeds between zero and 1500 rev/min.

Fig. 14 shows the ratio $\frac{h_N}{h_z}$ for truncated cones with apex angles of 0^{o}, 10^{o} and 20^{o}. The film on each of these cones starts at diameter d = 0.493 m and the ratio of $\frac{h_N}{h_z}$ is taken at a distance from the starting point of x = 0.2 m. The curve for the 0^{o} cone or cylinder shows, as was expected, no change in heat transfer coefficient with increases in speed. The curve for the 10^{o} truncated cone shows that although the improvement in heat transfer is more marked at any given speed, speeds approaching 1000 rev/min are still required before the transition curve becomes asymptotic.

Two of the experimental cones are truncated and have apex angles of 10^{o} and 20^{o}. The starting point of condensation on these cones is 0.493 m and 0.532 m respectively and each has a working slant length of approximately 0.2 m. Over the experimental speed range, these cones should show a 2 to 3 fold improvement in heat transfer coefficient providing that the film remains in laminar flow.

There is a similarity in the shape of the curves on fig. 13 and on fig.14, but for the latter curves the asymptotic equation takes a slightly different form because the condensate film starts at cone diameter d. Equation (3.3.7) and (3.3.11) give the equation for the asymptote for the curves on fig.14. The equation for the asymptote is:-

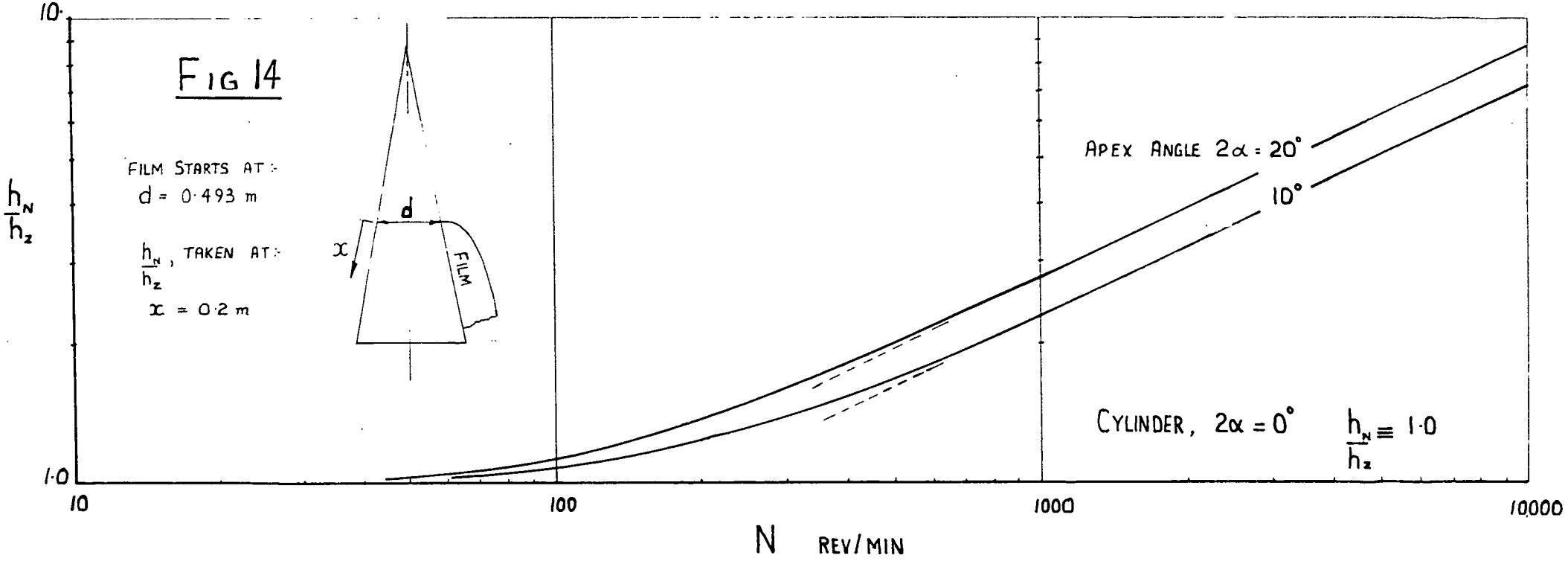
FIG 14
FILM STARTS AT :-
d = 0·493 m
$\frac{h_N}{h_z}$, TAKEN AT :-
x = 0·2 m
d
x
FILM
APEX ANGLE 2α = 20°
10°
CYLINDER, 2α = 0°
$\frac{h_N}{h_z} \equiv 1·0$
$\frac{h_N}{h_z}$
10·
1·0
10
100
1000
10000
N REV/MIN

$$\frac{h_N}{h_z} = \left\{ \frac{8}{7} \frac{D\omega^2 \sin\alpha}{2g\cos\alpha} \frac{D}{d} \right\}^{1/3} \left[\frac{\left(\frac{D}{d}\right)^{7/3} - 1}{\left(\frac{D}{d}\right)^{8/3} - 1} \right]^{\frac{1}{4}}$$

Where D is the cone diameter at the point x. The ratio of the centrifugal and gravitational acceleration, both resolved in the X direction, again appears in the equation for the asymptote, but with an additional term

$$\left\{ \frac{D}{d}^{1/3} \left[\frac{\left(\frac{D}{d}\right)^{7/3} - 1}{\left(\frac{D}{d}\right)^{8/3} - 1} \right]^{\frac{1}{4}} \right\}$$

As the ratio $\frac{D}{d}$ approaches 1.0, the above term reduces to 0.967 When $\frac{D}{d}$ exceeds a value of 2.0, the term approaches unity and reduces the asymptotic equation to that given for the curves in fig. 13, for which $\frac{D}{d}$ is always infinite.

The general similarity in the shape of the curves in figs. 13 and 14, coupled with the fact that both sets of curves have similar asymptotes makes it possible to plot the ratio $\frac{h_N}{h_z}$ for all values of x and for all speeds of rotation on two curves. One curve is for the special case where the film starts at the apex, and the second curve is for the film starting at some distance away from the apex. These curves are produced by using the term

$$\left[\frac{D\omega^2 \sin\alpha}{2g\cos\alpha} \right]^{\frac{1}{4}}$$

from the equation for the asymptotes, as the new abscissa. Fig.15 shows the two curves. The two curves differ only in the region of the transition from the low speed asymptote to the high speed asymptote. The upper curve is for cones where

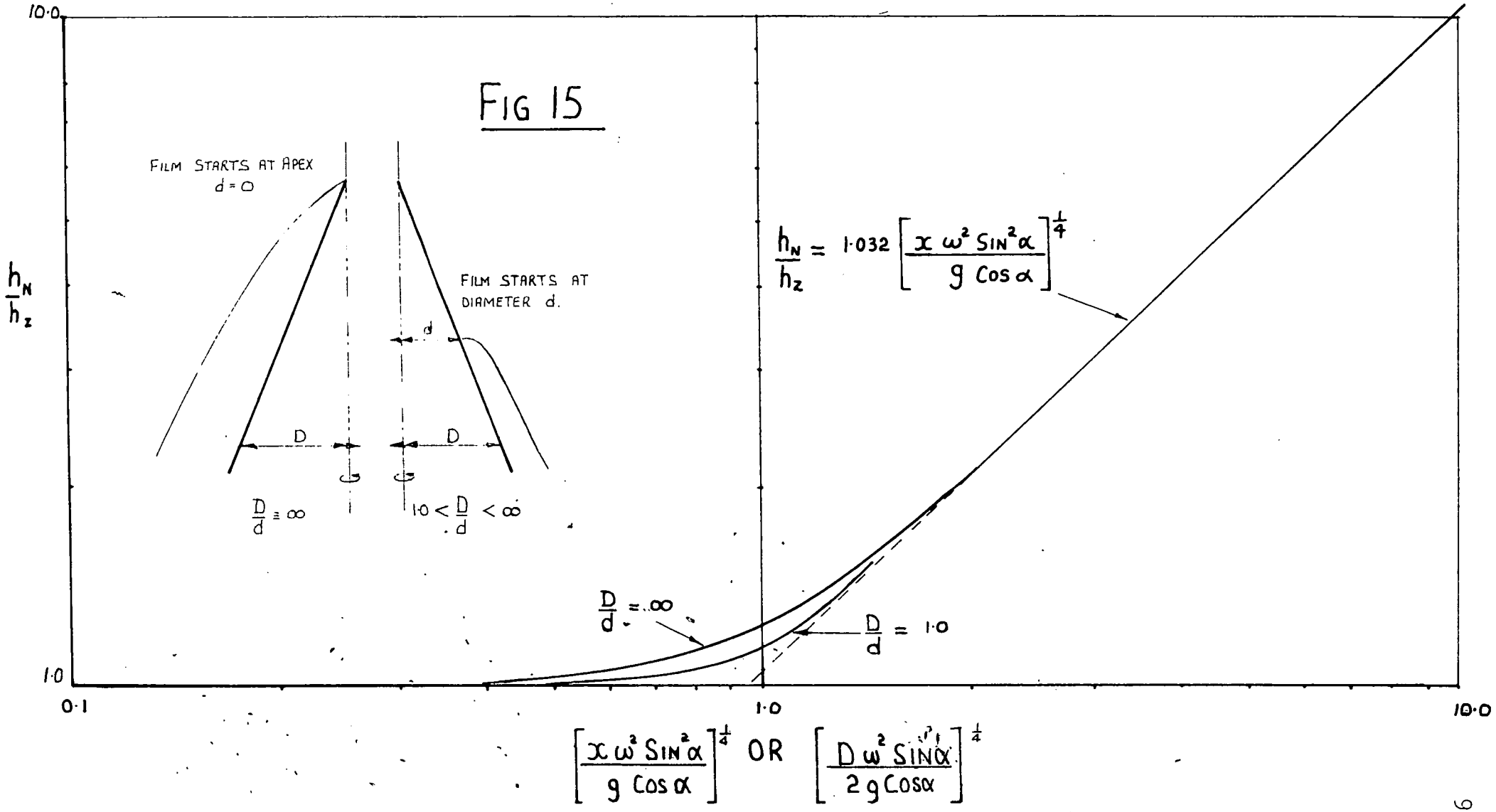
FIG 15
FILM STARTS AT APEX
d = 0
FILM STARTS AT
DIAMETER d.
D
D
d
D/d = ∞
1·0 < D/d < ∞
h_N/h_z = 1·032 [x ω² Sin²α / g Cos α]^¼
D/d = ∞
D/d = 1·0
10·0
1·0
0·1
1·0
10·0
h_N/h_z
[x ω² Sin²α / g Cos α]^¼ OR [D ω² Sinα / 2g Cosα]^¼

the condensate film starts at the apex, i.e. for the upper limit where the ratio $\frac{D}{d}$ is infinite. The lower curve is for the film starting at some cone diameter d where the ratio $\frac{D}{d}$ can attain the lower limit of unity. At any intermediate value of the ratio $\frac{D}{d}$, the transition curve will lie between these two.

The point where the transition curves intersect the asymptotes defines the two extreme conditions where either gravitational acceleration or centrifugal acceleration dominates the film drainage and the heat transfer. Both transition curves are very close to the high speed asymptote at

$$\left[\frac{D\omega^2 \ \mathrm{Sin}\alpha}{2 \ g \ \mathrm{Cos}\alpha}\right]^{\frac{1}{4}} = 2.0$$

The curve for $\frac{D}{d}$ = unity being the closer of the two. The ratio of the resolved accelerations $D\omega^2 \ \mathrm{Sin}\alpha : g \ \mathrm{Cos}\alpha$ is 16:1. Both curves are very close to the low speed asymptote at

$$\left[\frac{D\omega^2 \ \mathrm{Sin}\alpha}{2 \ g \ \mathrm{Cos}\alpha}\right]^{\frac{1}{4}} = .5$$

At this point the ratio of the resolved accelerations $D\omega^2 \ \mathrm{Sin}\alpha : g \ \mathrm{Cos}\alpha$ is 1 : 16. The relative magnitude of these two acceleration components has a wide range of variation between these extreme limits. It is over this intermediate range that the governing equation has the most value, because it furnishes the transition curve between the two extremes.

For the practical point of view, the upper transition curve shows that the maximum departure from either of the asymptotes only amounts to just over 20% when $\frac{D\omega^2 \ \mathrm{Sin}\alpha}{2} = g \ \mathrm{Cos}\alpha$.

When $\frac{D\omega^2 \sin\alpha}{2}$ is less than $g \cos\alpha$, the effect of rotation on heat transfer coefficient could be accounted for by adding a small correction to equation (3.3.13) which considers the film to be drained only by gravitational acceleration. Similarly when $\frac{D\omega^2 \sin\alpha}{2}$ is larger than $g \cos\alpha$, the effect of gravitational acceleration on heat transfer coefficient could be accounted for by adding a small correction to equation (3.3.9) which considers the film to be drained only by centrifugal acceleration.

3.6 The effect of cone apex angle on the heat transfer coefficient.

Since the experimental results from the present work will cover a range of cones with apex angles of 10^{o}, 20^{o} and 60^{o}, it would be relevant to make a comparison between the theoretical heat transfer coefficients for various cones. Where conditions of uniform film thickness occur, Sparrow and Hartnett (68) showed that providing all other variables remain constant, the heat transfer coefficient for a rotating cone should always be less than that for a rotating disc by the fraction $(\text{Sin } \alpha)^{\frac{1}{2}}$. It has been shown in the last section that conditions of uniform film thickness do not always exist therefore we shall reconsider the relationship between the heat transfer coefficients for cones and for discs in the light of the present theory.

Fig. 16 shows curves for the ratio $\frac{\text{h cone}}{\text{h disc}}$ against the speed of rotation N, on a log-log scale. The curves are for cones with apex angles of 0^{o}, 10^{o}, 60^{o}, 120^{o}, 170^{o} and 180^{o}; the latter being the disc. The ratio $\frac{\text{h cone}}{\text{h disc}}$ is taken at $x = 0.25$ m and the condensate film starts at the apex.

The curve for the disc is represented by the line $\frac{\text{h cone}}{\text{h disc}} = 1.0$. The curve for the cylinder or 0^{o} truncated cone has the equation $\frac{\text{h cyld}}{\text{h disc}} = .784 \left[\frac{g}{x\omega^{2}}\right]^{\frac{1}{4}}$ which is derived from equations (3.3.14) and (3.3.8). This curve retains its negative slope of -0.5 with increases in speed. At speeds below 100 rev/min, the family of curves tend to become dominated by gravitational acceleration. Each curve becomes

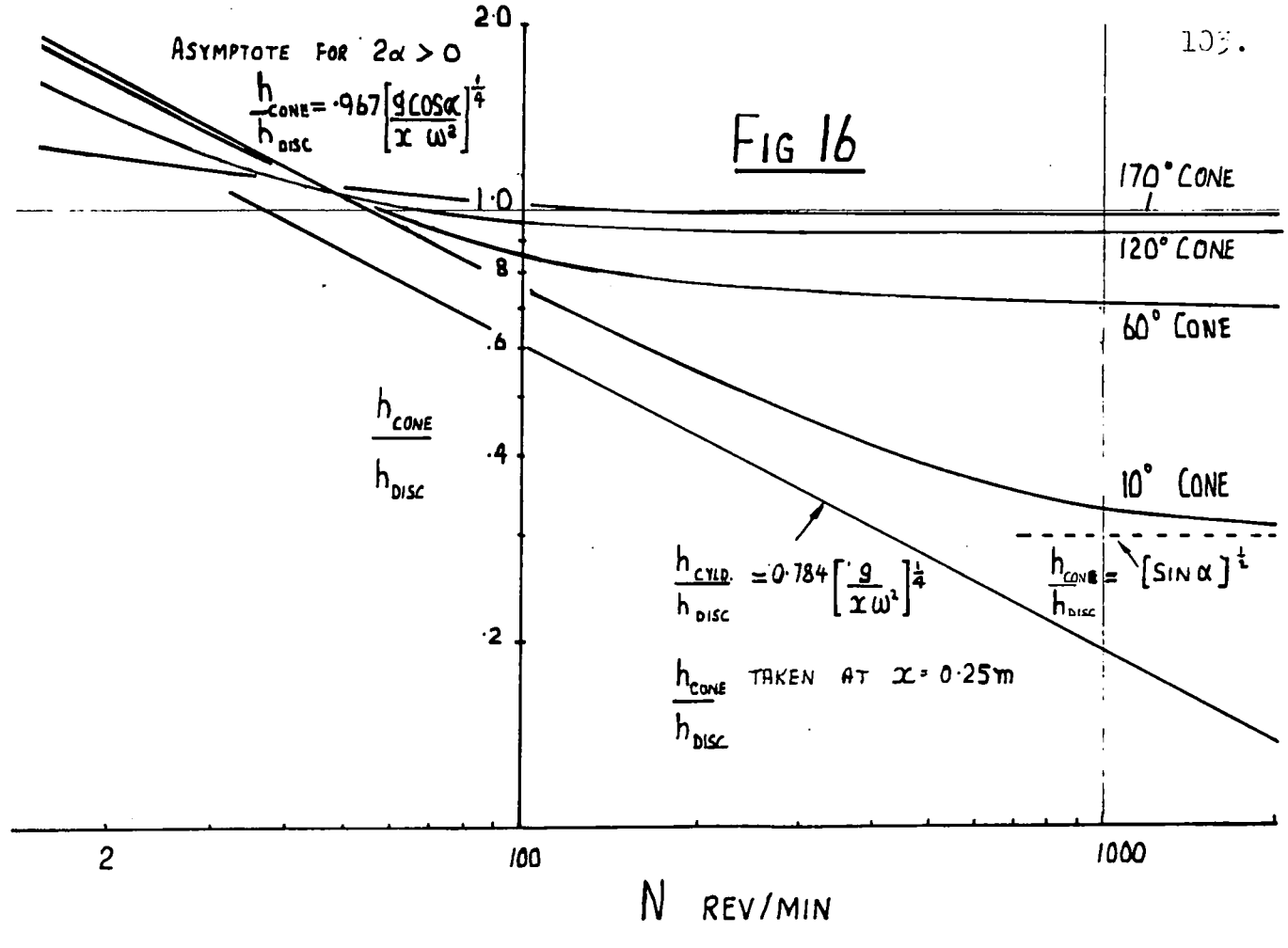
ASYMPTOTE FOR 2α > 0
$\frac{h_{CONE}}{h_{DISC}} = .967\left[\frac{g\cos\alpha}{x\omega^2}\right]^{\frac{1}{4}}$
2·0
1·0
·8
·6
·4
·2
$\frac{h_{CONE}}{h_{DISC}}$
170° CONE
120° CONE
60° CONE
10° CONE
$\frac{h_{CYLD.}}{h_{DISC}} = 0.784\left[\frac{g}{x\omega^2}\right]^{\frac{1}{4}}$
$\frac{h_{CONE}}{h_{DISC}} = [\sin\alpha]^{\frac{1}{2}}$
$\frac{h_{CONE}}{h_{DISC}}$ TAKEN AT $x = 0.25m$
2
100
1000
N REV/MIN

FIG 16

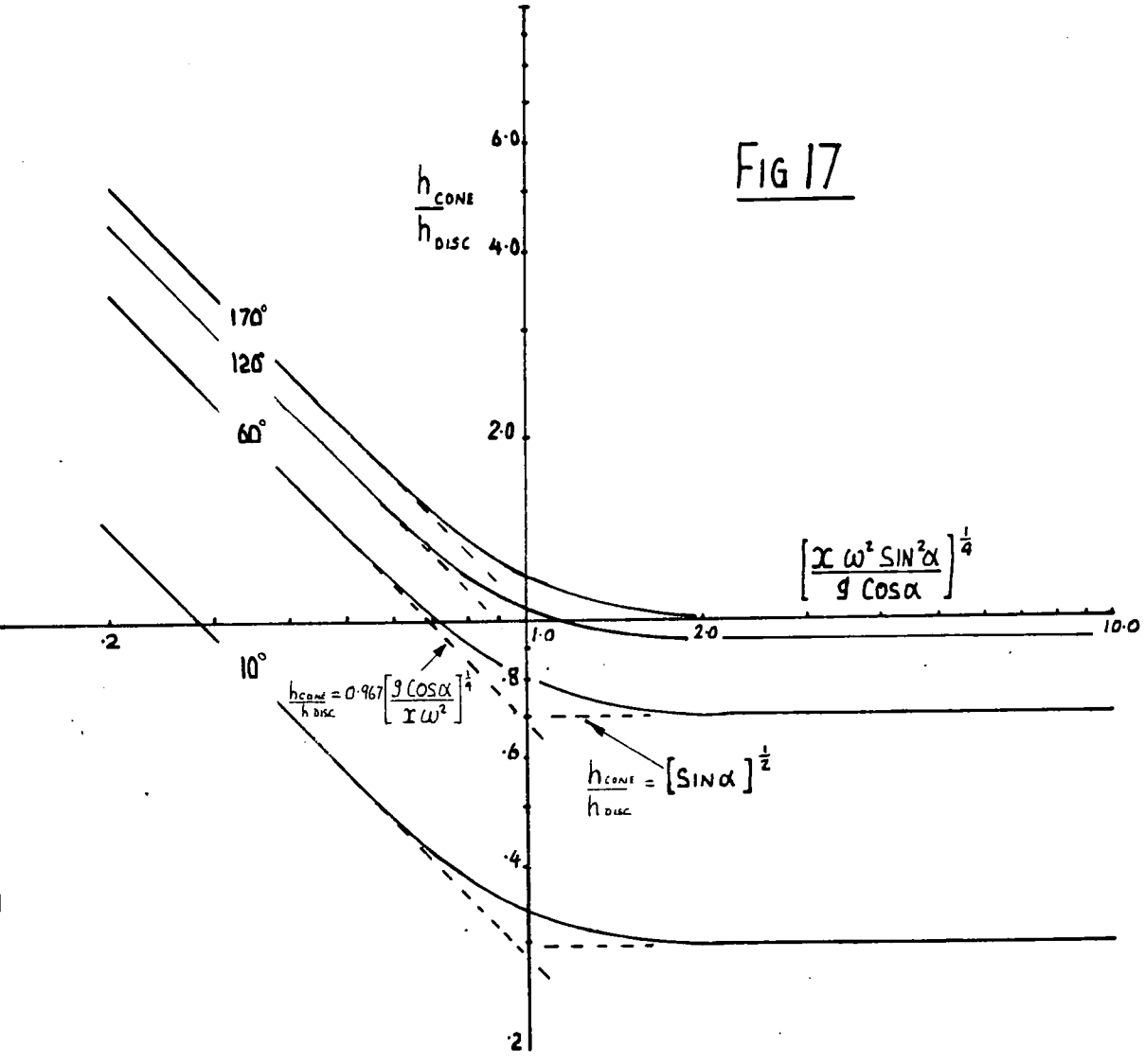
$\frac{h_{CONE}}{h_{DISC}}$
6·0
4·0
2·0
·8
·6
·4
·2
170°
120°
60°
10°
$\left[\frac{x\omega^2\sin^2\alpha}{g\cos\alpha}\right]^{\frac{1}{4}}$
·2
1·0
2·0
10·0
$\frac{h_{CONE}}{h_{DISC}} = 0.967\left[\frac{g\cos\alpha}{x\omega^2}\right]^{\frac{1}{4}}$
$\frac{h_{CONE}}{h_{DISC}} = [\sin\alpha]^{\frac{1}{2}}$

FIG 17

parallel to the 0^{o} curve and become asymptotic to the line

$$\frac{\text{h cone}}{\text{h disc}} = 0.967\left[\frac{g\ \text{Cos}\alpha}{x\omega^{2}}\right]^{\frac{1}{4}}$$

This equation cannot be applied to the 0^{o} cone for the reason given in section (3.3.3). At higher speeds the 0^{o} curve and the 180^{o} curve act as the lower and upper boundaries respectively, for the family of curves. In this region the slope of each curve increases and the curve becomes asymptotic to $\frac{\text{h cone}}{\text{h disc}} = (\text{Sin}\alpha)^{\frac{1}{2}}$ which is the limiting value predicted by Sparrow and Hartnett.

By using the parameter $\left[\frac{x\omega^{2}\ \text{Sin}^{2}\alpha}{g\ \text{Cos}\alpha}\right]^{\frac{1}{4}}$ as a non-dimensional abscissa we can again produce curves for the ratio $\frac{\text{h cone}}{\text{h disc}}$ which are independent of x. Fig.16 shows the ratio $\frac{\text{h cone}}{\text{h disc}}$ against $\left[\frac{x\omega^{2}\ \text{Sin}^{2}\alpha}{g\ \text{Cos}\alpha}\right]^{\frac{1}{4}}$ on a log-log scale. The individual curves from the original family have changed their shape and have become separated from one another to clearly show the two extreme conditions where either gravitational acceleration or centrifugal acceleration dominates the film drainage. When $\left[\frac{x\omega^{2}\ \text{Sin}^{2}\alpha}{g\ \text{Cos}\alpha}\right]^{\frac{1}{4}}$ is less than 0.5 the curves join the asymptote $\frac{\text{h cone}}{\text{h disc}} = 0.967\left[\frac{g\ \text{Cos}\alpha}{x\omega^{2}}\right]^{\frac{1}{4}}$. When $\left[\frac{x\omega^{2}\ \text{Sin}^{2}\alpha}{g\ \text{Cos}\alpha}\right]^{\frac{1}{4}}$ exceeds 2.0, the curves have joined the asymptote $\frac{\text{h cone}}{\text{h disc}} = (\text{Sin}\alpha)^{\frac{1}{2}}$.

3.7 The condensation of steam in laminar films on bodies whose profiles are formed by circular arcs.

In this section the study of the behaviour of the laminar film thickness and of the heat transfer coefficient is extended to cover axisymmetrical bodies whose generators are formed by smooth curves. The scope of the study is confined to a class of axisymmetrical bodies which represent part of a turbine rotor where the shaft joins a blade disc. This class of bodies has an outer surface which may be described as concave, because the radius of curvature of the curved generator always lies outside the body. The choice of curve for the generator, which makes the transition from the shaft to the blade disc, depends to some extent on the method of manufacture, but the shape of the curve is always governed by the stresses acting on the rotor. To eliminate undue stress concentrations the curves are free from sudden changes in curvature, but the chosen curves usually do not have simple geometrical descriptions.

If a power series in terms of the cartesian co-ordinates η and ξ can be used to describe the generator curve, this will be of great assistance when applying the present theory. It may be possible to obtain a very close approximation to the chosen curve by using a combination of either exponential parabolic or circular arcs.

In the present study a circular arc is chosen to be representative of these curves. The arc subtends an angle of $\frac{\pi}{2}$ radians and is tangential to the shaft and to the disc. Selecting a circular arc for the generator curve has several advantages:-

(i) the position of the centre of curvature and the radius of curvature of the arc are constant,

(ii) both the angle α and the diameter D may be expressed in terms of x by very simple equations which do not require the use of the co-ordinates η and ξ .

The body generated by the circular arc is shown in fig. 18 and has a vertical axis of rotation, because the moving parts of the experimental apparatus, which will be described later, also has a vertical axis of rotation. The distance x along the curve is measured from the point where the arc meets the shaft, which is also the point where the condensate film is assumed to start and where the angle is zero.

Angle α is expressed in terms of x by

$$\alpha = \frac{x}{r} \text{ radians.} \qquad \ldots\ldots\ldots (3.7.1)$$

which gives

$$\frac{d\alpha}{dx} = \frac{1}{r} \qquad \ldots\ldots\ldots (3.7.2)$$

The reason why $\frac{d\alpha}{dx}$ is always given as the reciprocal of the radius of curvature is given in section (3.2).

The diameter of the body in terms of x is given by the expression

$$D = d + 2r\,(1 - \text{Cos}\alpha) \qquad \ldots\ldots\ldots (3.7.3)$$

which gives

$$\frac{dD}{dx} = 2\ \text{Sin}\alpha \qquad \ldots\ldots\ldots (3.7.4)$$

FIG 18

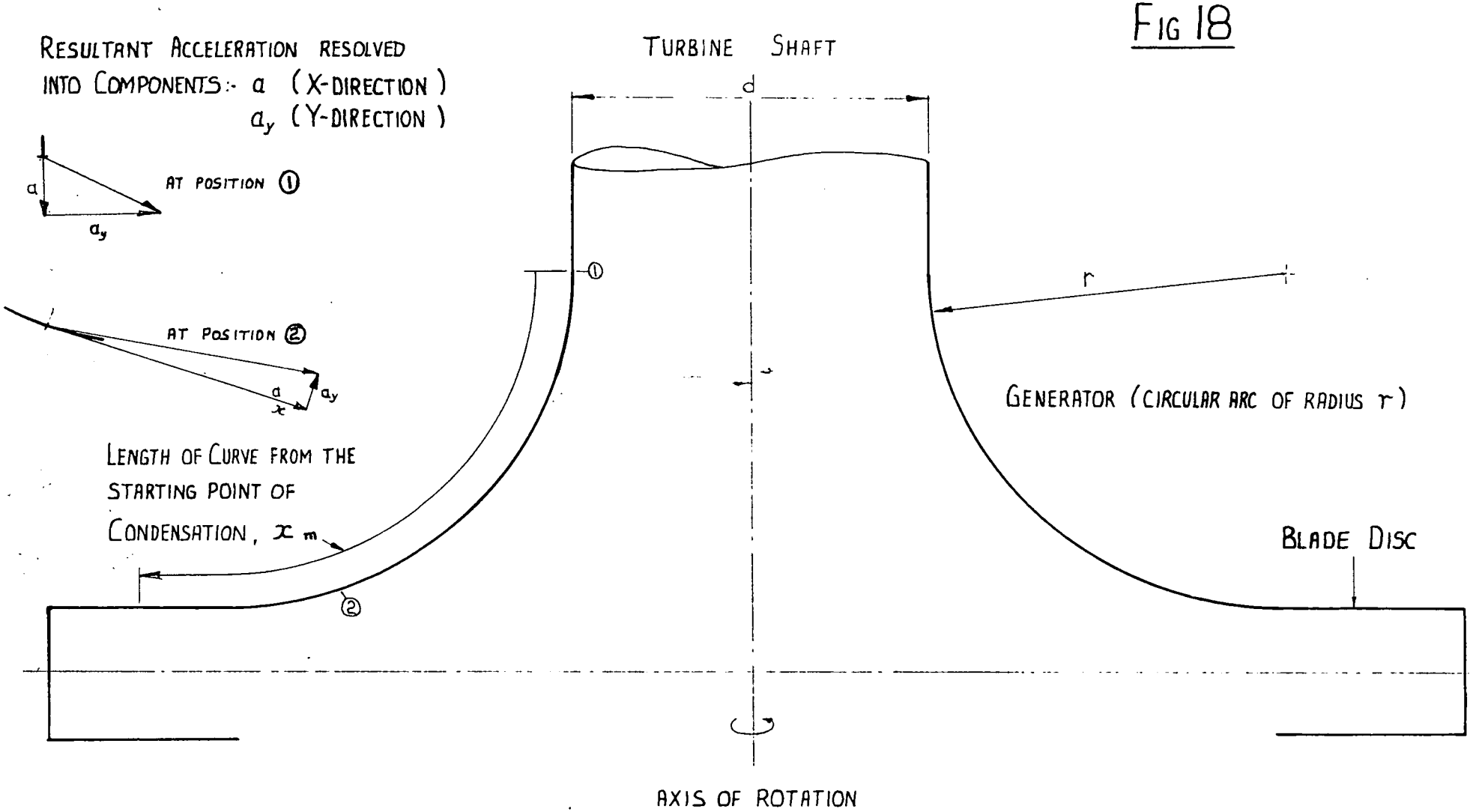
RESULTANT ACCELERATION RESOLVED INTO COMPONENTS:- a (X-DIRECTION)
a_y (Y-DIRECTION)
a
a_y
AT POSITION ①
AT POSITION ②
a
a_y
x
LENGTH OF CURVE FROM THE STARTING POINT OF CONDENSATION, x_m
TURBINE SHAFT
d
①
②
r
GENERATOR (CIRCULAR ARC OF RADIUS r)
BLADE DISC
AXIS OF ROTATION

When the axis of symmetry of the body is vertical, the accelerations resolved in the X direction and in the Y direction are given by equations (3.2.13) and (3.2.14) respectively. These equations are repeated here for convenience:-

(i) In the X direction

$$a = \tfrac{1}{2} D\omega^2 \operatorname{Sin}\alpha + g \operatorname{Cos}\alpha$$

(ii) In the Y direction

$$a_y = \tfrac{1}{2} D\omega^2 \operatorname{Cos}\alpha - g \operatorname{Sin}\alpha$$

Equation (3.2.13, above) shows that at the starting point of the film the drainage is governed by gravitational acceleration alone, irrespective of the speed of rotation. Equation (3.2.13) gives

$$\frac{d\alpha}{dx} = \omega^2 \operatorname{Sin}^2\alpha + \frac{(\tfrac{1}{2} D\omega^2 \operatorname{Cos}\alpha - g \operatorname{Sin}\alpha)}{r} \quad \ldots\ldots (3.7.5)$$

The above equation contains a new term derived from the radius of curvature of the arc and the acceleration in the Y direction. This term is lost when the equation is used for cones because the radius of curvature becomes infinite.

The governing equation for the film thickness, equation (3.2.26) now becomes:-

$$\frac{d\delta}{dx} = H - \frac{\delta^4}{3}\left[\frac{2\omega^2 \operatorname{Sin}^2\alpha + \frac{2g \operatorname{Sin}\alpha \operatorname{Cos}\alpha}{D} + \frac{(\tfrac{1}{2} D\omega^2 \operatorname{Cos}\alpha - g \operatorname{Sin}\alpha)}{r}}{\delta^3 (\tfrac{1}{2} D\omega^2 \operatorname{Sin}\alpha + g \operatorname{Cos}\alpha)}\right] \quad \ldots\ldots\ldots (3.7.6)$$

Equation (3.7.6) has a partial analytical solution with a form similar to that given for equation (3.1.15) in section (3.3). In the partial solution the fluid properties and θ are separated from the geometrical terms x, r, d and α, and from the acceleration a. Therefore the film thickness will be a function of $\theta^{\frac{1}{4}}$ if all other terms remain constant.

The numerical method of integration outlined in section (3.4) was applied to equation (3.7.6) to calculate the film thicknesses and the heat transfer coefficients presented in this section. Calculations were performed for three bodies with shaft diameters of 0.002, 0.2 and 0.6 m, but each with a radius of curvature of 0.2 m. Each body was given speeds of rotation over the range zero to 10,000 rev/min, together with common values of temperature difference θ = 10° C and of Pr = 1.37. Because the film thicknesses and heat transfer coefficients are very dependent on the choice of r and d, these parameters are presented together with some comments on the general behaviour of equation (3.7.6).

Following the method given in sub-section (3.1.8), some of the general trends in the behaviour of the governing equation can be found by rearranging the equation in terms of δ^4 to give:-

$$\frac{d\delta^4}{dx} = 4\left\{\frac{H-\frac{\delta^4}{3}\left[2\omega^2\sin^2\alpha + \frac{2g\sin\alpha\cos\alpha}{D} + \left(\frac{\frac{1}{2}D\omega^2\cos\alpha - g\sin\alpha}{r}\right)\right]}{\left(\frac{1}{2}D\omega^2\sin\alpha + g\cos\alpha\right)}\right\} \quad \ldots\ldots\ldots (3.7.7)$$

Two extremes of rotation are considered.

When the speed of rotation is zero, equation (3.7.7) reduces to

$$\frac{d\delta^4}{dx} = 4\left\{\frac{H}{g\cos\alpha} - \frac{\delta^4}{3}\left[\frac{2\sin\alpha}{D} + \frac{\tan\alpha}{r}\right]\right\} \quad \ldots\ldots\ldots (3.7.8)$$

Inspecting the term $\frac{2\sin\alpha}{D} - \frac{\tan\alpha}{r}$ shows that

(i) while $\frac{\tan\alpha}{r}$ remains less than $\frac{2\sin\alpha}{D}$, the slope, which refers to $\frac{d\delta^4}{dx}$ will decrease with x

(ii) when $\frac{\tan\alpha}{r}$ is equal to $\frac{2\sin\alpha}{D}$, the slope remains

positive and finite at $\frac{d\delta^4}{dx} = \frac{8Hr}{gD}$

(iii) when $\frac{\tan\alpha}{r}$ is greater than $\frac{2\ \mathrm{Sin}\alpha}{D}$, the slope starts to increase and eventually becomes infinite.

Film thicknesses for three stationary bodies are plotted against distance x in fig. 19. The initial film growth on each body is shown to be close to that given by Nusselt for condensation on vertical surfaces (equation 3.3.14), but at other positions along the generator, the ratio $\frac{d}{r}$ affects the film growth. As $\frac{d}{r}$ approaches 2, the angle α at which $\frac{\tan\alpha}{r} = \frac{2\ \mathrm{Sin}\alpha}{D}$ approaches zero. Therefore as $\frac{d}{r}$ becomes large the slope $\frac{d\delta^4}{dx}$ increases with x from x = o and provides the film with a faster rate of growth, as is shown in fig. 19 by curve (i). As $\frac{d}{r}$ becomes small, the angle at which $\frac{\tan\alpha}{r} = \frac{2\ \mathrm{Sin}\alpha}{D}$ approaches 60°, and a lower rate of growth occurs in the early stages of film development to produce the thinner films shown by curves (ii) and (iii). Fig. 19 also indicates that the heat transfer coefficient decreases with increasing shaft diameter d which is the diameter at the starting point of condensation. In section (3.5) the heat transfer coefficients for stationary cones were also shown to decrease with d.

By a variation of the parameters in the integration program, the films on these stationary bodies would always appear to grow monotonically between $\alpha = 0$ and $\alpha = \frac{\pi}{2}$. Acceleration a is zero when $\alpha = \frac{\pi}{2}$. Curves (i), (ii) and (iii) in fig. 19 show that at $\alpha = \frac{\pi}{2}$ drainage ceases and the theoretical film thickness becomes infinite. In practice the film thickness will remain small because of drainage over the lower edge of the body.

If gravitational acceleration becomes negligible, equation

FIG 19

θ = 10°C
P_r = 1·37
N = ZERO

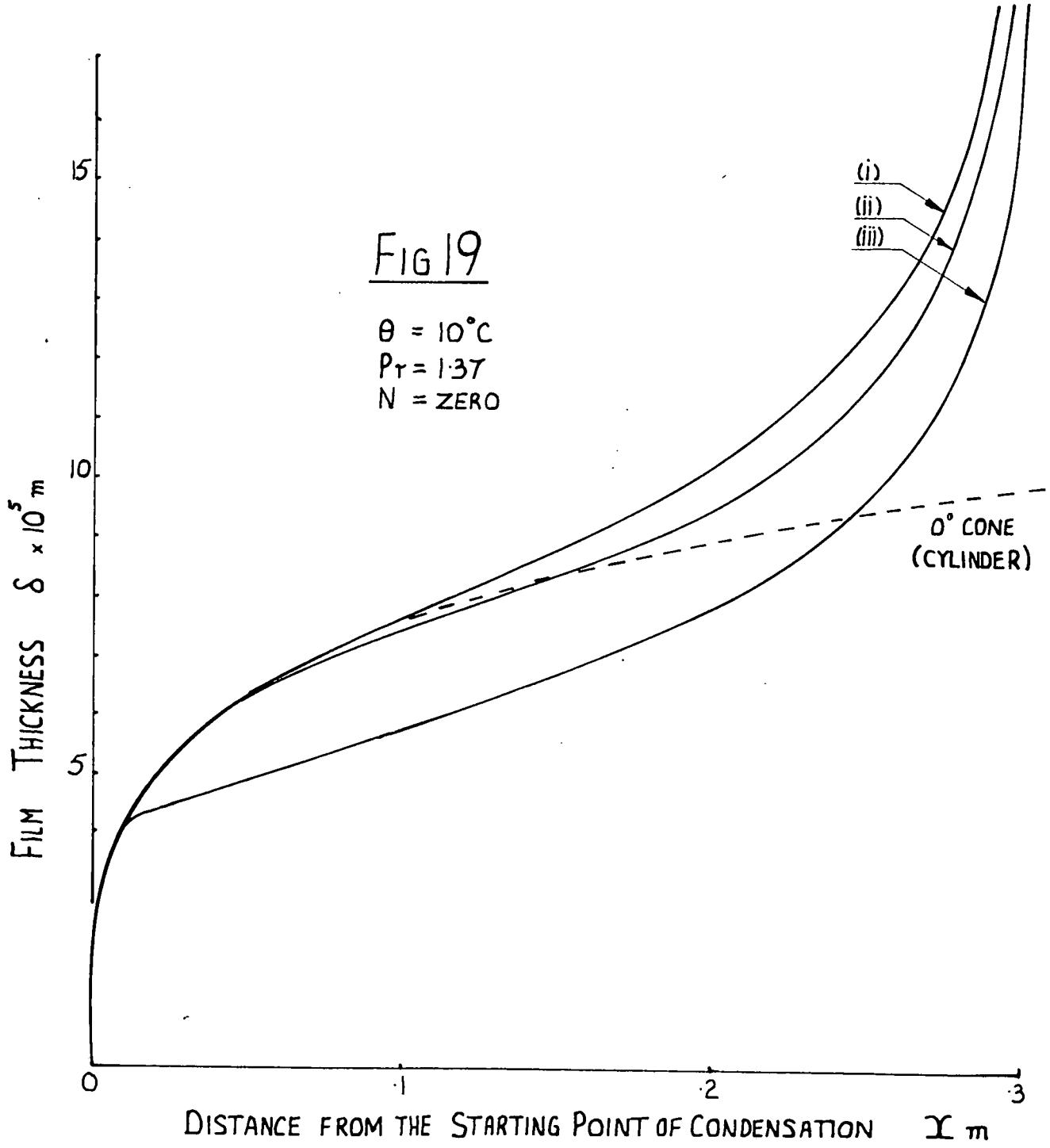

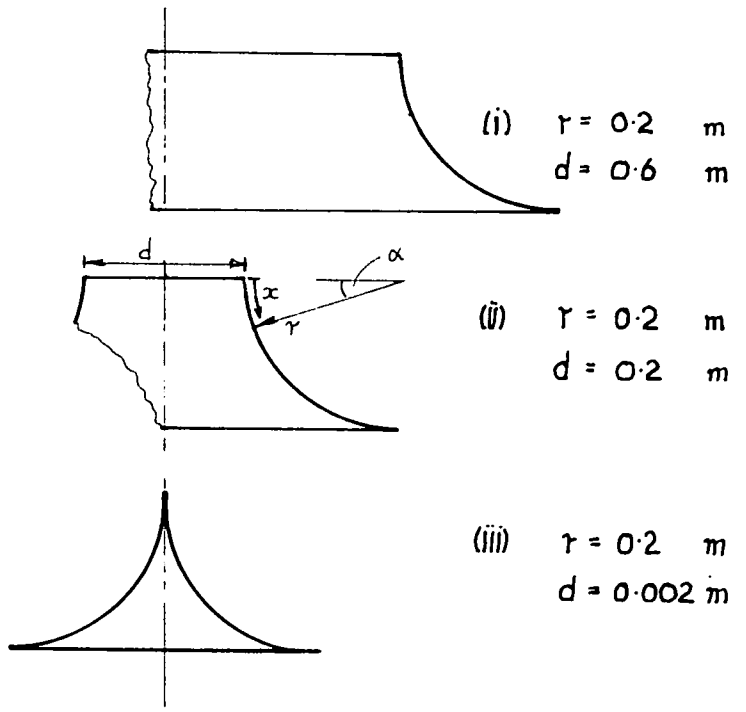

(i) r = 0·2 m
d = 0·6 m

(ii) r = 0·2 m
d = 0·2 m

(iii) r = 0·2 m
d = 0·002 m

111.

(3.7.7) reduces to:-

$$\frac{d\delta^4}{dx} = 8\left\{\frac{H}{D\omega^2 \operatorname{Sin}\alpha} - \frac{\delta^4}{3}\left[\frac{2\operatorname{Sin}\alpha}{D} + \frac{\operatorname{Cot}\alpha}{2r}\right]\right\} \ldots (3.7.9)$$

Inspecting the term

$$\frac{2\operatorname{Sin}\alpha}{D} + \frac{\operatorname{Cot}\alpha}{2r}$$

shows that at small angles the term is dominated by $\frac{\operatorname{Cot}\alpha}{2r}$, but as the angle increases $\frac{2\operatorname{Sin}\alpha}{D}$ becomes dominant. When this latter condition is attained, equation (3.7.9) reduces to equation (3.1.29) which shows that the film thickness becomes uniform with x when angle α is constant; as it is for cones. In the present case α is a variable, and the film thickness will become asymptotic to

$$\delta = \left[\frac{3H}{2\omega^2 \operatorname{Sin}^2\alpha}\right]^{\frac{1}{4}}$$

Since α is increasing in the direction of flow, the film thickness will decrease in that direction. Fig. 20 illustrates this reduction in film thickness for the rotating body which has the shaft diameter d = 0.002 m.

The initial film growth is dominated by gravitational acceleration alone and the film thickness increases. Once the centrifugal acceleration starts to have a significant influence on drainage, the film thickness starts to decrease and approach the asymptote. As the speed increases the point at which centrifugal acceleration dominates the drainage moves towards the starting point of the film. Fig. 21 shows film thicknesses for the rotating body which has a shaft diameter of 0.2 m. For any given speed the larger shaft diameter produces a stronger acceleration field at all finite values of x and this improves the drainage at an earlier stage in the growth of the film. At speeds N = 1000 and N = 10,000 rev/min the film thickness is seen in fig. 21

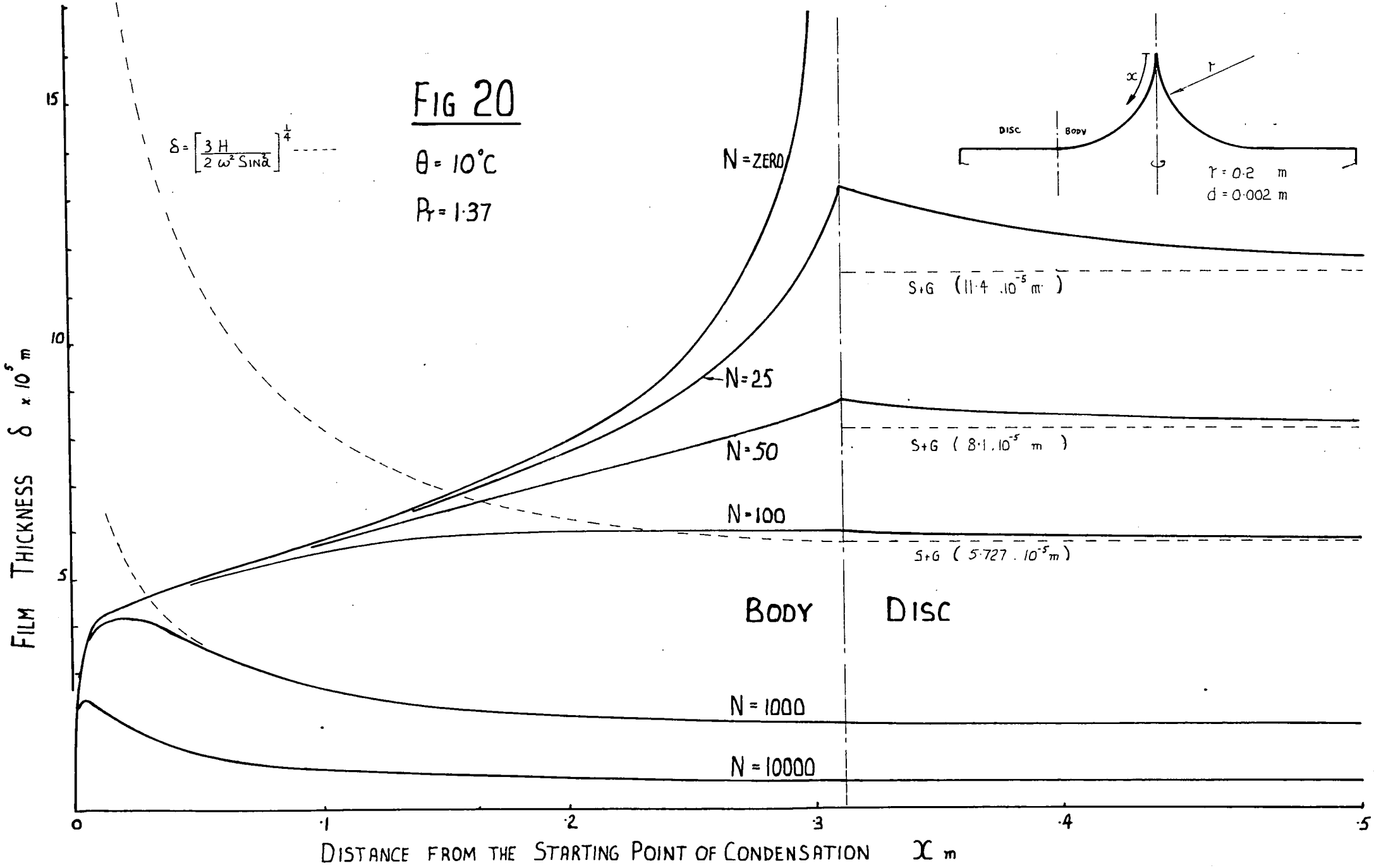
FIG 20
θ = 10°C
Pr = 1·37
δ = [3 H / 2 ω² Sin α]^¼
N = ZERO
N = 25
N = 50
N = 100
N = 1000
N = 10000
S+G (11·4 .10⁻⁵ m)
S+G (8·1 .10⁻⁵ m)
S+G (5·727 . 10⁻⁵ m)
BODY
DISC
DISC
Body
α
r
r = 0·2 m
d = 0·002 m
FILM THICKNESS δ x 10⁵ m
DISTANCE FROM THE STARTING POINT OF CONDENSATION x m
15
10
5
0
·1
·2
·3
·4
·5

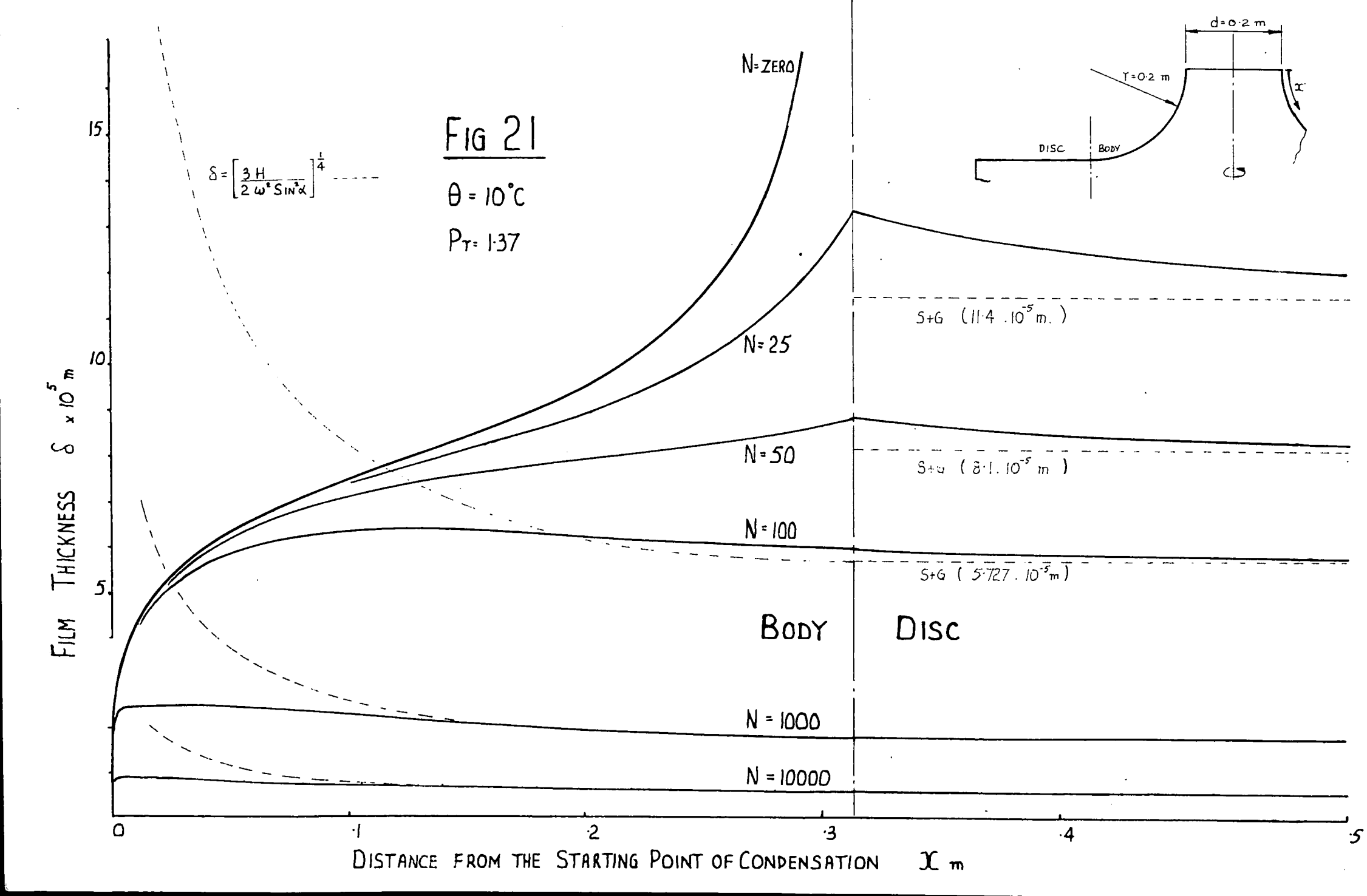
FIG 21
θ = 10°C
P_T = 1·37
δ = [3H / 2ω²Sin³α]^¼
N=ZERO
N=25
N=50
N=100
N=1000
N=10000
S+G (11·4 .10⁻⁵ m.)
S+G (8·1. 10⁻⁵ m)
S+G (5·727. 10⁻⁵m)
BODY
DISC
d=0·2 m
r=0·2 m
x
DISC
BODY
FILM THICKNESS δ x 10⁵ m
15
10
5
0
·1
·2
·3
·4
·5
DISTANCE FROM THE STARTING POINT OF CONDENSATION x m

almost to become uniform over the full length of the generator and to make little departure from the film thickness on the disc given by $\delta = \left[\frac{3}{2}\frac{H}{\omega^2}\right]^{\frac{1}{4}}$.

If the angle α becomes constant at any point on the generator, as it does in the present example where the arc joins the disc, then the radius of curvature becomes infinite. When this occurs the equation governing the film thickness reverts to that for cones. At high speeds the slope $\frac{d\delta^4}{dx}$ will not experience much change as the film flows onto the disc, but if the effects of gravitational acceleration remain important, the slope will suffer a substantial reduction in value. Figs. 20 and 21 show that at low speeds the curve of film thickness forms a cusp at the point where the arc joins the disc. After passing onto the disc, the film thickness decreases to become asymptotic to a value given by:-

$$\delta = \left[\frac{3}{2}\frac{H}{\omega^2}\right]^{\frac{1}{4}}$$

The film thicknesses presented in figs. 19, 20 and 21 depend upon the choice of d and r and as such they are of restricted interest. It is possible to draw some general conclusions about the behaviour of the films thickness and of the heat transfer coefficient on bodies with curved generators, by adopting the approach given in section (3.5), where the ratio $\frac{h_N}{h_z}$ for cones was plotted against $\left[\frac{D\omega^2 \sin\alpha}{2g \cos\alpha}\right]^{\frac{1}{4}}$ (fig. 15).

Fig. 22 shows the ratio $\frac{h_N}{h_z}$, which is equivalent to the ratio $\frac{\delta_z}{\delta_N}$, for the three bodies. The curves for $\frac{h_N}{h_z}$ are seen to be speed dependent, but they follow the same trend as those for cones and turn from unity to the high speed asymptote

FIG 22

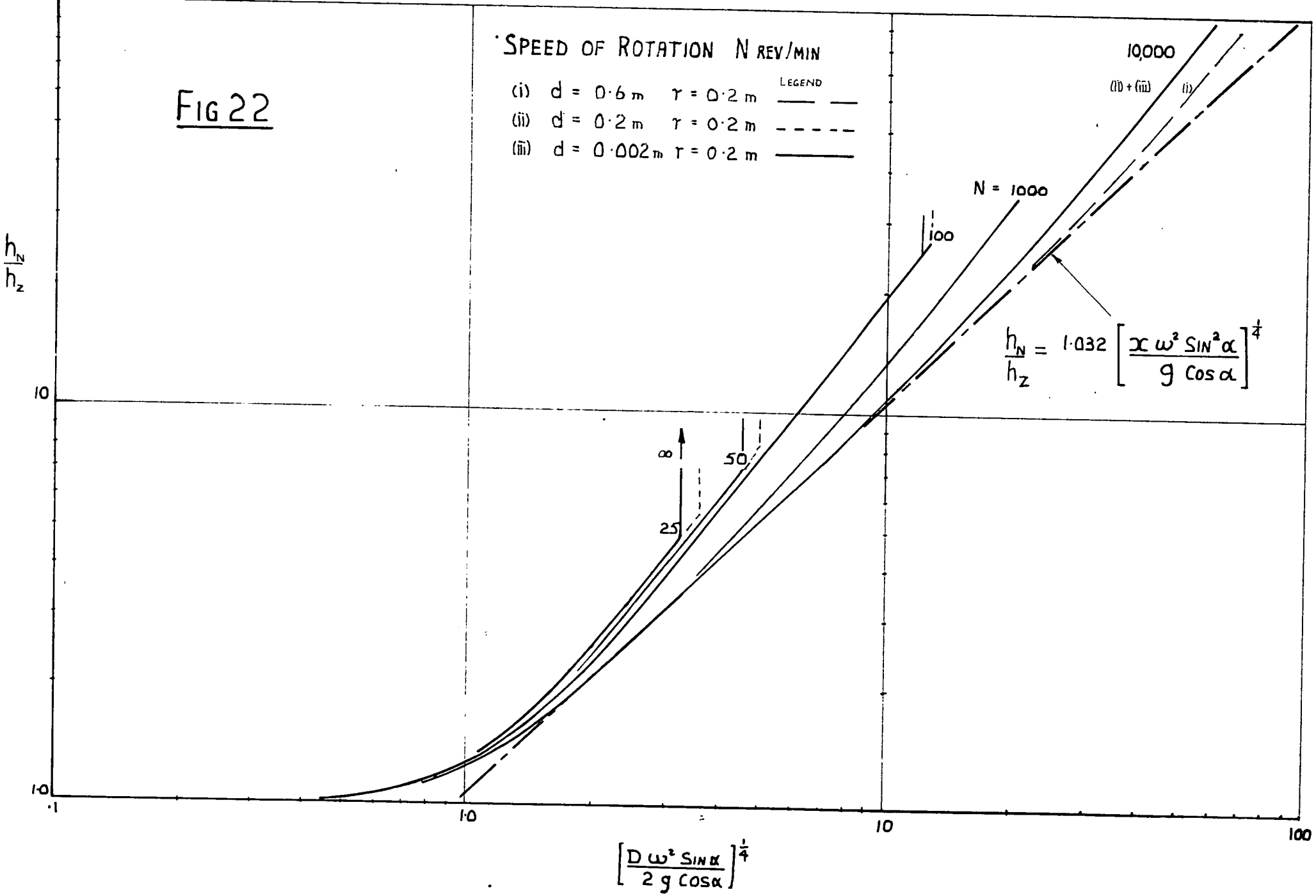
SPEED OF ROTATION N REV/MIN
LEGEND
(i) d = 0·6 m r = 0·2 m
(ii) d = 0·2 m r = 0·2 m
(iii) d = 0·002 m r = 0·2 m
10,000
(ii) + (iii)
(i)
N = 1000
100
50
25
∞
$\frac{h_N}{h_Z} = 1.032 \left[\frac{x\omega^2 \sin^2\alpha}{g \cos\alpha}\right]^{\frac{1}{4}}$
$\frac{h_N}{h_Z}$
10
1·0
·1
1·0
10
100
$\left[\frac{D\omega^2 \sin\alpha}{2g\cos\alpha}\right]^{\frac{1}{4}}$

$\frac{h_N}{h_z} = 1.032 \left[\frac{D\omega^2 \, Sin\alpha}{2g \, Cos\alpha} \right]^{\frac{1}{4}}$. As the generator becomes radial, h_z approaches zero and makes the ratio $\frac{h_N}{h_z}$ go to infinity at all speeds. If the centrifugal acceleration becomes dominant at an early stage in the growth of the film, as it does in figs. 20 and 21 when the speed exceeds 1000 rev/min, the curves of $\frac{h_N}{h_z}$ follow those for cones and close on the high speed asymptote at $\left[\frac{D\omega^2 \, Sin\alpha}{2g \, Cos\alpha} \right]^{\frac{1}{4}} = 2.0$. If this ratio of accelerations exists near the starting point of the film, the subsequent film thickness approaches $\delta = \left[\frac{3}{2} \frac{H}{\omega^2 \, Sin^2\alpha} \right]^{\frac{1}{4}}$ and decreases with x. The point at which the centrifugal acceleration becomes dominant at any given speed depends on the shaft diameter d and on the radius of curvature r which governs the length of the generator x. If the centrifugal acceleration becomes dominant only along the latter part of the generator, the dominant effect cannot influence the film growth long enough to cause any significant reduction in film thickness or any improvement in heat transfer coefficient. Thus in fig. 22 at N = 25 to N = 100 rev/min the curves of $\frac{h_N}{h_z}$ make a turn towards infinity before they can close on the asymptote.

If the generator became tangential to a cone with an apex angle of less than 180° (disc), the ratio $\frac{h_N}{h_z}$ would not be forced to make a premature turn towards infinity, because drainage by gravitational acceleration would continue and h_z would remain finite.

Film drainage by the formation and detachment of drops in the Y direction has been neglected. Some comments on the conditions necessary for the occurrence of drop detachment

can be made while referring to the film thicknesses in figs. 20 and 21. which are only for drainage in the X direction.

When the body shown in fig. 18 is rotating, the resultant acceleration will lie above the outer surface at the starting point of the film. As x increases, the angle made between the resultant and the local tangent to the surface will decrease and possibly become negative. This means that the component a_y decreases with x, even though the magnitude of the resultant increases along the generator. In practical terms the reduction in a_y means that the possibility of the formation and detachment of drops from the film decreases as the generator curve becomes radial. Hoyle and Matthews (58) showed that drop formation occurred more readily as the shaft diameter decreased. At high speeds the film thicknesses in figs. 20 and 21 have a maximum value near the starting point of the film at the shaft and the magnitude of the maximum increases as the shaft diameter decreases. These two factors will favour the formation and detachment of drops. However, the possibility of drop detachment is not improved by the fact that the largest value of a_y occurs near the shaft, where the acceleration field has its lowest strength.

On a steam turbine where the rotor usually has a horizontal axis of rotation, some qualification is required for the above statements. At low speeds of rotation the rotor will experience non-axisymmetrical acceleration fields, although symmetry is restored as the speed increases and gravitational acceleration becomes negligible. Hoyle and

FIG 23

$\theta = 10°C$

$P_r = 1{\cdot}37$

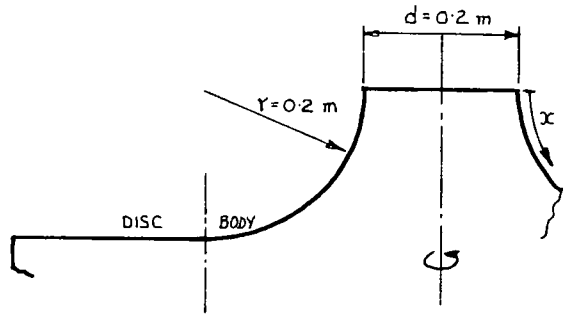

HEAT TRANSFER COEFFICIENT $h \times 10^{-4}$ $\frac{W}{m^2 C}$

BODY | DISC

N = 10000

N = 1000

N = 100

N = ZERO

N = 25

0 ·2 ·3 ·4 ·5

DISTANCE FROM THE STARTING POINT OF CONDENSATION x m

Matthews (58) show that at all speeds the film of condensate drains from a horizontal shaft by the formation and detachment of drops. At low speed the drops are detached from the underside of the shaft, but as the speed increases the drainage becomes symmetrical. Therefore at the shaft part of the rotor drainage will occur in the Y direction at all speeds. At high speeds this mode of drainage will tend to cease where the generator becomes radial.

Fig. 23 shows the heat transfer coefficients for the body with a diameter d = 0.2 m. Even with this small shaft diameter there is not a great deal of variation in heat transfer coefficient along the generator. If the film of condensate on the turbine rotor remains laminar during a cold start, the large surface to volume ratio of the blade disc will ensure that this part of the rotor is the first to attain the operating temperature. If the film does not remain laminar at the shaft the drop detachment occurs, this will give the shaft part of the rotor, which has a relatively small surface to volume ratio, a well needed improvement in the local heat transfer coefficient. The conditions favourable to Y direction drainage and to the presence of waves in the film of condensate must be determined experimentally.

3.8 Temperature distribution across the cone wall.

One of the main purposes of the experimental work is to provide measured values of heat flux and of heat transfer coefficient for known test conditions. The heat flux,or time rate of energy transfer across the wall per unit area, is obtained from a product of the temperature gradient in the cone material at the outer surface and the thermal conductivity of the material at the point. The temperature gradient is derived from the experimental readings of temperature taken at the inner and outer surfaces of the cone.

In this section the temperature distribution and the temperature gradient across the walls of hollow cones is investigated. Two types of cone materials are considered. The first has a constant thermal conductivity, but the second material has a thermal conductivity which is linearly dependent on temperature.

In the steady state and where the thermal conductivity is constant, energy transfer across the wall of flat plates is accompanied by linear temperature distributions and uniform temperature gradients, because the area of the plate between the inner and outer surfaces is constant. It is more precise to say that the distribution is linear because there is negligible change in curvature between the two surfaces of the flat plate. For bodies such as thick-walled tubes where there are large changes in curvature between the inner and outer surfaces, energy transfer in the steady state is accompanied by non-linear temperature distributions and non-uniform temperature gradients. A combination of these

two types of temperature distribution can occur across the walls of hollow cones.

Hollow cones with walls of constant thickness exhibit a difference in curvature between the inner and outer surfaces, but this difference is not constant and decreases with increasing axial distance from the apex of the cone. Consequently, near the apex where the radius of the inner surface becomes small, the difference in curvature between the inner and outer surfaces may become substantial and influence the temperature distribution.

The investigation commences with the development of a differential equation for the temperature distribution across the wall in a direction perpendicular to the cone surface.

Consider the small element shown in fig. 24. The cross-section of the element has a length Δx and a thickness Δy. Rotating the element about the vertical axis forms a control volume within the material of the cone.

The inner surface of the control volume is:-

$$A = \pi \operatorname{Sin} \alpha \left[2x\,\Delta x + (\Delta x)^2\right] \qquad \ldots\ldots\ldots (3.8.1)$$

The rate of change of surface area with respect to y becomes:-

$$\frac{dA}{dy} = \pi \operatorname{Sin} \alpha \left[2\,(x + \Delta x)\,\frac{d\Delta x}{dy} + 2\,\Delta x\,\frac{dx}{dy}\right] \ldots\ldots\ldots (3.8.2)$$

since Δx is constant, $\frac{d\Delta x}{dy} = 0$

and where $y = x \tan \alpha$, then $\frac{dx}{dy} = \frac{1}{\tan \alpha}$

therefore $\frac{dA}{dy} = 2\pi \operatorname{Cos} \alpha . \Delta x \qquad \ldots\ldots\ldots (3.8.3)$

Fig. 25 shows the control volume placed between the inner and outer surfaces of the wall of a hollow cone.

FIG 24

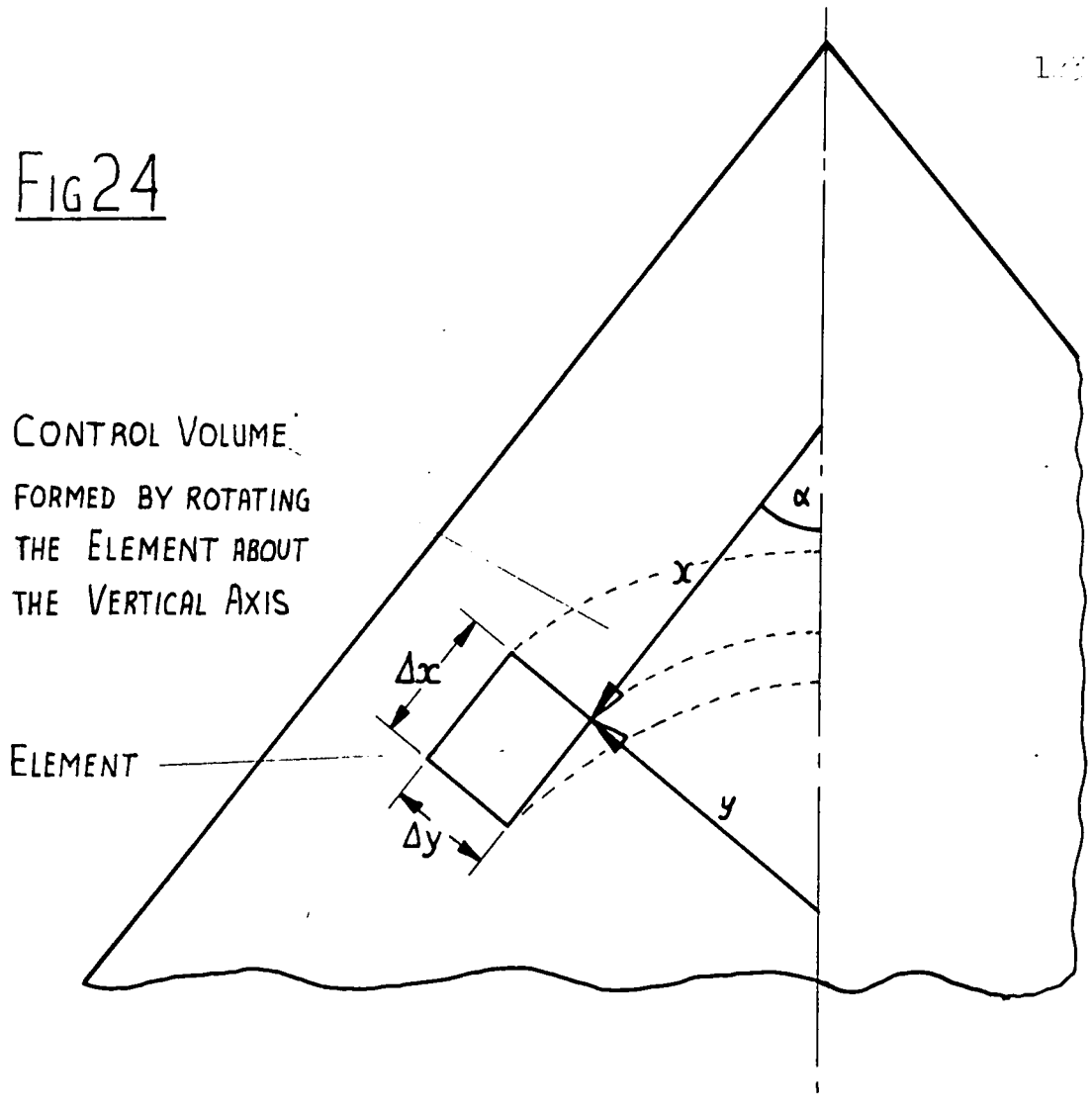
CONTROL VOLUME
FORMED BY ROTATING
THE ELEMENT ABOUT
THE VERTICAL AXIS
ELEMENT
α
x
Δx
Δy
y

FIG 25

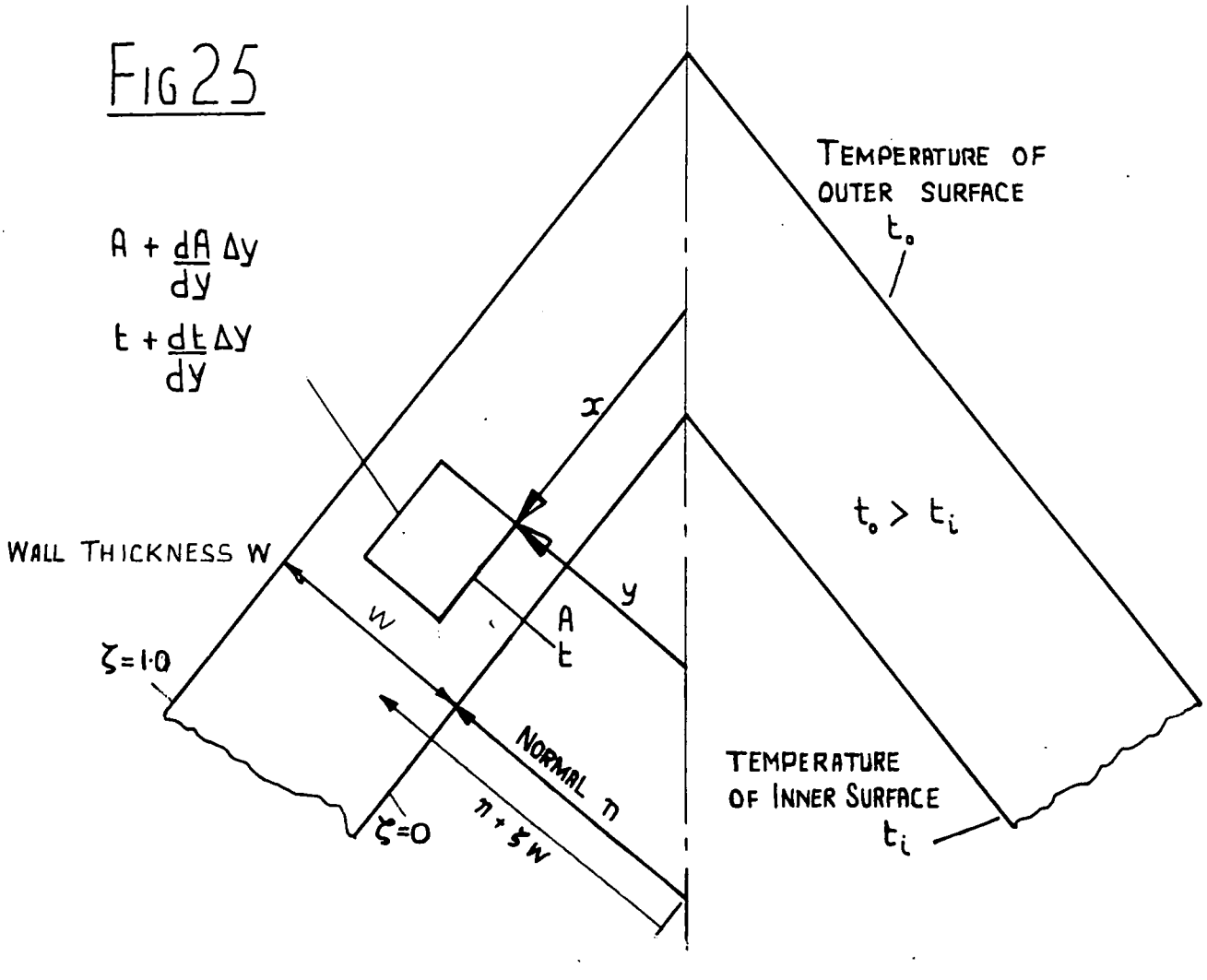
A + dA/dy Δy
t + dt/dy Δy
TEMPERATURE OF
OUTER SURFACE
t_o
x
$t_o > t_i$
WALL THICKNESS W
y
w
A
t
ζ=1·0
NORMAL n
n + ζw
ζ=0
TEMPERATURE
OF INNER SURFACE
t_i

The energy flow across the control volume in a direction perpendicular to the cone surface, that is in the Y direction, may be written for the inner surface of the element, as:-

$$Q = - k A \frac{dt}{dy} \qquad \ldots\ldots\ldots (3.8.4)$$

Differentiating equation (3.8.4) with respect to y gives

$$\frac{dQ}{dy} = - k\left[A \frac{d^2t}{dy^2} + k \frac{dt}{dy} \frac{dA}{dy} + A \frac{dt}{dy} \frac{dk}{dy}\right] \ldots\ldots (3.8.5)$$

If the energy flow in the X direction is negligible, then the energy flow in the Y direction remains constant and

$$\frac{dQ}{dy} = 0$$

Thus equation (3.8.5) becomes:-

$$k A \frac{d^2t}{dy^2} + k \frac{dA}{dy} \frac{dt}{dy} + A \frac{dt}{dy} \frac{dk}{dy} = 0 \qquad \ldots\ldots\ldots (3.8.6)$$

If the thermal conductivity at any temperature t can be represented by

$$k = k_o (1 + \beta t)$$

where k_o is the thermal conductivity at 0^o C and β is the temperature coefficient, then

$$\frac{dk}{dy} = \frac{dk}{dt} \frac{dt}{dy}$$

and equation (3.8.6) reduces to the following when

$$\Delta x \longrightarrow 0$$

$$\frac{d^2t}{dy^2} + \frac{1}{y} \frac{dt}{dy} + \frac{\beta}{1 + \beta t}\left[\frac{dt}{dy}\right]^2 = 0 \qquad \ldots\ldots\ldots (3.8.7)$$

and becomes the general equation for the temperature distribution across the cone wall.

If the cone material has a thermal conductivity which is independent of temperature, then $\beta = 0$ and equation (3.8.7)

reduces to

$$\frac{d^2t}{dy^2} + \frac{1}{y}\frac{dt}{dy} = 0 \qquad \ldots\ldots\ldots (3.8.8)$$

This equation has a standard solution of the form

$$t = C_1 + C_2 \ln y \qquad \ldots\ldots\ldots (3.8.9)$$

The boundary conditions at the inner and outer surfaces are shown in fig. 25.

At the inner surface

$$y = n \; ; \; t = t_i$$

and at the outer surface

$$y = (n + w) \; ; \; t = t_o$$

Where n is the distance in the Y direction from the vertical axis to the inner surface and w is the thickness of the cone wall.

Introducing these boundary conditions makes

$$C_2 = \frac{\theta_w}{\ln\left[\frac{n+w}{n}\right]} \quad \text{and} \quad C_1 = t_i - \theta_w \frac{\ln(n)}{\ln\left[\frac{n+w}{n}\right]}$$

where $\theta_w = (t_o - t_i)$

Hence equation (3.8.9) becomes

$$t = t_i + \theta_w \frac{\ln\left[\frac{y}{n}\right]}{\ln\left[\frac{n+w}{n}\right]} \qquad \ldots\ldots\ldots (3.8.10)$$

The value of y in the above equation lies between n and (n + w). It is more appropriate to express this value of y as

$$y = n + \zeta w \qquad \ldots\ldots\ldots (3.8.11)$$

where ζ is a fraction $\quad 0 \leqslant \zeta \leqslant 1$

ζ is zero at the inner surface and unity at the outer surface. Thus for materials with constant thermal conductivity the temperature distribution across the cone wall becomes:-

$$t = t_i + \theta \frac{\ln\left[\frac{n + \zeta w}{n}\right]}{\ln\left[\frac{n + w}{n}\right]} \qquad \ldots\ldots\ldots (3.8.12)$$

The form of this equation shows that for all values of n and w, the temperature distribution is non-linear. By a simple series expansion of the ln terms in the equation it can be shown that

$$t = t_i + \theta_w \frac{\left\{\left[\frac{\zeta w}{n}\right] - \frac{1}{2}\left[\frac{\zeta w}{n}\right]^2 + \ldots\right\}}{\left\{\left[\frac{w}{n}\right] - \frac{1}{2}\left[\frac{w}{n}\right]^2 + \ldots\right\}} \qquad \ldots\ldots\ldots (3.8.13)$$

When n becomes very large compared with w, the equation (3.8.12) reduces to

$$t = t_i + \theta_w \zeta$$

which indicates that under such conditions the temperature distribution tends to become linear.

When equation (3.8.12) is applied to the two possible extremes of the cone, i.e to the 180^o cone or disc and to the 0^o truncated cone or cylinder, the two standard forms for their respective temperature distributions are obtained.

For the disc, the value of n is always infinite at any distance along the surface from the centre. When n is infinite,

$$t = t_i + \theta_w \zeta$$

which is the equation for the temperature distribution across a plane wall.

For the cylinder, n becomes the inside radius r_i, $(n + w)$ becomes the outside radius r_o, and $(n + \zeta w)$ becomes the intermediate radius r, and equation (3.8.12) reduces to

$$t = t_i + \theta_w \frac{\ln\left[\frac{r}{r_i}\right]}{\ln\left[\frac{r_o}{r_i}\right]}$$

which is the standard equation for the temperature distribution across a thick-walled cylinder. The general similarity in form between the above equation and that for the hollow cone suggests that the temperature distribution across the wall of a hollow cone can be evaluated from the equation for thick-walled cylinders if the various cylinder radii are replaced by their corresponding normals on the hollow cone.

From equation (3.8.12) the temperature gradient becomes:-

$$\frac{dt}{dy} = \frac{\theta_w}{(n + \zeta w) \ln\left[\frac{n + w}{n}\right]} \qquad \ldots\ldots\ldots (3.8.14)$$

or

$$\frac{dt}{d\zeta} = \frac{\theta_w}{\ln\left[\frac{n + w}{n}\right]}\left[\frac{w}{n + \zeta w}\right] \qquad \ldots\ldots\ldots (3.8.15)$$

which is a non-dimensional equation for the temperature gradient. These two equations show that the temperature gradient will attain its highest value at the inner surface where $\zeta = 0$ and decline in magnitude as ζ increases towards unity. At the limit where $n = 0$, the gradient becomes infinite at $\zeta = 0$ and the temperature distribution will become

$$t = t_o$$

Fig. 26 shows the cross-section of a cone with an apex angle of 60^o and a wall thickness of 0.025 m. The outer surface of the cone and the inner surface have uniform temperatures of 150^o C and 50^o C respectively. The temperature distributions shown are obtained from equation (3.8.12) for the given conditions.

At large distances away from the apex, where the change in curvature between the inner and outer surfaces becomes small, the temperature distribution is almost linear.

FIG 26

APEX ANGLE $\alpha = 60°$
OUTER SURFACE TEMPERATURE $t_o = 150°C$
INNER SURFACE TEMPERATURE $t_i = 50°C$

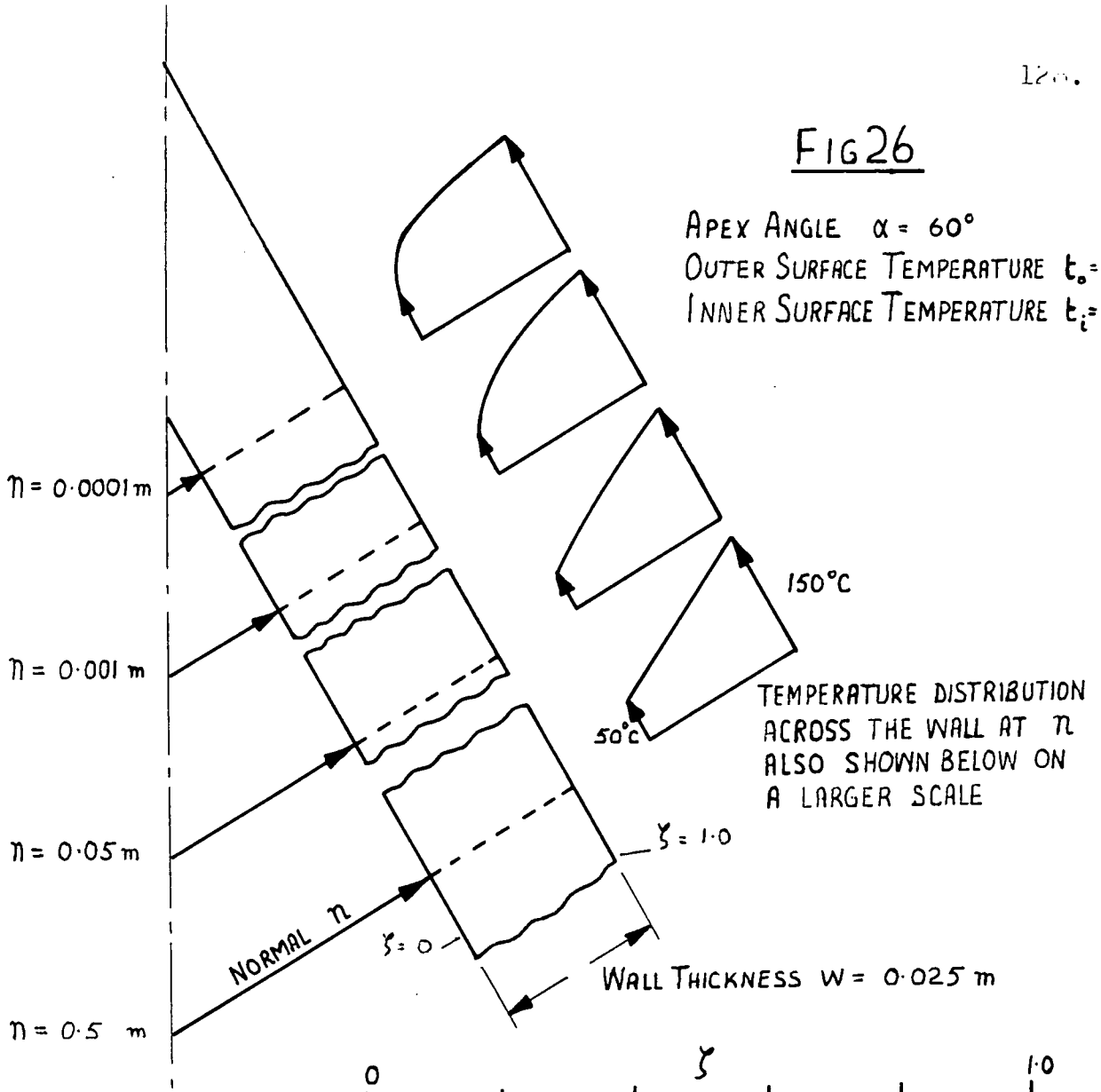

TEMPERATURE DISTRIBUTION ACROSS THE WALL AT η ALSO SHOWN BELOW ON A LARGER SCALE

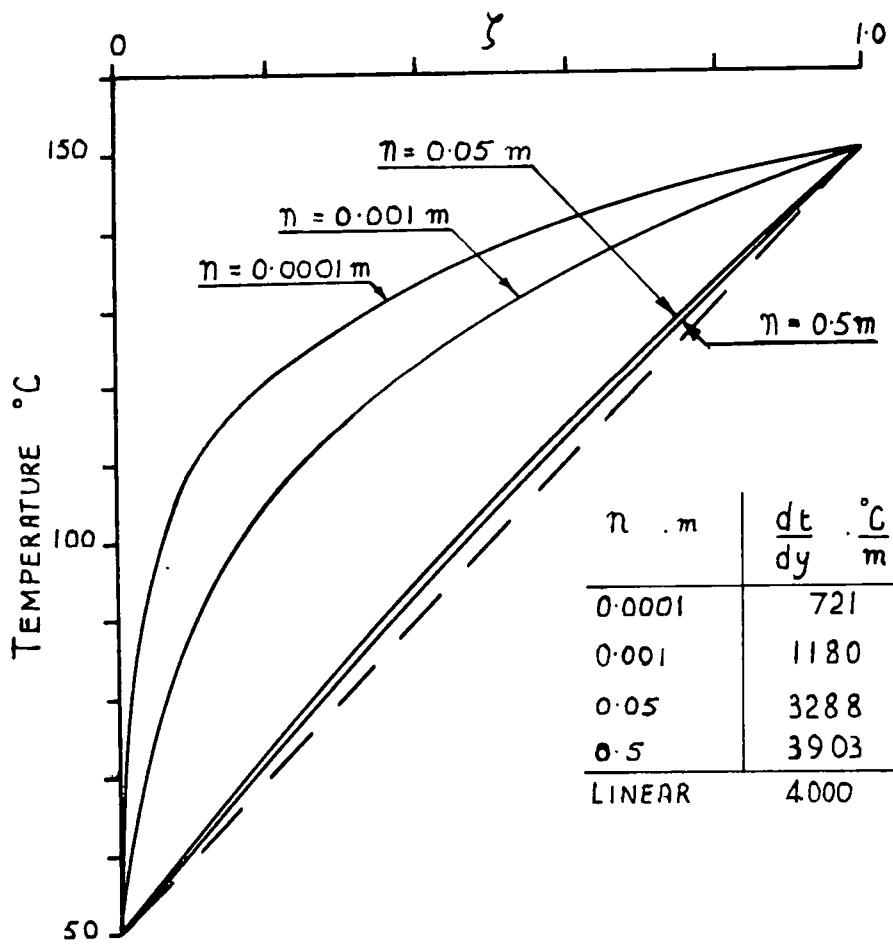

η . m	$\frac{dt}{dy}$. $\frac{°C}{m}$
0·0001	721
0·001	1180
0·05	3288
0·5	3903
LINEAR	4000

At n = .5 m the temperature gradient at the outer surface is 3903 $\frac{^{o}C}{m}$ or .975 times the linear temperature gradient. Conversely nearer the apex, where the change in curvature across the wall becomes large, the temperature distribution shows a considerable departure from linearity. At n = 0.05 m the temperature gradient at the outer surface is 3288 $\frac{^{o}C}{m}$ or .82 times the linear temperature gradient. In the limit as n approaches zero, the temperature gradient becomes very large at $\zeta = 0$ and tends towards zero at $\zeta = 1$. Two important points arise from these curves. The first point is that the heat flux does not remain uniform along the surface with uniform inner and outer surface temperatures, because as n decreases, the increasing curvature reduces the temperature gradient at the outer surface. The second point is that only at the inner and at the outer surfaces, where ζ is 0 and 1 respectively, can the temperature remain uniform with n. At any given intermediate value of ζ the temperature increases as n decreases. In effect this means that there is a rise in temperature within the wall in the -X direction and this rise in temperature is coupled with an energy transfer from the apex, that is in the positive X direction. This energy flow is greatest at the smaller values of ζ because the temperature is increasing in the negative X direction from $t = t_i + \theta_w \zeta$ at large n, to $t = t_o$ at $n = 0$.

Equation (3.8.12) was obtained by neglecting the energy transfer in the X direction but the solution has clearly shown that this energy transfer cannot be neglected. To fully account for this energy transfer along the wall and for that across the wall, the region near the apex must be

treated as a three-dimensional conduction problem. Having made that statement does not invalidate equation (3.8.12), because it is possible to define the region where the energy transfer in the X direction becomes negligible.

By differentiating equation (3.8.12) with respect to n while holding ζ constant, the temperature gradient $\frac{dt}{dn}$ is obtained. Denoting the temperature gradient in the X direction by $\frac{dt}{dX}$

$$\frac{dt}{dX} = \frac{dt}{dn} \cdot \frac{dn}{dx'},$$

where x' is the distance from the apex of the inner surface to the point where the normal n intersects the inner surface.

Hence $n = x' \tan \alpha$ and $\frac{dn}{dx'} = \tan \alpha$

Therefore
$$\frac{dt}{dX} = \frac{\theta_w \tan\alpha}{\ln\left[\frac{n+w}{n}\right]} 2\left\{-\frac{\zeta w}{n(n+\zeta w)} \ln\left[\frac{n+w}{n}\right] + \frac{w}{n(n+w)} \ln\left[\frac{n+\zeta w}{n}\right]\right\} \quad \ldots\ldots\ldots (3.8.16)$$

By integrating the above equation with respect to ζ between the limits of $\zeta = 0$ and $\zeta = 1$, the average value of the gradient $\frac{\overline{dt}}{dX}$ may be determined and this average gradient represents the energy flow per unit area in the X direction at any given position along the wall.

Thus
$$\frac{\overline{dt}}{dX} = \frac{\theta_w}{w} \tan\alpha \left\{1 - \frac{1}{b\,(b+1)\left[\ln\left(\frac{b+1}{b}\right)\right]^2}\right\} \quad \ldots\ldots\ldots (3.8.17)$$

where $n = b\,w$

The multiplier $\frac{\theta_w}{w}$ is the linear temperature gradient across the wall in the Y direction, therefore the average gradient can be conveniently expressed as

$$\frac{\overline{dt}}{dX} = \left.\frac{dt}{dy}\right|_{\text{linear}} \cdot \tan\alpha \left[f\,(b)\right] \quad \ldots\ldots\ldots (3.8.18)$$

where $$f(b) = \left\{ 1 - \frac{1}{b\,(b+1)\left[\ln\left[\frac{b+1}{b}\right]\right]^2} \right\}$$

If the energy flow in the X direction is considered to be negligible when

$$\frac{dt}{dX} = B \left.\frac{dt}{dy}\right|_{linear}$$

then equation (3.8.18) reduces to

$$B = \tan\alpha.(f(b)) \qquad \ldots\ldots\ldots (3.8.19)$$

The curve of f (b) against b, shown in fig. 27, may be used to obtain the distance from the inner apex to where

$$\frac{dt}{dX} = B \left.\frac{dt}{dy}\right|_{linear}$$

At any distance greater than x', the equations for the temperature distribution and temperature gradient may be used with negligible error.

For the 60° cone shown in fig. 27, the average gradient has become less than $0.1 \left.\frac{dy}{dy}\right|_{linear}$ at $x' = 0.56\ w$.

At $x' = w$ and at $x' = 3\ w$ the average gradient in the X direction decreases to $0.02 \left.\frac{dt}{dy}\right|_{linear}$ and $0.01 \left.\frac{dt}{dy}\right|_{linear}$ respectively, and may therefore be considered as negligible in this region.

The values of x' given for the 60° cone are not representative for all cones, because equation (3.8.19) shows that the value of x' is dependent on the apex angle of the cone. The curves given in fig. 28 are for x'/w plotted against semi apex angle α and show that for any given value of B, $\frac{x'}{w}$ reaches a maximum value. As B increases, the magnitude

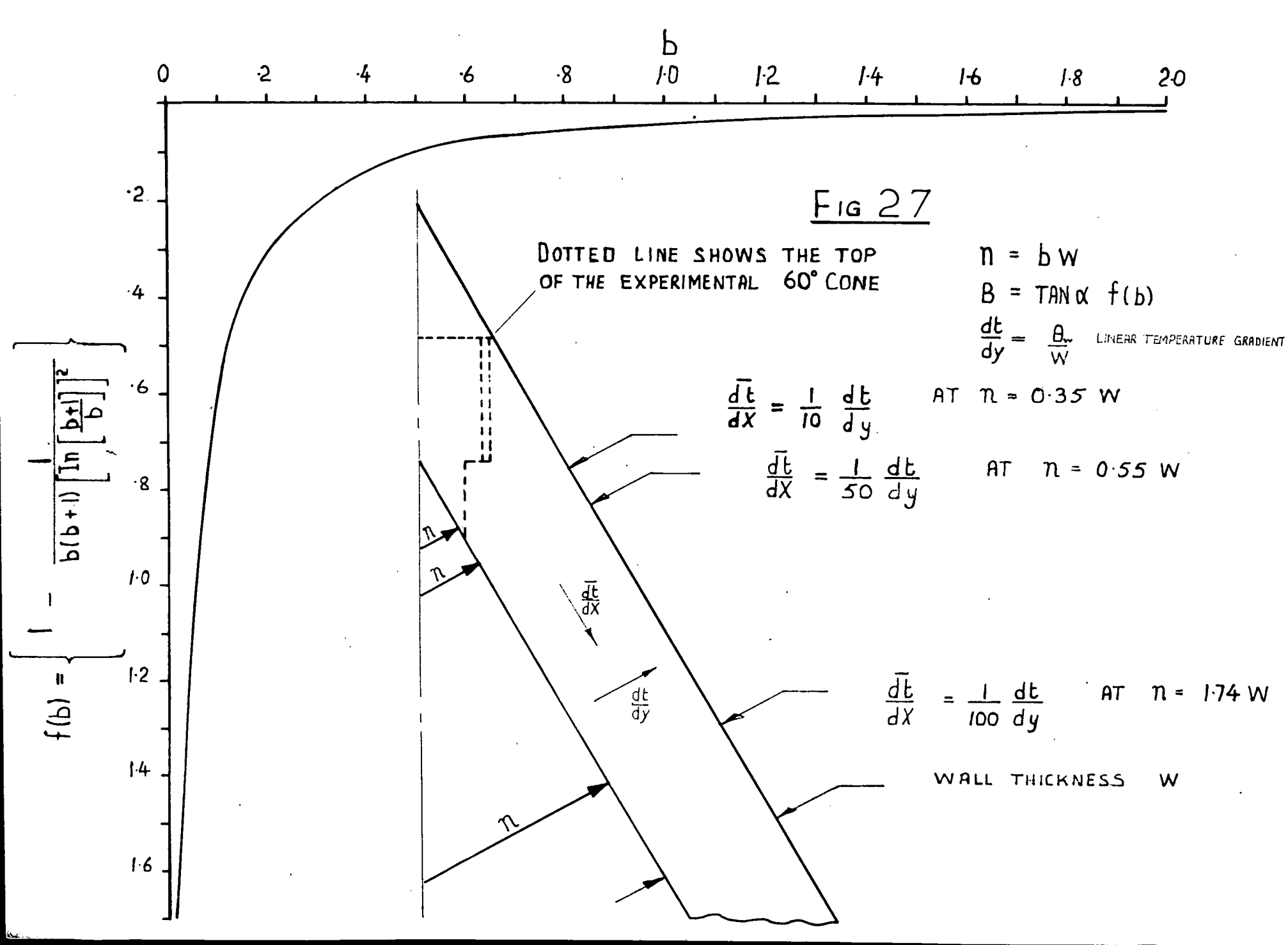

FIG 27

DOTTED LINE SHOWS THE TOP OF THE EXPERIMENTAL 60° CONE

$\eta = b\,W$

$B = \tan\alpha\ f(b)$

$\frac{dt}{dy} = \frac{\theta_w}{W}$ LINEAR TEMPERATURE GRADIENT

$\frac{\bar{dt}}{dX} = \frac{1}{10}\frac{dt}{dy}$ AT $\eta = 0{\cdot}35\ W$

$\frac{\bar{dt}}{dX} = \frac{1}{50}\frac{dt}{dy}$ AT $\eta = 0{\cdot}55\ W$

$\frac{\bar{dt}}{dX} = \frac{1}{100}\frac{dt}{dy}$ AT $\eta = 1{\cdot}74\ W$

WALL THICKNESS W

of the maximum value decreases and angle α , where the maximum value occurs, increases. The value of $\frac{x'}{w}$ is heavily dependent on the semi-apex angle α near the extremes of 0^o and 90^o. At these two extremes $\frac{x'}{w}$ is zero for all B, because with the cylinder, the difference in curvature between the inner and the outer surfaces is uniform with x making $\frac{dt}{dX} = 0$. With the disc, $\frac{dt}{dy}$ is linear and $\frac{dt}{dX}$ becomes zero.

Since $\tan \alpha = \frac{n}{x'}$ and $n = b\,w$ equation (3.8.19) may be written as

$$B = \frac{w}{x'}\, b\,(f\,(b)) \qquad \ldots\ldots\ldots (3.8.20)$$

Equation (3.8.20) can be used to replace the family of curves shown in fig. 28 by a single curve which is shown in fig. 29. The single curve shows that the maximum value of $\frac{Bx'}{w}$ occurs at $b = 0.1762$ and has a value of $b\,(f\,(b)) = 0.0597$. The maximum distance x' occurs at

$$x' = 0.0597\,\frac{w}{B} \qquad \ldots\ldots\ldots (3.8.21)$$

and at a semi-apex angle

$$\alpha = \tan^{-1}\,(2.8908\,B) \qquad \ldots\ldots\ldots (3.8.22)$$

The locus of the maxima shown in fig. 28 was obtained from equations (3.8.21) and (3.8.22).

The second type of cone material to be considered is one with a thermal conductivity which has a linear dependence on temperature. Thus the temperature coefficient β remains finite, although for most common metals β remains small. Introducing a variable thermal conductivity means that the complete form of equation (3.8.7) must be solved. This solution can be readily achieved with the aid of several

FIG 28

$$\frac{dt}{dX} = B \left.\frac{dt}{dy}\right|_{\text{LINEAR}}$$

x' DISTANCE IN THE X DIRECTION FROM THE APEX OF THE INNER SURFACE.
W WALL THICKNESS.

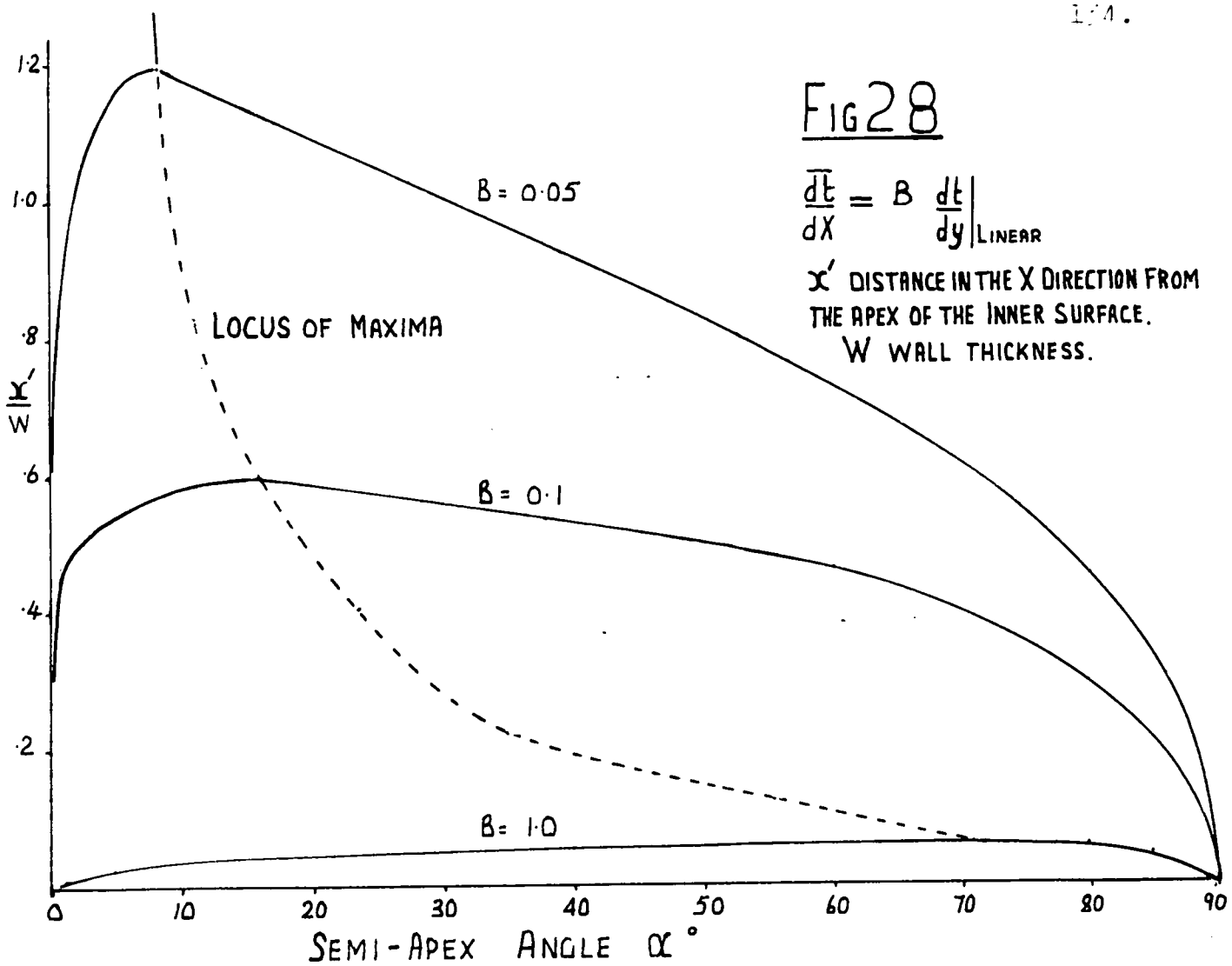

FIG 29

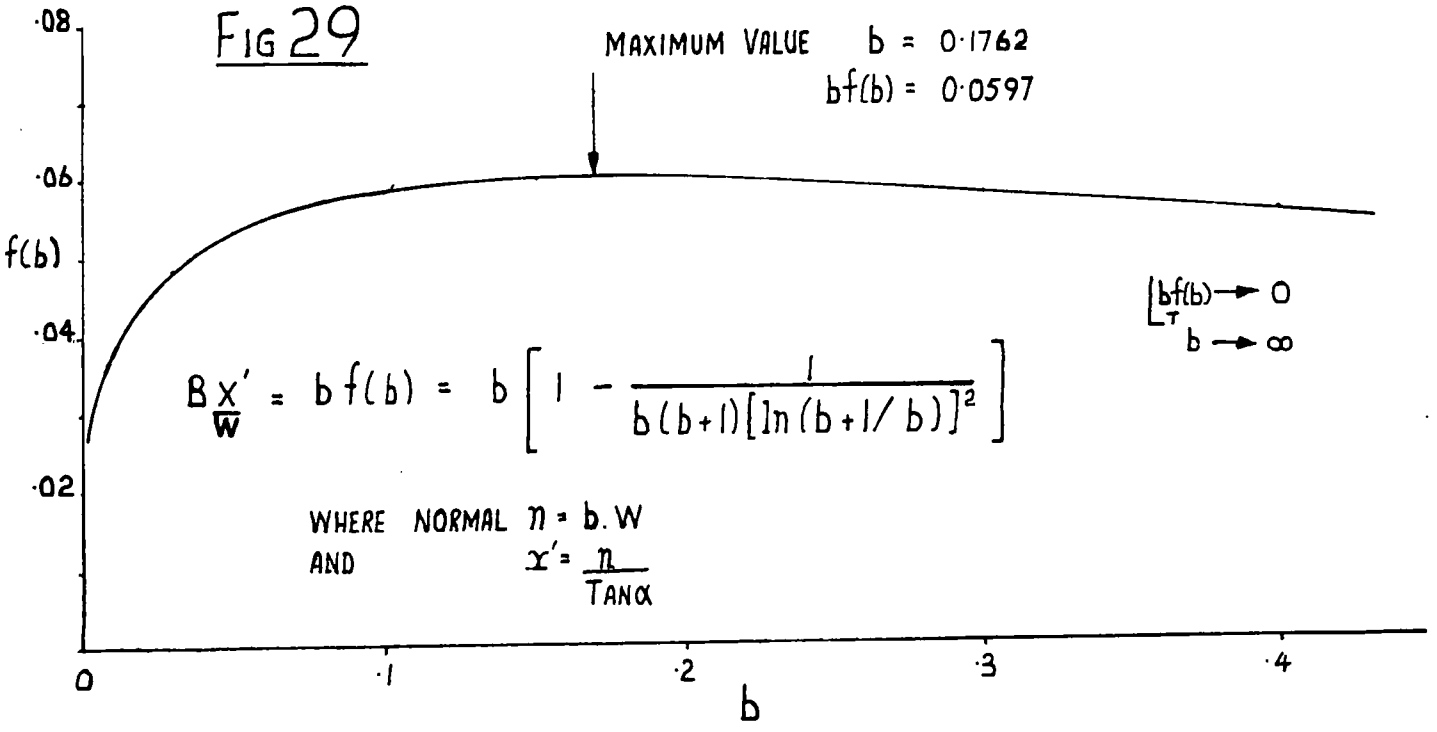

$$\frac{Bx'}{W} = bf(b) = b\left[1 - \frac{1}{b(b+1)[\ln(b+1/b)]^2}\right]$$

WHERE NORMAL $n = b.W$
AND $x' = \frac{n}{\tan\alpha}$

substitutions. The equation to be solved is

$$\frac{d^2t}{dy^2} + \frac{1}{y}\frac{dt}{dy} + \frac{\beta}{(1+\beta t)}\left[\frac{dt}{dy}\right]^2 = 0 \qquad \ldots\ldots\ldots (3.8.7)$$

let $R = 1 + \beta t$

then $\frac{dR}{dy} = \beta\frac{dt}{dy}$ and $\frac{d^2R}{dy^2} = \beta\frac{d^2t}{dy^2}$

hence equation (3.8.7) becomes:-

$$\frac{d^2R}{dy^2} + \frac{1}{y}\frac{dR}{dy} + \frac{1}{R}\left[\frac{dR}{dy}\right]^2 = 0 \qquad \ldots\ldots\ldots (3.8.23)$$

This equation may be reduced to a simpler differential equation by the introduction of a new and as yet unknown function Z of y

let $R = e^{\int Z\,dy}$

then $\frac{dR}{dy} = Z\,e^{\int Z\,dy}$ and $\frac{d^2R}{dy^2} = \left[\frac{dZ}{dy} + Z^2\right] e^{\int Z\,dy}$

hence equation (3.8.23) becomes:-

$$\frac{dZ}{dy} + \frac{Z}{y} + 2Z^2 = 0 \qquad \ldots\ldots\ldots (3.8.24)$$

or

$$\frac{dP}{dy} - \frac{P}{y} = 2 \qquad \ldots\ldots\ldots (3.8.25)$$

where $P = \frac{1}{Z}$ and $\frac{dP}{dZ} = -\frac{1}{Z^2}\frac{dZ}{dy}$

The integrating factor for equation (3.8.25) is $\frac{1}{y}$ which reduces equation (3.8.25) to

$$\frac{d\left[\frac{P}{y}\right]}{dy} = \frac{2}{y}$$

Hence $P = y\,(2\ln(y) + C_3)$

and $Z = \frac{1}{y\,(2\ln(y) + C_3)}$

Since $R = e^{\int Z\,dy}$

or $R = e^{\int \frac{1}{y\,(2\ln(y) + C_3)}\,dy}$

after integration R becomes:-

$$R = C_4 \left(2 \ln (y) + C_3\right)^{\frac{1}{2}} \qquad \ldots\ldots\ldots (3.8.26)$$

By introducing the boundary conditions shown in fig. 25, the constants C_3 and C_4 may be evaluated.

At $y = n$; $\quad t = t_i$

therefore $R_i = 1 + \beta t_i$ $\qquad \ldots\ldots\ldots (3.8.27)$

and $R_i = C_3 \left(2 \ln (n) + C_3\right)^{\frac{1}{2}}$ $\qquad \ldots\ldots\ldots (3.8.28)$

At $y = n + w$; $\quad t = t_o$

therefore $R_o = 1 + \beta t_o$ $\qquad \ldots\ldots\ldots (3.8.29)$

and $R_o = C_4 \left(2 \ln (n + w) + C_3\right)^{\frac{1}{2}}$ $\qquad \ldots\ldots\ldots (3.8.30)$

Equations (3.8.28) and (3.8.30) give

$$\frac{R_o}{R_i} = \frac{1 + \beta t_o}{1 + \beta t_i} = \left[\frac{2 \ln (n + w) + C_3}{2 \ln (n) + C_3}\right]^{\frac{1}{2}}$$

Hence

$$C_3 = \frac{2\left\{\left(\ln (n + w) - \left[\frac{R_o}{R_i}\right]^2 \ln (n)\right\}\right.}{\left[\frac{R_o}{R_i}\right]^2 - 1} \qquad \ldots\ldots\ldots (3.8.31)$$

and

$$C_4 = \frac{R_i}{\left(2 \ln (n) + C_3\right)^{\frac{1}{2}}} \qquad \ldots\ldots\ldots (3.8.32)$$

Finally, the solution of the equation for the temperature distribution with variable thermal conductivity becomes:-

$$t = \frac{1}{\beta}\left\{\left[\frac{R_o^{\,2} \ln \left(\frac{n + \zeta w}{n}\right) + R_i^{\,2} \ln \left(\frac{n + w}{n + \zeta w}\right)}{\ln \left(\frac{n + w}{n}\right)}\right]^{\frac{1}{2}} - 1\right\} \qquad \ldots\ldots\ldots (3.8.33)$$

where $\quad 0 < \zeta \leq 1.0$

The temperature gradient may be obtained from equation (3.8.33)

$$\frac{dt}{dy} = \frac{R_o^{\,2}}{2\beta(n+\zeta w)\left\{\ln(n+w)\left[R_o^{\,2} \ln\left(\frac{n+w}{n}\right) + R_i^{\,2} \ln\left(\frac{n+w}{n+\zeta w}\right)\right]\right\}^{\frac{1}{2}}} \qquad \ldots\ldots\ldots (3.8.34)$$

At the outer surface where $\zeta = 1.0$, the above equation reduces to

$$\frac{dt}{dy} = \frac{R_o^2 - R_i^2}{2 \beta R_o (n + w) \ln\left(\frac{n + w}{n}\right)} \qquad \ldots\ldots\ldots (3.8.35)$$

Equation (3.8.33) shows that at the outer surface, the temperature gradient, at any position n and for any wall thickness w, is a function of the temperature t_i and t_o and of the temperature coefficient . As β becomes large ($>.05$) the term $\frac{R_o^2 - R_i^2}{2 R_o}$ tends to $\frac{t_o^2 - t_i^2}{2t_o}$

Fig. 30 shows the temperature distribution with variable thermal conductivity, for two positions along the cone wall. Temperature coefficients of $\beta = 0$, 0.002 and 0.02 $\frac{1}{\sigma_C}$ have been used to produce the curves from equation (3.8.32) and the temperature gradients at the outer surface from equation (3.8.34). The effect of introducing variable thermal conductivity with positive temperature coefficients is to make the temperature distribution depart further from linearity. Conversely if a negative temperature coefficient was used, the temperature distribution would be moved in the opposite direction and back towards linearity or even to pass through that condition. Increasing the temperature coefficient from zero to + 0.002, which is approximately the value for the test cones, reduces the temperature gradient by 8% at n = 0.05 m and at n = 0.5 m. Increasing the temperature coefficient from zero to 0.02 reduces the gradient by 13% at these two positions. For small values of temperature coefficient, of the order 0.002, equation (3.8.35) can be used to show that the heat flux may be calculated by equation

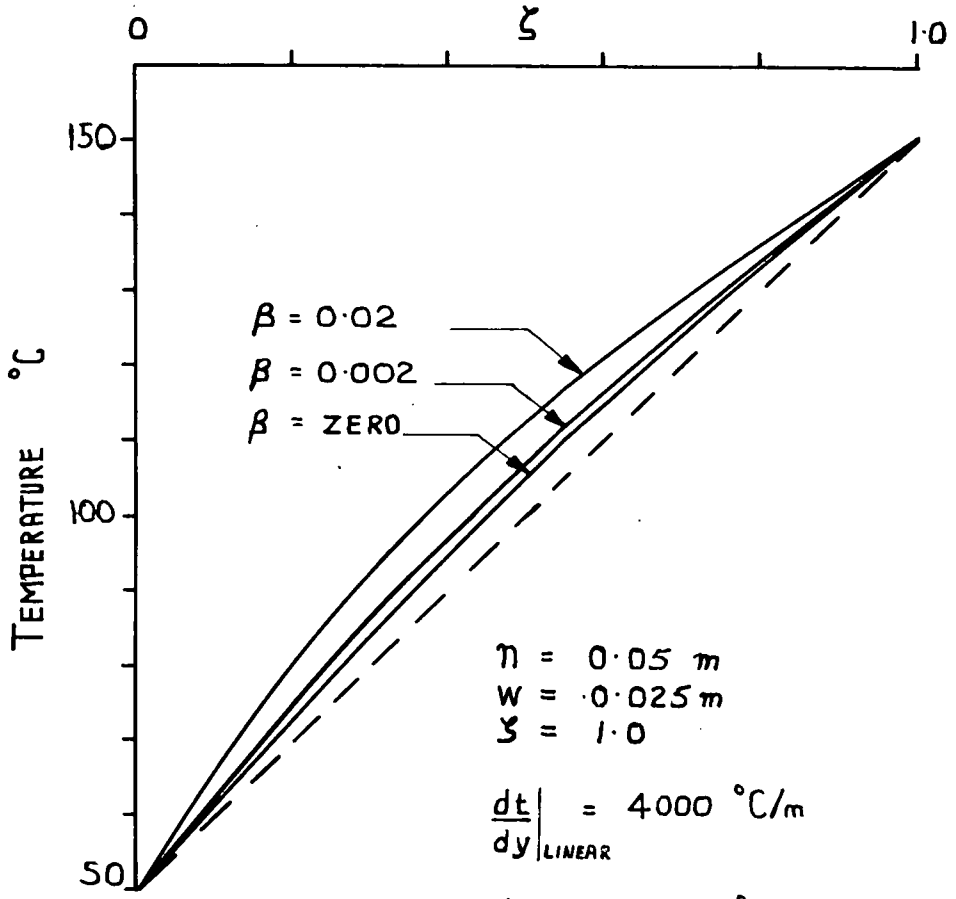

η = 0·05 m
W = 0·025 m
ζ = 1·0

$\left.\frac{dt}{dy}\right|_{LINEAR}$ = 4000 °C/m

$\frac{dt}{dy}$ = 3288 °C/m β = ZERO

$\frac{dt}{dy}$ = 3035 °C/m β = 0·002

$\frac{dt}{dy}$ = 2466 °C/m β = 0·02

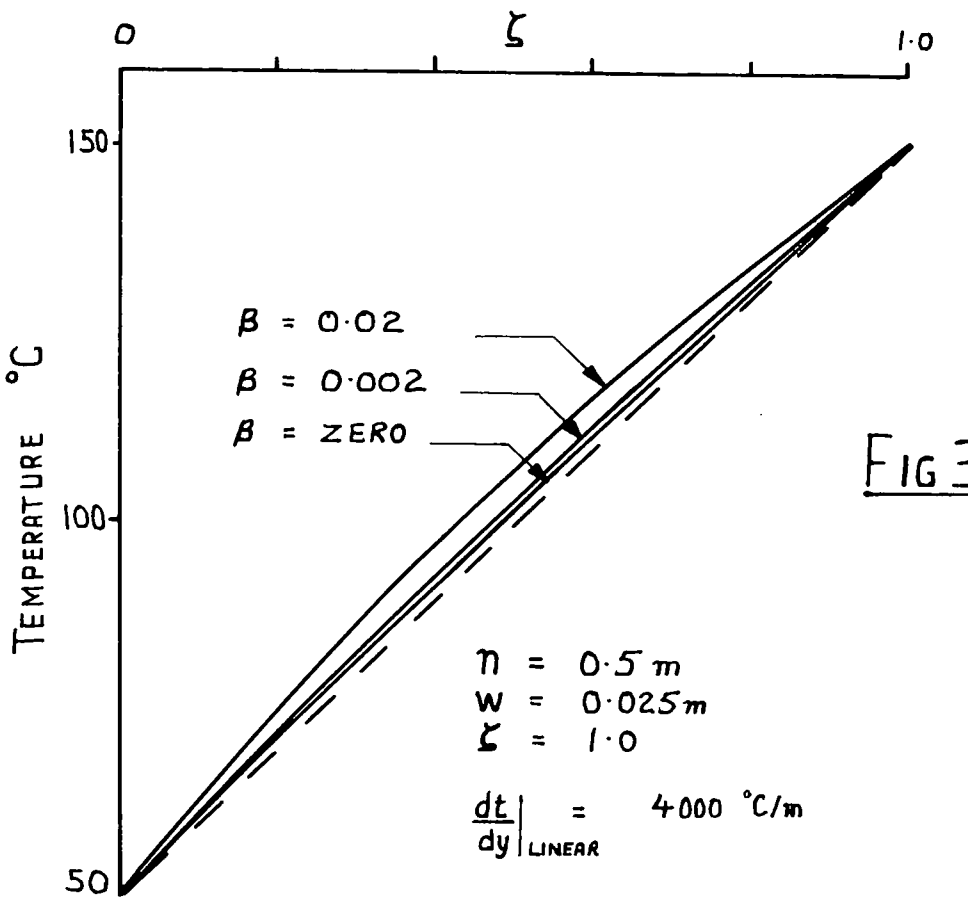

FIG 30

η = 0·5 m
W = 0·025 m
ζ = 1·0

$\left.\frac{dt}{dy}\right|_{LINEAR}$ = 4000 °C/m

$\frac{dt}{dy}$ = 3903 °C/m β = ZERO

$\frac{dt}{dy}$ = 3605 °C/m β = 0·002

$\frac{dt}{dy}$ = 2928 °C/m β = 0·02

(3.8.14), if the thermal conductivity is evaluated at the mean wall temperature.

The effects of variable thermal conductivity in the materials used for the experimental cones are shown to be significant, and need to be included in the calculation of the experimental heat flux.

Remarks made earlier concerning the small region near the apex of the cone where the equations for temperature distribution and temperature gradient become inaccurate, also apply to equations (3.8.33) and (3.8.34). After removing the apex from the 60° experimental cone to accommodate the small shaft (fig. 27) the energy transfer in the X-direction remains negligible at the start of the working slant length where $x' = 1.74\ w$. The equations for temperature distribution and gradient are also valid for the experimental truncated 10° and 20° combined cones, because the film starts at cone diameter $d = 0.493$ m. The effects of energy transfer along the wall of the combined cone has been investigated by field plotting with teledeltos paper. Energy transfer to the wall from the end cover plates has been shown to be negligible at a distance along the wall equal to the wall thickness w.

4.0 APPARATUS

4.0 Introduction.

The construction of the basic apparatus shown in fig. 31 from the design and preparation of working drawings through to the final commissioning was jointly undertaken by the author and Mr. B.T. Robson. At this early stage in the project each designer was ultimately concerned with only one of the two particular aspects of the research,

(i) the heat transfer from steam to the rotating cone, and

(ii) the fluid mechanics of the film of condensate.

Each designer, therefore, paid particular attention to the overall design from his own point of view. This arrangement produced an integrated design capable of satisfying the research needs of both workers.

The work-load for the design of the basic apparatus including the 60° cone was divided equally between the two designers, with each designer checking the others calculations. The author designed and commissioned a second conical body incorporating cones with apex angles of 10°, 20° and 150°, together with it's ancillary equipment including the cooling water system.

As far as the author is aware, no apparatus of similar size has been constructed for research into the condensation of steam on cold rotating bodies; a fact which makes this equipment unique.

One of the prime design considerations in this project was for the general safety of personnel, both operating and

working, in the vicinity of the apparatus while under test conditions.

Apart from being safe to use, the apparatus had to be functional and meet the diverse requirements specified in this research programme. Consideration was also given to possible future research requirements, such as steam condensing on other cones and on rotating axi-symmetrical bodies having curved profiles. Thus the designers had to consider not only the short term needs but also as many as possible of the foreseable requirements in the long term.

A preliminary working design was drawn up for the complete apparatus required to contain rotating cones with various apex angles, but all with a 0.61 m base diameter. The size of the base diameter decided the scale of the apparatus. Major items of the apparatus were designed and put out to tender as a costing exercise, and an estimate of the total cost of the numerous minor items of equipment was made. This was done to ascertain a cost analysis of the project and hence to determine whether or not the final cost would fall within the fixed sum set aside for apparatus.

Early in 1967 the basic design was completed and final tenders were called for major items such as the pressure vessel and the motor unit.

To save money many parts of the apparatus, including the main shaft, were manufactured in the University workshops by the Author and Mr. B.T. Robson and by the resident technicians. Being one of the co-designers and playing a

direct part in all stages from design through to final commissioning proved extremely useful in ensuring that the required accuracy of manufacture was always maintained and that design modifications could be effected quickly. High precision in manufacture and in assembly was essential on apparatus of this size to ensure that the rotating parts moved with precision and with the minimum of vibration.

Various design criteria, together with other relevant details concerning individual items of equipment, are discussed in the following sections of this chapter.

4.1 Specification.

The following specification was drawn up in 1966 and formed the basic requirements in the design for the research apparatus:-

(1) Steam pressure; variable up to 13.8 bar.

(2) Steam condition; dry saturated.

(3) Cone base diameter; 0.61 m.

(4) Apex angles; 60°, 90°, 120°, 150°.

(5) Speeds of rotation of the cone variable between 0-2000 rev/min.

(6) The outside surface temperature of the cone should be capable of controlled variation, but in the first series of tests, should be kept at a uniform temperature.

(7) Condensate forming on the interior surface of the pressure vessel should not drip on the cone.

(8) All cones should be capable of being viewed both tangentially and normally while under test.

(9) Windows in the pressure vessel should be capable of withstanding the working steam pressure and temperature, and allow the cones to be photographed.

(10) The polar axis of the cones should be vertical.

(11) The cones should be capable of being rotated with the minimum of vibration.

(12) The steam supply should be free from non-condensable gases.

The condensing elements were made as large as possible to reduce scale effects if the test results were to be used to calculate the thermal stresses in turbine rotors. A base diameter of 0.61 m gave a large area of condensing surface regardless of the apex angle of the cone.

An apex angle of 60° was chosen for the first cone. This was consistent with work being carried out in the Department at that time by Holgate (71) whose interest was with the wave formation in constant flow rate water films on conical surfaces. His apparatus for this work also used a 60° cone with a base diameter of 0.61 m. Although condensation was not taking place on Holgate's cone, having both cones the same size made it possible to compare some of the results obtained from each piece of apparatus.

The second experimental body was completed in early 1971 and featured truncated cones of 10° and 20° apex angle with a cover plate in the form of a 150° cone. The 10° and 20°

angles were chosen to give film drainage by the formation and detachment of drops which had not been observed on the 60^{o} cone, where drainage occurred in a direction along the surface.

As explained in section 2.4, the film of condensate on a rotating body can drain either in a direction along the surface of the body or in a direction perpendicular to the surface of the body; or possibly in both directions simultaneously. The speed of rotation at which these modes of drainage would occur on the proposed experimental cones was unknown at the design stage, therefore a wide range of speeds 0-2000 rev/min was called for in the specification.

The theoretical studies of condensation on rotating bodies assume that the body rotates in an infinite volume of vapour. A minimum clearance of 0.3 m was left between the cone and the walls of the pressure vessel to minimise drag between the steam and the walls.

4.2 General arrangement of the apparatus.

Fig. 31 shows the main features of the research apparatus and a general view of the complete assembly. Item numbers are assigned to the important parts of the apparatus shown on fig. 31 and these item numbers are also used in the following sub-sections.

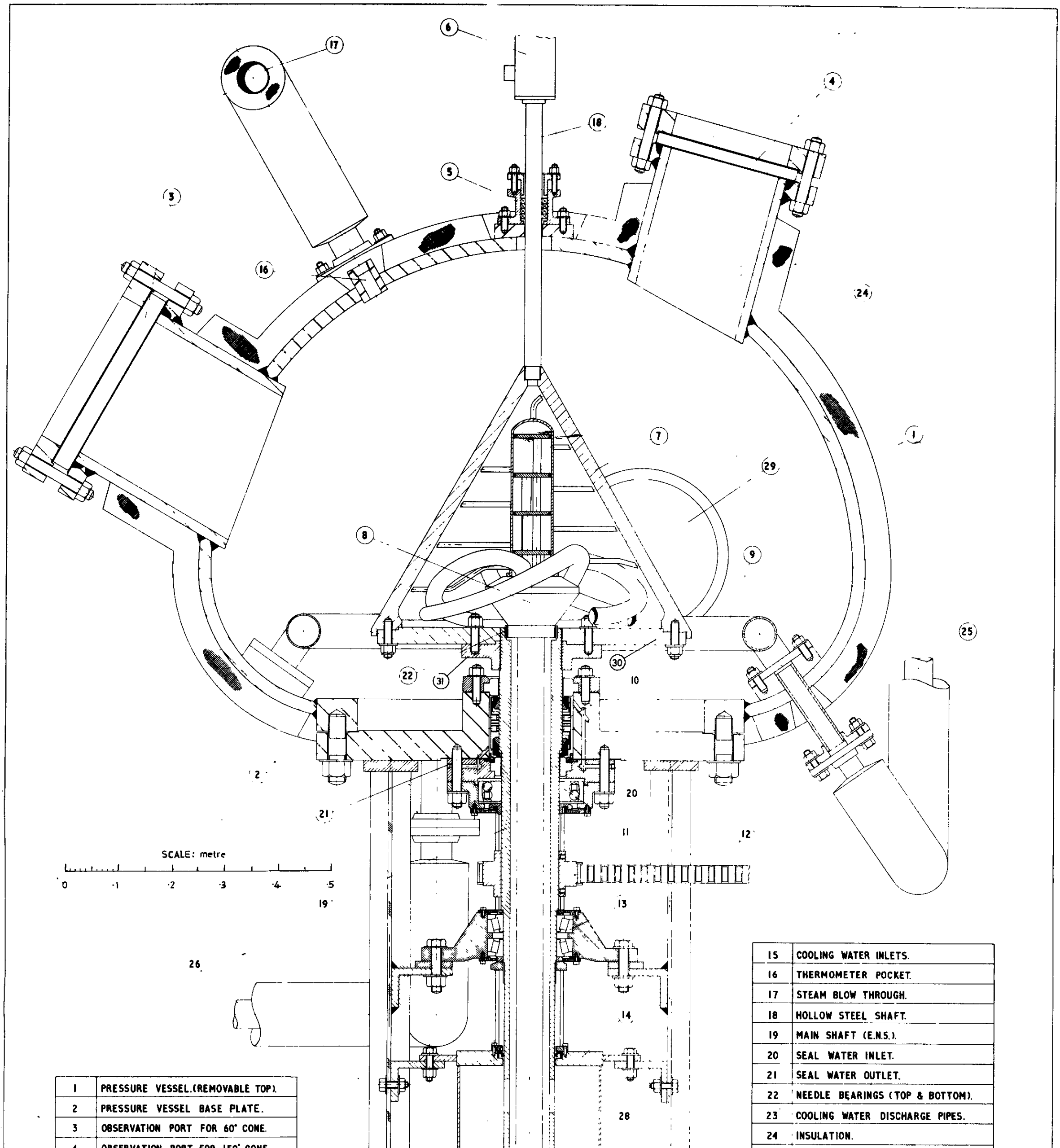

1	PRESSURE VESSEL.(REMOVABLE TOP).
2	PRESSURE VESSEL BASE PLATE.
3	OBSERVATION PORT FOR 60° CONE.
4	OBSERVATION PORT FOR 150° CONE.
5	STUFFING BOX.
6	SLIP RING UNIT.
7	60° ALUMINIUM BRONZE CONE.
8	WATER SPRAY AND COLLECTOR UNIT.
9	STEAM DISTRIBUTOR.
10	MECHANICAL SEAL UNIT.
11	LOCATING BEARING.
12	TIMING BELT AND PULLEY WHEEL
13	THRUST BEARING.
14	PERSPEX COLLECTOR.

15	COOLING WATER INLETS.
16	THERMOMETER POCKET.
17	STEAM BLOW THROUGH.
18	HOLLOW STEEL SHAFT.
19	MAIN SHAFT (E.N.S.).
20	SEAL WATER INLET.
21	SEAL WATER OUTLET.
22	NEEDLE BEARINGS (TOP & BOTTOM).
23	COOLING WATER DISCHARGE PIPES.
24	INSULATION.
25	STEAM INLET.
26	CONDENSATE DRAIN.
27	SUPPORTING STEELWORK.
28	COOLING WATER DISCHARGE FROM SHAFT.
29	HORIZONTAL OBSERVATION PORT.
30	CONE BASE PLATE
31	SHAFT FLANGE

FIG 31

4.3 Pressure Vessel.

The pressure vessel was designed and built to class II of the British Standard Specification 1500:1950; the specification for Fusion Welded Unfired Pressure Vessels. A maximum working pressure of 13.8 bar for dry saturated steam gave the vessel a design pressure and temperature of 15.2 bar and 200° C respectively.

Essentially the vessel (see fig. 31) consisted of two detachable parts, (i) a thick base cover (item 2) capable of housing the main shaft together with its locating bearing and seal, and (ii) a domed head (item 1) to which the observation ports were attached. These two main elements were bolted together. To compensate for loss of strength due to observation port openings in the shell, the general shell thickness of the dome was increased to 0.0254 m. The basic shell of the dome was formed by butt-welding together two hot-pressed dished ends, one hemispherical and one semi-elipsoidal.

In manufacture the centres of the ports were positioned within a tolerance of $\pm$ 0.003 m and the port flanges, which had been thickened to allow for final machining, were faced off to within $\pm$ 0.1 degrees of the required angle. Provision was also made for a stuffing-box gland to be housed on the crown of the dome and for a pressure gauge, a thermometer pocket and a blow-off valve to be positioned as convenient in areas of the dome not reserved for observation ports.

Steam inlet pipes, together with the semi-circular

distributor pipes (item 9), were installed in the lower portion of the dome.

The availability of thick toughened armour-plate glass discs governed the maximum observation port diameter. Messrs. Pilkington Brothers Ltd. recommended that 0.372 m diameter by 0.032 m thick and 0.273 m diameter by 0.022 m thick armour-plate glass would give clear 'sight size' ports of 0.3 m and 0.24 m diameter respectively, and would withstand both the working and the proof-testing conditions. This firm kindly undertook to supply the discs as a special order.

Rings of steam jointing placed on both faces of the glass discs provided a soft seating and prevented glass to metal contact with the retaining flanges.

Port geometry.

The two modes of viewing required for photography by the original specification were (i) perpendicular to and (ii) tangential to the condensing surfaces of the cones.

To minimise the effects of distortion due to the thickness of the glass windows, the ports were made large enough or increased in number to give full coverage of the cone generator from the perpendicular direction. The following observation ports were arranged on the dome as shown in fig. 32 to enable the surfaces of the four original cones to be viewed from the perpendicular direction.

Cone apex angle	Port	No.	Sight size
60°	A1, A2	2	0.3 m diameter
90°	B	1	0.3 m diameter
120°	C	1	0.24 m diameter
150°	D	1	0.24 m diameter

SECTION A2 D

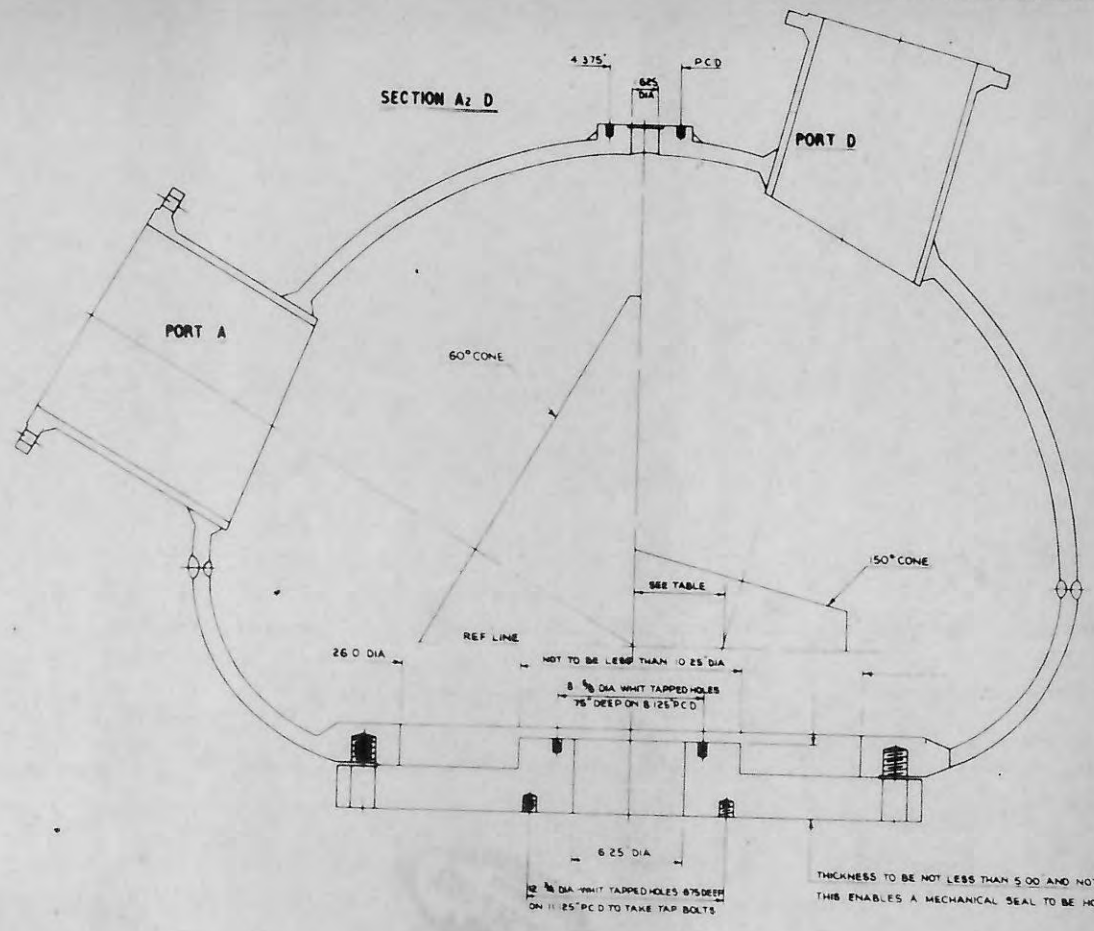

THICKNESS TO BE NOT LESS THAN 5.00 AND NOT MORE THAN 5.25"
THIS ENABLES A MECHANICAL SEAL TO BE HOUSED

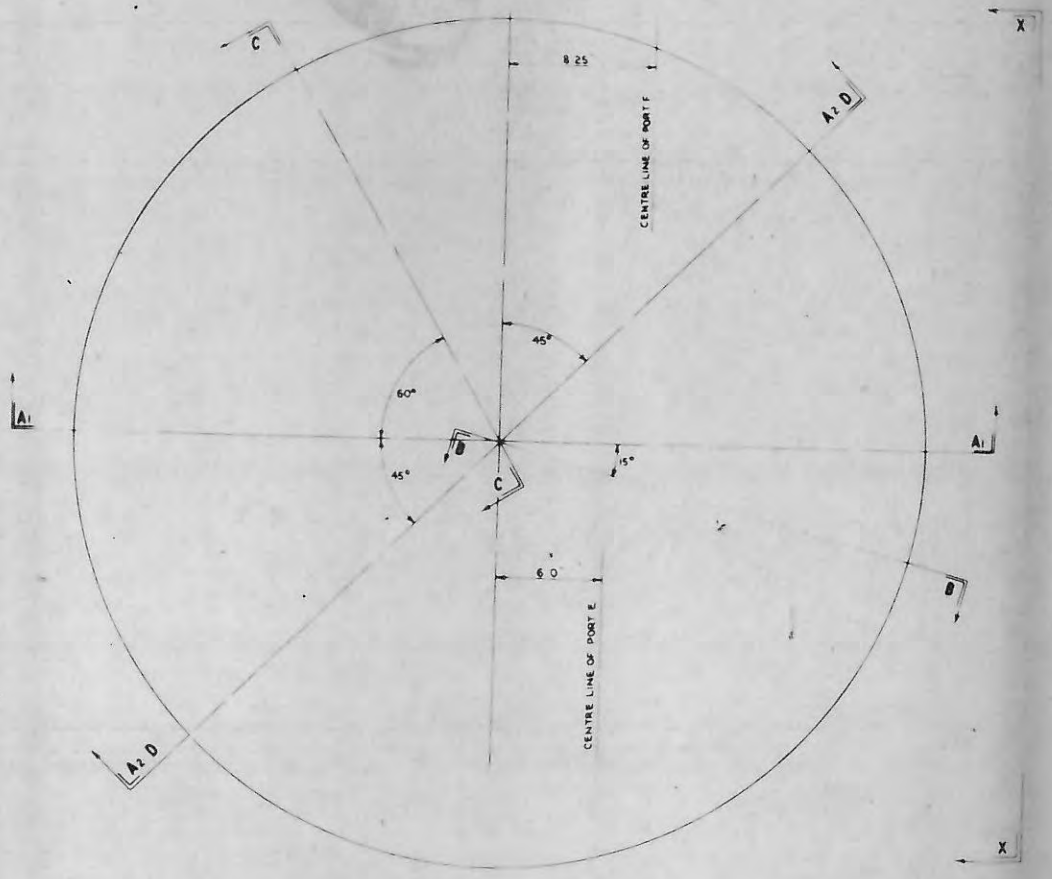

SECTION A1 A1

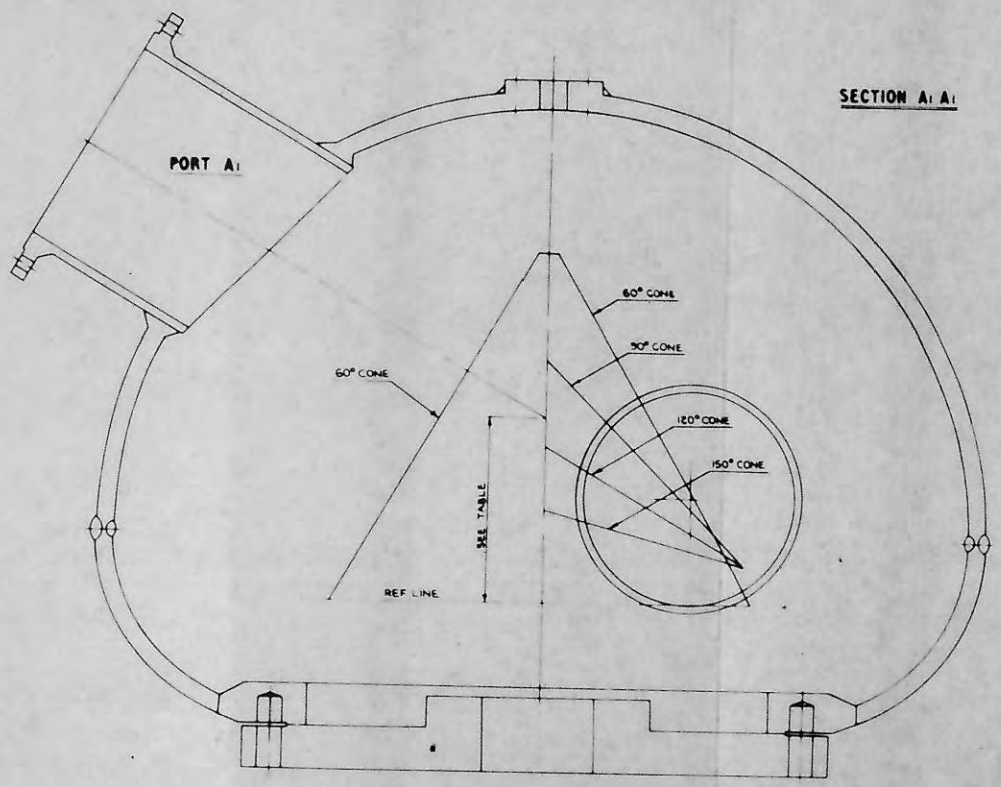

FIG 32

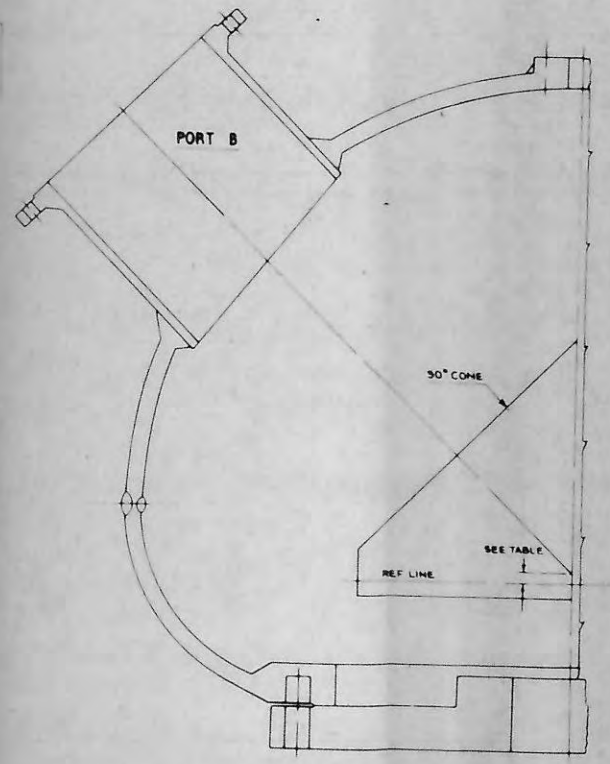

SECTION B B

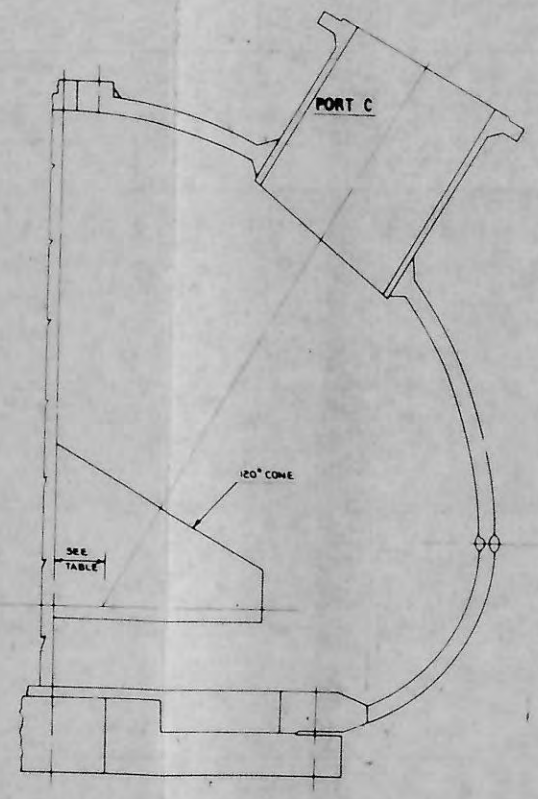

SECTION C C

TITLE	DRAWING No.	ISSUE
GEOMETRICAL REQUIREMENT FOR RESEACH PRESSURE VESSEL.	2a	

NOTE 1. ALL PORTS TO HAVE AN OUTSTAND OF ABOUT 9.0" AND COMPLY WITH DRAWING No. 8

2. THE REFERENCE LINE REPRESENTS THE BASE LINE OF CONES AND MUST BE MAINTAINED AT 9.5" ABOVE OUTSIDE OF BASE PLATE AS SHOWN

PORT	SIGHT SIZE OR NOZZLE BORE	TYPE OF VIEW GIVEN BY PORT	POSITION OF PORT CENTRE LINE OR INTERSECTION WITH REF PLANE OR VERTICAL CENTRE LINE			
			"a"	"b"	"c"	ANGLE TO VERTICAL "E"
A_1	12·0" DIA.	NORMAL TO 60° CONE	—	10·375"	—	60°
A_2	12·0" DIA.	NORMAL TO 60° CONE	0·0"	0·0"	0·0"	60°
B	12·0" DIA.	NORMAL TO 90° CONE	—	0·625"	—	45°
C	9·0" DIA.	NORMAL TO 120° CONE	2·875"	—	—	30°
D	9·0" DIA.	NORMAL TO 150° CONE	5·0"	—	—	15°
E	12·0" DIA.	TANGENTIAL TO EDGES OF ALL CONES.	AS SHOWN ON THIS DRAWING			90°
F	12·0" DIA.					90°

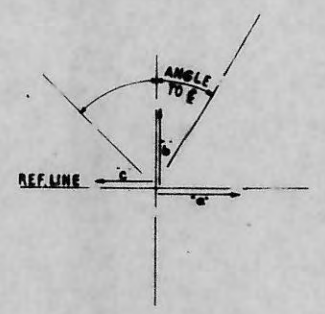

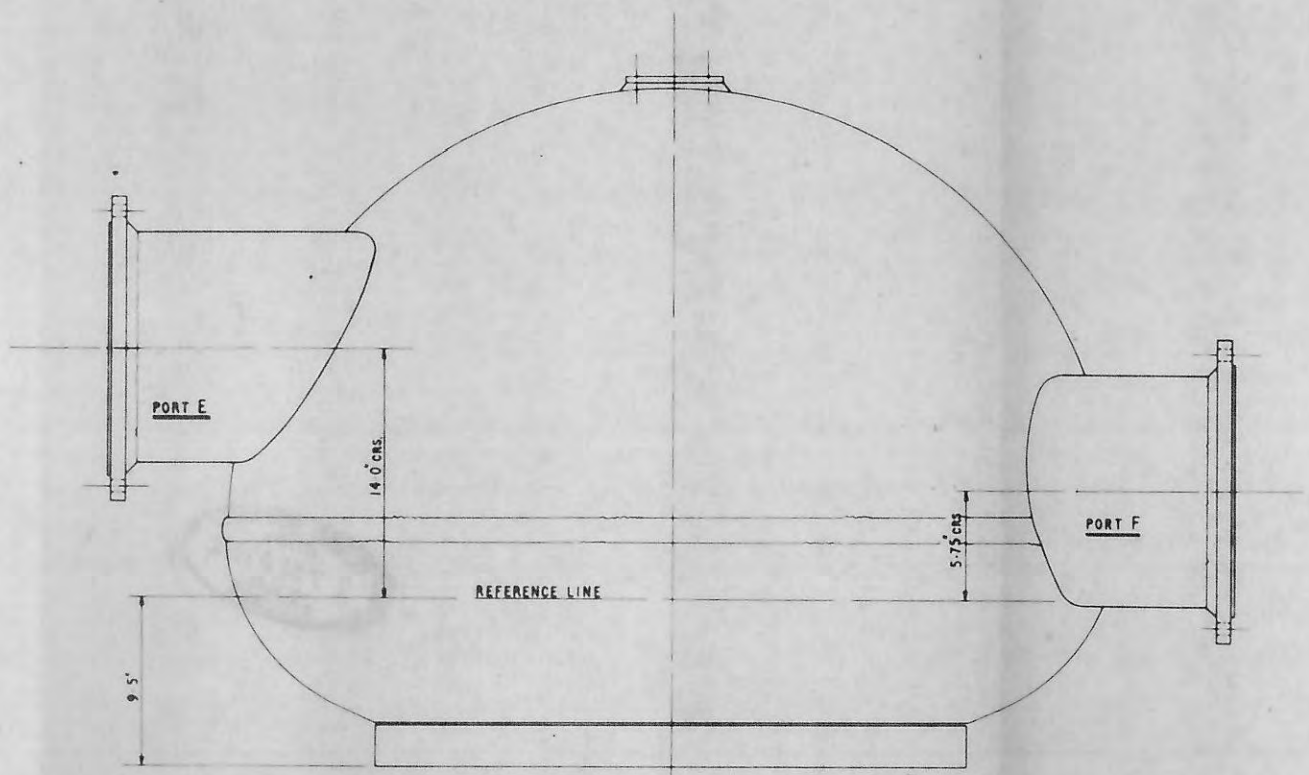

VIEW IN DIRECTION OF ARROW XX

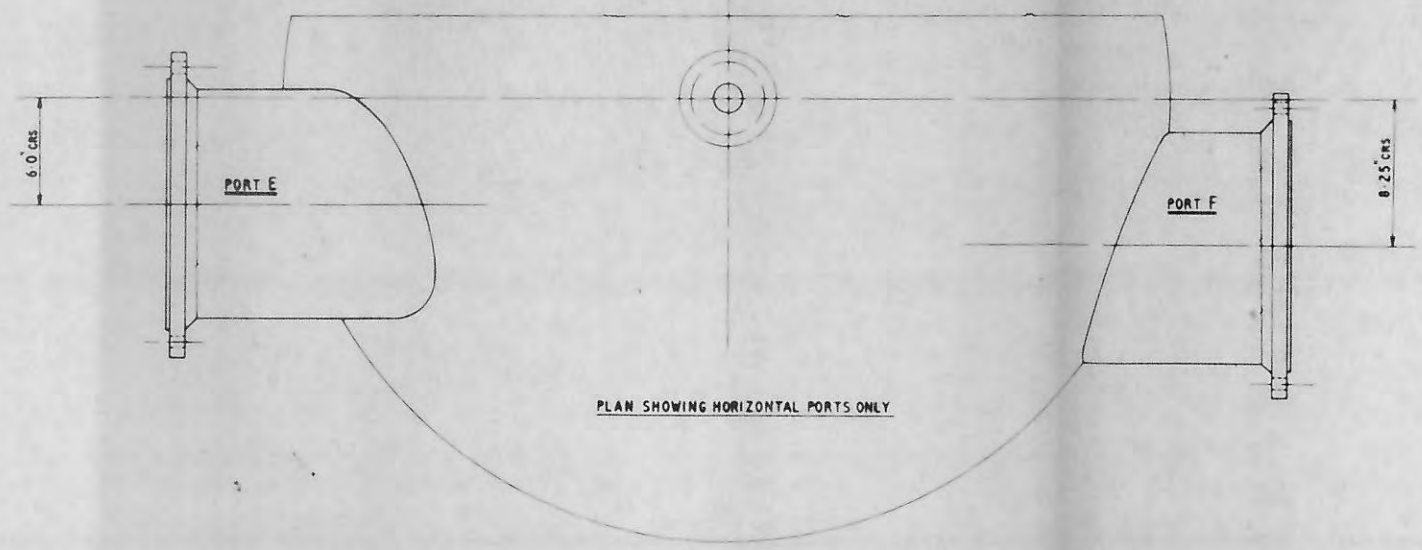

PLAN SHOWING HORIZONTAL PORTS ONLY

DESIGN CONDITIONS TO B.S. 1500 1515

WORKING FLUID	DRY SATURATED STEAM AT ALL PRESSURES
WORKING PRESSURE	5 – 200 $\frac{lbf}{in^2}g$
DESIGN PRESSURE	220 $\frac{lbf}{in^2}g$
HYDRAULIC TEST PRESSURE	300 $\frac{lbf}{in^2}g$ AT 60°
MAXIMUM WORKING TEMPERATURE	400°F

MATERIAL SPECIFICATION

MATERIAL FOR MANUFACTURE OF VESSEL TO COMPLY WITH BS 1501-151 GRADE 28A
BOLTING TO B.S. 1750 GRADE B7

FIG 33

TITLE	DRG. No.	ISSUE
GEOMETRICAL REQUIREMENT FOR RESEARCH PRESSURE VESSEL.	2b	

Two 0.3 m diameter horizontal ports were provided for tangential viewing fig. 33. These ports were positioned to allow the generator of each cone to be viewed tangentially through one, or through a combination of the two ports. Bearing in mind that at some future date condensing elements other than cones might be used, the view through the two ports was overlapped to give the greatest continuous coverage of area in the tangential plane.

An 0.05 m coating of magnesia plastic and an 0.012 m coating of finishing cement applied to the vessel after completion gave effective insulation against thermal losses.

4.4 Experimental cones.

4.4.1 The 60^{o} experimental cone.

The first experimental cone had an apex angle of 60^{o} (item 7). Several important factors were considered during the design and construction of the 60^{o} cone and of subsequent cones.

(i) The physical properties of the cone material. Aluminium-bronze BS 1400 AB1.C was chosen as the casting material for the 60^{o} cone. When cast by the Durville process, which involved tilting the mould during the pouring operation, this alloy formed pore-free castings. Also the alloy had good machining qualities and formed a surface film of oxide which was stable and had resistance to corrosion from any of the steam conditions likely to be encountered inside the pressure vessel.

(ii) Thermal energy transfer across the cone wall.

The thermal conductivity of the casting material and the wall thickness of the cone were directly related to the flow of thermal energy across the wall for any given surface heat transfer coefficient and temperature difference. At the time of design a practical limit was imposed on the energy flow by the available supply of cooling water, which was limited by the recirculation and cooling rates of the closed circuit cooling system in the laboratory. One feature considered necessary for the apparatus was that the total cooling-water demand for all purposes should be within the continuous recirculation and cooling rate of this system. Estimates of the experimental heat transfer coefficient and of the thermal conductivity of the cone material were used to obtain the wall thickness of 0.0248 m for the 60^{o} cone.

The 60^{o} cone had a 0.4 m working length along the generator, between outside diameters 0.09 m and 0.535 m. The working length was free from temperature disturbances due to thermal energy flowing into the cone wall from both the small shaft at the top end and from the cone flange at the lower end.

The thermal conductivity of a metal sample taken from the 60^{o} cone was measured using the method described in appendix B and found to be given by the equation

$$k = 39.45 + 0.0889\ t \quad \frac{W}{m\ ^{2o}C}$$

(iii) The structural strength of the cone.

Loads from three sources were imposed on the cone:-

(1) external pressure from steam,

(2) centrifugal forces,

(3) thermal stresses.

The final design for the 60° cone was stressed for the external pressure loading using a method described in BS 1500 section 3.G.

The hoop stress due to rotation was calculated approximately by assuming that the cone was built up from a series of thin rings with increasing diameters.

Heat transfer across the cone wall from steam to the cooling water produced a temperature gradient, which gave rise to compressive stresses at the outer surface and tensile stresses at the inner surface.

At the outer surface, the stresses due to loadings (1) and (3) tend to cancel the stress due to (2). At the inner surface, the stresses due to loadings (2) and (3) tend to cancel the stresses due to (1). The approximate calculations for the stresses acting on the cone showed that the net stress was about half of the proof stress for the cone material and this safety margin gave a measure of confidence in the design.

(iv) Dynamic balancing.

At the design stage an attempt was made to minimise the initial out of balance of the assembled shaft and cone. This was achieved by calling for the inside surface of the cone and the socket which locates the base of the cone to the base-plate (item 30), to be machined during one operation

to ensure maximum concentricity. In addition to this requirement, the outside surface of the cone had to be machined concentric with the locating socket to within $\pm$ 25μm. A ring of metal 0.0095 m by 0.0143 m in section position at the base of the cone provided spare metal for removal during the dynamic balancing operation.

The thermocouple wires were bonded in place and the loose ends were coiled and fastened on the inside of the cone near the apex before the cone was despatched for balancing. Two special jigs were manufactured to support the cone between the two bearings of the balancing machine. Balancing was performed with the cone running at a speed of 500 rev/min.

The cone base-plate, the shaft flange, and the driving pulley, were attached to the main shaft to make a sub-assembly of the rotating parts. This sub-assembly was dynamically balanced (see section 4.5). The balanced cone was attached to the balanced sub-assembly to form a complete assembly of the rotating parts. This complete assembly was mounted on the balancing machine and given a trial spin at 500 rev/min to verify that the overall dynamic balance was maintained.

4.4.2 Combined 10°, 20° and 150° experimental cones.

The second experimental body fig. 34 incorporated 10°, 20° and 150° conical surfaces. The main part of this unit was formed by the intersection of two truncated cones which had apex angles of 10° and 20° and minor diameters of 0.493 m and 0.53 m respectively. A 0.18 m working length along the

FIG 34

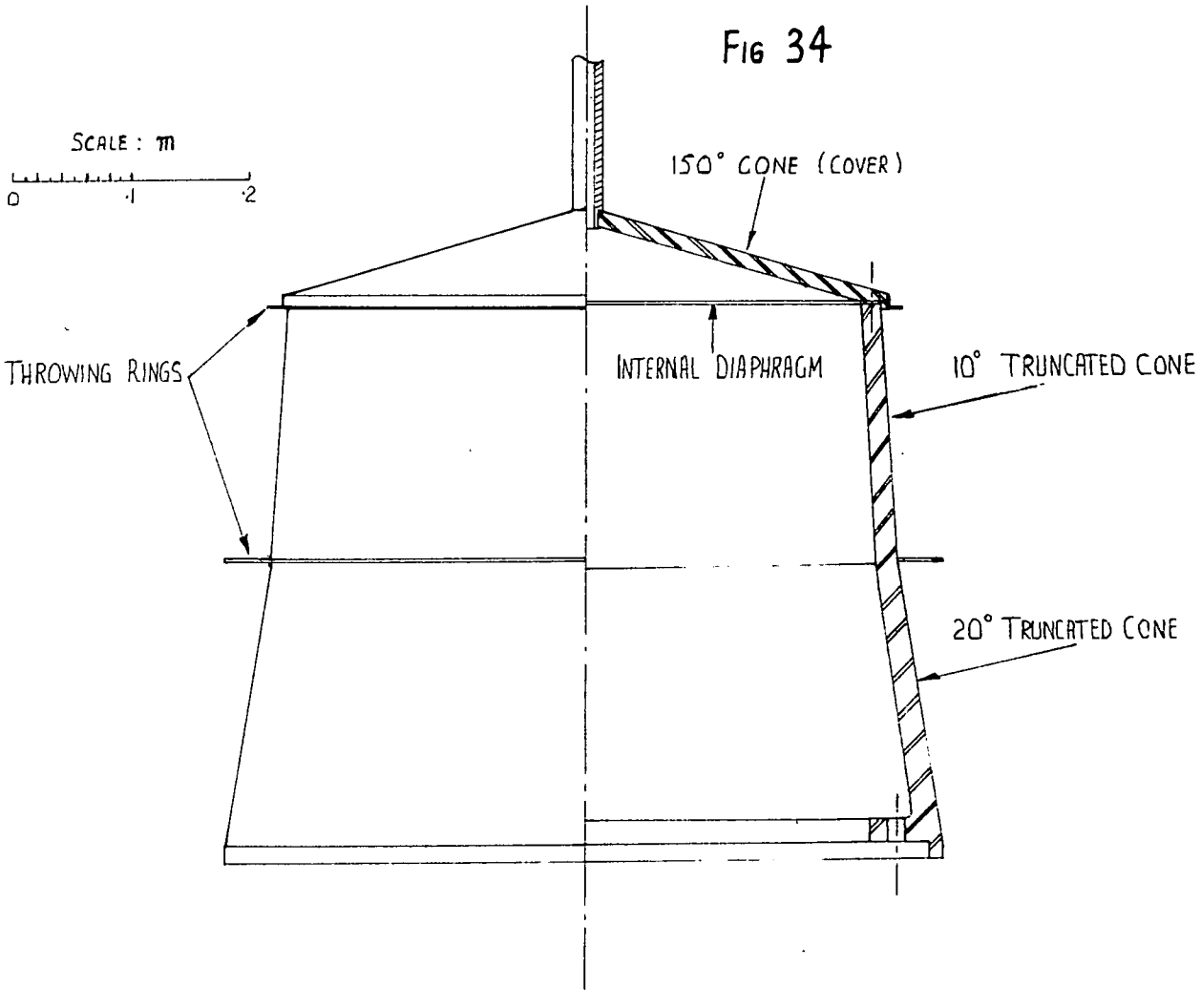

CROSS-SECTION OF STATIONARY PIPE SHOWING INDEPENDENT PASSAGES FOR INLET COOLING WATER

FIG 35

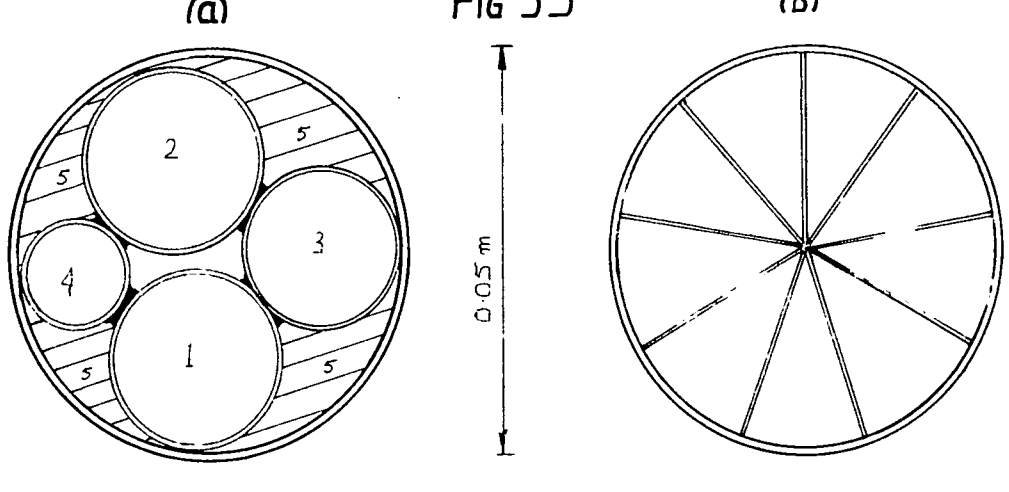

60° CONE
(FIVE PASSAGES)

10° AND 20° CONES
(NINE PASSAGES)

generator of each section was accompanied by a uniform wall thickness of 0.0172 m. Steam was excluded from the top end of the 10^{o} and 20^{o} section by a 150^{o} cone which acted as a cover plate. The 150^{o} cone had a working length of 0.2 m and a wall thickness of 0.0175 m.

Each of the cones could not be tested separately in the strict sense of the word, although several features were built in to the unit to minimise the effect of one condensing surface on a neighbour. For the first series of tests, which concentrated on the 10^{o} and 20^{o} sections of the unit, an internal diaphragm was installed between the top of the 10^{o} section and the 150^{o} cover. The diaphragm prevented cooling water reaching the inner surface of the cover thus minimising condensation on the outer surface of the cover. A throwing ring was installed on the outside of the unit at the same level as the diaphragm to prevent condensate from the cover running onto the 10^{o} section. At the intersection of the 10^{o} and 20^{o} cones, a throwing ring was attached to the outer surface to prevent condensate from the 10^{o} section running onto the 20^{o} section. This throwing ring was designed to be detached and removed from the inside of the vessel via a port, should it be necessary to allow condensate from the 10^{o} section to run onto the 20^{o} section.

Design considerations similar to those given for the 60^{o} cone were applied to the combined unit, with several exceptions.

The casting material was changed to manganese bronze BS 1400 HTB1, because of the increased cost of the aluminium

bronze, which was used for the 60^{o} cone. Manganese bronze has corrosion resistance and strength characteristics comparable with aluminium bronze, but has a higher thermal conductivity. A metal sample taken from the unit was used to determine the equation for the thermal conductivity $k_m = 80.6 + 0.121\ t \frac{W}{m\ 2^{o}\ C}$

An improved supply of cooling water to the apparatus relaxed the limitation on the maximum thermal load for the combined unit.

4.5 Main shaft, bearings, cone base-plate and shaft flange.

The maximum working speed of the main shaft (item 19) was 2000 rev/min. Ker Wilson (72) recommended that the working speed of a shaft should be below 0.8 of the first critical speed. To comply with this requirement the main shaft was designed to have a first critical speed in excess of 3000 rev/min.

To ease the task of boring out the centre of the main shaft, which was necessary to create a passage for cooling water flowing into and out of the cone, the shaft was machined from hot-drawn En 5 steel tube.

After the machining operation the entire surface of the shaft was given protection against corrosion by an electro-plated coating of nickel-phosphorous alloy 80 μm in thickness.

Steam pressure acting over the cross-sectional area of shaft inside the vessel created a maximum thrust of 15.8. 10^{3}N which was supported, together with the weight of the shaft and

its attachments of 2.0. 10^3N, by a pair of high precision tapered roller-bearings (item 13). These bearings were mounted back to back and limited the shaft run out to 8μm at the bearing position. The thrust from the bearing was equally distributed to brackets welded to the four legs supporting the pressure vessel. A double-row spherical seating ball-bearing (item 11) mounted in a sliding housing, acted as a locating bearing at the upper position.

Extra attention was paid to the design of the cone base-plate (item 30) which was subject to a complex loading by centrifugal and compound steam forces, together with a thermal stress arising from the temperature gradient across the plate. Normal atmospheric pressure inside the cone caused the steam pressure loading. Stressing was performed by considering the rotational and steam pressure loadings separately. Centrifugal forces acting on the flange while rotating at 2000 rev/min were calculated approximately by assuming that the flange was a thin disc of uniform thickness with zero axial stress.

Stresses due to the compound steam loading on the cone base-plate were assessed by dividing the loading into two parts:-

(i) Full steam pressure acting on the underside of the cone base-plate.

(ii) Net thrust on the cone due to the difference between the steam and the atmospheric pressures acting over the cross-sectional area of the end of the main shaft. The thrust was transferred from the cone to the shaft via the cone base-plate and the shaft flange.

In order to simplify the stress analysis the base-plate was assumed to be a thin disc with edges rigidly fixed.

The net stress on the base-plate from all sources was estimated to be less than 0.3 of the ultimate tensile stress for the base-plate material En 3, and this level of working stress was considered to be acceptable.

After the machining operation the base-plate also received a coating of nickel-phosphorous alloy to prevent oxidation corrosion from either the cooling water or the steam. The plating was also effective in reducing electrolytic corrosion between the steel of the base-plate and the bronze of the cone and between the base-plate and stainless steel of the shaft flange.

The shaft flange (item 31) was manufactured from stainless steel to enable the spigot which locates the base-plate, to be finish machined without plating allowances. Before this final machining operation, the shaft flange was secured firmly in place at the top of the main shaft by four locking screws. This assembled unit was mounted in a precision lathe at the Sunderland works of Messrs. Rolls Royce Ltd., and the two bearing positions on the shaft, and both the seating face and the locating spigot on the shaft flange, were precision ground to make these primary locating positions concentric to within 8 μm.

The cone base-plate and the driving pulley (item 12) were attached to the main shaft-shaft flange unit to form a sub-assembly of the rotating parts. Since this sub-assembly was a permanent feature of the apparatus, the sub-assembly was

dynamically balanced as an independent unit (see section 4.4.1.iv). Balancing was achieved by the removal of metal from two planes; from the edge of the cone base-plate and from the driving pulley.

4.6 Shaft seals.

A type 109, 109B balanced mechanical seal (item 10) manufactured by Crane Packing Ltd., provided an effective means of sealing the main rotating shaft where it entered the pressure vessel. For this particular application the seal ran in a housing which was separately pressurized by water at 1 to 2 bar above the vessel pressure. A water flow rate of 0.5 m^3/h was required to cool and to lubricate the seal. Using water to lubricate the seal reduced the risk of contamination entering the pressure vessel.

Dry asbestos packing and P.T.F.E. tape were used to pack the gland which sealed the small shaft (item 5). Being dry and self lubricating meant that the packing did not introduce contamination into the pressure vessel.

4.7 Cooling water.

4.7.1. 60^{o} cone.

A primary inlet manifold divided the cooling water into five independent supplies (item 15). Each one of these supplies was controlled with a separate regulating valve.

The five water supplies were connected to five separate passages inside a 0.05 m diameter stationary pipe which conducted them to the cone along the central hole in the main shaft fig. 35a. This 0.05 m pipe was located inside the main shaft at both ends by needle roller bearings. Each of the water supplies terminated in one of the five water-tight chambers of the sprayer head (item 8). Water was carried from these chambers to the inner surface of the cone by a number of 0.005 m bore tubes. The number of tubes leading from each compartment increased with the cone diameter to deliver water to the cone in quantities proportional to surface area. During test runs this basic cooling water distribution was found to need little alteration to obtain a uniform temperature on the inner surface of the cone.

At the lower end of the cone the cooling water was collected by four stationary 0.025 m diameter scoops and carried into the annular passage between the stationary central inlet pipe and the bore of the rotating shaft. To assist the cooling water flow out of the scoops and into the annular passage, the outlet from the scoops was angled 10^{o} to the vertical; giving the water a helical motion. The torque created by cooling water entering the scoops was transmitted by the central water pipes to an anchoring arm attached to one of the pressure vessel legs.

A sealed perspex box (item 14) mounted over two 0.064 m diameter holes in the shaft collected the cooling water discharged from the annular passage.

4.7.2 10^{o} and 20^{o} cones.

The 10^{o} and 20^{o} sections of this unit required nine independent supplies of cooling water; four for each section and one where the sections intersected. To meet this requirement four more valves were added to the primary inlet manifold. The inside of the 0.05 m diameter pipe which conveyed the cooling water along the bore of the main shaft to the inside of the unit, was divided into nine separate passages by a group of radial fins running the full length of the pipe, fig. 35b. This fin structure was manufactured separately and was then soldered into the inside of the pipe to form water tight passages. Each passage vented into separate sections of the modified sprayer head which delivered cooling water to the inner surface of the cone through a number of small bore tubes. The number of tubes increased with cone diameter to give a water delivery in amounts proportional to the inner surface area. Cooling water was collected and removed from the cone unit by scoops.

4.8 Motor Drive

A preliminary estimate of the power required to drive the rotating parts at the maximum speed was made by considering the following:-

(i) Running losses and break out torque for the mechanical seal.

(ii) Oil seal power loss.

(iii) Bearing power loss.

(iv) Cooling water. This power requirement varied with cooling water flow rate and represented the angular momentum given to the water by the viscous drag from the inner surface of the rotating cone.

(v) Angular momentum given to the condensate and to the steam. At the design stage the condensation rate was unknown, but the momentum given to the condensate was estimated to be much less than that given to the cooling water.

An estimate of the power requirement showed that from the available choice of motors a 11.5 kW d.c. motor with a 200% overload starting torque was required. To accommodate low running speeds the motor was force cooled by a separate fan unit.

The motor was mounted with its shaft parallel to the main shaft on a right angled frame which was separate from other parts of the apparatus and bolted to the concrete floor. A timing belt transmitted power from the motor to the main shaft through a 1:1 ratio. Moulded teeth on the timing belt meshed with teeth on the pulley wheels to give a low tension drive with negligible back-lash.

A d.c. tachometer incorporated in the non-drive end of the armature shaft of the motor gave a speed indication on the control panel.

The power supply to the motor was provided by a control unit, comprising of a 400-440 V, 3 phase, 50 Hz thyristor

bridge rectifier for armature supply, together with a single-phase bridge rectifier for field supply.

The drive features are as follows:-

(a) Control of the motor speed between 50 and 2000 rev/min.

(b) Constant torque output for speeds up to 1500 rev/min with constant power output between 1500 and 2000 rev/min.

(c) A continuous overload capacity of two times the full load torque for the motor and three times the full load torque for the control unit.

(d) A speed holding accuracy to within 1% of the maximum speed for a 100% change in load.

(e) A 0.1% drift in speed over several hours at constant load.

Long connecting wires between the control unit and the motor permitted the control unit to be moved to any part of the apparatus. The load current to the motor and the motor speed were indicated by an avometer and tachometer respectively. These instruments were mounted on the instrument panel of the control unit, together with the speed control wheel.

A more accurate indication of the motor speed was obtained by applying a hand tachometer to the end of the motor shaft. The precision hand tachometer used during tests runs, recorded an average value of the speed over a period of several seconds.

4.9 Thermocouples

4.9.1 Temperature - e.m.f. characteristic.

Copper - constantan thermocouples were used to measure temperatures on the apparatus. In order to achieve a consistency of temperature e.m.f. characteristic, all of the thermocouples were constructed from single reels of each material. The conductors had a diameter of 0.0002 m and were insulated with a coating of temperature resistant enamel. Although the junctions were made by spot welding a small quantity of high melting point solder was also applied to the junction to give additional strength.

Six thermocouples were made to determine the temperature - e.m.f. characteristic. Standard reference temperatures for 100^{o} C and 0^{o} C were provided by boiling distilled water at atmosphere pressure and by a mixture of ice and water respectively. The six thermocouples exhibited a reasonable consistency of e.m.f. characteristic by showing a maximum deviation of $\pm$ 5 μV; equivalent to $\pm$ 0.1^{o} C. The average e.m.f. given by the thermocouples at 100^{o} C was 14 μV down on the reference value of 4.239 mV for copper-constantan at 100^{o} C. Readings of e.m.f. were taken at several intermediate temperatures, which were measured with an accurate mercury in glass thermometer, to obtain the temperature - e.m.f. characteristic for the thermocouple material. This measured characteristic was found to deviate little from the standard characteristic given in BS1828:1961.

4.9.2 Thermocouples on the 60° experimental cone.

Thermocouples used on the 60° cone measured point temperatures on the inner and outer surfaces. The 33 available slip-rings on item 6 placed an upper limit on the number of thermocouples that could be placed on the cone. Using the circuit shown in fig. 36a enabled a total of 32 junctions to be used. This circuit required that all constantan leads should be connected to one slip ring, while each of the copper leads was connected to an individual slip-ring. If the junctions were in electrical contact with one another through the metal of the cone, an average temperature would be read by the common junctions instead of a point value which was required. When the junctions were being cemented in place, care was taken to ensure that they did not make electrical contact with one another.

Twenty thermocouples were distributed over the outer surface of the 60° cone to give a coverage of one thermocouple for every 0.025 m of length along the generator, fig. 37a. Ten meridional grooves, which were equally spaced at 36° intervals about the axis of symmetry, were used to take the leads from these thermocouples to holes drilled through the cone wall near the apex. On passing through to the inside of the cone the leads were taken, together with those from the twelve junctions on the inner surface of the cone, into the small hollow shaft and out of the pressure vessel up to the slip-ring unit. The thinnest cutting wheel available at the time of machining the grooves on the 60° cone,

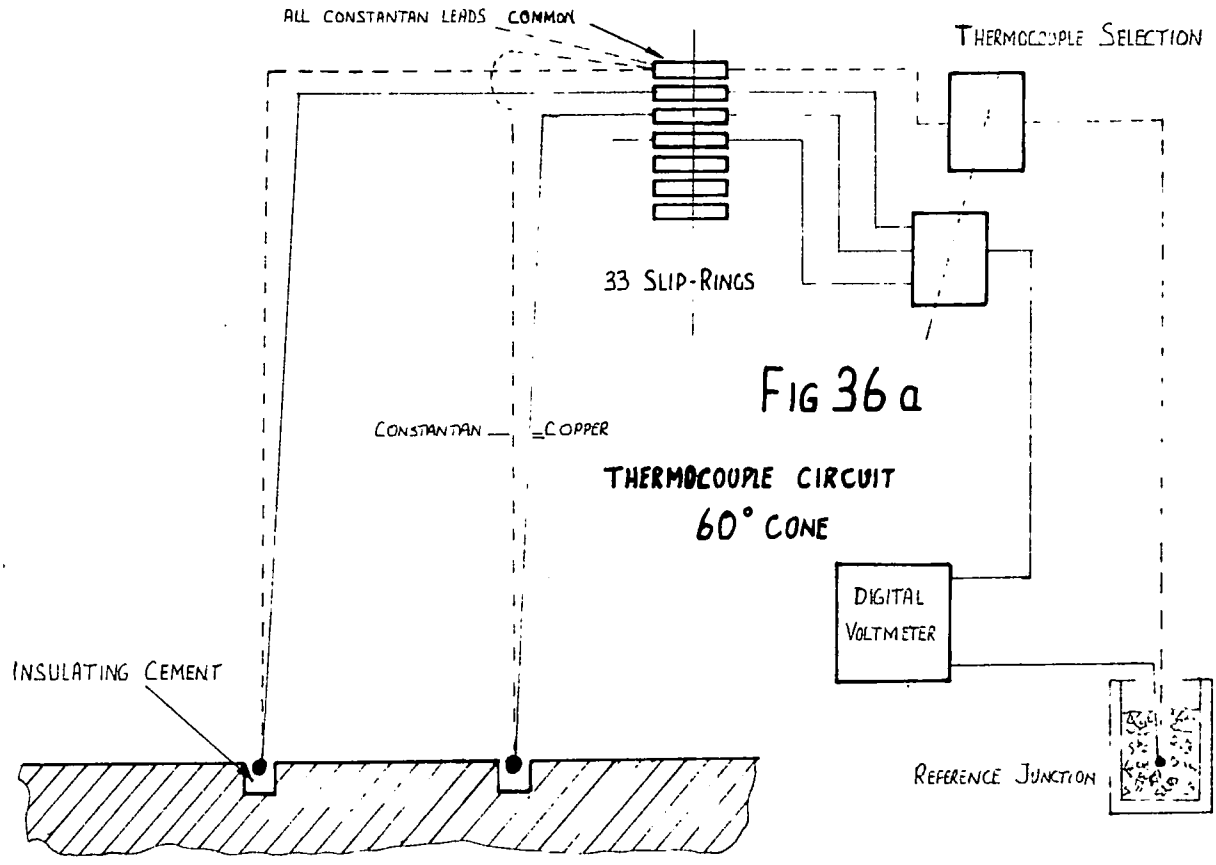

FIG 36a

THERMOCOUPLE CIRCUIT
60° CONE

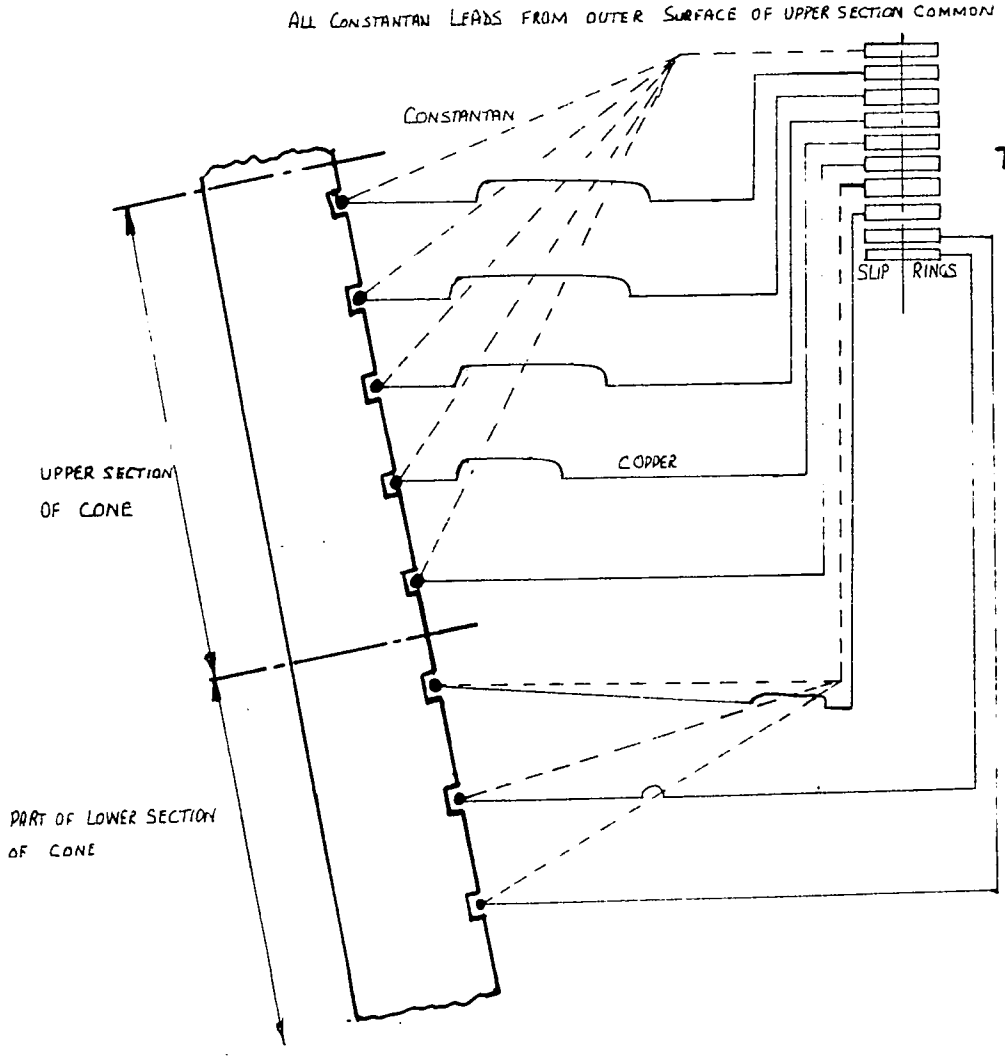

FIG 36b

THERMOCOUPLE CIRCUIT
10° AND 20° CONES

dictated the groove width of 0.0008 m, which was also the depth of the grooves, fig. 37b. The twelve thermocouples on the inner surface of the cone were carried to the apex in six equally spaced grooves running up the inner surface.

Both the junctions and the leads were held in the grooves on the 60° cone by a temperature resistant insulating cement Bostik 1160. This cement remained wettable during tests and as such did not interfere with the film of condensate. After curing the cement in an hot air oven for 2 hours at 180° C, the surplus cement was removed from the cone surface to preserve the contour. Local pitting in the cement was observed after some 30 hours of testing. Repairs could be made with the 60° cone in situ by a local application of cement. The manufacturers attributed this failure of the cement to the strain at the cement - metal interface on the groove and not to erosion by either steam or condensate. This cement only achieves its maximum bonding strength when applied in thin films and looses strength when applied to other configurations such as grooves.

Each of the 32 junctions was placed at least 0.04 m inside a different isothermal region on the surface of the cone. Having a junction in an isothermal region eliminated the conduction of energy away from the junction. Fig. 37a shows the junctions in isothermal regions on the outer surface of the 60° cone. Planes normal to the axis of the cone were considered to be isothermal regions by the

FIG 37

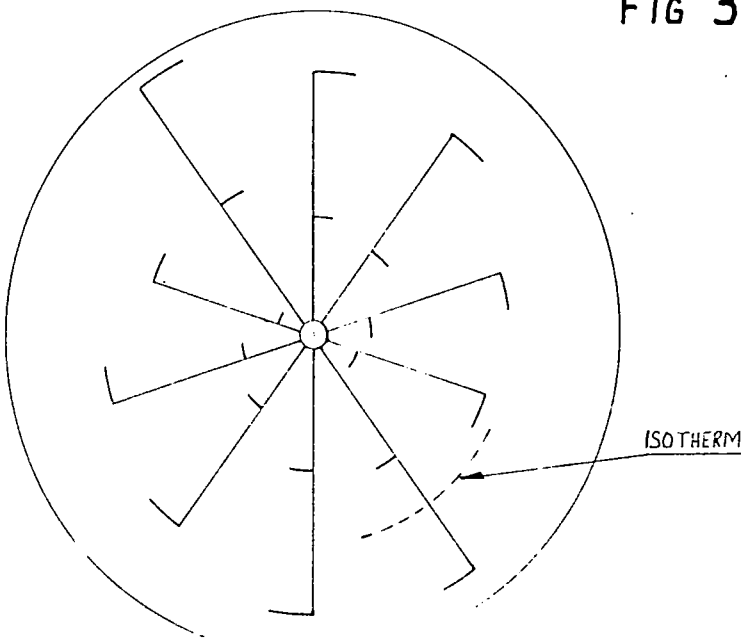
ISOTHERM

(a)

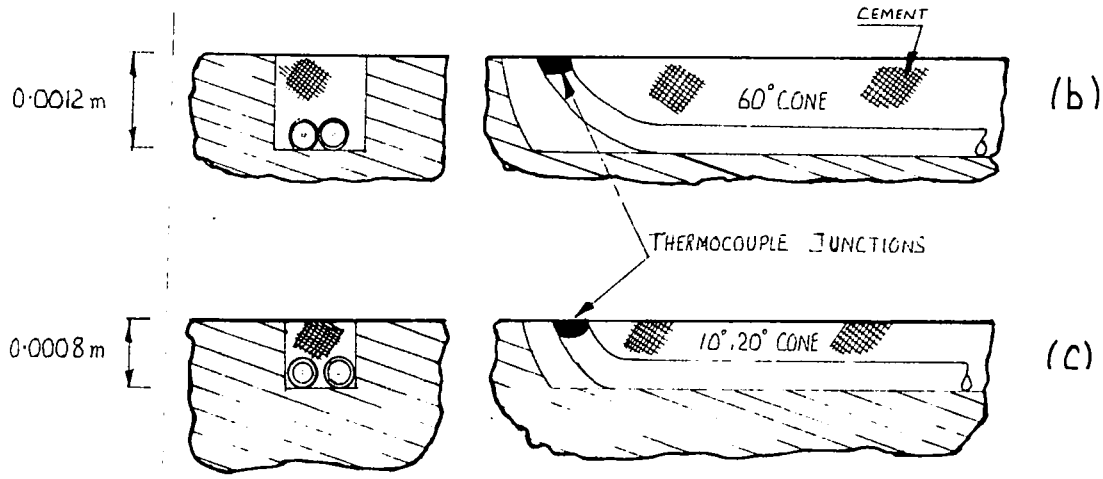
0·0012 m
CEMENT
60° CONE
(b)
THERMOCOUPLE JUNCTIONS
0·0008 m
10°, 20° CONE
(c)

assumption of axial symmetry. Care was also taken to ensure that the junctions were at the condensing surface, but a large scale electrical analogue was used to examine the effects on temperature measurement of a junction lying at some position within the groove, which was three wire diameters in depth. Details of the analogue and of the text results are given in appendix C. The test results show that if a temperature difference of 100° C existed across the cone wall (0.0248 m) a junction positioned near the bottom of the groove, i.e. 0.0008 m from the true condensing surface, would read a temperature≈2° C less than the surface temperature.

4.9.3 Thermocouples on the 10° and 20° experimental cones.

Fig. 38 shows the arrangement of thermocouples on the outer surface of the 10° and 20° sections of the cone. Nineteen thermocouples were used on the outer surface and nine on the inner surface. The wall thickness of the 10° and 20° sections of the second experimental cone was 0.0172 m, which was 0.695 times the wall thickness of the 60° cone. To provide a slight reduction in possible error due to a thermocouple junction not lying exactly at the outer surface of the cone, the depth and the width of the grooves in the isothermal regions was reduced to almost two wire diameters (0.0005 m), fig. 37c. The smaller grooves required less insulating cement and this helped both to enhance the bonding strength and to reduce the strain at the cement - metal interface.

fig. 38

Thermocouples on the 10^{o} cone.

10^{o} cone

20^{o} cone

20^{o} cone

In an attempt to avoid the deterioration found with Bostik 1160 after some hours of testing, the make of insulating cement was changed to Araldite AY105 and HT972 hardener with a priming coating of DZ80. It was possible to make running repairs to the pitted Bostik with the 60^{o} cone in situ, because that cement was soluable in methylated spirits and there was room to handle the wires in their grooves. However, the insolubility of the cured Araldite and the narrow grooves on the 10^{o} and 20^{o} cones made running repairs impossible without risking severe damage to junctions. Thus a second failure of the cement could only be remedied by dismantling the apparatus.

Although point readings of temperature were required from each thermocouple on the 10^{o} and 20^{o} cones, a safeguard was built into the thermocouple circuit to permit useful tests to continue for some time in the event of a second failure of cement, which could cause the thermocouples to become electrically connected and thus to read an average temperature. This safeguard consisted of grouping thermocouples into separate circuits to ensure that if junctions became electrically connected they would read an average temperature of certain sections of the cone surface. The outer surface of each cone was divided into upper and lower sections and the inner surface of each cone was likewise divided; making four separate sections of surface on each cone. Each section had a length along the generator of about 0.09 m. Thermocouple leads from

each section were connected to sets of slip-rings as shown in fig. 36b. While junctions remained electrically insulated local heat fluxes could be calculated from the point readings temperature but the safeguard enabled average heat fluxes to be calculated for the upper and the lower halves of each cone if the junction became electrically connected. The latter case could be detected during tests by two or more junctions reading exactly the same e.m.f.

In addition to the 34 slip rings on item 6, 2 extra slip rings were made available for thermocouples on the 10^{o} and 20^{o} cones from a new six-way slip-ring unit which was mounted on top of item 6. The remaining four slip rings were used by Smith (73) who was measuring condensate film thicknesses on the 10^{o} and 20^{o} cones using electrical resistance transducers.

A prolonged series of tests over a period of 100 hours showed that pitting did not occur in the Araldite in the isothermal grooves. Some of the thermocouples on the outer surface failed when bonding between the cement and one of the vertical grooves eventually broke down. Although a partially successful repair was made to the cement, that group of wires eventually became proud of the cone surface and were damaged when the cone surface was cleaned with abrasive paper (see section 6.1). The series of tests was concluded when only one half of the thermocouples remained.

4.9.4 Stationary thermocouples.

Inlet cooling water temperature measurements were made

at the primary inlet manifold and at each of the sections inside the sprayer head. Outlet cooling water temperatures were measured at the mouth of each of the scoops and at entry into the water collection box. Leads from these stationary thermocouples passed along the bore of a 0.003 m pipe for protection during their passage down the central water pipe. The temperature of steam inside the vessel, the temperature at the multi-way switch, and the temperature at the input and at the output terminals on the slip-ring unit, were also measured with thermocouples.

4.10 Slip-ring unit and air filter.

The thermocouple e.m.f. was taken from the 60^{o} experimental cones by a thirty-four way packaged slip ring unit (item 6), which was mounted on the top of the small shaft (item 18). Thirty three of the slip rings were used for thermocouples on the 60^{o} cone and one slip ring was allocated to Robson's experiments.

The slip-ring unit was manufactured by I.D.M. Electronics Ltd. and had 80%-20% silver graphite brushes running on silver rings. This type of slip-ring unit was chosen because of its negligible noise characteristic; an attribute that was demonstrated by Ogale (74). But before the thirty-four way slip ring unit was ordered, several tests were performed on a worn six-way unit to determine the effect on e.m.f. due to brush friction increasing the temperature of the unit.

A thermocouple was attached to the shaft of the slip-ring unit and arranged to run immersed in an oil bath. The e.m.f. from this rotating thermocouple was taken to the digital voltmeter through a pair of slip rings. Leads from a second thermocouple were taken directly from the oil bath to the digital voltmeter to provide a reference temperature reading. Several tests were carried out over a speed range of 0 to 5000 rev/min without cooling air to the slip ring unit. The results showed that after running for a while at any speed, a noticeable change in e.m.f. was given by the rotating thermocouple as the operating temperature of the slip-ring unit increased. When cooling air was introduced to the slip-ring unit, the difference in e.m.f. between the two thermocouples was reduced to 10 μV; the equivalent of 0.25° C. This small difference in e.m.f. was attributed to the existance of a small temperature difference between the lead connections at the input and the output to the slip-ring unit. An oscilloscope was later connected in the circuit to measure noise, but none could be detected. This result confirmed Ogale's findings, but showed the necessity for air cooling to maintain uniform temperatures in the slip-ring unit.

Smith (73), who required extra slip-ring capacity for his measurements of condensate film thickness using an electrical resistance technique, mounted a new six-way slip-ring unit on top of the 34 way unit. Two of the slip-rings were made available for thermocouples from the 10° and 20° cones.

Compressed air from the laboratory air-line was contaminated by water, rust and oil, and required filtering before it could be used for cooling the slip-ring units. The air was cleaned and dried by an Aerox Carbon Adsorber Filter, which consisted of three sub-units, (a) a porous ceramic pre-filter for removal of gross liquid impurities, (b) a powdered-carbon adsorber unit for the removal of vapour and odours, and (c) a second ceramic filter to prevent ingress of carbon into the air-stream.

4.11 Steam supply.

Steam with a dryness fraction of 0.99 was supplied at 10 bars by an English Electric automatically regulating oil-fired package boiler unit, which could, if required, supply steam at a pressure of 15 bar.

The pressure of the steam supply to the pressure vessel was controlled by a 0.019 m bore reducing valve which could produce reduced pressures over the range 0.05 to 0.8 of the supply pressure.

Three separate valve springs were required to cover the full range of reduced pressure. A modification was made to the screw-down cap which loaded the spring and thereby controlled the reduced steam pressure. Four spokes with insulated handles were attached to the top of the cap to form a capstan wheel. This enabled the reduced pressure to be adjusted with greater ease and accuracy. The presence

of this valve in the supply line also tended to reduce pressure fluctuations, which occurred in the small steam receiver on the boiler whenever the secondary burner flame was either ignited or extinguished.

Throttling the steam down to the desired pressure caused a certain degree of superheat. Passing the steam through a water jacketed heat exchanger before entry into the pressure vessel, enabled the steam quality to be returned to the dry saturated state. Steam for quality testing was supplied from either a tapping point positioned in the steam line between the reducing valve and the de-superheater, or directly from the pressure vessel.

4.12 Measuring equipment and multi-way switch.

Cooling water flow.

The volumetric flow of cooling water was measured by a Kent type 253 Pottermeter lying in the main water feed pipe before the manifold. This unit produced pulsed output information directly proportional to volumetric flow, because the six blade impellor on the rotor unit rotated at a speed directly proportional to the mean velocity of the fluid. A reluctance type pick-off coil sensed the passage of each of the ferritic stainless steel blades on the rotor unit as they crossed the magnetic field created by the coil. The sinusoidal wave-form generated by the coil was transmitted to a type 2000 digital totaliser which continuously indicated the pulse count on a six digit electro-mechanical register.

Errors in flow measurement can occur in rotor-type flow meters if the water has preliminary axial rotation about the centre line of the pipe. This rotation may be caused by the presence of valves and bends in the pipe-line. To minimise this error a flow-straightening device, which consisted of a 0.4 m long cruciform vane, was placed in the bore of a straight section of the water-main immediately in front of the impellor.

The steam pressure in the pressure vessel was measured with a 0.25 m diameter Bourdon test gauge which had an accuracy of $\pm$ 0·009 bar over the full range of pressure 0 to 8 bar. The gauge was connected to the end of an extension pipe from the pressure vessel to help keep the gauge at the calibration temperature of 20^{o} C.

Condensate flow.

The quantity of condensate from the rotating elements inside the pressure vessel could be measured in two ways. The condensate could be flashed off to an auxiliary condenser working at a vacuum condition and then collected in a calibrated measuring tank. This method was useful for high condensing rates and for low condensing rates taken over a period of hours. The second method was used to collect small volumes of condensate over a period of minutes. With this method, condensate was collected and measured in a well of known volume which was formed inside the base of the pressure vessel.

Thermocouple e.m.f.

A Solartron type LM 1420.2 digital voltmeter was used

to measure the e.m.f. generated by the thermocouples. This instrument had a 0 to 20 mV scale and a sensitivity multiplication switch which gave a maximum sensitivity of 2.5 μV on the 4 x range. The input resistance to the digital voltmeter was 50 M ohms and this ensured that the resistance of the lead wires was negligible by comparison.

Thermocouple selector switch.

A Cropico type SP2 fifty-one way selector switch working on the break before make principle allowed the leads from individual thermocouples to be switched into the digital voltmeter and cold junction circuit. The gold-silver alloy contacts of the switch unit reduced the switching resistance to less than 0.001 ohm and thermal e.m.f. due to rapid switching to less than 0.2 μV.

Dryness - fraction of steam.

The quality of the steam atmosphere inside the vessel, together with any gas content, was measured using the authors adaption of the barrel-type calorimeter, fig. 38. One of the essential features of this calorimeter was a tubular condensing coil through which the steam sample passed. The coil was cooled by the water content of the calorimeter. Steam in the sample condensed in the coil, while the gas content flowed through to be collected in a closed glass vessel which was graduated for volumetric measurement. Both the condensing coil and the measuring vessel were housed in a thermally insulated water-tight container. The dryness fraction was

FIG 39.

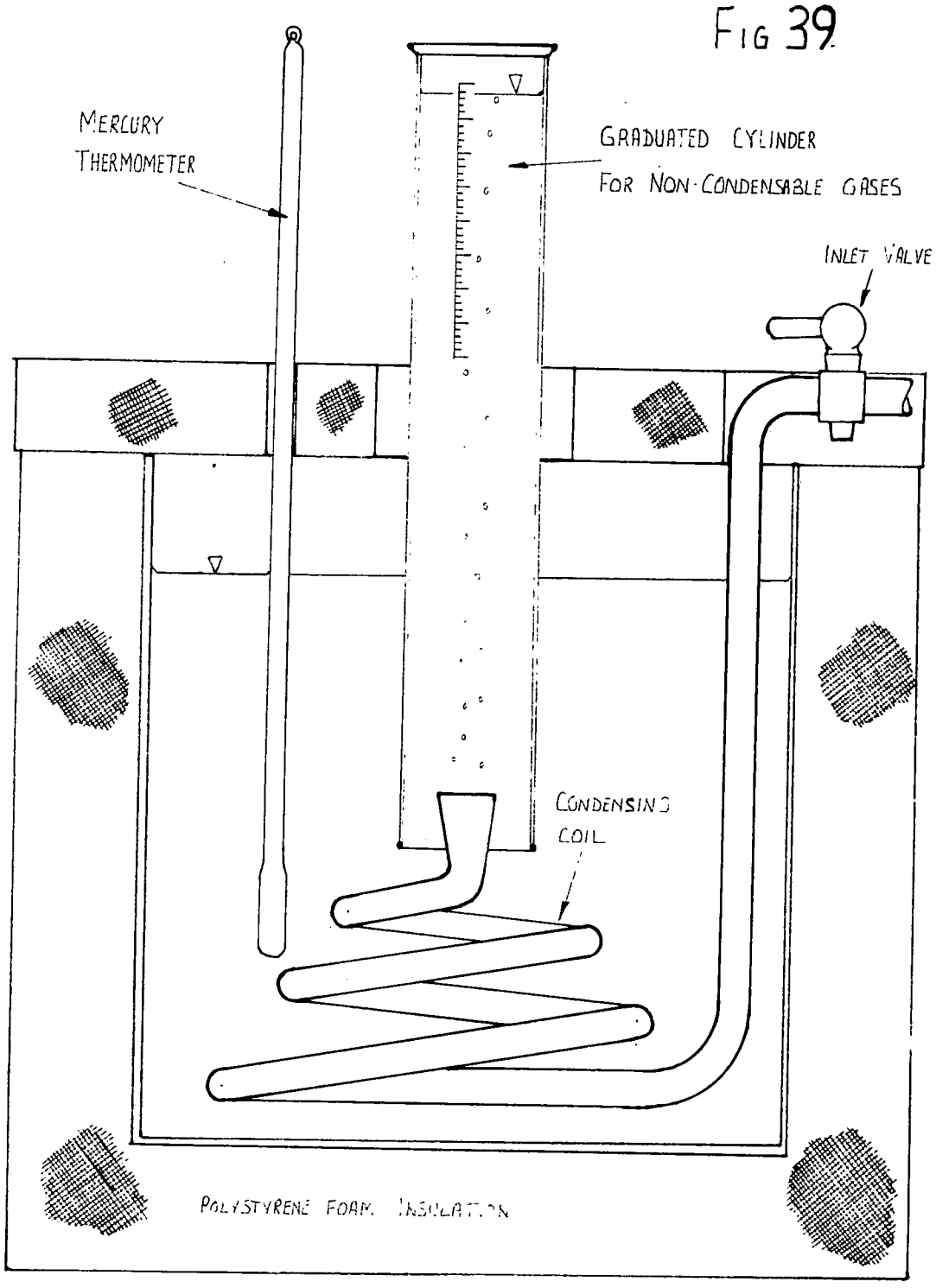
MERCURY
THERMOMETER
GRADUATED CYLINDER
FOR NON-CONDENSABLE GASES
INLET VALVE
CONDENSING
COIL
POLYSTYRENE FOAM INSULATION

obtained by a simple energy balance and an estimate of the volume of non-condensable gases was obtained by a direct reading using the methods shown in appendix D.

4.13 Photography.

The formation and drainage of the films of condensate on the 10^{o} and 20^{o} cones was studied with the aid of still photographs taken through windows in the pressure vessel.

A large format (0.101 m x 0.127 m) monorail plate camera was used to take the still photographs. Illumination was provided by a Hadland 2 μs flash unit which could provide a 50 J flash every 30 s.

5.0 Commissioning tests.

5.1 Performance of slip-ring unit.

Some preliminary test runs on the assembled apparatus revealed that the supply of cooling air to the slip-ring unit was not maintaining the unit at a uniform temperature. Since copper-silver and constantan-silver connections were made at the input and output terminals of the slip-ring unit, it followed from the 'Law of Intermediate Metals' that a temperature difference across the terminals would introduce a secondary e.m.f. into the thermocouples from the cone. Although the thermal e.m.f. between copper and silver is extremely small, the thermal e.m.f. between constantan and silver is of the same order as that between copper and constantan. The same secondary e.m.f. was created in each pair of copper-constantan leads passing through the slip-ring unit. Thus the effects of the secondary e.m.f. would be cancelled out when taking the difference between the temperature of the outer and inner surfaces of the cone, and the measurements of heat flux derived from the temperature difference across the cone wall would remain unaffected by the secondary e.m.f. However, the secondary e.m.f. affects the readings of temperature value, and influences the measured difference between the temperature of the outer surface of the cone and the steam. Leaving the secondary e.m.f. uncorrected would introduce an error into the calculation of the heat transfer coefficient. Temperatures at the input and output terminals of the slip-ring unit were measured,

therefore the readings of temperature value taken on the cone could be corrected for the secondary e.m.f. using the following procedure given by Benedict (75). If the temperature of the input terminal on the slip-ring unit was greater than the temperature at the output terminal, the temperature difference between the two terminals was added to readings of the temperature value from thermocouples on the cone, to correct for the secondary e.m.f.

However, an outer casing was removed from the slip-ring unit to improve the circulation of cooling air and this proved effective in maintaining a uniform temperature across the input and output terminals, to within $\approx 5^{o}$ C.

5.2 Performance of thermocouples on the cone.

For several days, both steam and cooling water were kept away from the stationary cone to enable it to attain the ambient temperature of the laboratory. After attaining this uniform temperature, the consistency of the e.m.f. readings from thermocouples on the cone and on the cooling water system inside the cone were measured. The readings of e.m.f. were found to be consistent to within $\pm$ 5 μV or $\pm$ 0.1^{o} C which was in agreement with the consistency of e.m.f. measured on the six thermocouples mentioned in section 4.9.1. This consistency of $\pm$ 0.1^{o} C was maintained when the cone was rotating at speeds up to 1500 rev/min, but at these higher speeds the temperature at the input terminal of the slip-ring unit was found to be up to 5^{o} C higher than the temperature

at the output terminals. The small secondary e.m.f. introduced during these high speed tests depressed the readings of temperature value taken from the thermocouples on the rotating cone. However, the correction for secondary e.m.f. given by Benedict (75) and mentioned in section 5.1, was applied to the readings of temperature value taken from the cone; these corrected readings agreed with those taken from the thermocouples on the cooling system inside the cone to within $\pm 1^{o}$ C.

5.3 Warming through period.

Steam was supplied to the pressure vessel at 2 bars. The cooling water supply was adjusted to give a uniform temperature at the inner surface of the cone. Readings from thermocouples on the cone were monitored every five minutes. It was found that after 15 minutes a steady inside surface temperature could be attained. By this time the pressure vessel was also warmed through. Thus a warming through period of some 15 to 20 minutes was allowed before commencing a test run.

6.0 Test procedure.

6.1 Preparatory work on the outer surface of the cone.

Machine marks were removed from the outer surface of new cones by abrading the surface with various grades of wet and dry carborundum paper, down to grade 004. Between tests, grade 004 paper was also used during preparatory work on the surface of the cone.

The surface finish of the outer surface of experimental cones could not be measured because the cones were too large for the available bench-mounted 'Talysurf' machine. However, surface roughness was measured on small pieces of cone material which were abraded with grade 004 paper in the manner used for the experimental cones. The surface roughness of these samples had an average value of 0.5 microns C.L.A. across the abrasion marks and 0.3 microns C.L.A. in the direction of the marks.

To ensure that filmwise condensation would occur on the experimental cone, the outer surface of the cone was cleaned before a test while the apparatus was cold. Access to the cone was gained by removing one of the 0.3 m diameter glass windows. The cone was rotated during the cleaning process which commenced with a wash using a detergent and warm water to remove oil or other contamination. Two different detergents were used during the experimental program. Tepol was used for the 60^{o} cone and Decon 75 was used for the combined 10^{o} and 20^{o}

cones. Although both detergents were effective in removing contamination, the latter had the quickest action and reduced the cleaning time. The surface of the rotating cone was also lightly abraded with grade 004 paper and thus the abrasion marks ran in planes of axial symmetry. Therefore condensate travelling along the generator of the cone would cross the abrasion lines and encounter the roughest path of approximately 0.5 microns C.L.A. After the cleaning operation both the cone and the inside of the pressure vessel were given several rinsings with cold tap water to remove all traces of detergent. The outer surface of the cones retained part of the rinsing water in a complete film. This was taken as evidence of the wettability of the surface and of the likelihood that filmwise condensation would occur under test conditions.

6.2 Starting procedure.

The following procedure was evolved as the logical sequence of operations required to bring the apparatus up to a particular set of test conditions.

(i) Both the cooling water stop-valve and the drain valve were opened.

(ii) After starting the water-pump, the pressurized water supply to the mechanical seal was adjusted to give a flow of 0.5 $\frac{m^3}{h}$ at a pressure of 2 bar.

(iii) Cooling water was supplied to the inner surface of the cone by opening the main valve at the distribution manifold.

(iv) A supply of cooling air was delivered to the slip-ring unit from the Aerox filter.

(v) The motor-control unit was switched on and the speed of rotation of the cone was slowly increased up to the desired speed.

(vi) After opening the steam stop-valve, the pressure-reducing valve was adjusted to give the desired steam pressure in the pressure vessel. At the same time the water pressure at the mechanical seal was increased to be 1 to 2 bar above the vessel pressure.

(vii) The steam blow-off valve was opened for several minutes to purge both the steam supply system and the pressure vessel of their initial charge of air.

(viii) After the air purging, the steam pressure and the speed of rotation were checked, and if necessary, adjusted to the desired values.

(ix) A uniform temperature was obtained on the inner surface of the cone by adjusting the individual supplies of cooling water to the various cooling zones on the inner surface. This adjustment started at the uppermost cooling zone and progressed down successive zones. Adjustments to the cooling water supply were made while readings of temperature were taken from thermocouples on the inner surface of the cone.

(x) Condensate from the rotating parts was allowed to collect over the entrance to the condensate drain pipe (fig. 31 item 26) in the base of the pressure vessel. The condensate drain value was adjusted to maintain the condensate in the base of the pressure vessel at a constant depth.

These test conditions were maintained for 15 to 20 minutes to enable the temperatures of the cone and of the pressure vessel to become steady.

The steam blow-off valve was opened for 30 seconds while observing the e.m.f. readings from thermocouples on the cone to check for the presence of non-condensables before a test run started.

6.3 Test procedure.

The parameters that constituted the test conditions were:-

a) steam pressure and temperature,

b) speed of rotation,

c) cooling water flow rate,

d) point temperature readings from the inner and outer surfaces of the cone, and from the cooling water system.

Test runs lasted about 30 minutes during which time the test conditions were maintained constant. The surface of the cone was illuminated with stroboscopic light to check that the condensate remained filmwise.

During the test period the following measurements were taken.

(i) The steam pressure was measured and the equivalent saturation temperature was compared with the measured steam temperature.

(ii) The speed of rotation was read by a hand tachometer every 10 min.

(iii) Cooling water flow rate to the inner surface of the cone was measured over two 15 min periods.

(iv) A reading from each of the thermocouples on the inner and the outer surfaces of the rotating cone and from each of the thermocouples in the cooling water system and on the slip-ring unit, was taken at least 3 times during every test run.

(v) The flow of condensate was measured by either one of the methods given in section 4.11 depending on flow rate.

(vi) The dryness fraction of the steam and the concentration of non-condensable gas in the steam were measured during several tests on the 60^{o} cone.

The dryness fraction was found to be between 0.99 and 0.96 and the concentration of non-condensables was found to be less than 0.05%. Since the operating procedure for the boiler was strictly adhered to, the dryness fraction and the concentration of non-condensable gas were maintained within these limits and direct measurements of these

quantities were discontinued. A simple qualitative check for non-condensable gases was devised. The presence of non-condensable gases retards the heat transfer from steam to the outer surface of the cone (section 2.2) and thus lowers the temperature of the outer surface. Thus the presence of non-condensables in the pressure vessel were detected by venting the vessel while observing the surface temperature of the cone. It was found that if the pressure vessel was adequately vented during the starting procedure, non-condensables did not attain significant levels during the test period of 30 minutes.

7.0 EXPERIMENTAL RESULTS AND DISCUSSION

7.1 Independent variables and their range for the experimental work.

The independent variables in the experimental apparatus described in section 4 were as follows:-

(i) Apex angle of cone 2α

(ii) Cone diameter D

(iii) Speed of rotation N

(iv) Cooling water flow rate

(v) Steam temperature t_s

(vi) Steam pressure p

(vii) Cleanliness of the condensing surface

(viii) Roughness of condensing surface.

The experimental heat transfer results taken from the apparatus were a function of these independent variables.

The ranges of the independent variables were:-

(i) Apex angles of experimental cones; 10^o, 20^o and 60^o.

(ii) The range of cone diameter for the 10^o cone was

D = 0.493 m to D = 0.529 m.

The range of diameter for the 20^o cone was

D = 0.529 m to D = 0.60 m.

The range of diameter for the 60^o cone was

D = 0.08 m to D = 0.58 m.

(iii) Experiments were conducted over the speed range zero to 1450 rev/min. On the 10^o cone the ratio of accelerations $\frac{D\omega^2}{2g}$ was varied between zero and 600. On the 20^o cone the range of $\frac{D\omega^2}{2g}$ was zero to 670 and on the 60^o cone the range of $\frac{D\omega^2}{2g}$ was zero to 590.

(iv) The cooling water flow rate was varied over the range $\frac{3m^3}{h}$ to 13 $\frac{m^3}{h}$ and was delivered to the inner surface of the experimental cones to maintain the inner surface at a uniform temperature. Thus the temperature of the inner surface was dependent on the cooling water flow rate, and on the inlet temperature of the cooling water.

(v) (vi) Steam with a dryness fraction between 0.96 and 1.0 was used during all experiments therefore the steam temperature was related to the steam pressure. The steam was supplied to the apparatus at gauge pressures between 1 and 8 bar.

(vii) (viii) The outer surfaces of the cones were cleaned and polished for testing using the method given in section 6.1. The surface roughness on each cone was maintained almost uniform at 0.5 microns C.L.A. or better.

7.2 Behaviour of the film of condensate on the 10°, 20° and 60° cones.

Robson (70) made a photographic study of the behaviour of the film of condensate on the 60° cone. His findings were discussed in section 2.4.4.

The author has made a photographic study of the drainage of condensate from the 10° and 20° cones. A selection of these photographs taken at speeds between zero and 800 rev/min are shown for the 10° cone in fig. 40 and for the 20° cone in fig. 41. The photographs shown were taken with steam at a gauge pressure

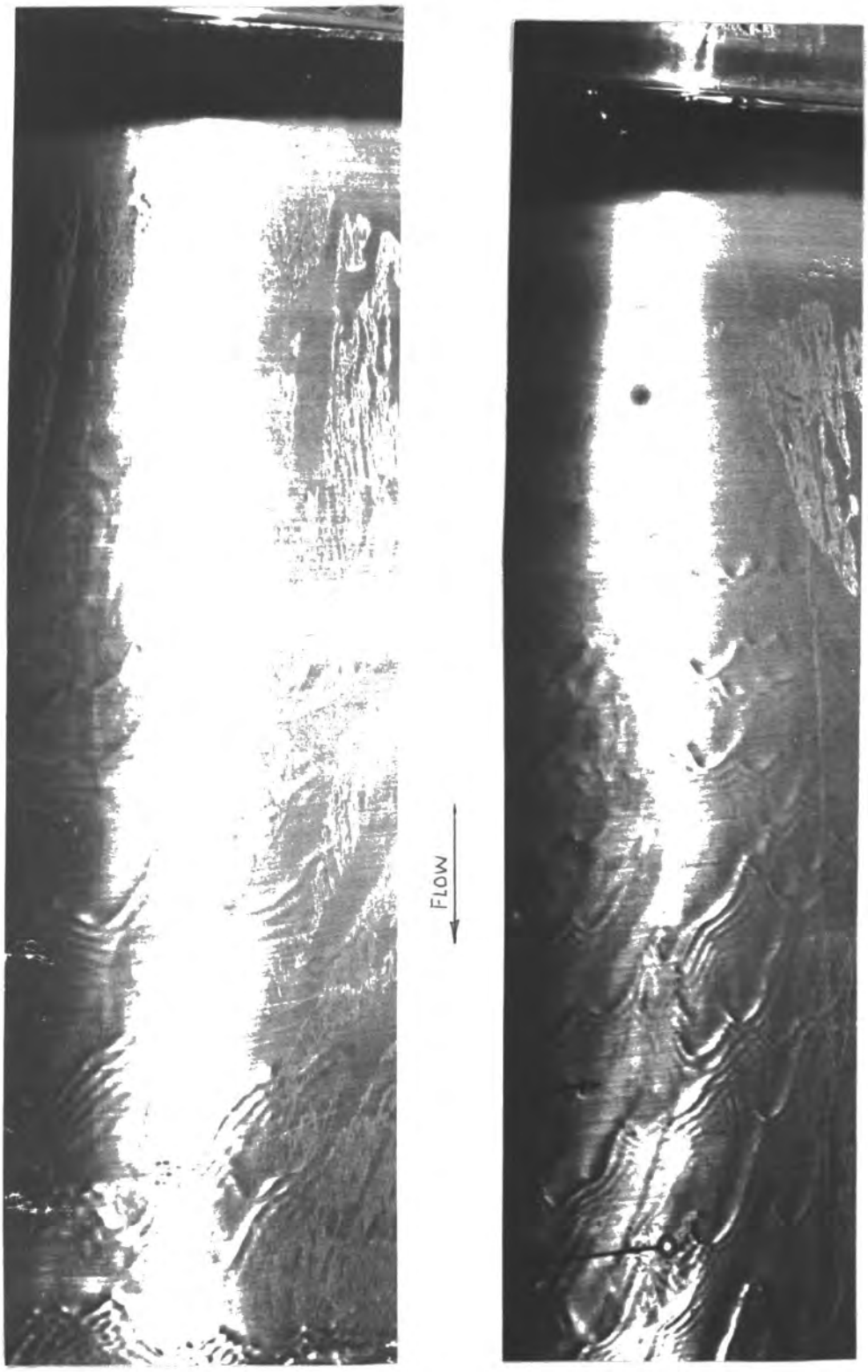

Roll waves

fig. 40(a) Speed of rotation N=zero

(b) Speed of rotation N=100 rev/min

Direction of rotation

Full-size

Uniform ridges

fig. 40(c)

N=200 rev/min

of 1.4 bar. The heat flux for the 10^{o} cone was between $2.6 \ 10^{5} \frac{W}{m^2}$ and $3.0 \ 10^{5} \frac{W}{m^2}$

Comments on the photographs of the 10^{o} cone.

Patterns of roll-waves are visible on the film over the lower 2/3rds of the 10^{o} cone at zero speed fig. 40a. The separation of the main waves appears to be irregular with wavelengths between 0.015 m and 0.03 m. Each of the main waves appears to be preceded by up to four smaller ripples.

On increasing the speed to 100 rev/min, at which $\frac{D\omega^2}{2g}$ on the 10^{o} cone is approximately 2.8, the wave front appears to become jagged (fig. 40b), and the ripples travelling in front of adjacent waves intersect. This type of wave pattern was also observed on the 60^{o} cone. The drainage path on the lower part of the cone is no longer along the generator of the cone, but along a path crossing the generator at an angle of approximately 10^{o}. The direction of drainage is in the opposite sense to the direction of rotation.

At a speed between 100 and 200 rev/min where $\frac{D\omega^2}{2g} \approx 11.5$ the jagged roll-wave regime degenerates into a very uniform pattern of ridges (fig. 40c). The centre line of each ridge makes an angle of approximately 20^{o} with the generator and the distance between the crests of adjacent ridges, or the pitch of the ridges, varies between 0.003 and 0.005 m. A regime of ridges similar to these were observed in the drainage of condensate under gravity from the underside of an inclined plate by Gerstmann and Griffith (38). The pitch of the ridges on this plate were approximately 0.01 m.

Drops leaving non-uniform ridges

Speed of rotation
N=400 rev/min

fig.40(d)
Full-size

(e)
2.Full-size

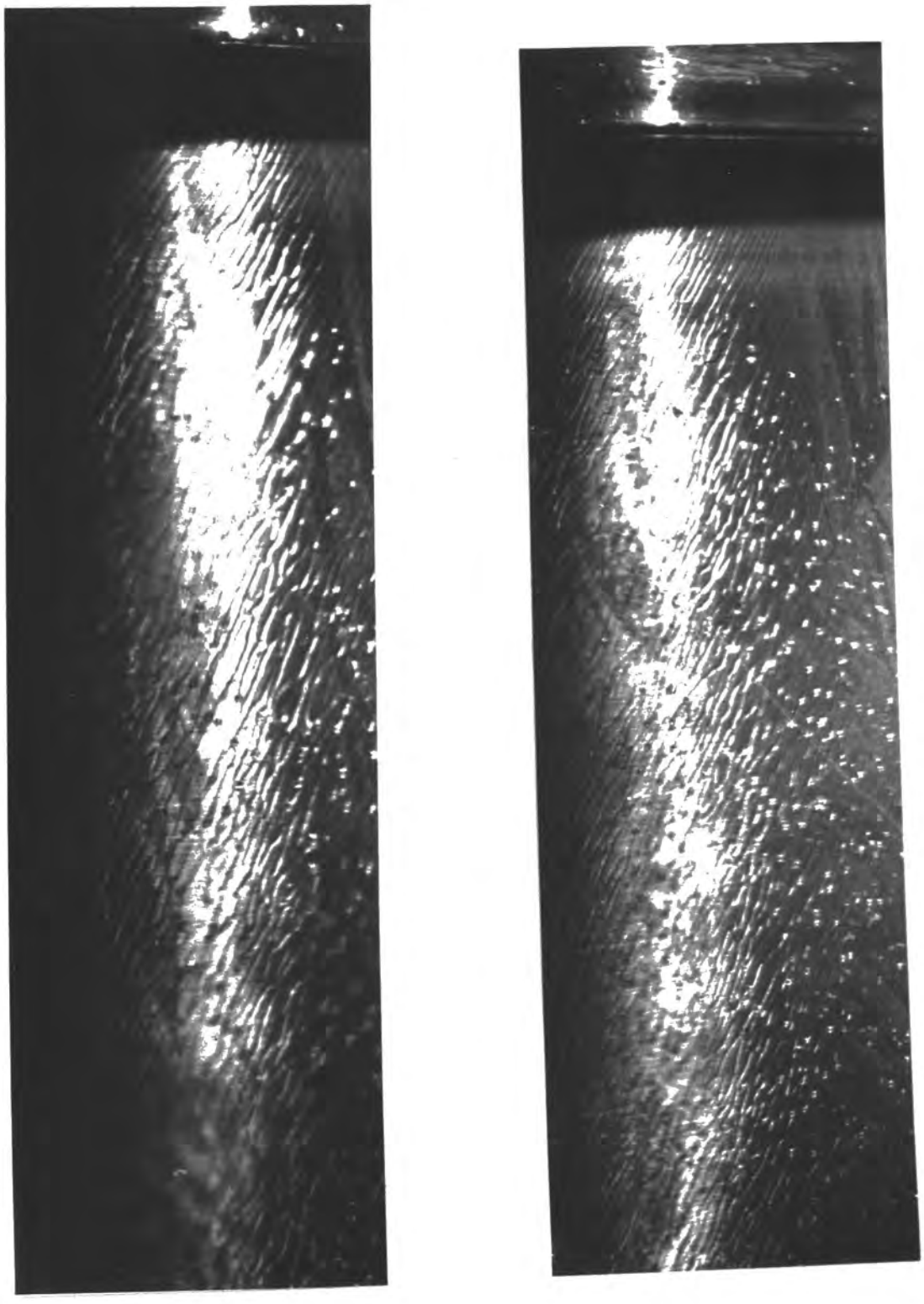

Drops leaving non-uniform ridges

fig.40(f)
N=600 rev/min

Full-size

fig.40(g)
N=800 rev/min

Heat transfer in the troughs of the ridges will be larger than at their crests. To maintain a stable ridge pattern, the condensate deposited at a trough must flow into the ridge which then acts as a drainage channel. Nusselt (9) showed that for a given acceleration along a surface, the velocity of drainage of a smooth laminar film of thickness δ was proportional to δ^2. If we assume that the velocity of flow in any thin film is also a function of film thickness, it follows that the velocity of drainage in the main part of the ridge beneath the crest is larger than at the trough where the film is thinnest. It would appear from the uniformity of the ridges at 200 rev/min that the ridge can accept the flow of condensate from the trough and provide adequate drainage along the surface of the cone.

At 400 rev/min (fig. 40d) where $\frac{D\omega^2}{2g} \approx 45$, the ridges become slightly irregular in shape and tend to join up with neighbouring ridges. Over the upper third of the 10° cone the pitch of the ridges is approximately 0.002 m, but over the lower two thirds of the surface the pitch of the ridges increases to between 0.0025 m and 0.006 m. However, by observing the shadows cast by the ridges, it would appear that the ratio of amplitude to width of the ridges remains substantially unchanged at a value near unity. The enlarged view (fig. 40e) taken from fig. 40d, illustrates the amplitude to width ratio for the ridge over the lower portion of the cone and also shows that comparatively large areas of the film are free from disturbances. Where ridges join with neighbours on this lower part of the cone the new ridge appears to become

overloaded with condensate some distance downstream from the point of intersection, and a drop of condensate forms on the ridge. These drops have a diameter of approximately 0.002 m and tend to travel along the ridge for some distance before they are detached from the ridge. The point at which drops are detached depends on the heat flux and on the ratio $\frac{D\omega^2}{2g}$, which does not vary much along the 10° cone at any given speed. On many of the ridges drops can be seen spaced at intervals between 0.002 m and 0.003 m. One could argue that the condensate draining from the undisturbed parts of the film into the ridge causes an overloading of the ridges capacity to drain the condensate along the surface. This overloading appears to be relieved periodically by the formation and detachment of drops.

The photographs taken at 600 rev/min (fig. 40f), where $\frac{D\omega^2}{2g} \approx 110$, show that the pitch of the ridges has decreased to approximately 0.0015 m and that ridges tend to join their neighbours more frequently. Drop detachment continues and the starting point of detachment moves up towards the starting point of the film of condensate. The intensity of drop detachment from the 10° cone is such that the view of the cone surface tends to be obscured and the inner surface of the windows in the pressure vessel become covered with a film of condensate which is continuously disturbed by the impact of drops.

The process of drainage by the throwing of drops continues with increasing speed and prevents clear photographs being taken. Thus the photograph taken at 800 rev/min (fig. 40g) where $\frac{D\omega^2}{2g} \approx 180$ is not too clear, but the ridges and drops can still be seen.

Fig. 41

(a)

N=Zero

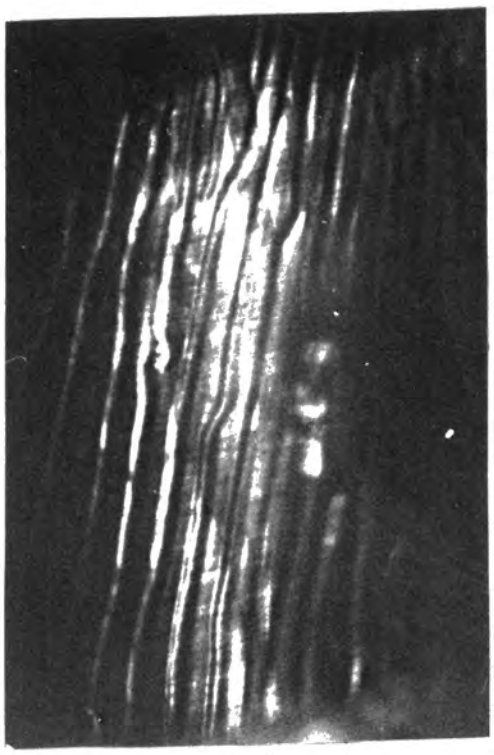

(b)

N=200rev/min

(c)

N=400rev/min

Full-size

20° Cone

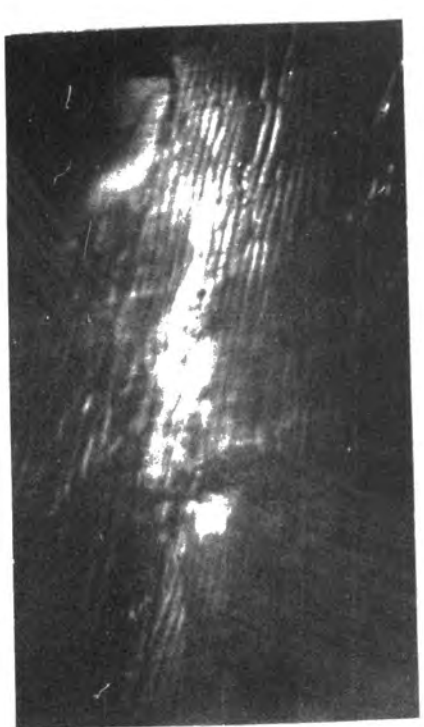

(d)

(d)

(e)

N=600rev/min

N=800rev/min

Comments on the photographs of the 20^{o} cone.

Only part of the 20^{o} cone between x = 0.04 m and x = 0.12 m is visible on the photographs shown in fig. 41.

At zero speed the roll-wave regime for condensate drainage along the surface can be seen in fig. 41a. The ripples which preceed the roll-waves are also visible. This regime exists up to speeds of between 100 and 150 rev/min, but between approximately 150 and 200 rev/min the roll-wave regime degenerates to a pattern of uniform ridges (fig. 41b). The pitch of these ridges is similar to the pitch of the ridges on the 10^{o} cone at this speed of rotation.

On increasing the speed of rotation to 400 rev/min where $\frac{D\omega^2}{2g} \approx 50$ the ridge regime is maintained, and drainage continues to be across the surface of the cone along a backward curving drainage path which makes an angle of approximately 20^{o} with the generator (fig. 41c). The pitch of the ridges is between 0.002 m to 0.004 m. There is little suggestion that drops have formed on the ridges at 400 rev/min, where as on the 10^{o} cone at this speed, many drops can be seen on the film of condensate.

The ridge regime is maintained on the 20^{o} cone at speeds up to 600 rev/min and 800 rev/min where $\frac{D\omega^2}{2g}$ is 113 and 200 respectively (fig. 41d and 41e), and there is some evidence to suggest that drops are being formed on the ridges. Since the heat flux on the 10^{o} and 20^{o} cones is similar, we can conclude that the increased component of the centrifugal acceleration resolved along the surface of the 20^{o} cone is sufficient to enable the condensate flowing into the ridge to drain predominantly along the surface of the cone.

Comments on the effect of the acceleration field on drop detachment.

From the preceeding discussions on the behaviour of the film of condensate on the 10^{o}, 20^{o} and 60^{o} cones, the question arises as to the conditions necessary for the formation and detachment of drops from a film of condensate on the surface of a given cone. This question cannot be answered properly without a much more detailed study than is given here. However, by using the results of the present study in conjunction with the findings of other workers, some general conclusions can be drawn on the influence that the acceleration field has on the mode of film drainage.

The drainage of a film of condensate from a body is governed by the action of the acceleration field which surrounds the body. Neglecting any effects that vapour drag might have in disturbing the film, it can be argued that only when a component of the acceleration field acts normal to and away from the condensing surface can there be any possibility of drop detachment. On the upper surface of a disc rotating with its axis of symmetry in the vertical, the centrifugal acceleration acts along the surface of the disc and gravitational acceleration acts normal to, but towards the surface. Therefore drops are not likely to be formed on such a body while film-wise condensation exists. Decreasing the apex angle of the cone while maintaining the same value of $\frac{D\omega^2}{2g}$, reduces the proportion of the centrifugal acceleration acting along the surface of the cone and increases the proportion of the centrifugal acceleration acting normal to and away from the surface.

While the proportion of the gravitational acceleration acting along the surface and normal to the surface increases and decreases respectively. Consequently at an apex angle of 0^{o} the centrifugal acceleration acts exclusively normal to and away from the surface while the gravitational acceleration acts exclusively along the surface.

On a stationary vertical cylinder the film of condensate will drain along the surface, but at a critical finite value of $\frac{D\omega^2}{2g}$, drainage of the film along the surface will be enhanced by the formation and detachment of drops. Thus the mode of drainage is influenced by the magnitude of the acceleration resolved along the surface of the cone (denoted by a in section 4.1.2) and by the acceleration resolved normal to the surface (denoted by a_y).

Nichol and Gaseca (59) did not discuss in detail the behaviour of the film of condensate on the vertical 0.025 m diameter rotating cylinder, but if we assume that drops were thrown from the film when the heat transfer coefficient started to show an increase with speed, their published results indicate that drops started to leave the film at speeds between 450 and 1000 rev/min for which $\frac{D\omega^2}{2g}$, or $\frac{a_y}{a}$ is between 2.5 and 12 respectively. The critical value of $\frac{D\omega^2}{2g}$ depended on the heat flux; as the heat flux increased the critical value decreased. This figure of $\frac{D\omega^2}{2g}$ between 2.5 and 12 is in good agreement with the value found by Hoyle and Matthews (60) for the detachment of drops from their 0.2 m diameter horizontal rotating cylinder. Gerstmann and Griffith (38) observed that drops started to fall from ridges in a film of condensate (freon 113) on the underside

of a stationary inclined plate after the angle of inclination between the plate and the horizontal decreased below 13^{o}. At 13^{o}, $\frac{a_y}{a} = 4.16$. Thus there is strong independent experimental evidence to show that drops are detached when $\frac{a_y}{a}$ is between 2.5 and 12 despite a difference in the magnitude of the individual accelerations between (38) and (60). Increases in the magnitude of a_y will reduce the diameter of the drops that leave the film.

The photographs for the 10^{o} cone showed that drops start to leave the film at a speed between 200 rev/min and 400 rev/min for which $\frac{a_y}{a}$ is between 5.7 and 9.0. This finding is in agreement with other workers and leads us to conclude that the ratio $\frac{a_y}{a}$ needs to be greater than approximately 2.5 before drops can form and be detached from the film.

On a rotating vertical cylinder the ratio $\frac{a_y}{a}$ is equal to $\frac{D\omega^2}{2g}$ and can increase without limit, but when the apex angle of the cone 2α becomes finite, $\frac{a_y}{a}$ cannot increase without limit. Using equation 3.1.1 and equation 3.1.3 it can be shown that as $\frac{D\omega^2}{2g}$ becomes large, $\frac{a_y}{a}$ for cones approaches the limit $\frac{1}{\tan\alpha}$

At $2\alpha = 10^{o}$ the limit of $\frac{a_y}{a} = 11.4$

at $2\alpha = 20^{o}$ the limit of $\frac{a_y}{a} = 5.6$

at $2\alpha = 60^{o}$ the limit of $\frac{a_y}{a} = 1.74$

Although drops were not observed on the 20^{o} cone at speeds up to 800 rev/min, the limiting value of $\frac{a_y}{a} = 5.6$ is within the range of $\frac{a_y}{a}$ where drops have been observed by other workers. Photographs could not be taken of the 20^{o} cone at speeds beyond 800 rev/min, but the heat transfer results could indicate a change in the mode of drainage at speeds over 800 rev/min.

Patterns of disturbances resembling ridges were observed on the 60^{o} cone at speeds between 600 rev/min and 1450 rev/min, but over the full range of test speeds drainage always occurred along the surface of this cone. It can be seen that $\frac{a_y}{a}$ for the 60^{o} cone cannot exceed 1.74 which is below the lowest value (2.6) at which drops have been observed to leave a film.

The foregoing discussion shows that as the apex angle becomes significantly greater than 20^{o}, the limiting ratio of $\frac{a_y}{a}$ decreases to reduce the probability of drop detachment. At these apex angles greater than 20^{o} the acceleration a becomes dominant and causes an improvement in film drainage along the surface.

In section 4.7 a laminar theory was developed for condensation on a rotating body with a curved generator. On this body the apex angle 2α as defined in fig. 4 increased with the distance x along the generator. On such a body the laminar film of condensate was assumed to start at a point where the apex angle 2α was zero and to drain along the generator and onto a disc where the apex angle was 180^{o}. In practice the film of condensate would not remain laminar and on current

evidence from rotating cylinders and cones, drops would form and leave the film where the apex angle was small. However, on this body the apex angle increases, therefore at a certain apex angle the detachment of drops should cease and the film should drain along the surface. It will be interesting to see whether the range of $\frac{a_y}{a}$ 2.5 to 12 necessary for drop detachment for cones has any significance in predicting the point where drops cease to be thrown from the body with a curved generator. The evidence to date strongly suggests that the ratio $\frac{a_y}{a}$ will be significant.

7.3 Energy balance.

It is usual practice to have a check for the measured energy transfer across the walls of the condensing element. This check can be provided by making a balance between the energy liberated by the measured flow of condensate from the condensing element and the energy gained by the cooling water flowing over the inner surface of the element. In the present series of tests the condensate from the conical surfaces and from the underside of the cone base-plate (fig. 31 item 30) were not kept separate during collection, therefore a meaningful energy balance for the conical surfaces of either the 10^{o} and 20^{o} cone and of the 60^{o} cone could not be made.

A device for collecting condensate from the 60^{o} cone was designed, but was not used because

(a) the collector would obscure the surface of the 60^{o} cone and interfere with Robson's (70) photographic study of the condensate drainage along the surface of that cone.

(b) the presence of a collector near the rotating surface of the cone might cause a disturbance in the steam flow and thus interfere with the heat transfer process.

(c) an undetermined amount of condensation would occur on the drops of under-cooled condensate as they passed through the steam between the cone and the collector.

At high speeds, drops of condensate were likely to leave the surfaces of the 10^{o} and 20^{o} cones at any point and also from the throwing rings (fig. 34). A suitable collector for condensate leaving the 10^{o} and 20^{o} cones would be much larger than the proposed device for the 60^{o} cone and could therefore have had an adverse effect on the flow of steam around the rotating cones.

The energy liberated by the total flow of condensate, that is from the cone and the base-plate together, was shown by Robson (70) to balance with the energy transferred to the cooling water, with an unaccounted loss of 2.4% of the total energy. Such an energy balance is useful in checking the accuracy of the cooling water flow rate and of the cooling water temperature measurement. However this overall energy balance is not an independent check on the accuracy of heat transfer results on the experimental cones, and makes little contribution towards the experimental results reported here.

Because the accuracy of the heat transfer results are dependent on the temperature measurements at the surfaces of the cones and on the thermal conductivity of the cone material, precautions were taken to ensure that these quantities

were accurately measured (section 4.9 and appendix B).

7.4 Typical temperature distributions on the experimental cones.

Typical temperature distributions along the inner and outer surfaces of the 10^{o} and 20^{o} experimental cones are shown in figs. 42 and 43 respectively and for the 60^{o} cone in fig. 44.

The 60^{o} cone was the first to be used in the experimental program and provided a proving ground for developing an experimental technique. The inner surface of the 60^{o} cone was cooled by five independent supplies of cooling water to the five cooling zones shown in fig. 44. The supply of cooling water to each zone was adjusted to make the temperature of the inner surface as near to being uniform as possible. As can be seen in fig. 31 the cooling water was distributed to the cone through a large number of small bore tubes. Thus at zero speed the uniformity of temperature over the entire inner surface was dependent on the axial distribution of cooling water in each of the cooling zones. Since the cooling water distribution was not at it's best at zero speed, the local variation in surface temperature was more noticeable. However, as the speed of rotation increased, the axial distribution of cooling water over the entire inner surface of the cone was greatly improved.

The presence of both the small shaft (fig. 31, item 18) on the apex of the 60^{o} cone and the base-plate (item 30) at the base of the cone, caused disturbances in the temperature distribution in the cone wall near these extremities.

FIG 42

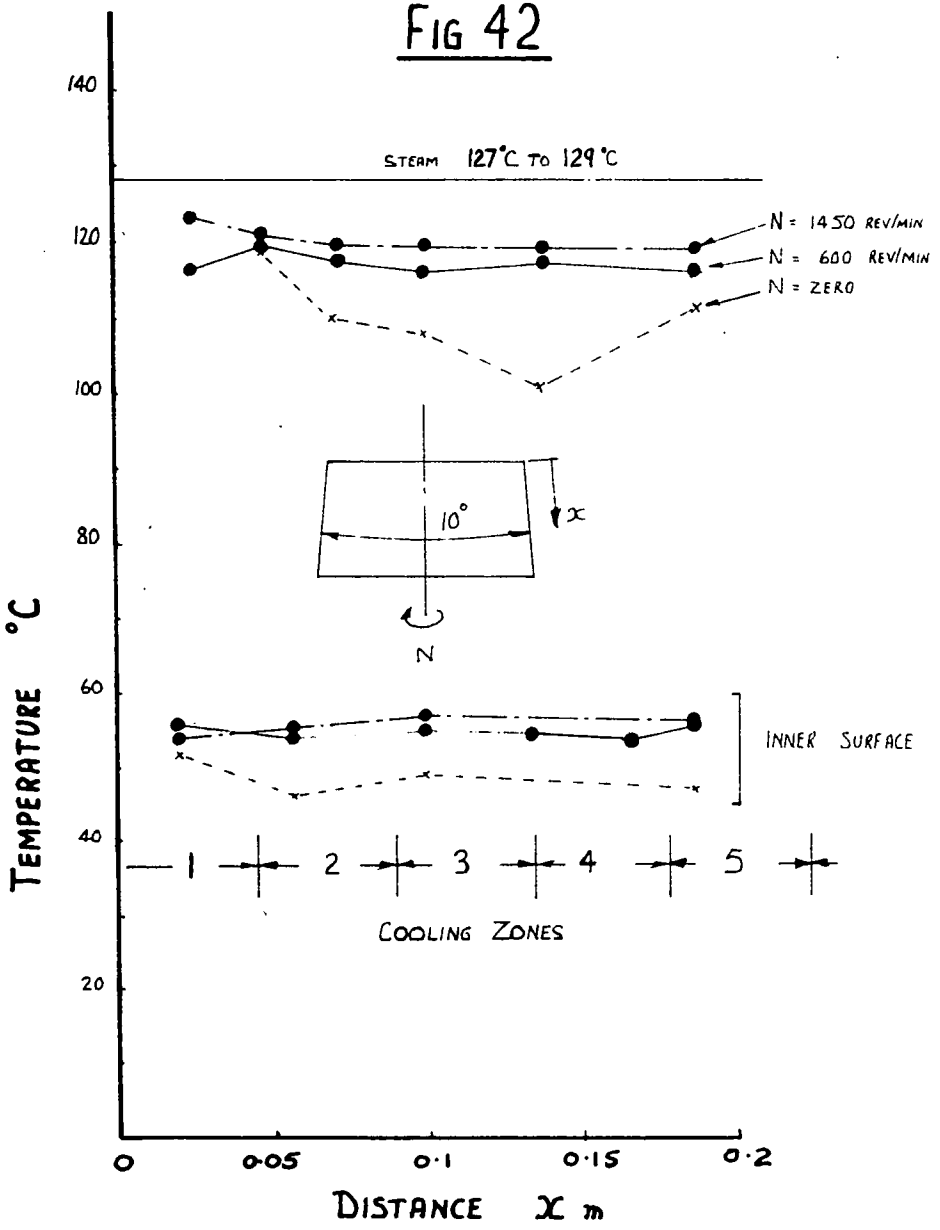
140
120
100
80
60
40
20
STEAM 127°C TO 129°C
N = 1450 REV/MIN
N = 600 REV/MIN
N = ZERO
10°
x
N
INNER SURFACE
1
2
3
4
5
COOLING ZONES
TEMPERATURE °C
0
0·05
0·1
0·15
0·2
DISTANCE x m

FIG 43

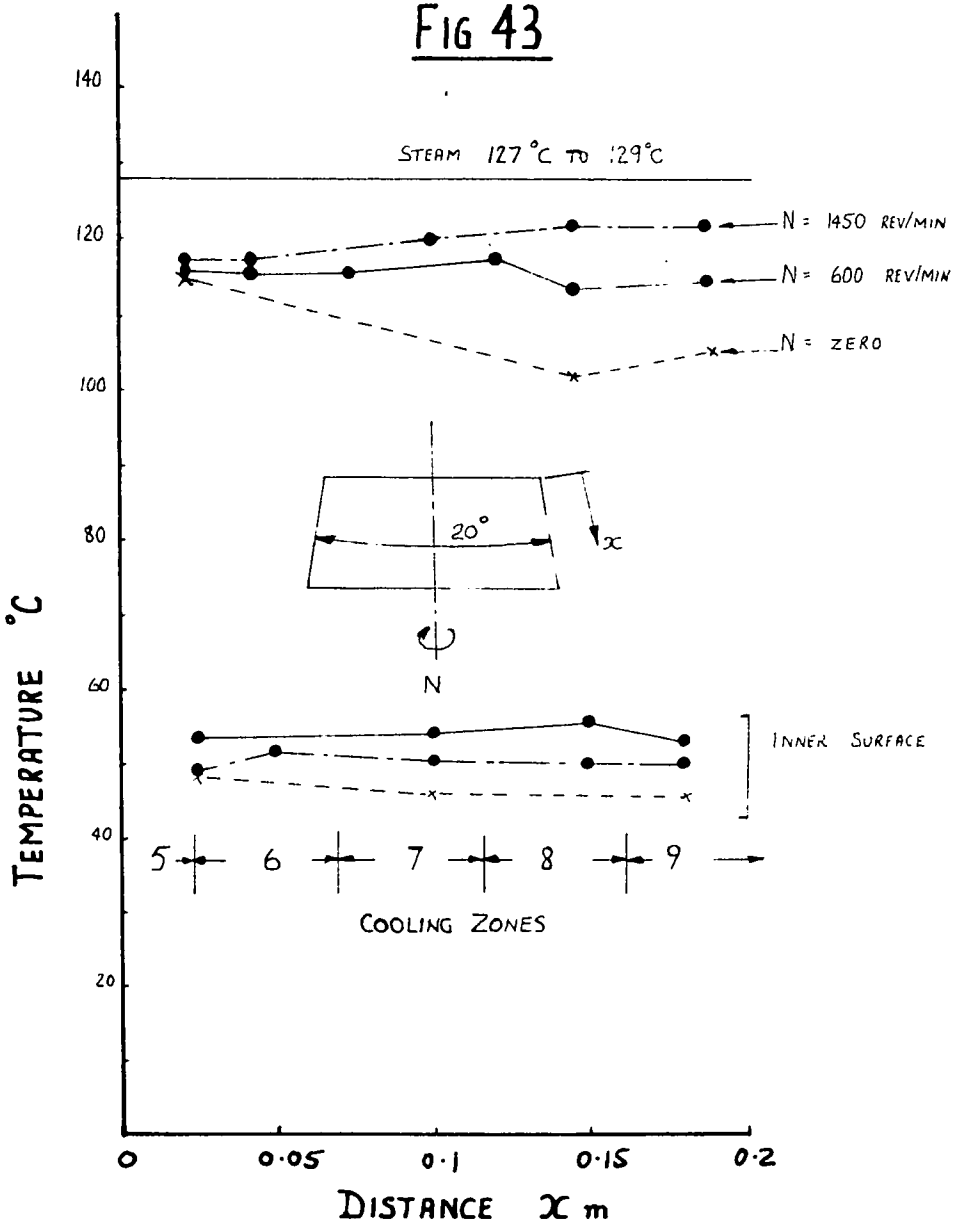
140
120
100
80
60
40
20
STEAM 127°C TO 129°C
N = 1450 REV/MIN
N = 600 REV/MIN
N = ZERO
20°
x
N
INNER SURFACE
5
6
7
8
9
COOLING ZONES
TEMPERATURE °C
0
0·05
0·1
0·15
0·2
DISTANCE x m

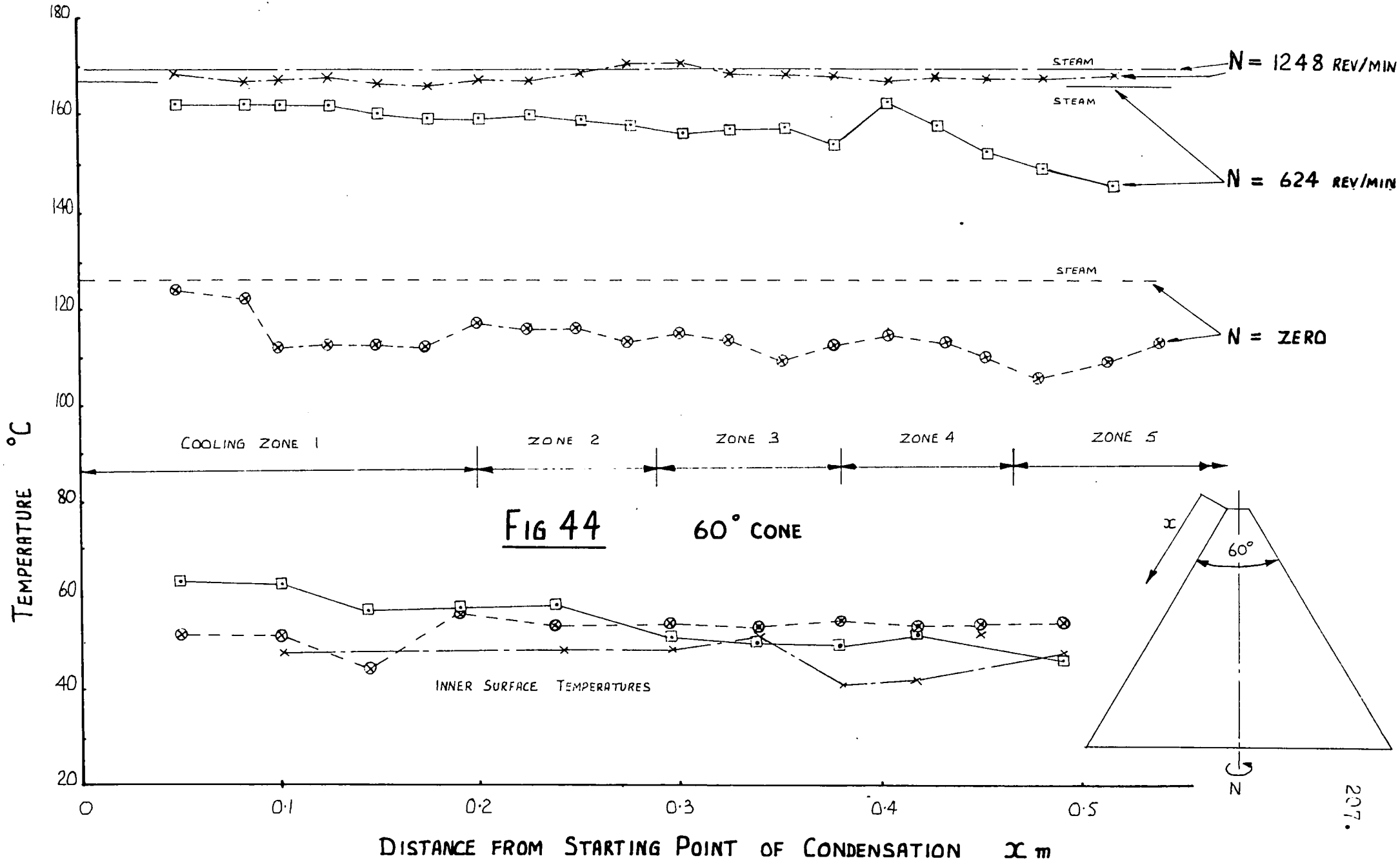

FIG 44 60° CONE

207.

The end effect caused by the apex of the cone and the small shaft was discussed in the latter part of section 3.8, where it was shown from theoretical considerations that the end effect on the 60^{o} cone became negligible at x greater than 0.04 m. In practice the temperature of the outer surface of the 60^{o} cone could not be maintained uniform very close to the apex of the cone, due largely to imperfect cooling in this region of the inner surface at all speeds. Consequently as x became less than approximately 0.04 m, the temperature of the outer surface of the cone gradually increased up to the steam temperature. To reduce errors in heat transfer measurements due to end effects, values of heat flux and heat transfer coefficient were calculated from measurements of temperatures taken between cone diameter D = 0.08 m and D = 0.58 m, which gave a length along the cone generator of approximately 0.5 m between x = 0.04 m and x = 0.54 m.

As can be seen on fig. 44, absolute uniformity in temperature on the inner surface of the cone between x = 0.05 m and 0.54 m could not be achieved but the greatest deviation was hardly more than $\pm$ 5^{o} C over the full range of test speeds. The temperature of the inner surface could have been maintained more uniform if a larger number of cooling zones had been used. This lesson was borne in mind when designing the cooling system for the 10^{o} and 20^{o} cones. The temperature on the outer surface of the 60^{o} cone was found to be uniform generally to within $\pm$ 5^{o} C.

Cleaning the outer surface of the 60^{o} cone with abrasive paper to obtain a wettable surface took a toll on the life

of thermocouples. Junctions needed to be inspected regularly and to be repaired when necessary as mentioned in section 4.9.2.

The ideal position for taking temperature measurements on each of the experimental cones was exactly at the inner and at the outer surfaces. However, the method of fitting thermocouple junctions to the cones, as described in sections 4.9.2 and 4.9.3, and the fact that the junctions were a finite size, probably introduced small positional errors to the junction. Consequently the measured temperature may not be the true surface temperature. If a junction was near the bottom of a groove on the 60° cone, i.e. 0.0008 m from the surface, the thermocouple was estimated in appendix C to be reading 2° C below the true surface temperature for every 100° C temperature difference across the wall of the cone. Assuming a mean thermocouple position of 0.0008 m from the surface the error in temperature reading becomes $\pm$ 2% of the temperature difference across the wall of the cone. From the possible sources of error in temperature measurement that have been discussed in this section and in sections 5.1 and 5.2, the error in wall temperature difference becomes $\pm$ 4% of the wall temperature difference. Thus for a wall temperature difference of 100° C, which was approximately the value at N = 624 and N = 1248 rev/min (fig. 34), the error was $\pm$ 4° C.

The two sources of error in the measurement of the outer surface temperature were $\pm$ 2% of the wall temperature difference and $\pm$ 1° C due to the correction for secondary e.m.f. (section 5.2).

The measured steam temperature was accurate to within $\pm$ 0.1° C, therefore the error in the measured film temperature difference at these speeds was probably very close to $\pm$ 3° C. The error introduced by the correction of secondary e.m.f. was evident at N = 1248 rev/min where the temperature of the outer surface measured by two thermocouples near x = 0.3 m was slightly above the measured steam temperature.

The effects of these errors in temperature measurement on the calculated values of local heat flux and of local heat transfer coefficient are discussed in section 7.4 and 7.5 respectively.

Typical temperature distributions are shown for the 10° and 20° cones in fig. 42 and 43 respectively. The nine cooling zones used over the 0.4 m length of the combined 10° and 20° cones enabled the inner surface of each cone to be maintained uniform to within approximately $\pm$ 3° C.

At the lower end of the speed range the film of condensate was observed to run along the surface of the 10° cone and onto the throwing ring. The throwing ring thus caused a disturbance in the flow of condensate and produced an increase in the temperature near the intersection of the 10° and 20° cones. The throwing ring also acted as an energy source and conducted energy to the outer surface of the body where the two cones joined.

It is also clear from the curves in figs. 42 and 43 that several thermocouples were broken both on the inner and outer surfaces. Shortly after the test at zero speed, the test program was brought to an end, because of these breakages.

The error in the wall temperature difference across the 10^{o} and 20^{o} cones was estimated to be $\pm$ $4\frac{1}{2}\%$ of the wall temperature difference θ_w. At $\theta_w = 65^{o}$ C, which was approximately the value at a speed of 1450 rev/min on the 10^{o} cone, the error in wall temperature difference was within $\pm$ 3^{o} C. The positional error in the measurement of outer surface temperature is $\pm$ $2\frac{1}{4}\%$ of the wall temperature difference and the error due to secondary e.m.f. was $\pm$ 1^{o} C at 1450 rev/min on the 10^{o} cone. Thus the error in the film temperature difference was within $\pm$ $2\frac{1}{2}^{o}$ C. The effect of these errors on the calculated values of heat flux and of heat transfer coefficient are discussed in subsequent sections.

7.5 Experimental heat flux.

Calculation of the experimental heat flux.

Experimental values of the local heat flux across the film of condensate in the Y direction were calculated from the measured heat flux across the wall of the cone. The measured temperature distribution along the inner and outer surfaces of the experimental cones was used with the theory for energy conduction across the walls of hollow cones (see section 3.8) to calculate the heat flux. Rearranging equation 3.8.4 gave the experimental local heat flux ϕ as

$$\phi = -k \frac{dt}{dy} \qquad \ldots\ldots\ldots (7.1)$$

where k = thermal conductivity of the cone material at the outer surface

and $\frac{dt}{dy}$ = the temperature gradient in the Y direction in the cone material at the outer surface.

The effects of variable thermal conductivity of the cone metal were shown in the latter part of section 3.8 to be significant, therefore the temperature gradient $\frac{dt}{dy}$ was evaluated from equation 3.8.35.

The typical temperature distributions given in figs. 42, 43, and 44, exhibit a slight non-uniformity of temperature along both the inner and the outer surfaces of the experimental cones. The theory developed in section 3.8 gives the correct heat flux only when the temperature of the inner and outer surfaces are uniform, and thus does not take into account the small X direction heat flux which results from this non-uniformity of temperature distribution. A three dimensional electrical analogue for the experimental cones would be needed to account for both the X direction and Y direction heat flux. In the majority of the experiments the non-uniformity of the temperature distribution along the surfaces of the cones was small compared with the temperature difference across the cone wall, therefore the X direction heat flux was neglected. In doing so, equation 7.1 slightly **under** estimated the Y direction heat flux.

Errors in the experimental heat flux.

The error in the calculated values of heat flux can be assessed from the known experimental errors. There are an insufficient number of tests carried out at a given set of

test conditions for the use of a statistically based method of error analysis, so the experimental errors were assessed in the following way.

The experimental heat flux ϕ was calculated from equation 7.1, which when applied to the 10° and 20° experimental cones reduces to

$$\phi = -k \frac{\theta_w}{w} \qquad \ldots\ldots\ldots (7.2)$$

where θ_w = wall temperature difference

w = wall thickness

k = thermal conductivity of the cone material.

Then $\frac{\Delta k}{k} = \pm 0.03$ from appendix B

$$\frac{\Delta \theta_w}{\theta_w} = \pm 0.045 \text{ from section 7.4}$$

$$\frac{\Delta w}{w} = \pm 0.001$$

By differentiating equation 7.2 and taking the modulus of the errors in the measured quantities

$$\frac{\Delta \phi}{\phi} = \frac{\Delta k}{k} + \frac{\Delta \theta_w}{\theta_w} + \frac{\Delta w}{w} = \pm 7.6\%$$

This method of analysis gives very pessimistic assessments of experimental errors.

For the 60° cone, where equation 7.1 reduces to equation 7.2 at large values of x,

$$\frac{\Delta k}{k} = \pm 0.03 \quad ; \quad \frac{\Delta \theta_w}{\theta_w} = \pm 0.04 \quad ; \quad \frac{\Delta w}{w} = \pm 0.001$$

Thus, for the 60° cone the error in the heat flux $\frac{\Delta \phi}{\phi} = \pm 7.1\%$.

No attempt has been made to make an accurate assessment of the error in the Y direction heat flux due to neglecting the X direction heat flux; such an assessment could not be made without the use of a three dimensional analogue. Since the X direction temperature gradients in the majority of experiments were less than 6% of the Y direction gradient, using equation 7.1 to calculate the heat flux would lead, at the worst, to errors of the same order as those predicted above.

Experimental heat flux plotted against distance x.

Experimental values of the local heat flux calculated from equation 7.1 and using the temperature distributions given in fig. 42, 43 and 44, are shown for the 10^{o} cone and 20^{o} cone in fig. 45 and 46 respectively and for the 60^{o} cone in fig. 47. In general the curves of heat flux against distance from the starting point of condensation x are not smooth, due partly to the unknown position of the thermocouple junctions and partly to neglecting the X direction heat flux. A three dimensional treatment of these test results would produce smoother curves of heat flux.

However figs. 45, 46 and 47 show that the experimental heat flux does change with x and the rate of change with x is dependent on the speed of rotation.

Typical heat flux for the 10^{o} cone.

Considering the experimental heat flux for the 10^{o} cone shown in fig. 45 it can be seen that at zero speed the heat flux decreases with x. At zero speed the film of condensate

10° CONE

FIG 45

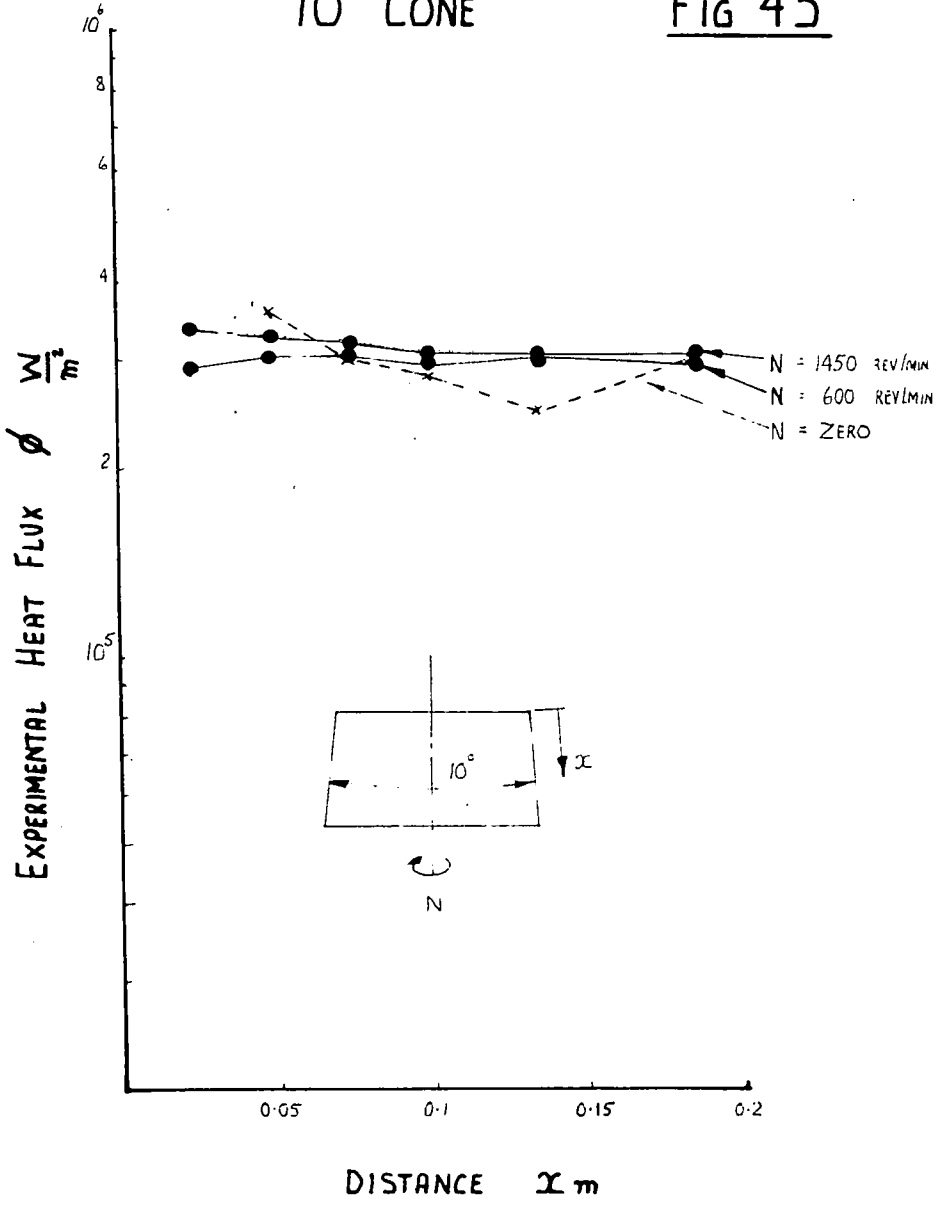

20° CONE

FIG 46

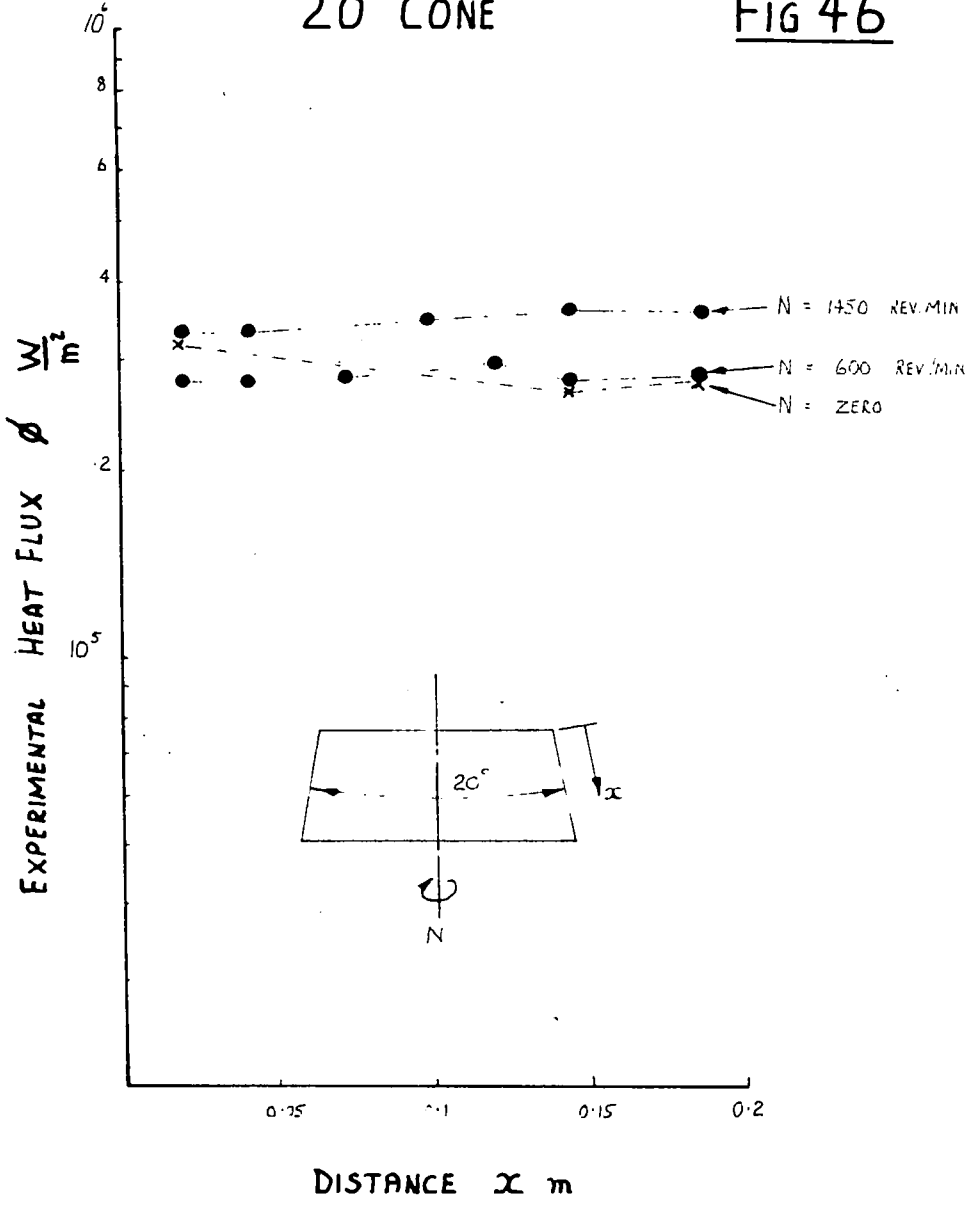

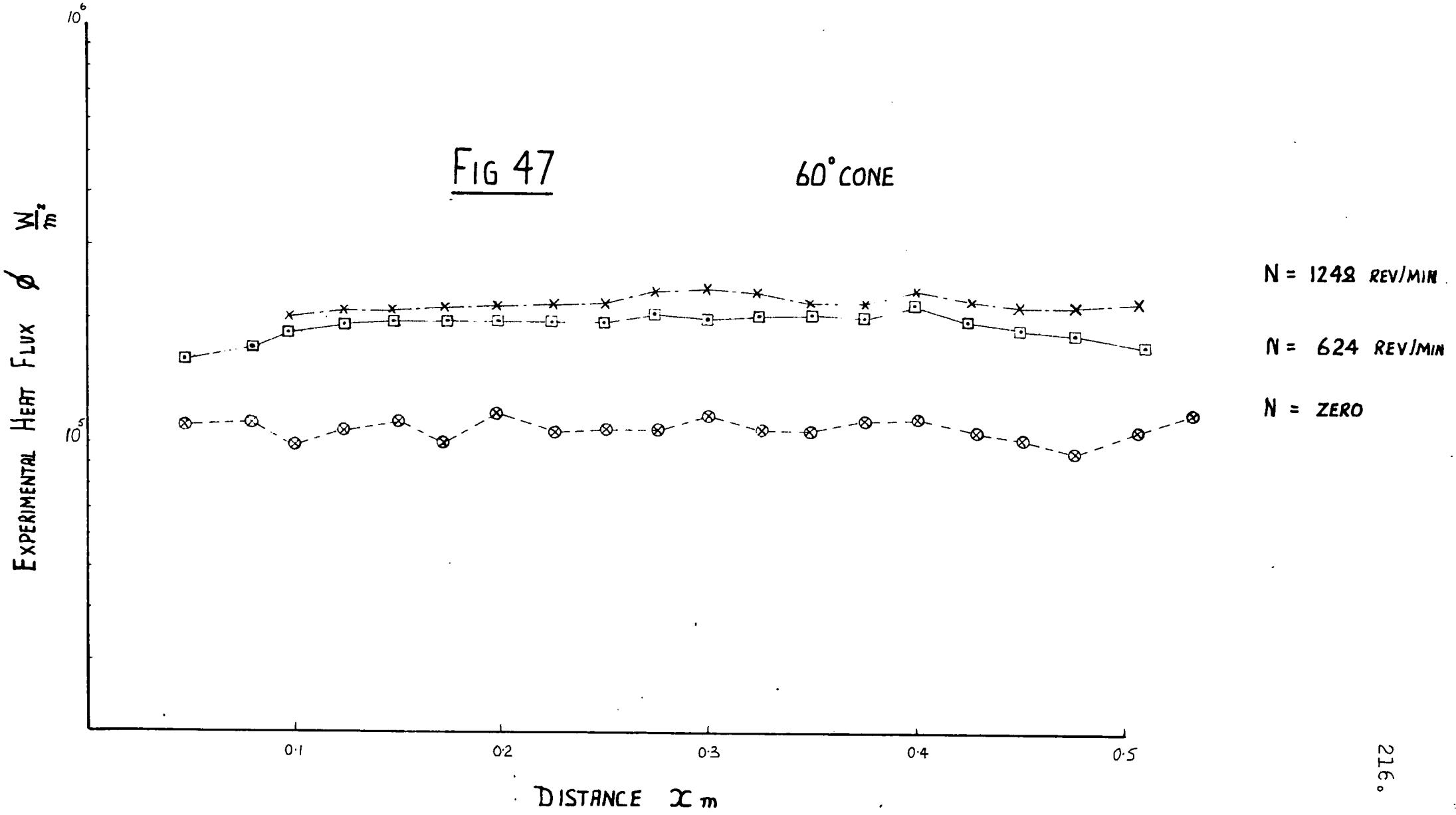
FIG 47
60° CONE
EXPERIMENTAL HEAT FLUX ϕ W/m²
10⁶
10⁵
0·1
0·2
0·3
0·4
0·5
DISTANCE x m
N = 1248 REV/MIN
N = 624 REV/MIN
N = ZERO

was seen in fig. 40a to drain along the generator of the 10^{o} cone, under the influence of gravitational acceleration. The laminar theory for the condensation of steam on cones developed in section 3.5 showed that the film of condensate on a stationary cone increased in thickness with x and that the heat flux should decrease with x. The curve for zero speed on fig. 45 shows that this trend has been found in practice.

With the 10^{o} cone rotating at 600 rev/min, photograph fig. 40e shows that over the lower 2/3rds of the 10^{o} cone the film of condensate drains partly along the surface of the cone and partly by the formation and detachment of drops normal to the surface of the cone. The detachment of drops should reduce the rate of increase in film thickness with x, and should thus lead to a more uniform distribution of the experimental heat flux with x. For this reason the experimental heat flux at both 600 rev/min and 1450 rev/min is more uniform with x.

Since there is a change in the mode of film drainage between zero and 1450 rev/min, it is at first sight perhaps surprising that the experimental heat flux should show such little change with speed. But this can be explained.

The experimental cones are water cooled heat exchangers for condensing steam. Although the curves in figs. 45 to 47 show the heat flux from the film of condensate to the outer surface of the cone, the energy liberated at the outer surface has also to be conducted across the wall of the cone and transferred to the cooling water. It follows that the thermal resistance of the wall and of the transfer of energy to the

cooling water also influence the heat flux. If U is the overall heat transfer coefficient between the steam and the cooling water then

$$\frac{1}{U} = \frac{1}{h_i} + \frac{w}{k_{cone}} + \frac{1}{h}$$

where h = heat transfer coefficient for the condensate to the outer surface of the cone

and h_i = heat transfer coefficient from the inner surface to the cooling water

w = wall thickness of the cone

k_{cone} = thermal conductivity of the cone wall.

Taking as an example, the 10^{C} cone at zero speed,

at $x = 0.17$ m

$$\frac{1}{h} = 4.3\ 10^{-5}\ \frac{m^2C}{w} \qquad \frac{1}{h_i} = 8.0\ 10^{-5}\ \frac{m^2C}{w} \qquad \frac{w}{k}\ 19.1\ 10^{-5}\ \frac{m^2C}{w}$$

From these figures it can be shown that the thermal resistance of the condensate layer is 13% of the total thermal resistance and as the speed increases to 1450 rev/min this fraction reduces to 10%. Thus the thermal resistance of the wall and of the process of transferring energy to the cooling water remain important, so it is perhaps not surprising that a change in the mode of drainage has a limited effect on the value of the experimental heat flux. The thermal resistance of the cone wall could be reduced in two ways.

(i) by using metals with high thermal conductivities; these metals are usually expensive, and have low strength and are difficult to cast,

(ii) by reducing the wall thickness of the cone; the wall thickness is strongly influenced by mechanical considerations.

Typical heat flux for 20^{o} cone.

The thermal resistance of the condensate layer at x = 0.17 on the 20^{o} cone is 30% of the total resistance at zero and 7% of the total at 1450 rev/min. Thus there is a greater change in the experimental heat flux with speed on the 20^{o} cone. At zero speed the heat flux shows a decrease with x as expected from the laminar theory.

The photographs of the condensate at speeds up to 600 rev/min show that the direction of drainage is exclusively along the surface of the 20^{o} cone. At 800 rev/min, several drops were visible (fig. 41e) on the ridges in the film of condensate. The improvement in the heat flux between 600 rev/min and 1450 rev/min could be due to an improvement in the film drainage by the detachment of drops from the film of condensate, although at present there is no photographic evidence to show that drops are being detached from the film.

Typical heat flux on the 60^{o} cone.

Fig. 47 shows typical values of local heat flux for the 60^{o} cone calculated from equation 7.1 using the experimental temperature distributions given in fig. 44. On the 60^{o} cone, the film of condensate starts near the apex where thermocouples were not placed, therefore the behaviour of the film near the starting point is not recorded in fig. 47. The test results for the 60^{o} cone show that the heat flux tends to decrease towards the apex due to the relatively large changes in curvature between the inner and the outer surfaces near the apex, as discussed in section 3.8.

Full range of heat flux on the 10^{o}, 20^{o} and 60^{o} cones.

The full range of the experimental heat flux on each of

the test cones can best be shown by using (i) the film temperature difference θ, which is the steam to surface temperature difference, and (ii) the steam temperature t_s. Both θ and t_s have been shown to influence the experimental heat flux and they can be conveniently linked by the Drew reference temperature $t_f = t_s - 0.75\,\theta$. The validity of the Drew reference temperature was discussed in section 2.2 ref. (21), and the use of this reference temperature was discussed in section 2.2 ref. (69) where it was argued that in a given acceleration field an increase in t_f improved the freedom of movement of the condensate. This improvement was obtained by both the viscosity and the surface tension of the condensate being reduced more rapidly than the density of the condensate.

The dependence of the experimental heat flux on the Drew reference temperature is illustrated in figs. 48 a b c for the 10^o, 20^o and 60^o cones respectively. The experimental local heat flux shown in fig. 48a and 48b are taken at a distance $x = 0.1$ m along the generator of the 10^o and 20^o cones respectively and the local heat flux for the 60^o cone is taken at a distance $x = 0.4$ m. At these values of x on each cone, the heat flux is least likely to be affected by energy transfer from the ends of the cones.

In figs. 48a (10^o cone) the heat flux over a given range of $\frac{D\omega^2}{2g}$ is shown to increase with t_f. Values of heat flux at $\frac{D\omega^2}{2g}$ less than 45, for which the film drainages is along the cone surface, lie along line $A_1\ A_1$. At $\frac{D\omega^2}{2g}$ above 100 film drainage is enhanced by the formation and detachment of drops.

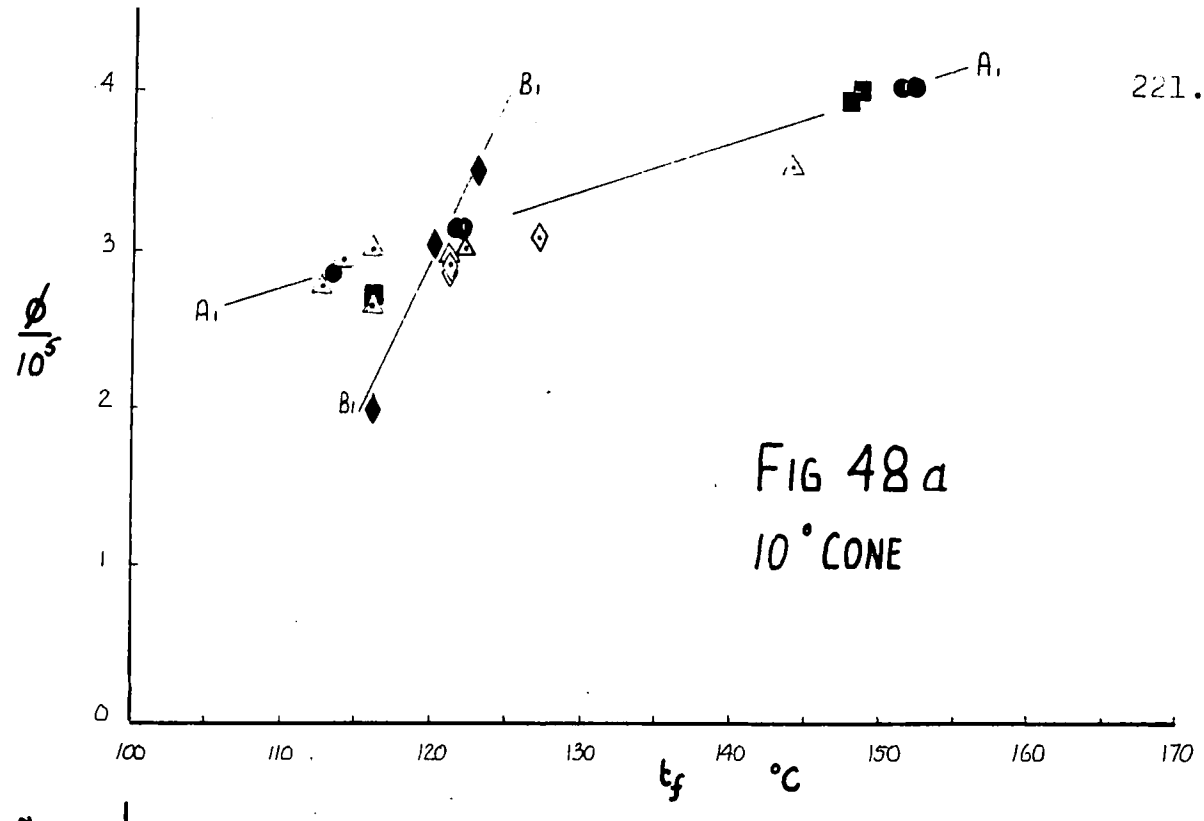

FIG 48a
10° CONE

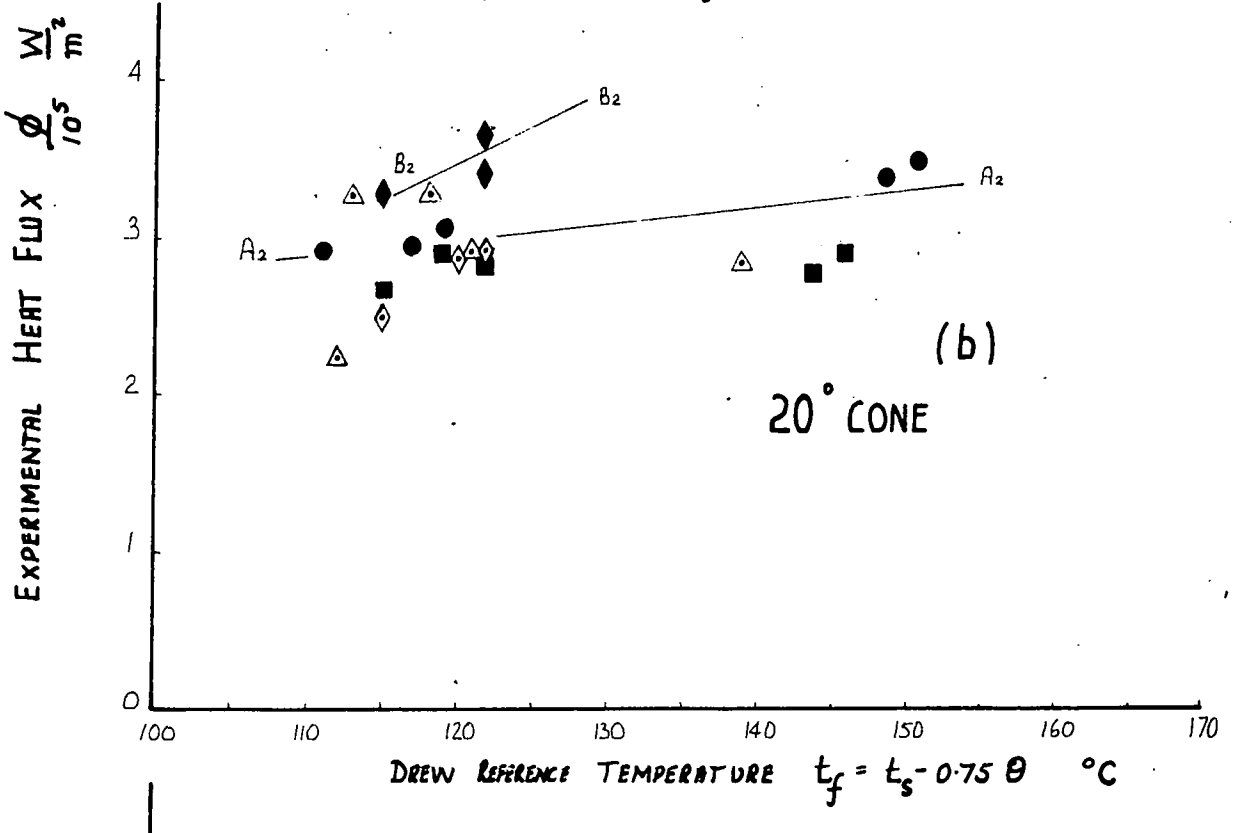

(b)
20° CONE

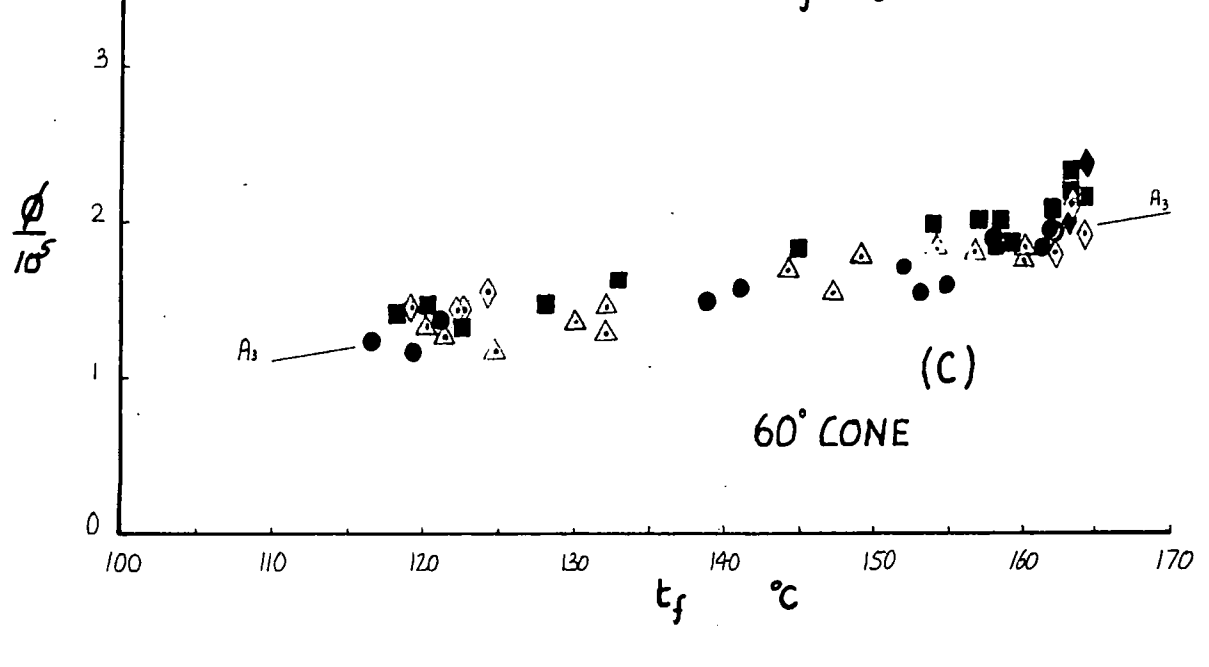

(C)
60° CONE

The heat flux at $\frac{D\omega^2}{2g} \approx 100$ lie close to line $B_1\ B_1$ which exhibits a larger increase in heat flux with t_f than does line $A_1\ A_1$. Clearly this trend cannot be confirmed without more experimental values of heat flux taken from tests at the upper end of the range of t_f and with values of $\frac{D\omega^2}{2g} > 100$.

On the 20^o cone the values of heat flux against t_f at $\frac{D\omega^2}{2g}$ less than 20 appear to lie near the line $A_2\ A_2$. At $\frac{D\omega^2}{2g} = 54$ the heat flux appears to remain unaffected by t_f over the range 115^o C to 146^o C, and to be slightly lower than the heat flux shown by line $A_2\ A_2$. The reason for this decrease in heat flux is not apparent, but it could be due to increases in either the thermal resistance of the film of condensate or of the energy transfer to the cooling water. More heat transfer results, together with direct measurements of the condensate film thickness over the range $\frac{D\omega^2}{2g}$ 20 to 54, are required to clear up this point.

At $\frac{D\omega^2}{2g}$ greater than 320, the heat flux shows a more marked improvement with t_f. As has been suggested before, this improvement could be due to the formation and detachment of drops from the ridges of the 20^o cone. More experimental points at a higher value of t_f would also be needed to confirm the trend shown by line $B_2\ B_2$.

Drainage of the film of condensate on the 60^o cone was studied by Robson (70) who found that the film drained along the surface over the ranges of both t_f and speed covered in the tests reported here. On the 60^o cone, the heat flux is shown to increase more rapidly with increases in t_f than with increases in $\frac{D\omega^2}{2g}$. At any $\frac{D\omega^2}{2g}$, the increase in heat flux with t_f shown by the slope of line $A_3\ A_3$, is not dissimilar from

FIG 49

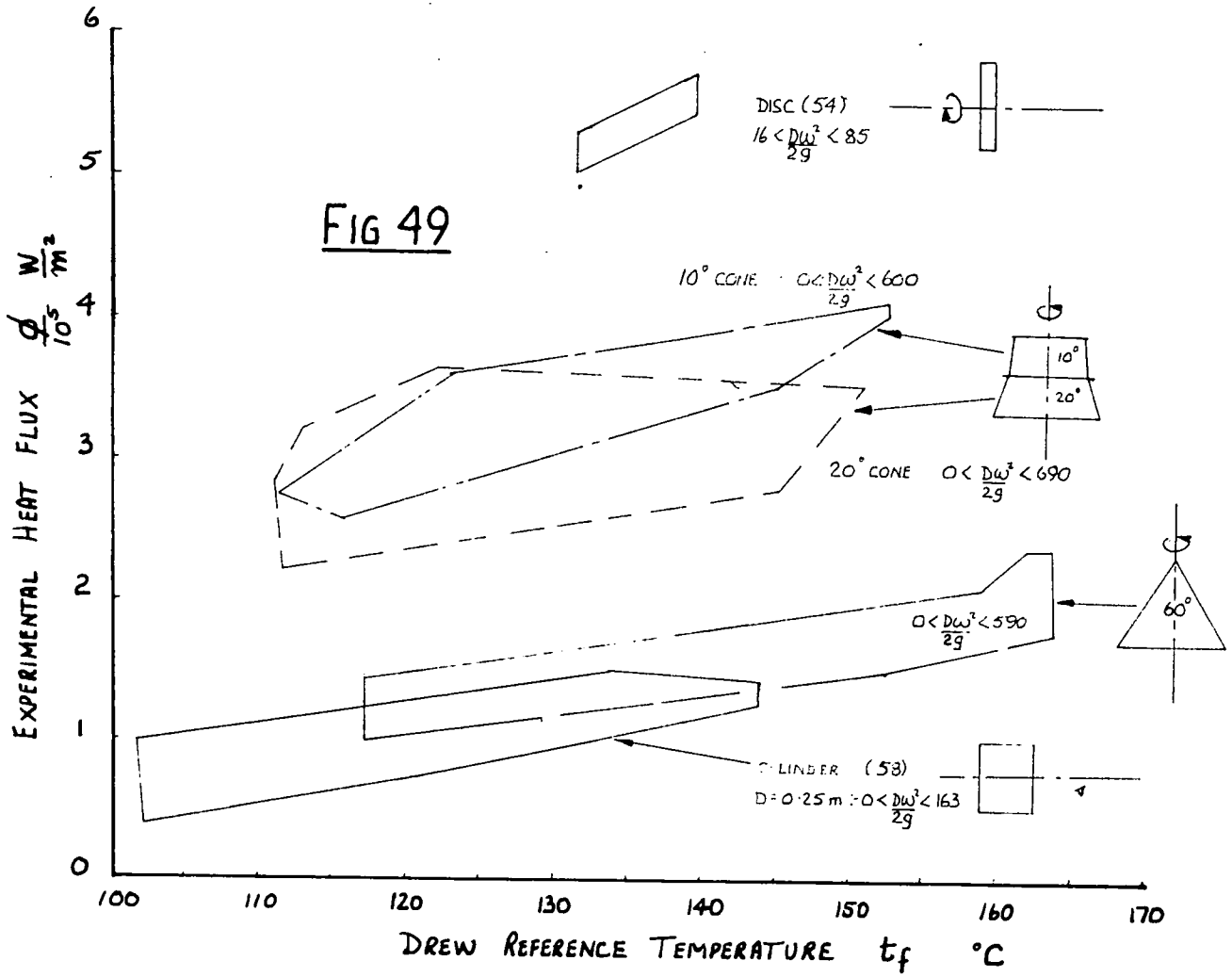
EXPERIMENTAL HEAT FLUX $\frac{q}{10^5}$ $\frac{W}{m^2}$
0
1
2
3
4
5
6
100
110
120
130
140
150
160
170
DREW REFERENCE TEMPERATURE t_f °C
DISC (54)
$16 < \frac{D\omega^2}{2g} < 85$
10° CONE $0 < \frac{D\omega^2}{2g} < 600$
10°
20°
20° CONE $0 < \frac{D\omega^3}{2g} < 690$
$0 < \frac{D\omega^2}{2g} < 590$
60°
CYLINDER (58)
D = 0·25 m $0 < \frac{D\omega^3}{2g} < 163$

the slope of lines A_1 A_1, and A_2 A_2, which are also for condensate drainage along the surface.

At this stage in the discussion of the results it is interesting to compare the experimental heat flux for the 10^o, 20^o and 60^o cones with the heat flux for condensation of steam on rotating cylinders (58) and on rotating discs (53). Such a comparison is readily made using the Drew reference temperature and is shown in fig. 49. Envelopes have been drawn around the arrays of points in figs. 48a, b, c, and around the points taken from (53) and (58). Only the envelope for each cone is shown in fig. 49.

Fig. 49 shows that the experimental heat flux for each body is only partly influenced by the behaviour of the film of condensate for the reasons given earlier in this section. The placing of the sets of heat transfer results is strongly influenced by the thermal conductivity of the body, so the effect of changes in apex angle on heat flux is masked. However, the sets of results for the disc and the cylinder have similar increases with $\frac{D\omega^2}{2g}$ as the authors results for the 10^o, 20^o and 60^o cones. Thus over the full range of apex angle, the thermal resistance of the film becomes negligible at high speeds of rotation. With regard to the calculation of the transient thermal stresses in turbine rotors during cold starting, it is only when the thermal resistance of the film is dominant in the overall heat transfer process, that the effect of changes in the speed of rotation on heat flux is important. This latter condition is satisfied in the early stages of the cold starting operation.

In an attempt to make the heat transfer results more applicable to cones in general, the heat transfer results are compared with the laminar theory for the condensation of steam on the outer surfaces of rotating cones developed in section 3. Such a comparison is made in the next section.

7.6 Heat transfer coefficient.

The ultimate aim in this section is to present to the designer a recommended equation for the experimental results. In the recommended equations the heat transfer results are characterised by the local Nusselt number $\frac{hx}{k}$, where h is the local heat transfer coefficient from the film of condensate to the outer surface of the cone. All of the heat transfer coefficients used in this section are local values and not average values.

The form of the recommended equation is based on the theoretical model of the condensation process described in section 3.1.

The theoretical model demanded that the film should be in laminar flow along the generator of the cone and that the film should be thin. The model was developed for films with $\frac{c\theta}{l}$ less than 0.1 and the experimental films of condensate complied with this requirement. However, the mode of drainage assumed for the model was rarely seen in practice except where the films were exceptionally thin. It was more common to see the film of condensate supporting waves in various patterns or to be throwing off drops, depending on the magnitude and direction of the acceleration field. In practice the films which supported

waves and ridges etc. were still thin and were thus strongly influenced by the viscosity. It is not unreasonable therefore to compare the experimental results with predictions from the simple laminar theory which also assumes that the drainage is strongly influenced by the viscosity.

As a prelude to the development of a recommended equation, the experimental heat transfer coefficients are compared with predictions of the laminar heat transfer coefficient made by the integration of equation 3.1.15.

Experimental heat transfer coefficient.

The experimental heat transfer coefficient h from the film of condensate to the outer surface of the cone may be calculated from

$$h = \frac{\phi}{\theta} \qquad \ldots\ldots 7.3$$

where ϕ is the local experimental heat flux derived from 7.1 and θ is the local film temperature difference.

It is possible to assess the errors in the experimental heat transfer coefficient from the assessment of the errors in both ϕ (section 7.5) and θ (section 7.4), although the assessment is a pessimistic one.

When the film temperature difference $\theta = 20^{\circ}$ C on the 10° and 20° cones the error in h becomes $\pm$ 22.6%, and when $\theta = 5^{\circ}$ C, the error in h is $\pm$ 67.6%. When the film temperature difference is 20° C on the 60° cone the error in h is $\pm$ 22.6% and when $\theta = 5^{\circ}$ C the error in h is $\pm$ 57.1%. The probable erros should be somewhat less than these.

Laminar heat transfer coefficient.

The equation 3.1.15, which governs the rate of growth of a laminar film, was numerically integrated for isothermal cones to show (section 3.5) the variation of the laminar heat transfer coefficient with the distance x, the apex angle and the speed of rotation. In the present section, equation 3.1.15 was used to predict the laminar film thickness and hence the laminar heat transfer coefficient corresponding to given temperature distributions along the outer surface of the experimental cones. Equation 3.1.15 was integrated using the method outlined in section 3.4, and a special input facility known as a 'function generator' was used to make the variation of the experimental θ with x available to the integration procedure.

Numerical integration of equation 3.1.15 commenced at the starting point of condensation, i.e. at x = 0. Thermocouples were not placed on the experimental cones exactly at the starting point of condensation, so the change in θ with x observed near the starting point was extrapolated for small values of x. On the 10° and 20° cones the first thermocouples were approximately 0.02 m from the starting point of condensation, while on the 60° cone the first thermocouple was at approximately x = 0.04 m. If the extrapolated film temperature was either very large, zero or negative, a small positive value of θ was used to start the calculation.

Since experimental values of θ were used in the integration of equation 3.1.15 the experimental error in θ also affected the laminar heat transfer coefficient. The effect on the laminar heat transfer coefficient of a given change in θ

was noticeably less than the effect on the experimental value. This follows from the discussion in section 3.5 where the laminar heat transfer coefficient for isothermal cones was shown to be a function of $\left[\frac{1}{\theta}\right]^{\frac{1}{4}}$; the power of $\frac{1}{4}$ tends to reduce the effect on heat transfer coefficient of changes in θ. Even with step changes in θ, the effect on the laminar heat transfer coefficient was small (see section 3.4).

Experimental and laminar heat transfer coefficients.

Typical experimental heat transfer coefficients for the 10^{o} and 20^{o} cones at speeds over the range zero to 1450 rev/min are shown in figs. 50 to 52. The experimental heat transfer coefficients were calculated from equation 7.3 using film temperature differences taken from figs. 42 and 43 for the 10^{o} and 20^{o} cones respectively, and values of heat flux taken from figs. 45 and 46 for the 10^{o} and 20^{o} cones respectively.

Fig. 50a and 50b show the experimental heat transfer coefficient for the 10^{o} and the 20^{o} cones at zero speed. The experimental heat transfer coefficient is large near the starting point of condensation and decreases with distance x. This was characteristic for films draining along the surface. Near $x = 0.2$ on the 10^{o} cone, where it joined the 20^{o} cone, the heat transfer coefficient increased. This increase was probably due to the mixing of condensate as it flowed onto the throwing ring at the intersection of the two cones. The throwing ring also acted as a fin and conducted energy from the steam to the outer surface of the cone.

Also shown in figs. 50a and 50b are the laminar heat transfer coefficients for the sets of test conditions given in

FIG 50

(a)

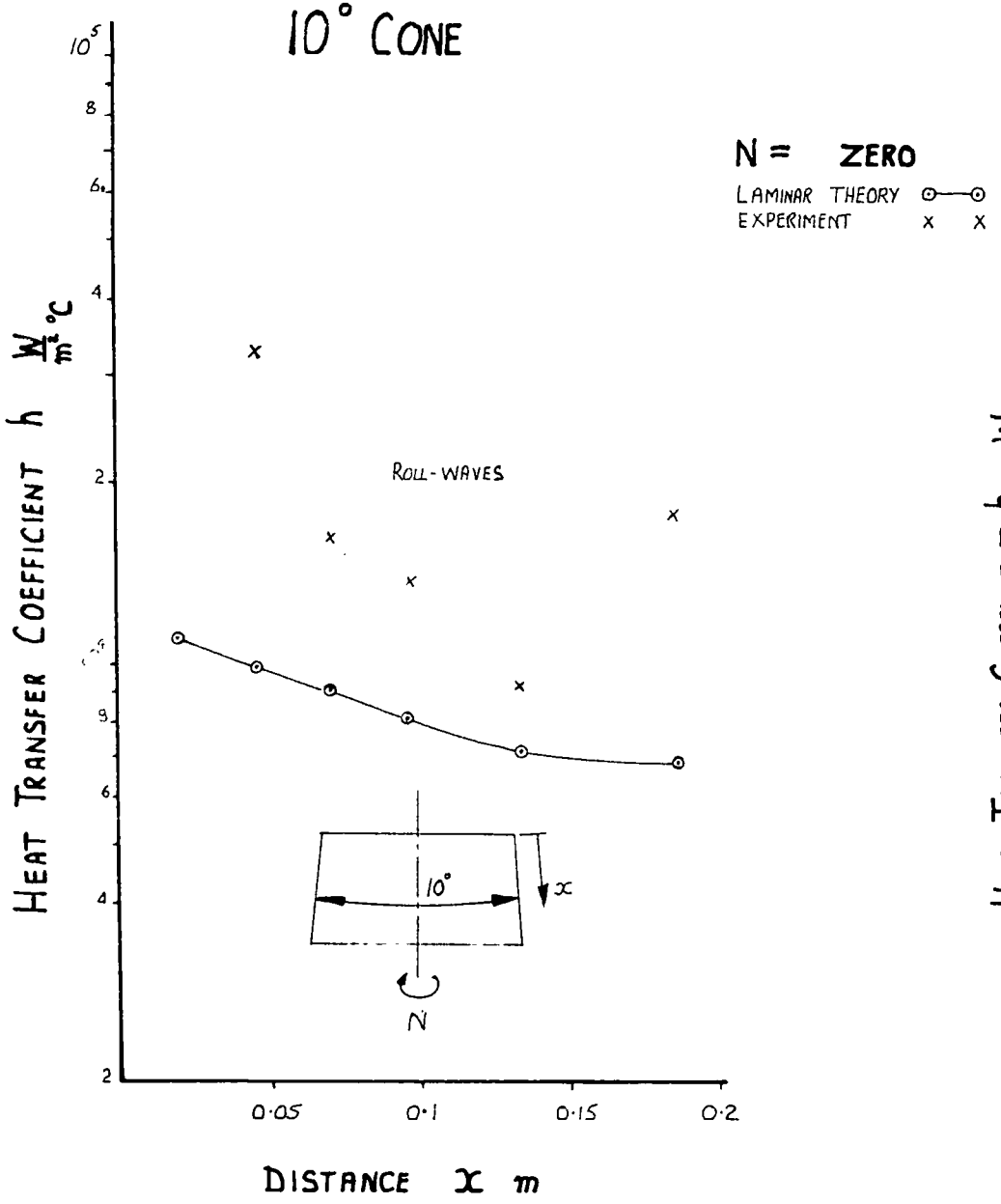
10° CONE
N = ZERO
LAMINAR THEORY
EXPERIMENT
ROLL-WAVES
HEAT TRANSFER COEFFICIENT h W/m² °C
DISTANCE x m
10°
x
N
10⁵
8
6
4
2
10⁴
0·05
0·1
0·15
0·2

(b)

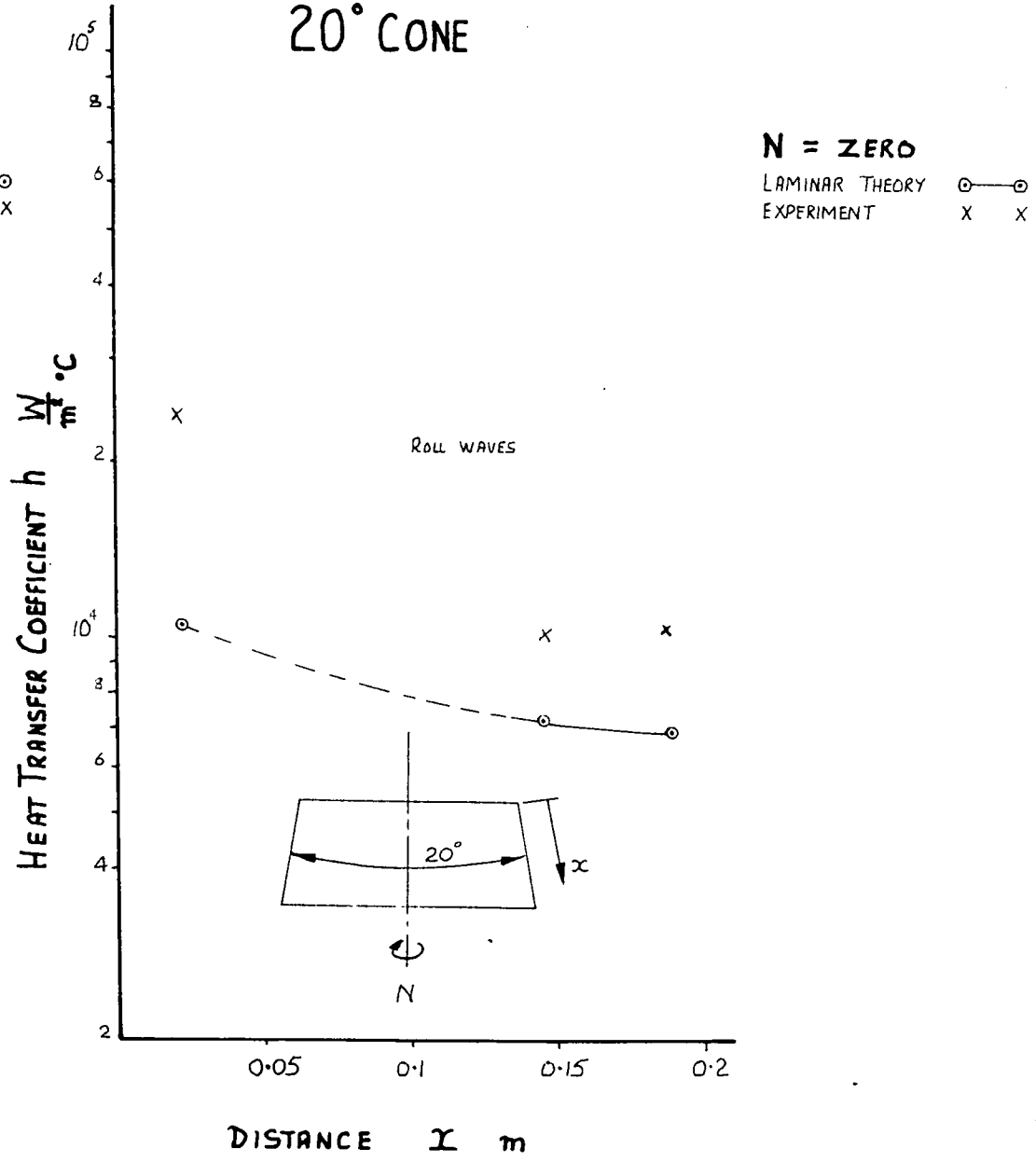
20° CONE
N = ZERO
LAMINAR THEORY
EXPERIMENT
ROLL WAVES
HEAT TRANSFER COEFFICIENT h W/m² °C
DISTANCE x m
20°
x
N
10⁵
8
6
4
2
10⁴
0·05
0·1
0·15
0·2

fig. 42 and 43. The laminar heat transfer coefficient on both cones at zero speed was lower than the experimental value, but also decreased with x. Figs. 50a and 50b show that the laminar heat transfer coefficient does not respond to changes in θ as rapidly as does the experimental value. From equation 7.3 it can be seen that if θ is increased by a factor of two at any distance x while the heat flux remains constant, the experimental heat transfer coefficient is reduced by a factor of two. As shown in section 3.4 the same change in θ near $x = 0.1$ m on a 60° cone reduces the laminar heat transfer coefficient by 6.5%; the same calculation performed for the 10° and 20° cones would produce a similar result. The effect of a given change in θ on the laminar heat transfer coefficient depends on the distance x and on the magnitude and direction of the acceleration field. Examining the behaviour of equation 3.1.24 (see section 3.1.8) shows that while the first term on the right-hand side of the equation remains dominant, rapid changes in θ produce significant changes in the laminar film thickness, and hence in the laminar heat transfer coefficient. This term tends to become insignificant as x increases and more rapidly so as the speed increases. From this discussion we can conclude that the laminar theory tends to smooth out the effects on heat transfer coefficient of rapid changes in θ with x. Such changes at zero speed produce the least effect at large distances from the starting point of condensation x, as can be seen from the curves in fig. 50a and 50b, and for the 60° cone in fig. 53. The curves in figs. 51 to 53 show that as the speed of rotation increases, the changes in θ have proportionately less effect on the laminar heat transfer

FIG 51

(a)

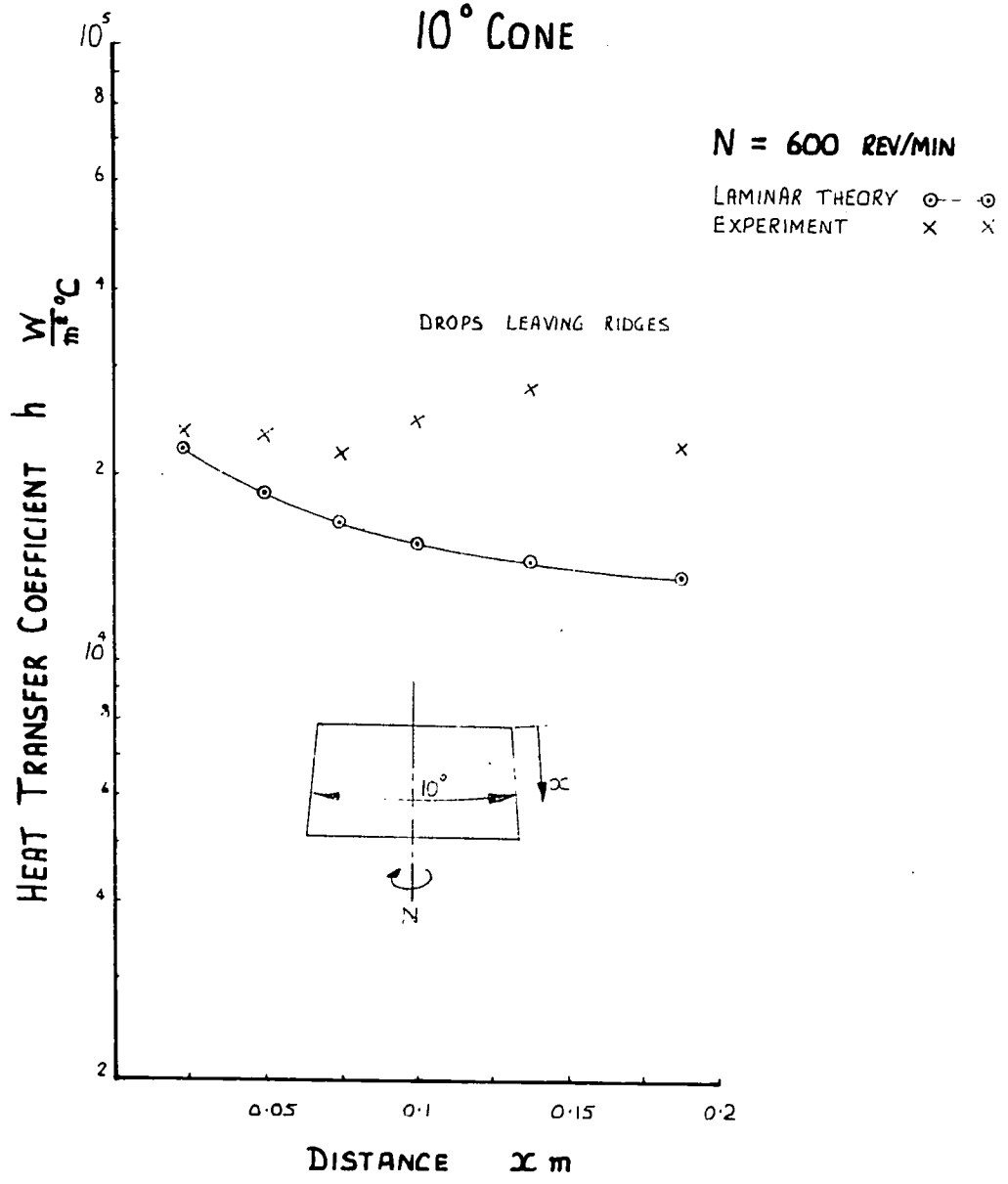
10° CONE
N = 600 REV/MIN
LAMINAR THEORY
EXPERIMENT
DROPS LEAVING RIDGES
HEAT TRANSFER COEFFICIENT h W/m²°C
10⁵
8
6
4
10⁴
8
6
4
2
10°
x
N
0·05
0·1
0·15
0·2
DISTANCE x m

(b)

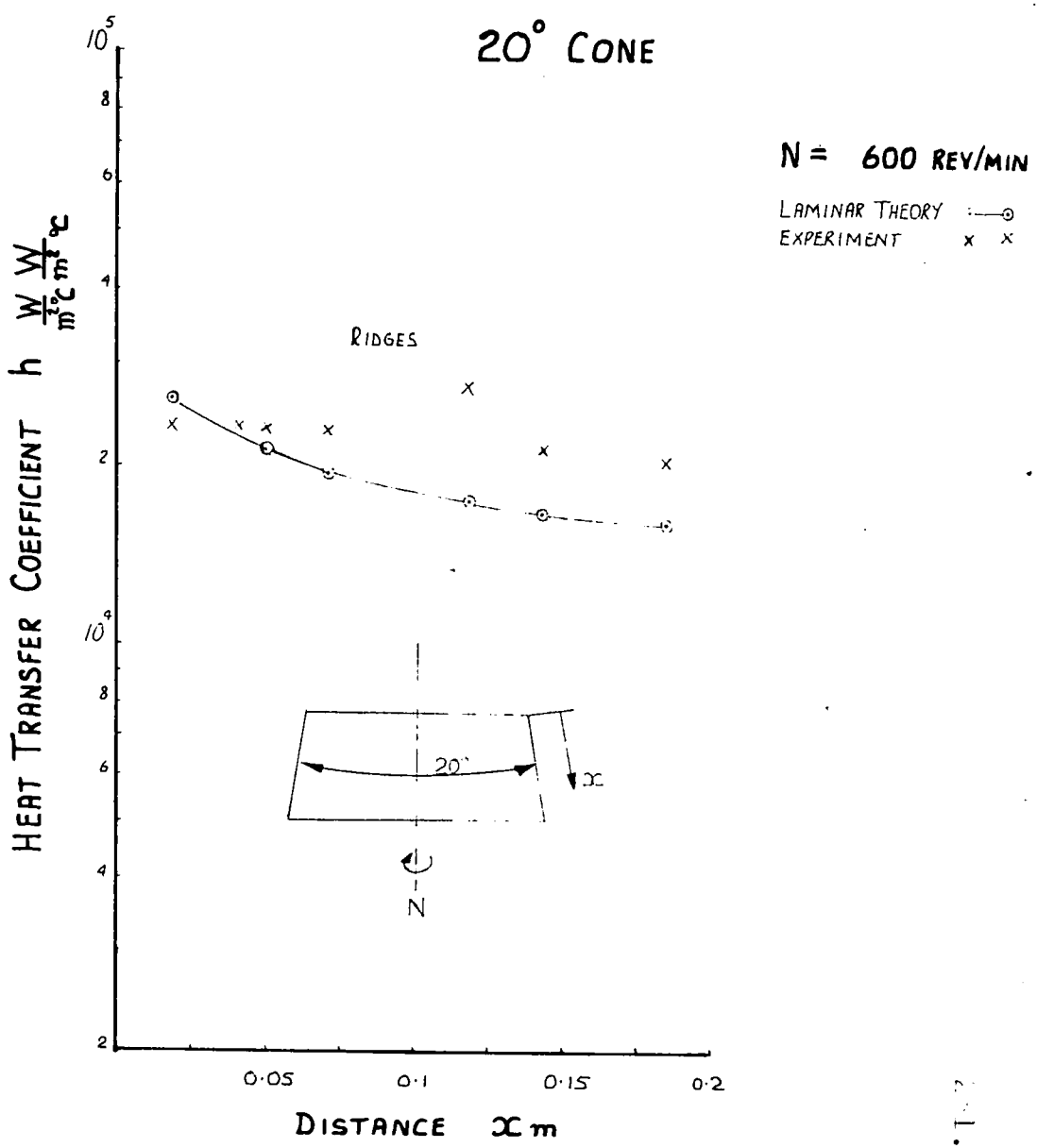
20° CONE
N = 600 REV/MIN
LAMINAR THEORY
EXPERIMENT
RIDGES
HEAT TRANSFER COEFFICIENT h W/m²°C
10⁵
8
6
4
10⁴
8
6
4
2
20°
x
N
0·05
0·1
0·15
0·2
DISTANCE x m

coefficient at all values of x.

Figs. 51a and 51b for the 10^{o} and 20^{o} cones respectively, show that at 600 rev/min, both the experimental and the laminar heat transfer coefficients generally increased beyond the corresponding values at zero speed.

At 600 rev/min the experimental and the laminar heat transfer coefficients on the 10^{o} cone are in good agreement up to the point $x = 0.07$ m, and both decrease with x. This decrease in the experimental value was expected since the film at this speed was observed to drain along the surface as far as $x = 0.07$ m. Downstream of this position, drainage was partly along the surface and partly by the detachment of drops. The region where drops were thrown from the film on the 10^{o} cone coincides with the region on fig. 51a, where the experimental heat transfer coefficient shows a marked increase to approximately 2 times the laminar value.

At 600 rev/min on the 20^{o} cone the condensate was observed to drain along the surface and the experimental heat transfer coefficient is between 0.8 and 1.6 times the laminar value.

At 1450 rev/min fig. 52a shows that the experimental heat transfer coefficient is generally above the values at 400 rev/min. At 1450 rev/min a substantial component of the centrifugal acceleration acts along the surface to improve laminar drainage in this direction. This improvement appears to make the experimental heat transfer coefficient follow the decrease with x shown by the laminar value; with the experimental value between 1.3 and 1.7 times the laminar value.

FIG 52

(a)

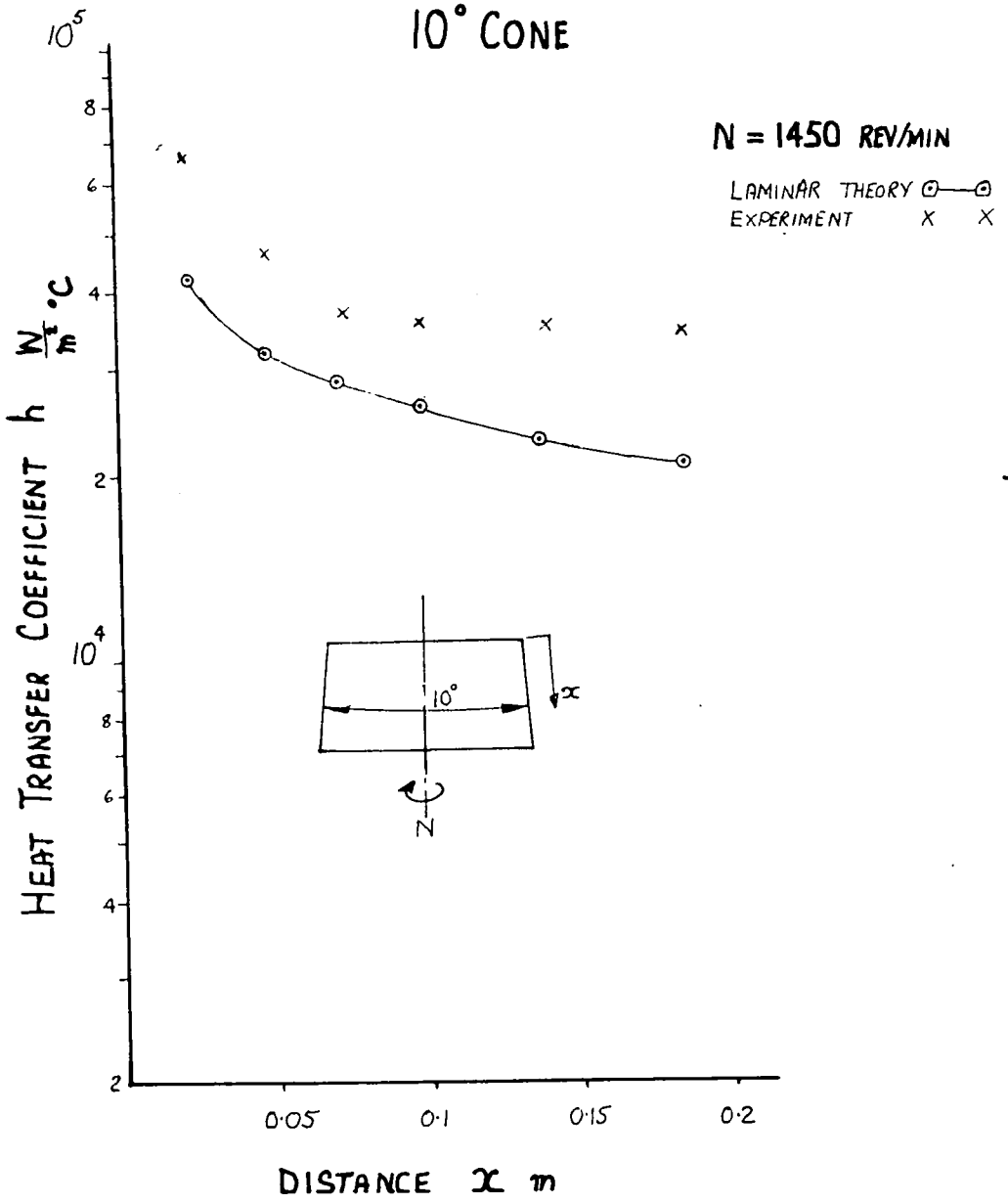
10° CONE
N = 1450 REV/MIN
LAMINAR THEORY
EXPERIMENT
HEAT TRANSFER COEFFICIENT h W/m² °C
DISTANCE x m
10°
x
N
10⁵
10⁴
0·05
0·1
0·15
0·2

(b)

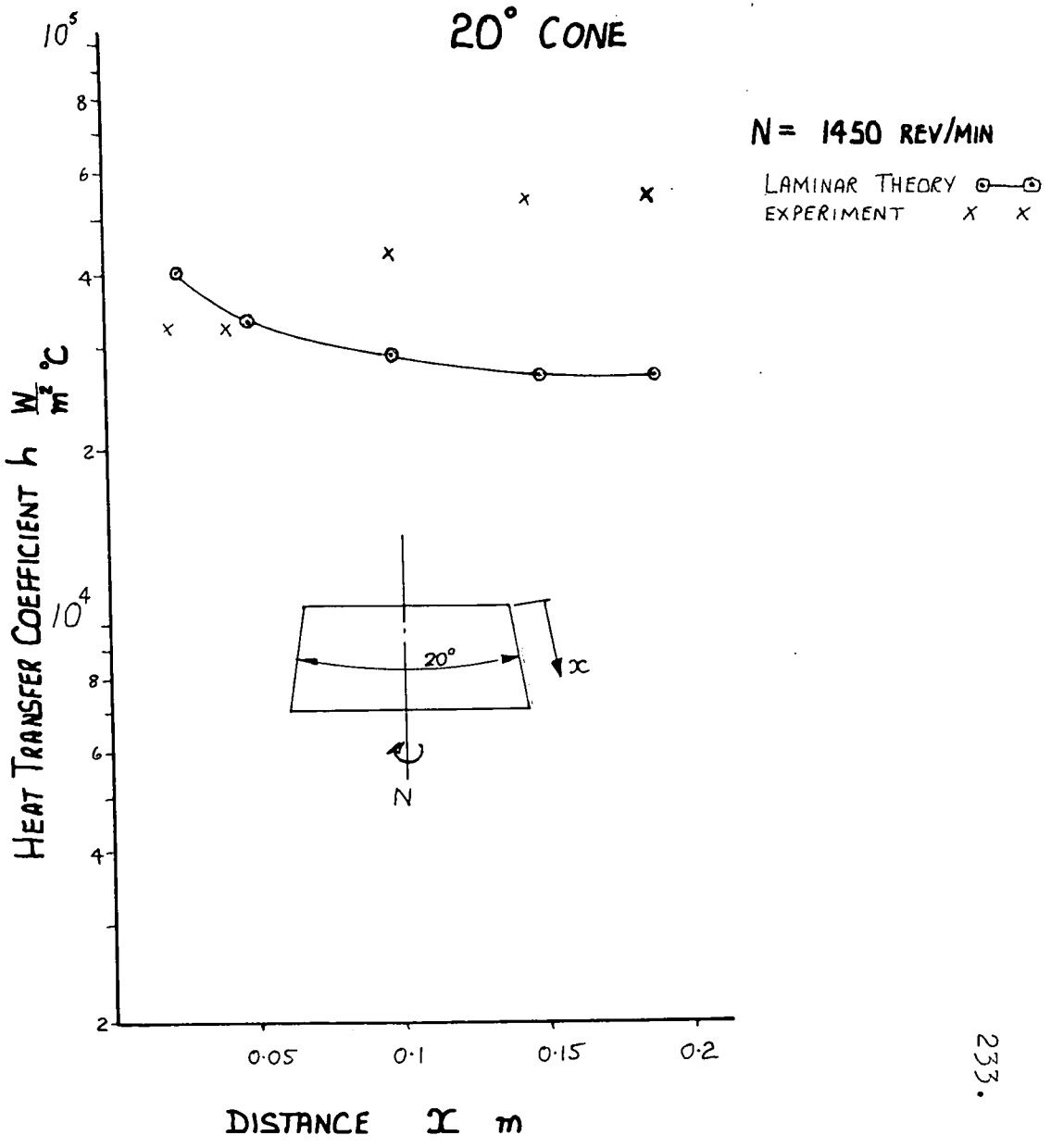
20° CONE
N = 1450 REV/MIN
LAMINAR THEORY
EXPERIMENT
HEAT TRANSFER COEFFICIENT h W/m² °C
DISTANCE x m
20°
x
N
10⁵
10⁴
0·05
0·1
0·15
0·2

At 1450 rev/min on the 20^{o} cone fig. 52b shows that the experimental heat transfer coefficient approaches two times the laminar value downstream of x = 0.05 m. This increase strongly suggests that the film drainage was being improved by the detachment of drops although there is no photographic evidence to support this claim.

Fig. 53 shows for the 60^{o} cone a comparison between the experimental heat transfer coefficient and the corresponding laminar values at speeds between zero and 1248 rev/min. These heat transfer coefficients were calculated from the temperature distributions given in fig. 44.

At zero speed both the experimental and the laminar heat transfer coefficients show the characteristic decrease with x. The change in θ from 4^{o} C to 12^{o} C between x = 0.09 m and x = 0.1 m causes the experimental heat transfer coefficient to drop sharply, but the laminar value does not exhibit the same response for the reasons given during the discussion of the results for the 10^{o} cone.

In the laminar theory the centrifugal acceleration dominates drainage over large portions of the 60^{o} cone at speeds above 300 rev/min, consequently the laminar heat transfer coefficient becomes uniform with x and is therefore relatively unaffected by changes in θ with x. The changes in θ with x continue to cause local variations in the experimental heat transfer coefficient which generally lies between 0.8 and 2.5 times the laminar value.

A comparison between the experimental and the laminar heat transfer coefficient was made for all of the test results.

FIG 53

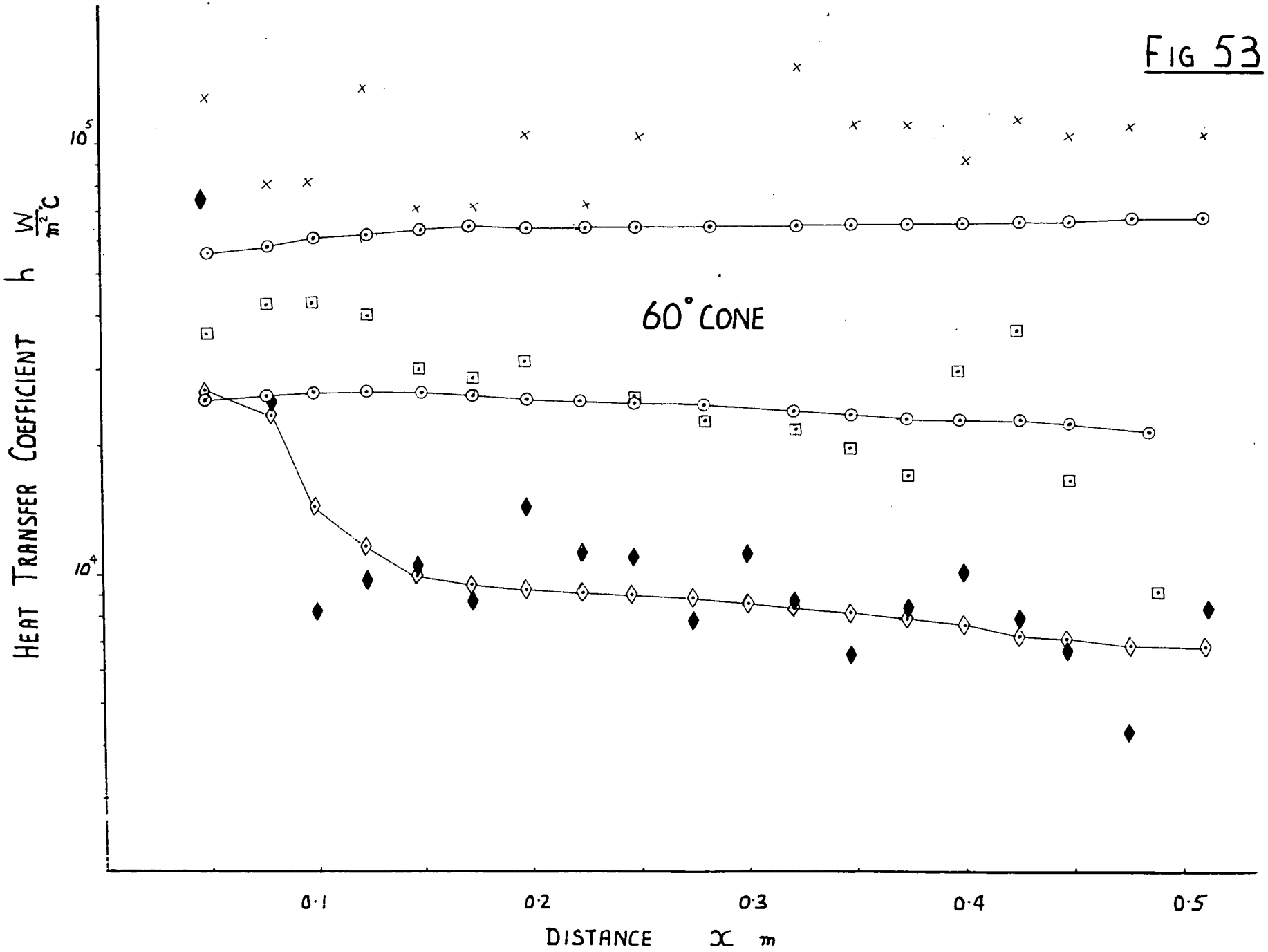
60° CONE
HEAT TRANSFER COEFFICIENT h W/m²°C
10⁵
10⁴
0·1
0·2
0·3
0·4
0·5
DISTANCE x m
N = 1248 REV/MIN
LAMINAR THEORY
EXPERIMENT
N = 624 REV/MIN
LAMINAR THEORY
EXPERIMENT
N = ZERO
LAMINAR THEORY
EXPERIMENT

The results are too numerous to be shown in the manner of Figs. 50 to 53 so they are presented in a modified way. Recommended equations for the 10^{o}, 20^{o} and 60^{o} cones.

The designer is often forced to assume the existence of an isothermal temperature distribution when in fact the temperature distribution may be non-isothermal. The recommended equations help the designer to predict the experimental heat transfer coefficient under these circumstances.

In appendix A two significant terms were derived from equation 3.1.15 and these were:-

(i) $Nu\ (3H)^{\frac{1}{4}} \left(\frac{\omega \mathrm{Sin}\alpha}{g\ \mathrm{Cos}\alpha}\right)^{3/2}$

where $H = \dfrac{c\theta\ \nu^2}{Pr\ (1 + \frac{3}{8}\ c\theta)}$

and (ii) $\dfrac{x\omega^2\ \mathrm{Sin}^2\alpha}{g\ \mathrm{Cos}\ \alpha}$

The above terms were shown to place the laminar heat transfer results for a given isothermal cone on a unique curve. As shown in appendix A the position of the curve depends on the position of the starting point of condensation on the cone. Term (ii) was also used in sections 3.4 to 3.6 to show the relative effects of centrifugal and gravitational accelerations on the theoretical heat transfer coefficients.

Terms (i) and (ii) can also be used to display the experimental heat transfer results at all values of x if the experimental Nusselt Number = $\dfrac{h_{exp}\ x}{k}$ is substituted for the laminar value, and the local film temperature difference θ is used in the value of H.

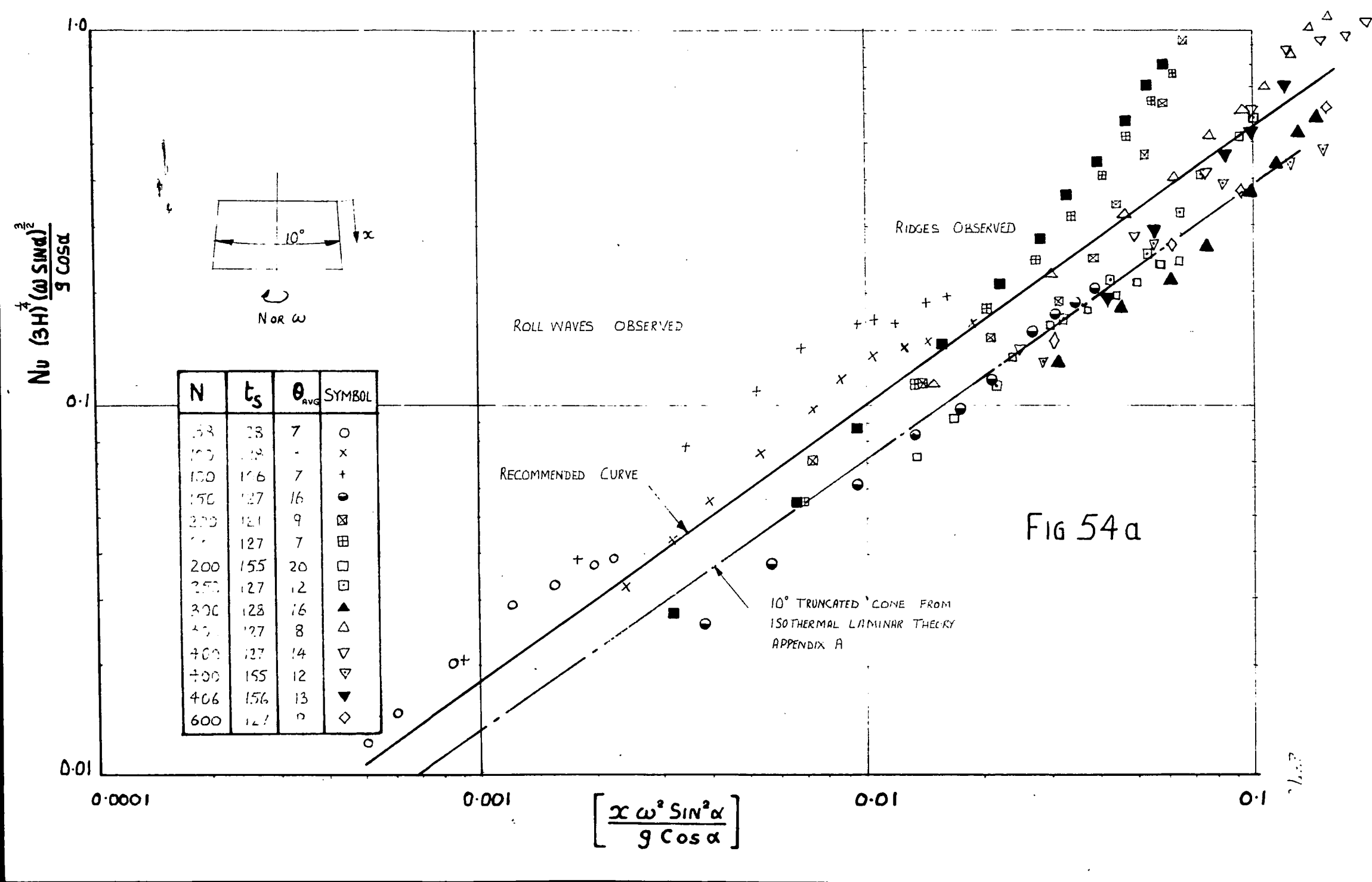
1·0
0·1
0·01
0·0001
0·001
0·01
0·1
$Nu\,(3H)^{\frac{1}{4}}\frac{(\omega \sin\alpha)^{\frac{3}{2}}}{g\cos\alpha}$
$\left[\frac{x\,\omega^2 \sin^2\alpha}{g\cos\alpha}\right]$
10°
x
N OR ω
ROLL WAVES OBSERVED
RIDGES OBSERVED
RECOMMENDED CURVE
10° TRUNCATED CONE FROM ISOTHERMAL LAMINAR THEORY APPENDIX A
FIG 54a
N | t_s | θ_{avg} | SYMBOL
.53 | 28 | 7 | ○
100 | 12 | - | ×
100 | 116 | 7 | +
150 | 127 | 16 | ◒
200 | 121 | 9 | ⊠
- | 127 | 7 | ⊞
200 | 155 | 20 | □
250 | 127 | 12 | ⊡
300 | 128 | 16 | ▲
- | 127 | 8 | △
400 | 127 | 14 | ▽
400 | 155 | 12 | ▽
406 | 156 | 13 | ▼
600 | 127 | 0 | ◇

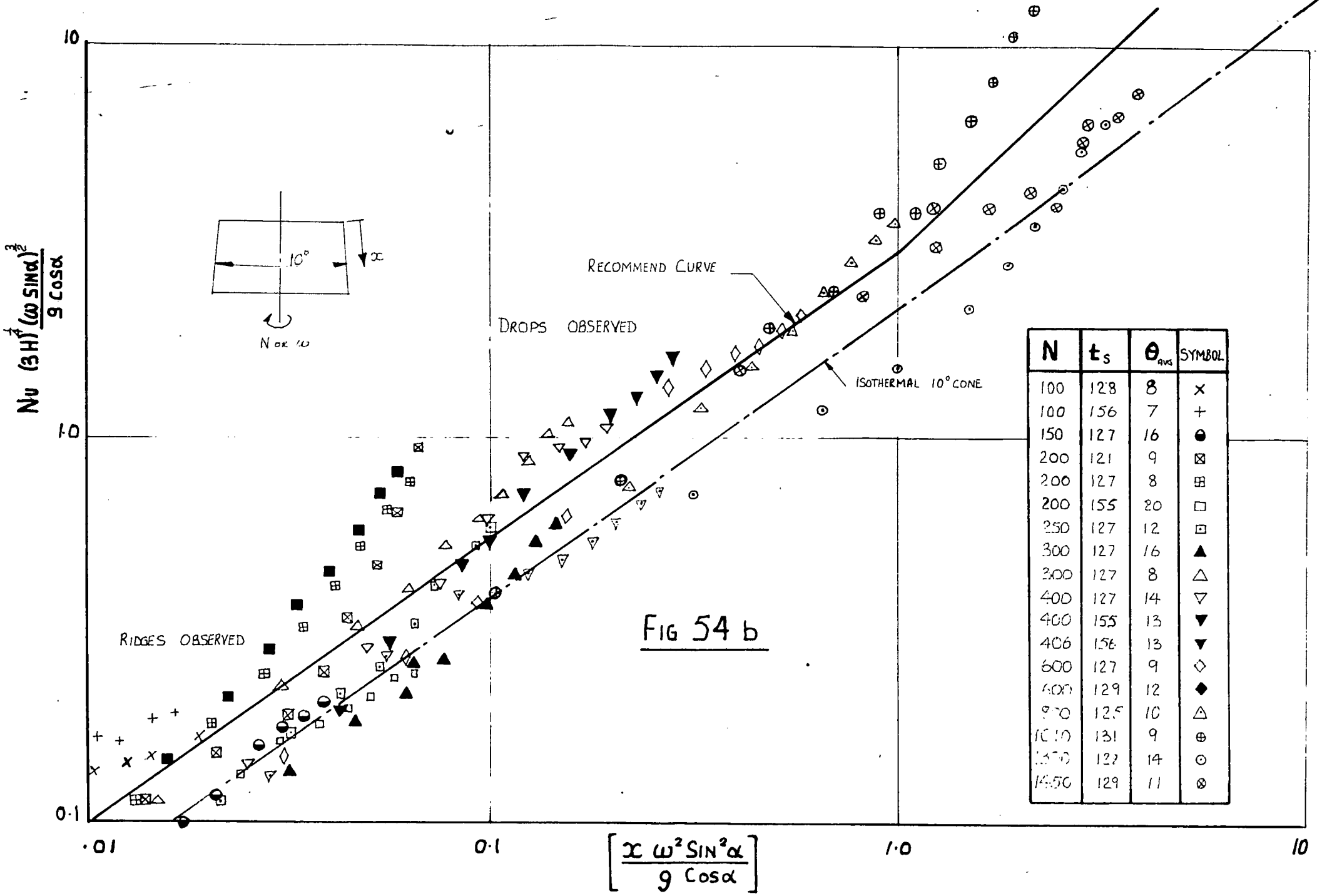
10
1·0
0·1
·01
0·1
1·0
10
$Nu\,(3H)^{\frac{1}{4}}\frac{(\omega \sin\alpha)^{\frac{3}{2}}}{9\cos\alpha}$
$\left[\frac{x\,\omega^2 \sin^2\alpha}{9\cos\alpha}\right]$
10°
x
N or ω
RECOMMEND CURVE
DROPS OBSERVED
ISOTHERMAL 10° CONE
RIDGES OBSERVED
N | t_s | θ_{avg} | SYMBOL
100 | 128 | 8 | ×
100 | 156 | 7 | +
150 | 127 | 16 | ●
200 | 121 | 9 | ⊠
200 | 127 | 8 | ⊞
200 | 155 | 20 | □
250 | 127 | 12 | ⊡
300 | 127 | 16 | ▲
300 | 127 | 8 | △
400 | 127 | 14 | ▽
400 | 155 | 13 | ▼
406 | 156 | 13 | ▼
600 | 127 | 9 | ◇
600 | 129 | 12 | ◆
900 | 125 | 10 | △
1010 | 131 | 9 | ⊕
1350 | 127 | 14 | ⊙
1450 | 129 | 11 | ⊗

FIG 54 b

The recommended equations for each cone are derived from curves drawn through the experimental points and have the general form

$$\underset{exp}{Nu}\,(3H)^{\frac{1}{4}}\left(\frac{\omega \operatorname{Sin}\alpha}{g \operatorname{Cos}\alpha}\right)^{3/2} = A_1\left[\frac{x\omega^2 \operatorname{Sin}^2\alpha}{g \operatorname{Cos}\alpha}\right]^{A_2}$$

where $$H = \frac{c\theta\,\nu^2}{Pr\,(1 + \frac{3}{8}c\theta)}$$

The fluid properties of the condensate c, k, ν were evaluated at the Drew reference temperature $t_f = t_s - 0.75\,\theta$ and the latent enthalpy l was evaluated at the steam temperature t_s.

Fig. 54a and 54b show the experimental heat transfer results for the 10^o cone plotted in terms of group (i) against group (ii).

The recommended equations for the 10^o cone are:-

For $0.001 < \frac{x\omega^2 \operatorname{Sin}^2\alpha}{g \operatorname{Cos}\alpha} < 1.0$

$$\underset{exp}{Nu}\,(3H)^{\frac{1}{4}}\left(\frac{\omega \operatorname{Sin}\alpha}{g \operatorname{Cos}\alpha}\right)^{3/2} = 3.36\left[\frac{x\omega^2 \operatorname{Sin}^2\alpha}{g \operatorname{Cos}\alpha}\right]^{0.75}$$

For $1 < \frac{x\omega^2 \operatorname{Sin}^2\alpha}{g \operatorname{Cos}\alpha} < 5$

$$\underset{exp}{Nu}\,(3H)^{\frac{1}{4}}\left(\frac{\omega \operatorname{Sin}\alpha}{g \operatorname{Cos}\alpha}\right)^{3/2} = 2.9\left[\frac{x\omega^2 \operatorname{Sin}^2\alpha}{g \operatorname{Cos}\alpha}\right]$$

There is a considerable scatter of experimental points which are for variable θ, but they lie close to the recommended curve. The extreme points deviate from the recommended curve by a factor of approximately 2; but the majority of points are in better agreement with the recommended curve.

Also shown in figs. 54a and 54b, is the unique curve for isothermal laminar heat transfer results on the 10^o cone. The curve passing through the experimental points is between 1.4 and 1.9 times the laminar value for an isothermal 10^o cone.

FIG 55a

N	t_s	θ	SYMBOL
38	128	12	○
100	128	14	×
100	156	9	+
150	127	20	◒
200	121	12	⊠
200	127	9	⊞
200	155	20	□
250	127	12	⊡
300	128	12	▲
300	127	7	△

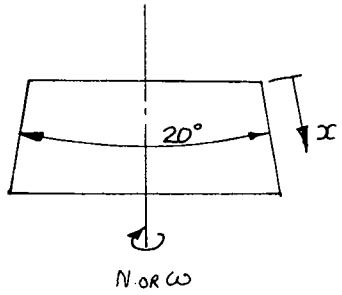

$Nu\ (3H)^{\frac{1}{4}} \left(\frac{\omega \sin\alpha}{g \cos\alpha}\right)^{\frac{3}{2}}$

1·0

0·1

0·01

0·0001

0·001

0·01

0·1

ROLL WAVES

RECOMMENDED CURVE AND CURVE FROM LAMINAR THEORY FOR ISOTHERMAL 20° CONE

$\left[\frac{x\,\omega^2 \sin^2\alpha}{g \cos\alpha}\right]$

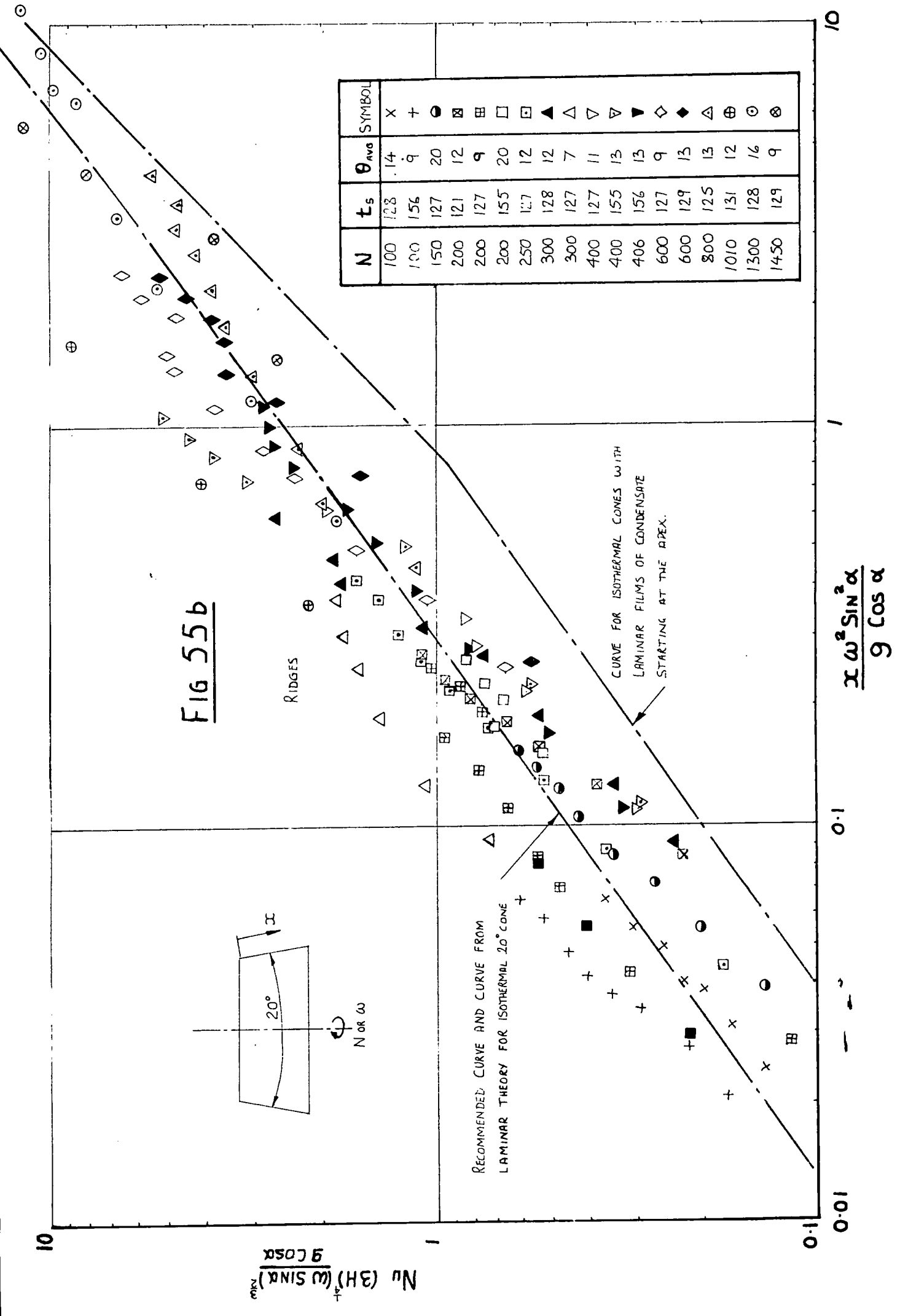
FIG 55b
RIDGES
CURVE FOR ISOTHERMAL CONES WITH LAMINAR FILMS OF CONDENSATE STARTING AT THE APEX.
RECOMMENDED CURVE AND CURVE FROM LAMINAR THEORY FOR ISOTHERMAL 20° CONE
20°
x
N OR ω
N
SYMBOL
θ avg
t s
10
1
0·1
0·01
0·1
1
10

Figs 55a and 55b show the experimental results for the 20^{o} cone and the recommended equation becomes:-

For $0.001 < \frac{x\omega^2 \sin^2\alpha}{g \cos\alpha} < 10$

$$Nu_{exp} (3H)^{\frac{1}{4}} \left(\frac{\omega \sin\alpha}{g \cos\alpha}\right)^{3/2} = 2.6 \left[\frac{x\omega^2 \sin^2\alpha}{g \cos\alpha}\right]^{0.75}$$

The extreme experimental points deviate from the recommended curve by a factor close on 2, but the majority of points are in better agreement. The above curve lies extremely close to the unique curve predicted for the 20^{o} cone from the isothermal laminar theory.

Figs. 56a and 56b show the experimental points for the 60^{o} cone. The recommended equations are:-

For $0.1 < \frac{x\omega^2 \sin^2\alpha}{g \cos\alpha} < 1.0$

$$Nu_{exp} (3H)^{\frac{1}{4}} \left(\frac{\omega \sin\alpha}{g \cos\alpha}\right)^{3/2} = 2.02 \left[\frac{x\omega^2 \sin^2\alpha}{g \cos\alpha}\right]^{0.75}$$

For $1 < \frac{x\omega^2 \sin^2\alpha}{g \cos\alpha} < 250$

$$Nu_{exp} (3H)^{\frac{1}{4}} \left(\frac{\omega \sin\alpha}{g \cos\alpha}\right)^{3/2} = 2.25 \left[\frac{x\omega^2 \sin^2\alpha}{g \cos\alpha}\right]^{0.90}$$

Also shown is the unique curve for the 60^{o} cone as derived from the isothermal laminar theory. Providing the film of condensate starts at the apex of the cone this curve can be used for cones with any apex angle. The recommended curve for the experimental results from the 60^{o} cone lies between 1.2 and 1.8 times the laminar value, with better agreement at high speeds of rotation.

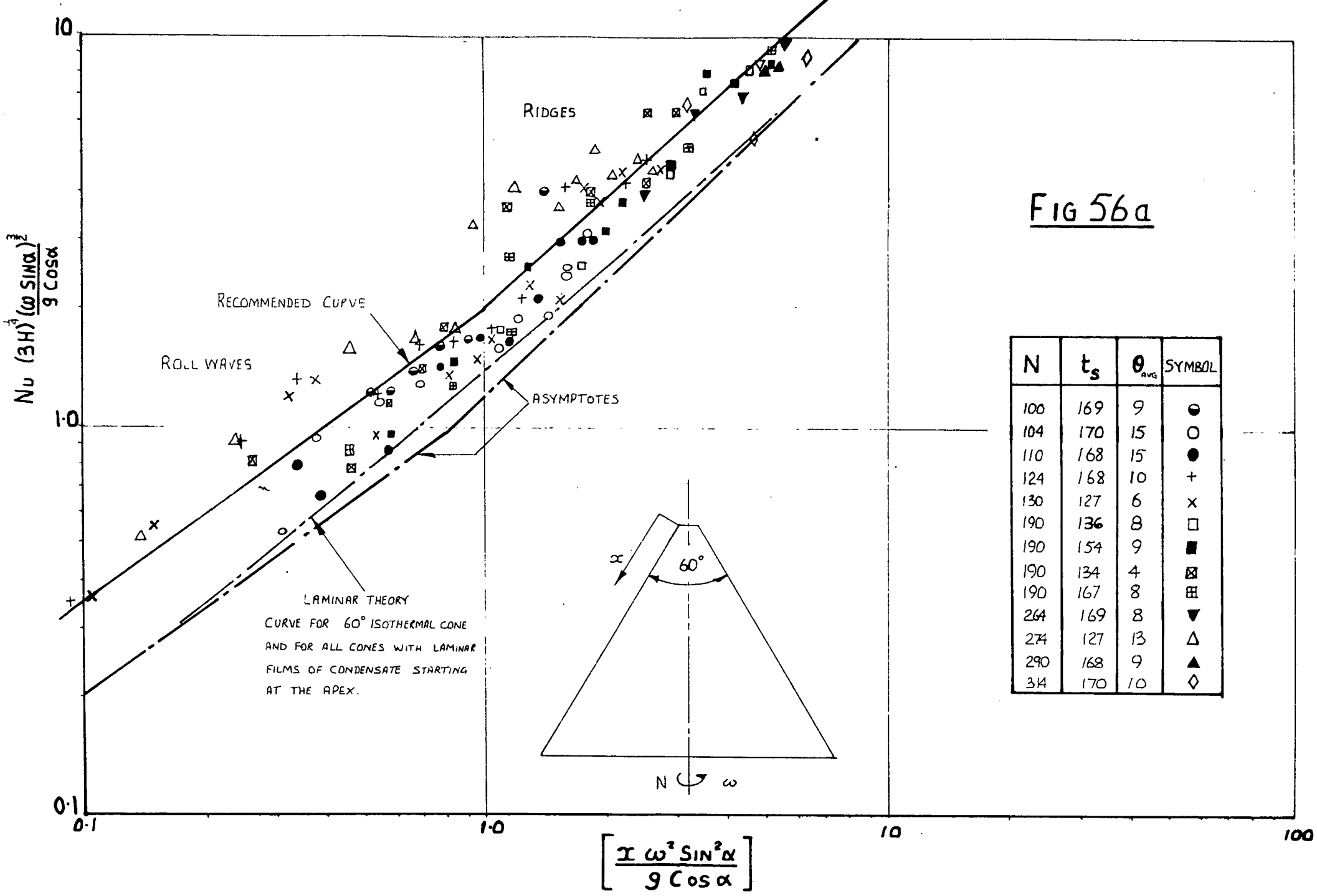

FIG 56a

N	t_s	θ_{avg}	SYMBOL
100	169	9	◒
104	170	15	○
110	168	15	●
124	168	10	+
130	127	6	×
190	136	8	□
190	154	9	■
190	134	4	⊠
190	167	8	⊞
264	169	8	▼
274	127	13	△
290	168	9	▲
314	170	10	◇

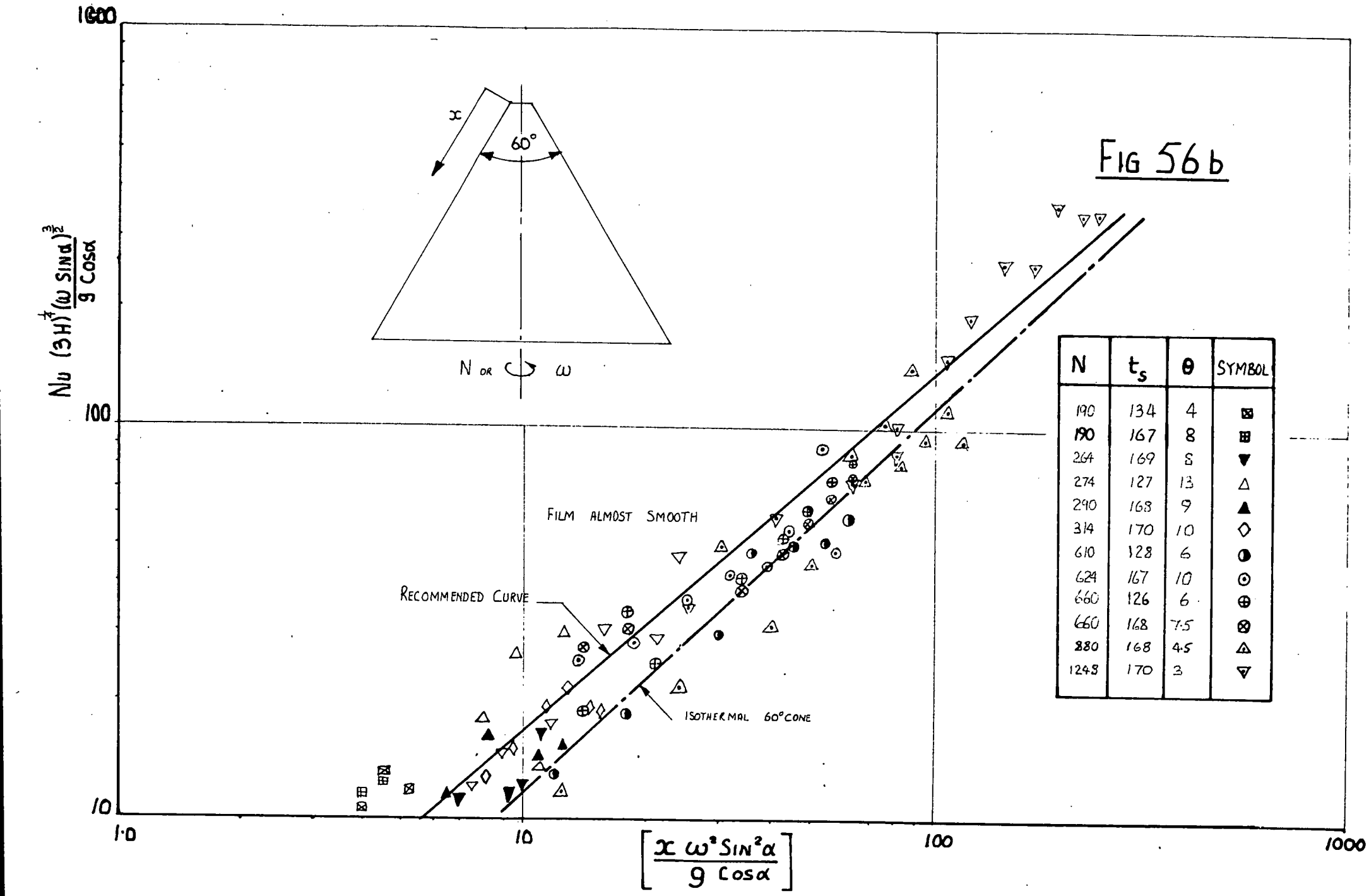
FIG 56b
$Nu\,(3H)^{\frac{1}{4}}\left(\frac{\omega \sin\alpha}{g\cos\alpha}\right)^{\frac{3}{2}}$
$\left[\frac{x\,\omega^2 \sin^2\alpha}{g\cos\alpha}\right]$
1000
100
10
1·0
10
100
1000
x
60°
N OR ω
FILM ALMOST SMOOTH
RECOMMENDED CURVE
ISOTHERMAL 60° CONE
N | t_s | θ | SYMBOL
190 | 134 | 4
190 | 167 | 8
264 | 169 | 8
274 | 127 | 13
290 | 168 | 9
314 | 170 | 10
610 | 128 | 6
624 | 167 | 10
660 | 126 | 6
660 | 168 | 7·5
880 | 168 | 4·5
1248 | 170 | 3

The effect of changes in the wave pattern or of the mode of film drainage on the experimental heat transfer coefficient is not clearly seen in figs. 54 to 56. These are two reasons for this:-

(i) the onset of a wave regime or of a change in the mode of drainage is dependent on the condensation rate, and the experimental results in figs. 54 to 56 cover a range of condensation rates at any value of $\frac{x\omega^2 \sin^2\alpha}{g \cos\alpha}$,

and (ii) reductions in the mean film thickness produced by changes in the wave pattern etc, generally cause reductions in the film temperature θ and this introduces larger experimental errors into the calculation of $h_{exp.}$

Fig. 57 shows on a smaller scale the envelopes enclosing the experimental points for the 10°, 20° and 60° cones, and the curves derived from laminar theory applied to isothermal cones. The general agreement between the experimental results from each cone can be seen, as can the relatively good agreement between the experimental results and the laminar theory.

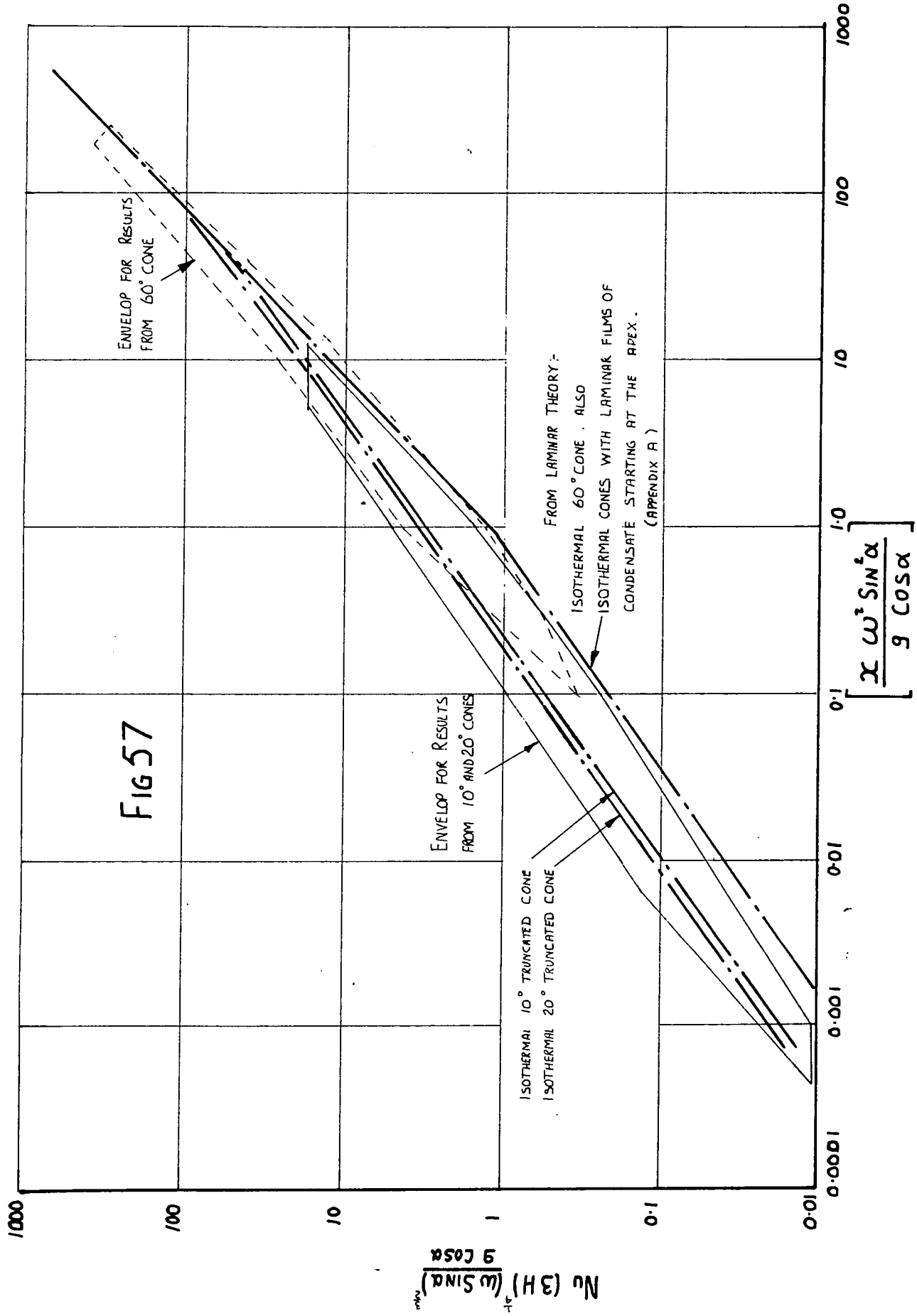
ENVELOP FOR RESULTS FROM 60° CONE
ENVELOP FOR RESULTS FROM 10° AND 20° CONES
FROM LAMINAR THEORY:-
ISOTHERMAL 60° CONE. ALSO
ISOTHERMAL CONES WITH LAMINAR FILMS OF CONDENSATE STARTING AT THE APEX. (APPENDIX A)
ISOTHERMAL 10° TRUNCATED CONE
ISOTHERMAL 20° TRUNCATED CONE
1000
100
10
1
0·1
0·01
0·0001
0·001
0·01
0·1
1·0
10
100
1000
$\left[\frac{x\,\omega^2 \sin^2\alpha}{g\cos\alpha}\right]$
$Nu\,(3H)^{\frac{1}{4}}\left(\frac{\omega \sin\alpha}{g\cos\alpha}\right)^{\frac{1}{2}}$

FIG 57

8.0 CONCLUSIONS

8.0 Conclusions.

The conclusions are a summary of the main points raised during discussions in various sections in the thesis.

The theory developed for the condensation of steam in thin laminar films on the outer surface of rotating cones assumed that the film drained along the generator of the cone under the combined influence of centrifugal and gravitational accelerations resolved along the surface. Analytical solutions of equation 3.1.15, which governed the rate of growth of the laminar film, for certain limiting values of speed of rotation and of apex angle, showed that the theory linked previous theories where drainage was by either centrifugal or gravitational acceleration alone.

A numerical method for integrating equation (3.1.15) was used to show the combined effect of centrifugal and gravitational accelerations on the laminar heat transfer coefficient on cones with various apex angles.

While the term $\left[\frac{x\omega^2 \operatorname{Sin}^2\alpha}{g \operatorname{Cos}\alpha}\right]^{\frac{1}{4}}$ was less than 0.5, gravitational acceleration dominated drainage and the laminar heat transfer coefficient decreased with the distance from the starting point of condensation. The reduction in gravitational acceleration resolved along the surface caused by increasing the apex angle from zero, resulted in a reduction in the laminar heat transfer coefficient at a given distance x. The laminar heat transfer coefficient was shown to be lower than at a given distance x, if the starting point of condensation, at which $x = 0$, was not at the apex of the cone.

When $\left[\frac{x\omega^2 \text{ Sin}^2\alpha}{g \text{ Cos}\alpha}\right]^{\frac{1}{4}}$ was greater than 2.0, the film drainage became dominated by centrifugal acceleration which made the laminar heat transfer coefficient become uniform with distance x. Increasing the apex angle at a given speed of rotation makes the point at which the centrifugal acceleration becomes dominant, move towards the apex of the cone.

The term $\left[\frac{x\omega^2 \text{ Sin}^2\alpha}{g \text{ Cos}\alpha}\right]^{\frac{1}{4}}$ also decided whether the ratio $\left.\frac{\text{h cone}}{\text{h disc}}\right|_{\text{lam}}$ was dominated by either gravitational or centrifugal acceleration.

In the former state, the ratio $\left.\frac{\text{h cone}}{\text{h disc}}\right|_{\text{lam}}$ was asymptotic to $0.976\left[\frac{g \text{ Cos}\alpha}{x\omega^2}\right]^{\frac{1}{4}}$, but when centrifugal acceleration dominated drainage, the asymptote was $(\sin\alpha)^{\frac{1}{2}}$ which agreed with Sparrow and Hartnett (68).

The assumption of plane laminar flow along the generator of the cone was seldom found during experiments, therefore the predictions made by the theory were not in exact agreement with the experimental results.

Film drainage

Photographic evidence shows that at certain speeds of rotation the film of condensate drains along the surface of the 10°, 20° and 60° cones; photographs for the latter cone are presented in (70). At zero speed, the film is free from waves near the starting point of condensation on each cone, but downstream, irregular patterns of roll-waves develop while the condensate drains along the generator of the cone.

At speeds of rotation between 100 rev/min and 200 rev/min on the 10^{o} and 20^{o} cones, and at speeds between 200 rev/min and 350 rev/min on the 60^{o} cone, the roll-wave regime degenerated into ridges. The transition to ridges depended on $\frac{D\omega^2}{2g}$, on the distance x and on the condensation rate; high condensation rates lead to transitions at a lower $\frac{D\omega^2}{2g}$ and distance x.

On the 10^{o} cone, drops developed on the ridges at speeds between 300 rev/min and 400 rev/min, and drops were observed to leave the film at speeds between 400 and 800 rev/min. At speeds up to 800 rev/min the photographs show that drainage from the 20^{o} cone was along the surface of the cone in a ridge regime.

Photographs of the 10^{o} and 20^{o} cones could not be taken at speeds above 800 rev/min because of the suspension of water droplets in the steam atmosphere. Presumably these drops were thrown from the 10^{o} cone, but certain tests for the 20^{o} cone show a sharp increase in the experimental heat transfer coefficient which suggests that the film drainage on this cone was also being enhanced by the detachment of drops.

It was argued that both the magnitude of the vector representing the acceleration field, and the direction of the vector relative to the surface of the cone would influence the mode of film drainage. The vector was resolved normal to the surface (a_y) and along the surface (a); the former acceleration encouraging drainage by drops, while the latter encouraged drainage along the surface. From published data for filmwise condensation on both stationary (38) and rotating surfaces (58) (59), the onset of drop detachment was shown

to occur at $\frac{a_y}{a}$ between 2 and 12. On cones, the ratio $\frac{a_y}{a}$ was shown to approach a limiting value which decreased as the apex angle increased from zero. On the 10^o cone the limiting value of $\frac{a_y}{a}$ was 11.4, and the onset of drop detachment occurred when $\frac{a_y}{a}$ was greater than 5.7, which was in keeping with the findings of other workers. The limiting value of $\frac{a_y}{a} = 5.6$ for the 20^o cone, was within the range where drops have been observed to leave films of condensate, so the proposed onset of drop detachment from this cone, as suggested by the heat transfer results, could not be ruled out.

The limiting value of $\frac{a_y}{a} = 1.74$ for the 60^o cone was below that observed for the detachment of drops. At speeds up to 1400 rev/min, photographs of the film (70) on the 60^o cone show that drainage continued along the surface of the cone.

As the speed increased, the film of condensate on each of the experimental cones drained along a path which spiralled downwards in the opposite direction to that of rotation. The angle made between the drainage path and the generator of the cone increased with speed from 0^o on stationary cones to a limit of approximately 30^o at speeds up to 1450 rev/min.

Heat flux.

Over the range of test conditions the experimental heat flux was shown to increase almost linearly with the Drew reference temperature $t_f = t_s - 0.75\,\theta$, at a given value of $\frac{D\omega^2}{2g}$.

In general, the heat flux from the condensate to the experimental cones increased with $\frac{D\omega^2}{2g}$ at a given t_f, but the heat flux increased more rapidly with t_f than with $\frac{D\omega^2}{2g}$. Experimental heat flux from published sources showed similar trends.

While the film of condensate drained along the surface of the 10^o and 20^o cones, the increase in heat flux with t_f was similar to that for the 60^o cone. When drops were thrown from the 10^o cone, and possibly from the 20^o cone, the few experimental points from these tests tended to indicate a slightly greater increase in heat flux with t_f. Additional experimental results at high speeds taken over a greater range of t_f are required to show this trend clearly.

Over certain ranges of speed, the heat flux to the 10^o, 20^o and 60^o cones, and to the disc and cylinders described in (54) (58), was shown to be limited by the thermal resistance of the solid beneath the condensing surface. When values of heat flux are required during the calculation of transient thermal stresses in rotors which are both warming through and accelerating, this limiting of the heat flux simplifies the calculation. If a large proportion of the temperature difference between the steam and the lowest temperature of the body, is across the body, the heat flux from the film will show little increase with increases in angular velocity. In general, the thermal resistance of the film is dominant only when the film temperature difference θ is a large fraction of the difference in temperature between the steam and the lowest temperature of the body.

Heat transfer coefficient.

The temperature distribution along the outer surface of

the experimental cones was non-isothermal. Changes in θ with x produce changes in both the experimental and laminar heat transfer coefficients. The experimental value was almost proportional to $\frac{1}{\theta}$ at any distance x, but the theoretical laminar value was almost proportional to $\left[\frac{1}{\theta}\right]^{\frac{1}{4}}$ while 4H was greater than $\frac{4}{3}\delta^4\left[\frac{da}{dx} + \frac{a}{D}\frac{dD}{dx}\right]$ (see section 3.1.8). The latter term became dominant with increases in speed and thereafter further changes in θ had little effect on the laminar heat transfer coefficient.

At zero speed, both the experimental and the laminar heat transfer coefficients tended to decrease with x. At high speeds where drainage was exclusively along the surface both heat transfer coefficients tended to become more uniform with x. The experimental heat transfer coefficient showed a marked increase downstream of the point where drainage was assisted by the detachment of drops.

Recommended equations.

The needs of the designer were borne in mind when developing the recommended equations. Equations predicting the experimental heat transfer coefficients were based on terms derived from the laminar theory for isothermal cones and had the following general form.

$$Nu\ (3H)^{\frac{1}{4}}\left(\frac{\omega \mathrm{Sin}\,\alpha}{g\ \mathrm{Cos}\alpha}\right)^{3/2} = A_1\left[\frac{x\omega^2\ \mathrm{Sin}^2\alpha}{g\ \mathrm{Cos}\ \alpha}\right]^{A_2}$$

where $Nu = \frac{h_{exp}\ x}{k}$ and $H = \frac{c\theta\ \nu^2}{Pr(1 + \frac{3}{8}c\theta)}$

The table below gives the constants A_1 and A_2 for the experimental cones.

Apex angle (2α)	$\frac{x\omega^2 \sin^2\alpha}{g \cos\alpha}$	A_1	A_2
10°	$0.001 < \cdot\cdot < 1.0$	3.36	0.75
	$1.0 < \cdot\cdot < 7.0$	2.9	1.0
20°	$0.001 < \cdot\cdot < 10.0$	2.6	0.75
60°	$0.1 < \cdot\cdot < 1.0$	2.02	0.75
	$1.0 < \cdot\cdot < 250.0$	2.25	0.9

Where the fluid properties of the condensate in the constant H namely c, k, ν are evaluated at the Drew reference temperature $t_f = t_s - 0.75\,\theta$, and the enthalpy of condensation l is evaluated at the saturation temperature t_s.

The above recommended equations are taken from curves passing through the experimental points which are scattered, due partly to the non-isothermal temperature distribution along the outer surface, and partly to the experimental error. Extreme points may differ by a factor of 2 times the value given by the curve, but most of the points were in better agreement.

Assuming isothermal conditions, the laminar heat transfer coefficients for each cone formed a unique curve expressed by an equation similar in form to that given for the recommended equations.

The constants A_1 and A_2 from the isothermal theory are

Apex angle (2α)	$\frac{x\omega^2 \sin^2\alpha}{g \cos\alpha}$	A_1	A_2
10°	less than 1.0	2.34	0.75
	1.0 20	2.1	0.875
	greater than 30	1.1	1.0
20°	less than 1.0	2.66	0.75
	1.0 35	2.5	0.875
	greater than 35	1.14	1.0
60°	less than 0.3	1.17	0.75
	0.3 5.0	1.17	0.875
	greater than 5.0	1.16	1.0

From these two tables and from the curves shown in figs. 55 and 58, it can be seen that the experimental curves are between approximately 1.0 and 1.9 times the isothermal theory.

The quotient $\frac{h_{cone}}{h_{disc}}$ predicted by the laminar theory cannot be verified from the experimental results, because there are insufficient values of the experimental heat transfer coefficients for the disc (54) and for the 0° (58), 10°, 20° and 60° cones, at a common value of θ. However, the experimental heat transfer coefficients for the disc, the 10°, 20° and 60° cones and the cylinders, have been compared with the laminar theory so $\left.\frac{h_{cone}}{h_{disc}}\right|_{exp}$ can be found indirectly if required.

Application of experimental data to rotating bodies with curved generators.

The laminar theory of condensation, which assumed drainage along the surface, was extended to include the condensation of steam on rotating bodies with curved generators. The theory was applied to a body resembling part of the turbine rotor where the shaft joins a blade disc.

The theoretical findings for such bodies at high speeds of rotation are of more general interest, because the assumed orientation of the axis of symmetry, which is also the axis of rotation, becomes unimportant.

The importance of the radius of curvature of the generator depended on its magnitude relative to the radius of the body. As the radius of the body increased for a given generator curve, the laminar film thickness at a given distance x along the curve was reduced and the laminar heat transfer coefficient was increased. At speeds of 100 rev/min the laminar heat transfer coefficient decreased for a short distance downstream of the starting point of condensation, at which $x = 0$, and thereafter increased to become asymptotic to $h_{\frac{2\alpha}{h}_{disc}} = (\mathrm{Sin}\alpha)^{\frac{1}{2}}$ where $h_{disc} = \left[\frac{2k^4 \nu^2}{3H}\right]^{\frac{1}{4}}$ and 2α is the local apex angle as defined in fig. 4. In laminar theory this asymptote holds for rotating bodies with generator curves other than circular arcs.

The experimental findings for cylinders and for the 10° and 20° cones shows that near the shaft part of the rotor where the angle α is small, the drainage should be assisted by the

formation and detachment of drops. This should lead to useful local improvements in the heat transfer coefficient in a region where the surface to volume ratio of the body is small. As with cones, the angle 2α at which drop detachment ceases will probably be closely related to the ratio of acceleration $\frac{a_y}{a}$. Accepting that this is so, the detachment of drops should cease as angle 2α increased beyond 20°. As the apex angle for cones increases towards 60°, the films of condensate tends to drain exclusively along the surface and should continue to do so up to 180°.

It can be shown that at high speeds, $\left.\frac{h_{60^\circ}}{h_{disc}}\right|_{exp}$ is close to $\left.\frac{h_{60^\circ}}{h_{disc}}\right|_{lam} = (\mathrm{Sin}\alpha)^{\frac{1}{2}}$. Since $\left.\frac{h_{2\alpha}}{h_{disc}}\right|_{lam}$ for the turbine rotor also closes on $(\mathrm{Sin}\alpha)^{\frac{1}{2}}$ at high speeds, one can argue that the experimental heat transfer coefficients on the rotor should be similar to those for cones over the range of 2α, 60° to 180°.

9.0 REFERENCES

(1) Erb, R.A. and Thelen, F.
'Promoting permanent dropwise condensation'
'65 Ind.Eng.Chem. 57, No. 10, 49-52.

(2) Tanner, D.W., Potter, C.J., Pope, D. and West, D.
'Heat transfer in dropwise condensation - Part I'
'65 Int.J.Heat.Mass Transfer, 8, 419-426,

(3) Tanner, D.W., Potter, C.J., Pope, D. and West, D.
'Heat transfer in dropwise condensation - Part II'
'65 Int.J.Heat.Mass Transfer, 8, 427-436.

(4) Umur, A. and Griffith, P.
'Mechanism of dropwise condensation'
'65 Trans.ASME Series C, 87, 275-282.

(5) McCormick, J.L. and Westwater, J.W.
'Drop dynamics and heat transfer during dropwise condensation of water vapour on a horizontal surface'
'66 Chem.Eng.Prog.Symposium Series No. 64, 62-120.

(6) Le Fevre, E.J. and Rose, J.W.
'Heat transfer measurements during the dropwise condensation of steam'
'64 Int.J.Heat.Mass Transfer, 7, 272-273.

(7) Rose, J.W.
'On the mechanism of dropwise condensation'
'67 Int.J.Heat.Mass Transfer, 10, 755-762.

(8) Mikic, B.B.
'On mechanism of dropwise condensation'
'69 Int.J.Heat.Mass Transfer, 12, 1311-1323.

(9) Nusselt, W.
'Die oberflachenkondensation des wasserdamfs'
'16 Z.Ver.dt.Ing, 60, 541

(10) Monrad, C.C. and Badger, W.L.
'Condensation of vapours'
'30 Ind.Eng.Chem. 22, No. 10, 1103-1112.

(11) Hampson, H. and Ozisik, N.
'An investigation into the condensation of steam'
'52 Proc.I.Mech.E. 1, Series B, 282-293.

(12) Bromley, L.A.
'Effect of heat capacity of condensate'
'52 Ind.Eng.Chem. 44, 2966-2969.

(13) Rohsenow, W.M.
'Heat transfer and temperature distribution in laminar-film condensation'
'56 Trans.ASME (78), 1645-1648.

(14) Sparrow, E.M. and Gregg, J.L.
'A boundary-layer treatment of laminar-film condensation'
'59 Trans.ASME Series C. 81, 13-17.

(15) Sparrow, E.M. and Gregg, J.L.
'Laminar condensation heat transfer on a horizontal cylinder'
'59 Trans.ASME Series C, 81, 291-296.

(16) Chen, M.M.
'An analytical study of laminar film condensation: Part I - flat plates'
'61 Trans.ASME, Series C, 83, 48-54.

(17) Koh, J.C.Y., Sparrow, E.M., Hartnett, J.P.
'The two phase boundary layer in laminar film of condensation'
'61 Int.J.Heat.Mass Transfer, 2, 69-82.

(18) Chen, M.M.
'An analytical study of laminar film condensation: Part II - single and multiple horizontal tubes'
'61 Trans.ASME, Series C, 83, 55-66.

(19) Sukhatme, S. and Rohsenow, W.M.
'Heat transfer during film condensation of a liquid metal vapour'
'66 Trans.ASME, Series C, 88, 19-29.

(20) Wilcox, S.J. and Rohsenow, W.M.
'Film condensation of potassium using copper condensing block for precise wall-temperature measurements'
'70 Trans.ASME, Series C, 92, 359-371.

(21) Poots, G. and Miles, R.G.
'Effects of variable physical properties on laminar film condensation of saturated steam on a vertical flat plate'
'67 Int.J.Heat.Mass Transfer, 10, 1677-1692.

(22) Kirkbride, C.G.
'Heat transfer by condensing vapour on vertical tubes'
'34 Am.Inst.Chem.Eng. 30, 170.

(23) Friedman, S.J. and Miller, C.O.
'Liquid films in the viscous flow region'
'41 Ind.Eng.Chem. 33, 885.

(24) Dukler, A.E. and Bergelen, O.P.
'Characteristics of flow in falling liquid films'
'52 Chem.Eng.Prog. 48, No. 11, 557.

(25) Grimley, H.
'Liquid flow conditions in packed towers'
'45 Trans.Inst.Chem.Engrs. 23, 228-235.

(26) Binnie, A.M.
'Experiments on onset of wave formation on film of water flowing down a vertical plane'
'57 J.Fluid.Mech. 2, 551-553.

(27) Kapitza, P.L. '48 Zh. Eksparim i. Teor Fiz. 18, 3
" " " " " " 18, 19
Translated in "collected works of Kapitza" Pergamon 1965.

(28) Brooke Benjamin, T.
'Wave formation in laminar flow down an inclined plane'
'57 J.Fluid.Mech. 2, 554-574.

(29) Yih, C.S.
'54 Proc.Second.U.S.Cong.Appl.Mech.ASME, 623.

(30) Colburn, A.P.
'The calculation of condensation where a portion of the condensate layer is in turbulent motion'
'34 Trans.Am.Inst.Chem.Engrs. 30, 187-193.

(31) Carpenter, E.F. and Colburn, A.P.
'The effect of vapour velocity on condensation inside tubes'
'51 Proc.of General Discussion on Heat Transfer I.Mech.E./ASME. 20-26.

(32) Seban, R.A.
'Remarks on film condensation with turbulent flow'
'54 Trans.ASME, 76, 299-303.

(33) Rohsenow, W.M., Weber, J.H. and Ling, A.T.
'Effect of vapour velocity on laminar and turbulent-film condensation'
'56 Trans.ASME. 78, 1637-1643.

(34) Dukler, A.E.
'Fluid mechanics and heat transfer in vertical falling film systems'
'60 Chem.Eng.Prog.Symposium Series No. 30, 56

(35) Lee, J.
'Turbulent film condensation'
'64 A.I.Chem.E.Journal 10, No. 4, 540-544.

(36) Kunz, H.R.
'Analytical study of liquid metal condensing inside tubes'
'65 NASA-CR-54352, Pratt and Witney.

(37) Dhir, V. and Leinhard, J.
'Laminar film condensation on plane and axisymmetric bodies in non-uniform gravity'
'71 Trans.ASME. Series C, 93, 97-100.

(38) Gerstmann, J. and Griffith, P.
'Laminar film condensation on the underside of horizontal and inclined surfaces'
'67 Int.J.Heat.Mass Transfer, 10, 567-579.

(39) Provan, T.F.
'Condensation of pure vapours in the presence of non-condensable gases'
National Engineering Laboratory, N.E.L. Report 114.

(40) National Engineering Laboratory.
Reports dealing with the effects of non-condensable gas on the performance of condensers.
Various authors.
'66 N.E.L. Reports No. 219.
'67 " " No. 270.
'67 " " No. 281.
'67 " " No. 294.
'71 " " No. 477.
'71 " " No. 483.

(41) Frankell, N.A. and Bankoff, S.G.
'Laminar film condensation on a porous horizontal tube with uniform suction velocity'
'65 Trans.ASME. Series C, 87, 95-102.

(42) Velkoff, H.R. and Miller, J.H.
'Trans.ASME Series C, 87, 197-207.

(43) Holmes, R.E. and Chapman, A.J.
'Condensation of freon 114 in the presence of a strong non-uniform alternating electric field'
'70 Trans.ASME. Series C, 92, 616-620.

(44) Terrel, B.J.
'The influence of thermal effects on manoeuvrability of marine steam turbines'
'53 Trans.N.E.Coast.Instn.Engrs. and Shipbuilders, 70, 93-101.

(45) Hall, J.S. and Britten, A.F.
'Rapid starting technique: Sone significant tests at Poole power station'
'54 Proc.I.Mech.E. 168, No. 27, 717-741.

(46) Moore, J.T.
'Engineering planning and design of large steam power plant for maximum availability'
'65 Proc.I.Mech.E. 179, Pt. (3I).

(47) Chow, C.L. and Hoyle, R.
'Temperature distribution in the rotor of a steam turbine during warm and hot starts'
'63 The Engineer, 215, 763-766.

(48) Hoyle, R. and Mahabir, H.E.
'Cold starting temperatures in rotors of marine steam turbines'
'63 The Engineer, 216, 353-356.

(49) Sparrow, E.M. and Gregg, J.L.
'A theory of rotating condensation'
'60 Trans.ASME. Series C, 81, 113-120.

(50) Nandapurka, S.S. and Beatty, K.O.
'Condensation on a horizontal rotating disc'
'59 3rd National Heat Transfer Conf.ASME. 130-137.

(51) Sparrow, E.M. and Gregg, J.L.
'The effect of vapour drag on rotating condensation
'60 Trans.ASME Series C, 71-72.

(52) Espig, H. and Hoyle, R.
'Waves in a thin liquid on a rotating disc'
'65 J.Fluid.Mech. 22, 671-677.

(53) Bromley, L.A., Humphreys, R.F. and Murray, W.
'Condensation and evaporation from radially grooved rotating discs'
'66 Trans.ASME Series C, 88, 80-86.

(54) Espig, H. and Hoyle, R.
'The transfer of heat from condensing steam to a cooled rotating disc'
'68 Proc.I.Mech.E. 182, Part 3H.

(55) Yeh, L.
'53 Ph.D. thesis, Imperial College of Science and Technology, London.

(56) Singer, R.M. and Preckshot, G.W.
'63 Proc. of the heat transfer and fluid mechanics institute, No. 14, 205-221.

(57) Kuo, C.T. et al.
'Heat transfer in rotating ducts'
'60 Trans.ASME Series C, 82, 139-151.

(58) Hoyle, R. and Matthews, D.H.
'The effect of diameter size and speed of rotation on the heat transfer from steam to cooled cylinders'
'64 Int.J.Heat.Mass Transfer, 7, 1223-1234.

(59) Nichol, A.A. and Gacesa, M.
'Condensation of steam on a rotating vertical cylinder'
'70 Trans.ASME, Series C, 92, 144-152.

(60) Hoyle, R. and Matthews, D.H.
'The effect of speed on the condensate layer on a cold cylinder rotating in a steam atmosphere'
'65 J.Fluid Mechanics, 22, Pt. 1, 105-112.

(61) Hickman, K.C.D.
'Centrifugal boiler compression still'
'57 Ind.Eng.Chem. 49, 786-800.

(62) Bromley, L.A.
'Prediction of performance characteristics of Hickman-Badger centrifugal boiler compression still'
'58 Ind.Eng.Chem. 50, 233-236.

(63) Bruin, S.
'Velocity distributions in a liquid film flowing over a rotating conical surface'
'69 Chem.Eng.Sci. 24, 1647.

(64) Wu, C.S.
'Three dimensional incompressable laminar boundary layer on a spinning cone'
'59 App.Sci.Res., Section A, 8, 140-146.

(65) Millsaps, K. and Pohlhausen, K.
'Heat transfer by laminar flow from a rotating disc'
'52 J.Aeronautical Sci. 19, 120-126.

(66) Sparrow, E.M. and Gregg, J.L.
'Heat transfer from a rotating plate to fluids of any Prandtl number'
'59 Trans.ASME. Series C, 81, 249

(67) Tien, C.L.
'Heat transfer by laminar flow from a rotating cone'
'60 Trans.ASME. Series C, 82, 252-253.

(68) Sparrow, E.M. and Hartnett, J.P.
'Condensation on a rotating cone'
'61 Trans.ASME. Series C, 101-102.

(69) Howe, M. and Hoyle, R.
'Heat transfer from condensing steam to a cooled cone rotating about a vertical axis'
'70 Proc.I.Mech.E. 184 (3G).

(70) Robson, B.
'The formation and drainage of a film of condensate on the surface of a rotating cone'
'70 M.Sc. thesis, University of Durham.

(71) Holgate, M.J.
'Stability of a fluid film on the surface of a cone'
'71 Ph.D. thesis, University of Durham.

(72) Ker Wilson, W.
'Practical solutions of torsional vibration problems'
Vol. 3, Strength calculations.
'65 Chapman Hall.

(73) Smith, D.B.
'Condensate film flow on the surface of rotating cones'
Ph.D. thesis, University of Durham.

(74) Ogale, V.A.
'Design and development of rotating slipring assembly for cooled gasturbine blade temperature measurements'
'65 Technische Hogeschool Delft.

(75) Benedict, R.P.
'Fundamentals of temperature, pressure and flow measurement'
'69 Wiley.

(76) Hanson, D. and Rodgers, C.E.
'The thermal conductivity of some non-ferrous alloys'
'32 J.Inst. Met. 48, 37-45.

(77) Smith, C.S. and Palmer, E.W.
'Thermal and electrical conductivities of copper alloys'
'35 Trans.Amer.Inst.Min.Met.Eng. 117, 225-243.

(78) Powell, R.W.
'Correltation of metallic thermal and electrical conductivities for both solid and liquid phases'
'65 Int.J.Heat Mass Transfer, Vol. 8, 1033-1045.

APPENDICES

Appendix A.

Equation (3.1.15) may be rearranged in the form

$$E = \frac{\delta}{x}\frac{d}{dx}\left[\frac{\delta^3 x}{\nu^2}\left(x\omega^2 \operatorname{Sin}^2\alpha + g \operatorname{Cos}\alpha\right)\right] \quad \ldots\ldots\ldots \text{A1}$$

where $$E = \frac{3\ c\ \theta}{Pr\ (1+\frac{3}{8}\ c\theta)}$$

Introducing a dimensionless variable L to characterise the distance along the cone from the starting point of the film.

$$L = \frac{x}{e} \quad \ldots\ldots\ldots \text{A2}$$

and $$\frac{dx}{dL} = e \quad \ldots\ldots\ldots \text{A3}$$

Introducing a dimensionless variable λ to characterise the film thickness at any value of L.

$$\lambda = \frac{\delta}{\gamma} \quad \ldots\ldots\ldots \text{A4}$$

and $$\frac{d\delta}{d\lambda} = \gamma \quad \ldots\ldots\ldots \text{A5}$$

Substituting equations A2 to A5 in A1 gives

$$E = \frac{\lambda}{L}\frac{d}{dL}\left[\frac{\lambda^3 L}{\nu^2}\left(\gamma^4\omega^2\operatorname{Sin}^2\alpha . L + g \operatorname{Cos}\alpha . \frac{\gamma^4}{e}\right)\right]$$

Now choose e and γ such that

$$\left.\begin{aligned} \frac{\gamma^4}{e\nu^2} g \operatorname{Cos}\alpha &= E \\ \frac{\gamma^4\omega^2\operatorname{Sin}^2\alpha}{\nu^2} &= E \end{aligned}\right\} \quad \text{giving}$$

$$\gamma = \left[\frac{\nu}{\operatorname{Sin}\alpha}\right]^{\frac{1}{2}} E^{\frac{1}{4}} \quad \ldots \text{A6}$$

$$e = \frac{g \operatorname{Cos}\alpha}{\omega^2 \operatorname{Sin}^2\alpha} \quad \ldots \text{A7}$$

Equations A6 and A7 reduce the equation A1 to

$$\frac{\lambda}{L}\frac{d}{dL}\left[\lambda^3 L\,(L+1)\right] = 1$$

which has the solution

$$\lambda^4 L^{4/3}(L+1)^{4/3} = \frac{4}{3}\int_o^L L^{4/3}(L+1)^{1/3}\,dL \qquad \ldots\ldots\ldots \text{A8}$$

Equation A8 is expressed in terms of the dimensionless variables λ and L, and has a form similar to equation 3.3.5.

The Nusselt number $\quad Nu = \frac{hx}{k}\Big|_{\text{laminar}}$

which reduces to $\quad Nu = \frac{x}{\delta}\Big|_{\text{laminar}}$

In terms of the dimensionless variables, $Nu = \frac{eL}{\gamma\lambda}$

or $\quad Nu\,\frac{\gamma}{e} = \frac{L}{\lambda} = f(L) \qquad \ldots\ldots\ldots \text{A9}$

Therefore

$$Nu(3H)^{\frac{1}{4}}\left(\frac{\omega \mathrm{Sin}\alpha}{g\mathrm{Cos}\alpha}\right)^{3/2} = f\left[\frac{x\omega^2\mathrm{Sin}^2\alpha}{g\mathrm{Cos}\alpha}\right] \qquad \ldots\ldots\ldots \text{A10}$$

Where $\quad H = \dfrac{c\,\theta\,\nu^2}{Pr\left(1 + \frac{3}{8}\,c\theta\right)}$

At high speeds of rotation, where centrifugal acceleration dominates the film drainage, equation A10 becomes:-

$$Nu(3H)^{\frac{1}{4}}\left(\frac{\omega \mathrm{Sin}\alpha}{g\mathrm{Cos}\alpha}\right)^{3/2} = C_1\left[\frac{x\omega^2\mathrm{Sin}^2\alpha}{g\mathrm{Cos}\alpha}\right] \qquad \ldots\ldots\ldots \text{A11}$$

Where $\quad C_1$ is a constant

The above equation expresses the findings of Sparrow and Hartnett (68).

At low speeds, where gravitational acceleration dominates drainage, equation A10 becomes:-

$$Nu(3H)^{\frac{1}{4}} \left(\frac{\omega \mathrm{Sin}\alpha}{g\mathrm{Cos}\alpha}\right)^{3/2} = C_2 \left[\frac{x\omega^2 \mathrm{Sin}^2\alpha}{g\mathrm{Cos}\alpha}\right]^{\frac{3}{4}} \quad \ldots\ldots\ A12$$

Where C_2 is a constant.

The above equation is comparable with the Nusselt type solution.

Laminar films of condensate on truncated cones.

The dimensionless film thickness λ is related to the dimensionless distance along the cone from the apex:-

$$\frac{4}{\lambda} L^{4/3} (L+1)^{4/3} = \frac{4}{3} \int_{L_o}^{L} L^{4/3} (L+1)^{1/3} \, dL \quad \ldots\ A8$$

or $$= I\ (L,\ L_o)$$

The right-hand side of equation A8 can also be written as

$$I\ (L,\ 0) - I\ (L_o,\ 0) = \frac{4}{3} \left[\int_o^L L^{4/3}\ (L+1)^{1/3}\ dL - \int_o^{L_o} L^{4/3}\ (L+1)^{1/3}\ dL \right]$$

Therefore

$$\left[\lambda\ (L,\ L_o)\right]^4 = \left[\lambda(L,\ 0)\right]^4 - \left[\lambda(L_o\ 0)\right]^4 \frac{L_o^{4/3}(L_o+1)^{4/3}}{L^{4/3}\ (L+1)^{4/3}}$$

Where $\lambda = 0$ at $L = L_o$

Knowing $\lambda(L,\ 0)$, which is the growth of the film when it starts at the apex, we can immediately form the corresponding film thickness when the film starts at any point away from the apex.

The definition of the Nusselt number in terms of the distance from the start of the film is:-

$$Nu(3H)^{\frac{1}{4}} \left(\frac{\omega \mathrm{Sin}\alpha}{g\mathrm{Cos}\alpha}\right)^{3/2} = \frac{L - L_o}{\lambda(L,\ L_o)} \quad \ldots\ldots\ A13$$

FIG A1

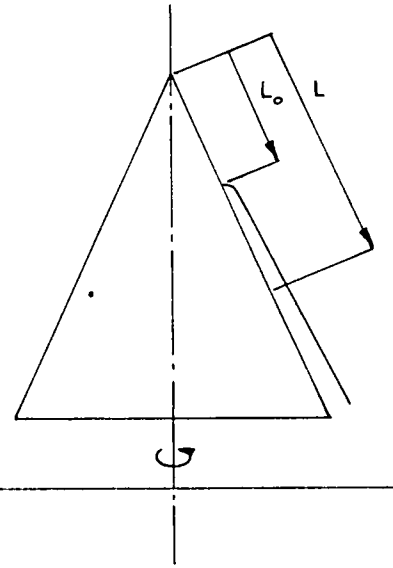

$Nu(3H)^{\frac{1}{4}}\left(\frac{\omega \sin\alpha}{9\cos\alpha}\right)^{\frac{3}{2}}$

10

1·0

$L_o = 1000$

$L_o = 100$

$L_o = 10$

$L_o = 0$

0·1

1·0

10

100

$L - L_o = \frac{x\omega^2 \sin^2\alpha}{9\cos\alpha}$

Therefore the left hand side of equation A13 can be plotted as a function of $L-L_0$ which is the parameter $\frac{x\omega^2 Sin^2\alpha}{gCos\,\alpha}$.

Fig. A1 shows the graph of $Nu(3H)^{\frac{1}{4}} \left(\frac{\omega Sin\alpha}{gCos\alpha}\right)^{3/2}$ against $\frac{x\omega^2 Sin^2\alpha}{gCos\alpha}$ for several values of L_0.

Appendix B.

The thermal conductivity of the cone material was derived from measurements of the electrical conductivity of the material.

In 1932, Hanson and Rodgers (76) gave a correlation between the thermal and electrical conductivities of several binary copper-alloys. Two years later, Smith and Palmer (77) extended the study to include commercial copper-alloys. More recently in 1965, Powell (78) reviewed the published data for the correlations of thermal and electrical conductivities for both solid and liquid phases of a wide range of metals.

The equation for the thermal conductivity of copper-alloys is given in (78) as:-

$$k_t = C_1 \sigma_t T + C_2 \qquad \ldots\ldots\ldots \text{B1}$$

where σ_t = electrical conductivity of the metal $\frac{1}{\Omega m}$

T = absolute temperature K

$C_1 = 2.39.10^8 \quad \frac{W\Omega}{K^2}$

$C_2 = 7.5 \quad \frac{W}{mK}$

Measurement of electrical conductivity.

The electrical resistance R of a sample of the cone material was measured at several temperatures between 20° C and 200° C with the circuit shown in Fig. B1.

The electrical conductivity was derived from:-

$$\sigma_t = \frac{1}{R_t A}$$

FIG B1

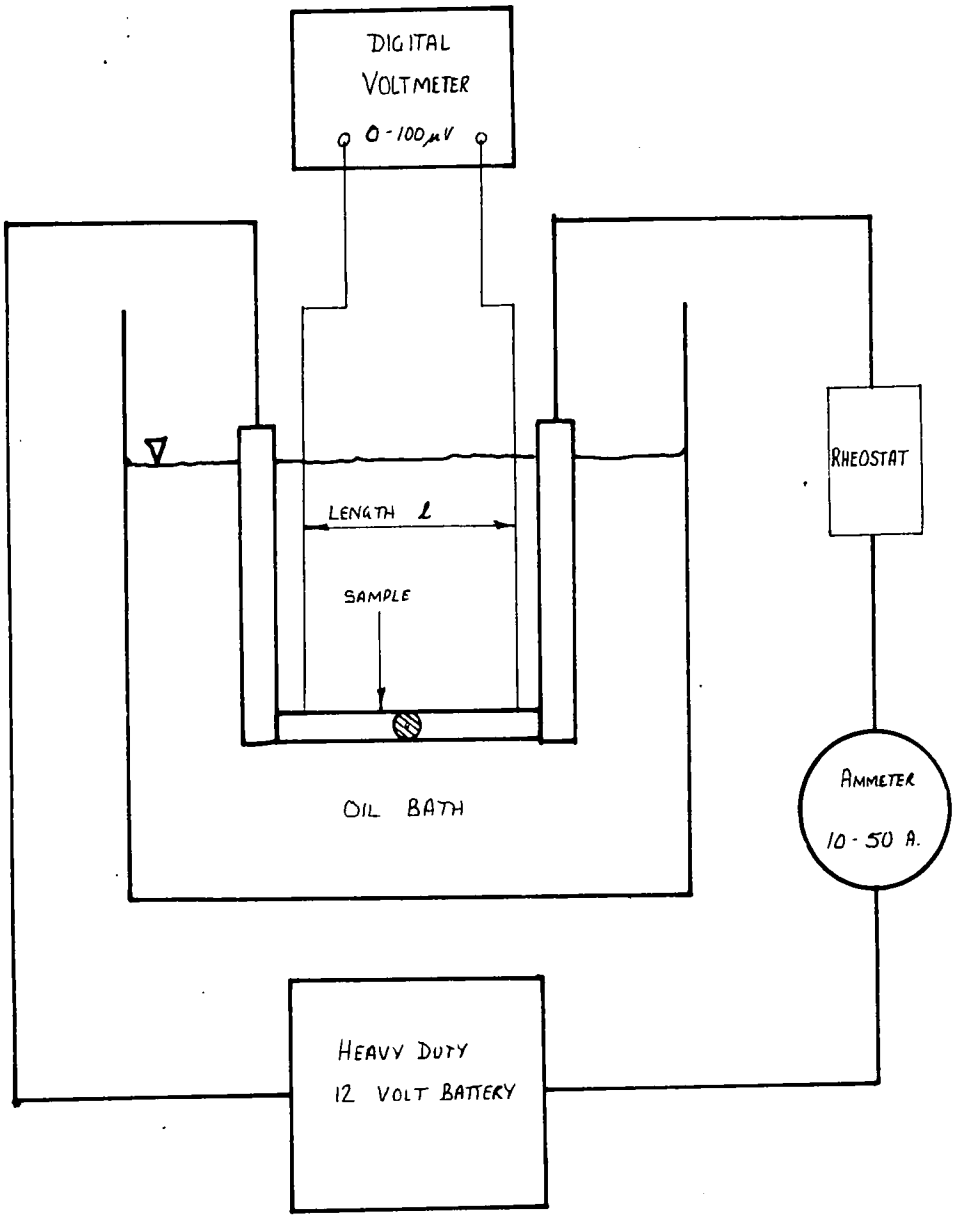
DIGITAL
VOLTMETER
0 - 100 μV
RHEOSTAT
LENGTH l
SAMPLE
OIL BATH
AMMETER
10 - 50 A.
HEAVY DUTY
12 VOLT BATTERY

where l = length of the sample

A = cross-sectional area of the sample

R_t = Electrical resistance of the sample at a given temperature.

A comparison between the thermal and electrical conductivities of copper-alloys (77) with compositions close to those of the cone materials showed that equation B1 predicted the thermal conductivity to within 3% of the measured value.

Appendix C.

The cross-section of the thermocouple groove was modelled with the apparatus shown in fig. C1.

A copper sulphate solution was used to represent the metal of the cone and a 50 to 1 dilution of the solution was used to represent the low thermal conductivity of the insulating cement.

Fig. C2 shows the model representing a thermocouple junction near the top of the groove.

Fig. C3 shows the model representing a junction near the bottom of the groove.

FIG C1

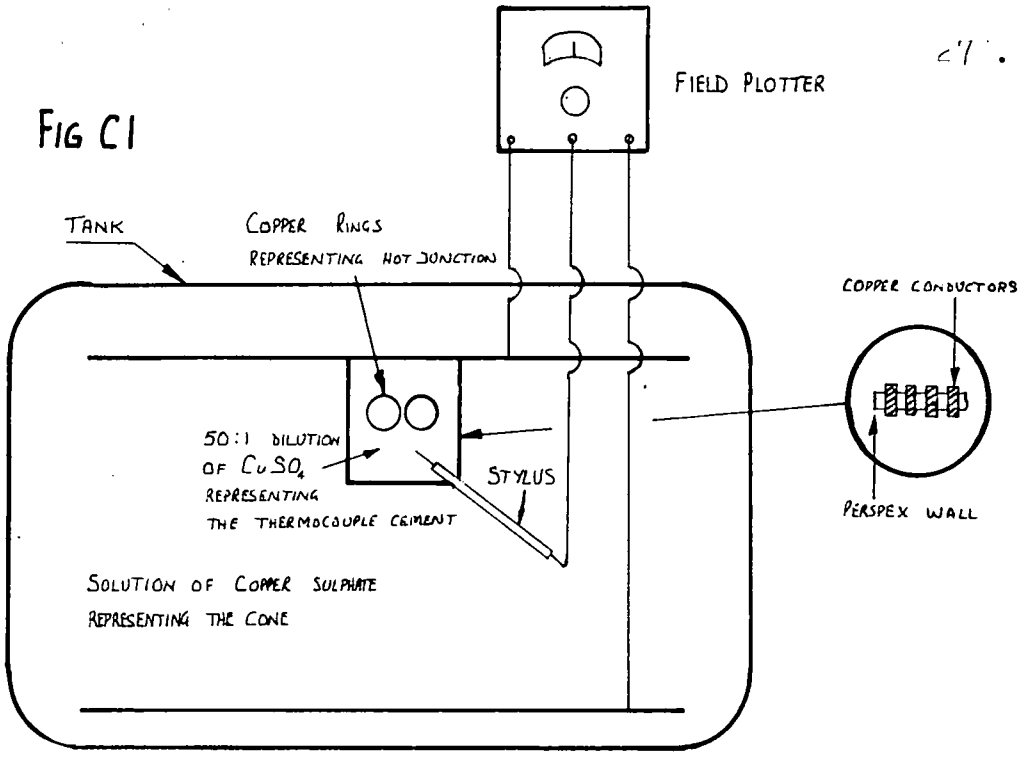

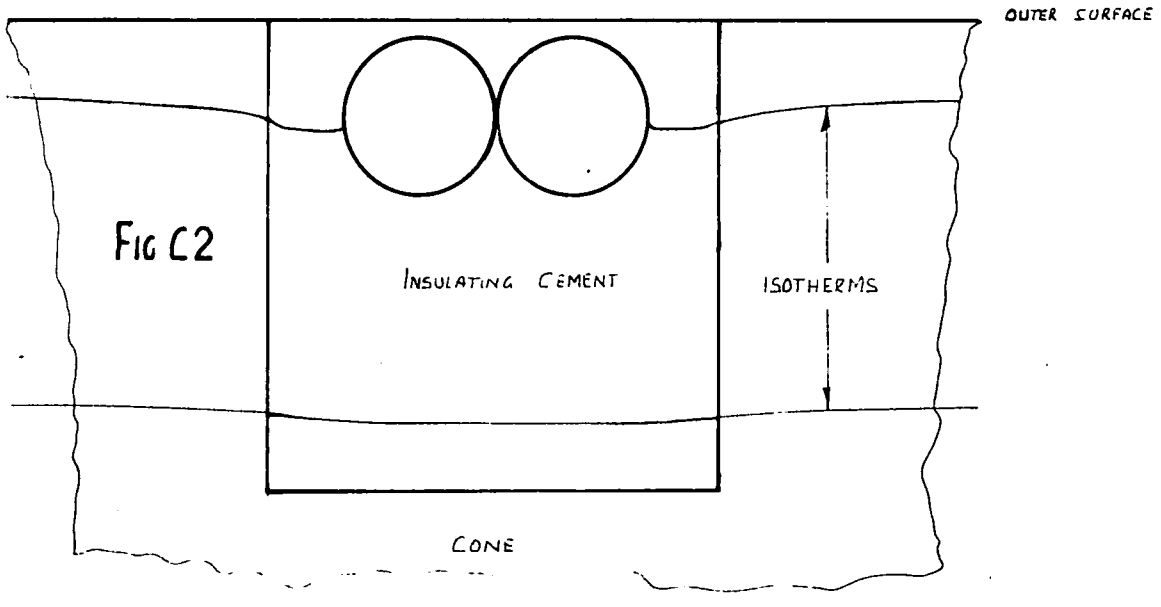

FIG C2

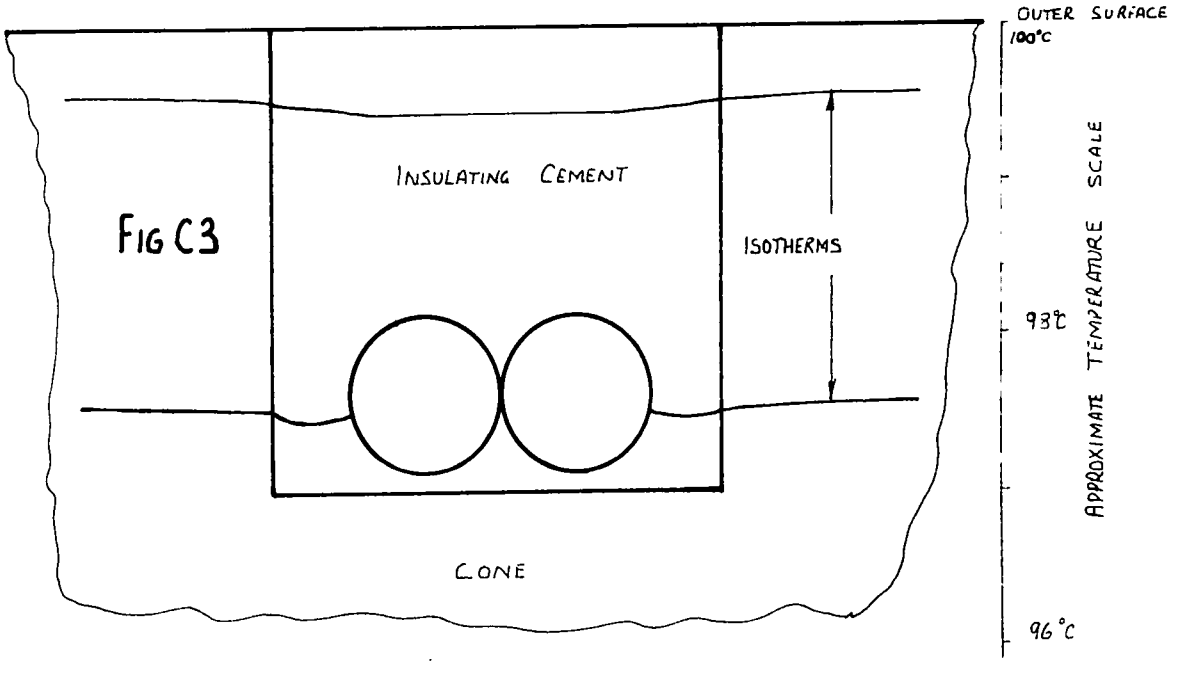

FIG C3

Appendix D.

The following procedure was used to take a sample of steam from the pressure vessel.

(i) The calorimeter, measuring cylinder and condensing coil, shown in fig. 39 were filled with cooling water.

(ii) The calorimeter was weighed on a precision balance.

(iii) The initial temperature of the calorimeter was measured.

(iv) A small flow of steam was passed along the insulated sampling pipe from the pressure vessel to purge the pipe of its gas content and to raise the temperature of the pipe to the steam temperature.

(v) A sample of steam from the sampling pipe was passed into the calorimeter. The flow rate was adjusted to allow the gas bubbles leaving the condensing coil to rise into the measuring cylinder.

(vi) The water content of the calorimeter was stirred and a final temperature was measured.

(vii) The calorimeter was reweighed on the precision balance.

Gas content of the steam.

The gas content of the steam sample is collected at the closed end of the measuring cylinder fig. 39. Assuming that the volume of the water displaced from the measuring cylinder is filled with gas, the mass of gas m_g is found from

$$m_g = \frac{p\ v}{R\ t}$$

where p = pressure of the gas:-

atmospheric pressure - head of water in the measuring cylinder.

v = volume of the gas.

t = temperature of the gas.

R = gas constant.

The mass of gas is somewhat less than this figure, because a small portion of the measured volume is vapour.

The mass of the steam sample m_g is given by the difference between weights (vii) and (ii).

Dryness fraction.

The energy introduced into the calorimeter by the air can be neglected when the concentration of air is small.

The following equation for the dryness fraction is derived from a simple energy balance on the calorimeter.

$$\text{dryness fraction} = \frac{C\left[\frac{m_1}{m_s}\Delta t + t_2\right] - h_f}{h_{fg}}$$

where m_1 = water equivalent of the apparatus before introducing the steam sample.

m_s = mass of steam sample.

t_1 = initial temperature of the calorimeter.

t_2 = final temperature of the calorimeter after introducing the sample of steam.

$\Delta t = (t_2 - t_1)$.

C = specific heat.

h_f = specific enthalpy of liquid phase } at the pressure

h_{fg} = specific enthalpy of condensation } in the vessel.